AD NUMBER

AD831118

NEW LIMITATION CHANGE

TO

Approved for public release, distribution unlimited

FROM

Distribution authorized to U.S. Gov't. agencies and their contractors; Administrative/Operational Use; Jan 1968. Other requests shall be referred to AFFDL/FDDA, Wright-Patterson AFB, OH 45433.

AUTHORITY

AFFDL ltr dtd 29 Oct 1973

AFFDL-TR-67-156

REFINEMENT OF SONIC FATIGUE STRUCTURAL DESIGN CRITERIA

JOHN R. BALLENTINE
FRED F. RUDDER, JR.
JAMES T. MATHIS
HARRY E. PLUMBLEE, JR.

LOCKHEED-GEORGIA COMPANY

TECHNICAL REPORT AFFDL-TR-67-156

JANUARY 1968

AIR FORCE FLIGHT DYNAMICS LABORATORY
AIR FORCE SYSTEMS COMMAND
WRIGHT-PATTERSON AIR FORCE BASE, OHIO

NOTICE

When Government drawings, specifications, or other data are used for any purpose other than in connection with a definitely related Government procurement operation, the United States Government thereby incurs no responsibility nor any obligation whatsoever; and the fact that the Government may have formulated, furnished, or in any way supplied the said drawings, specifications, or other data, is not to be regarded by implication or otherwise as in any manner licensing the holder or any other person or corporation, or conveying any rights or permission to manufacture, use, or sell any patented invention that may in any way be related thereto.

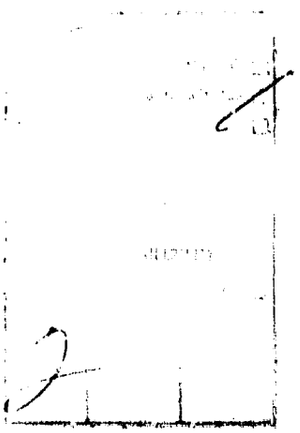

Copies of this report should not be returned unless return is required by security considerations, contractual obligations, or notice on a specific document.

200 - April 1968 - CO455 - 30-629

ABSTRACT

Accurate nomographs and computer programs for designing conventional skin-stringer and honeycomb sandwich construction to meet sonic fatigue requirements are presented. The nomographs were derived from the results of sonic fatigue tests of 30 skin-stringer and 30 honeycomb sandwich designs, totaling 60 test specimens for each design. Emphasis is also placed on assessing the effect of structural curvature on sonic fatigue and structural response. Nomographs for determining the curvature effects are included.

REFINEMENT OF SONIC FATIGUE STRUCTURAL DESIGN CRITERIA

JOHN R. BALLENTINE
FRED F. RUDDER, JR.
JAMES T. MATHIS
HARRY E. PLUMBLEE, JR.

FOREWORD

This report was prepared by the Lockheed-Georgia Company, Marietta, Georgia for the Aero-Acoustics Branch, Vehicle Dynamics Division, Air Force Flight Dynamics Laboratory, Wright-Patterson Air Force Base, Ohio, under contract AF33(615)-3816. The work described herein is a continuing part of the Air Force Systems Command's exploratory development program to establish tolerance levels and design criteria for sonic fatigue prevention for flight vehicles. The work was directed under Project 1471, "Aero-Acoustic Problems", and Task 147101, "Sonic Fatigue". Mr. A. S. Gray and later Mr. D. L. Smith of the Aero-Acoustics Branch were the task engineers.

This report concludes the work on contract AF33(615)-3816, which covered a period from August 1966 to December 1967.

The authors gratefully acknowledge the assistance rendered by J. R. Bay, L. V. Mazzarella, and H. T. Watson in performing the experimental work, data collection, and data reduction; R. N. Maddox for his frequency analysis of simple curved panels with elastic supports; and K. Francke, M. J. Cote, and D. Quinlin for data analysis and preparation of the computer data. The Lockheed-Georgia Company report identification number is ER-9546.

The manuscript was released by the authors on 11 October 1967 for publication.

This technical report has been reviewed and is approved.

WALTER J. MYKYTOW
Asst. for Research & Technology
Vehicle Dynamics Division

TABLE OF CONTENTS

TABLE OF CONTENTS (Continued)

LIST OF ILLUSTRATIONS

LIST OF ILLUSTRATIONS (Continued)

LIST OF ILLUSTRATIONS (Continued)

LIST OF ILLUSTRATIONS (Continued)

LIST OF ILLUSTRATIONS (Continued)

LIST OF TABLES

LIST OF SYMBOLS

A	aspect ratio of a curved panel
A_{ij}	coefficients defined by Equation (120)
$[{}_rA_{ij}]$	operator matrix for the r^{th} layer of a honeycomb panel
a	width of a flat panel; arc length of a curved panel
a_1, a_2	defined by Figure 6
$[B_{mnk}]$	matrix of assumed modes
b	length of a flat or curved panel
b_1, b_2	defined by Figure 6
C	extensional rigidity of a curved panel
$[{}_rC_{ij}]$	elastic constants for the r^{th} layer of a honeycomb panel
c	G_{xy}/G_{yz}
D	flexural rigidity of a panel
$[d_i]_i$	deflection vector at station i on the i^{th} element
E	Young's modulus of elasticity
$F_i(x)$	i^{th} mode shape of a one-dimensional structure
F	generalized acoustic pressure force for the fundamental mode.
f_i	frequency of the i^{th} mode in Hz
$G_p(X_A, X_B; \omega_i)$	cross-spectral density function of the excitation pressure at x_A and x_B
G_i	shear modulus for the i^{th} stiffener element
G_{ij}	stiffness parameter - Section F.2.a; shear modulus - Section F.3.a.
$[G]$	defined by Equation (73)
g	t/h
$[H]$	defined by Equation (70)
h	core thickness of honeycomb panel
h_1	$h/2$

I_{ij}	element in the inertia matrix
I_i	second area moment of inertia of the i^{th} stiffener element
J	St. Venant's torsion constant
J_{ii}	mass parameter - Section F.2.a
K	modal stiffness of fundamental mode defined by Equation (102) - Section F.2.b; in-plane spring constant - Section F.2.c
$[K]$	stiffness matrix
K_1, K_3	defined by Equation (135)
K_2, K_4	defined by Equation (134)
L	b/t - Section F.2.a b/h - Section F.3.a
L_i	Length of i^{th} stiffener element
L_{ij}	coefficients defined by Equation (131)
M	modal mass of fundamental mode
M_i	modal mass of i^{th} mode
M_x	bending moment about y axis in a plate moment about x axis of stiffener element - Section D.2.a
M_z	moment about z axis of stiffener element
M_{mn}	generalized mass of $(m,n)^{th}$ mode
$M_i(m)$	defined in Table I
$[M]$	mass matrix
$[\overline{M}]$	eigenvalues of the mass matrix
m_p	mass of plate inertia element
m_R	mass of rib inertia element
m_S	mass of stringer inertia element
$N_i(n)$	defined in Table I
P_o	acoustic pressure amplitude
P_1	$b_1^2 - b_1 b_2 + b_2^2$
P_2	$a_1^2 - a_1 a_2 + a_2^2$

P_3	$b_2 - b_1$
P_4	$a_2 - a_1$
P_y	force in the y direction
$[P_i]_i$	load vector at station i on the i^{th} element
$\overline{Q}^2_{mn}$	mean-square generalized acoustic pressure force for the $(m,n)^{th}$ mode
$[Q]$	a real symmetric matrix
q_{mnk}	k^{th} generalized coordinate for the $(m,n)^{th}$ mode of a curved honeycomb plate
R	aspect ratio function, $3(b/a)^2 + 3(a/b)^2 + 2$
r	radius of cylindrical panel
S_1, S_2	defined by Equation (133)
s	$(1 - \nu^2)G_{yz}/E$
T	kinetic energy
$[T]_i$	coordinate transformation matrix for the i^{th} stiffener element
t	thickness of a panel or facing sheet (if t appears in the argument of a function, it denotes time)
U	strain energy
U_{mn}	generalized coordinate for the displacement u in the $(m,n)^{th}$ mode
$_rU_o$	strain energy density for the r^{th} layer of a honeycomb panel
u	displacement in the x direction
u_k	displacement of the k^{th} coordinate
V_{mn}	generalized coordinate for the displacement v
v	displacement in the y direction
W	transverse displacement
W_o	transverse displacement due to a uniform static pressure of unit magnitude
W_{mn}	generalized coordinate for the displacement w
$\overline{W}_{mn}$	root mean square response at resonance for the $(m,n)^{th}$ mode for arbitrary input
w	displacement in the z direction

$X_m(x)$	mode shape for m^{th} mode in the x direction
$[X]$	column matrix of coordinates
$[\overline{X}]$	column matrix of amplitudes
x	coordinate direction
$Y_n(y)$	mode shape for the n^{th} mode in the y direction
$Y_n^*(y)$	mode shape defined by Equation (118)
$[\overline{Y}]$	column matrix of transformed coordinates
y(t)	transverse rigid body displacement of inertia element - Section D.3
y	coordinate direction
y_R	rigid body displacement of rib
y_S	rigid body displacement of stringer
$[Z]$	column matrix of transformed coordinates
z	coordinate direction section modulus - Section C.2.a
α_i	defined by Equation (58)
β_i	$(EI/L^3)_i$ - Section D.2.a
γ_i	defined by Equation (58)
δ	viscous damping ratio for fundamental mode
δ_{mn}	viscous damping ratio for the $(m,n)^{th}$ mode
δ_i	defined by Equation (58)
δ_y	deflection in the y direction - Section D.2.a
δ_{y_i}	deflection in the y direction at the i^{th} grid point
$_r\epsilon_i$	strain in the r^{th} layer of a honeycomb panel in the i^{th} direction
η_i	structural damping factor for the i^{th} mode
θ	variable of integration - Section C.1.a subtended angle a/r - Section F.3.a
θ_{x_i}	rotation about x axis at the i^{th} grid point
θ_{zi}	rotation about z axis at the i^{th} grid point

κ_i	defined by Equation (58)
λ	an eigenvalue - Section D.4 dimensionless frequency parameter defined by Equation (95)
λ_i	defined by Equation (58)
μ_i	defined by Equation (58)
ν	Poisson's ratio
ξ	in-plane restraint factor - Section F.2.c
$\xi(t)$	generalized coordinate
π	3.141592654 (approx.)
ρ	mass per unit area of a plate or shell mass per unit volume - Section F.2.c
ρ_i	defined by Equation (58)
ρ_P	mass per unit area of a plate inertia element
ρ_R	mass per unit length of rib inertia element
ρ_S	mass per unit length of stringer inertia element
σ, σ_{ij}	denotes bending stress
σ_i	defined by Equation (58)
$_r\sigma_i$	stress in the r^{th} layer of a honeycomb plate in the i^{th} direction
τ_{ij}	shearing stress
τ_i	$(GJ/L)_i$ - Section D.2.a
$\left[\Phi_m\right]$	eigenvectors of the mass matrix - Section D.4
Φ_{mn}	generalized coordinate for the $(m,n)^{th}$ mode
$\Phi(f)$	mean square pressure density
ϕ	variable of integration - Section C.1.a subtended angle, a/r, Section F.2.a coordinate direction - Section F.3.a
χ_i	defined by Equation (58)
Ψ_{mn}	generalized coordinate for $(m,n)^{th}$ mode
ψ	coordinate direction

Ω	dimensionless frequency parameter defined by Equations (121) and (132)
ω	undamped natural circular frequency of the fundamental mode
ω_i	undamped natural circular frequency of the i^{th} mode
ω_{mn}	undamped natural circular frequency of the $(m,n)^{th}$ mode

Notation

$[\ ]$	rectangular matrix
$[\ \searrow]$	diagonal matrix
$[\ ]^T$	transpose of a matrix
$[\ ]^{-1}$	inverse of a matrix
$\dot{}$	over-dot denotes differentiation with respect to time
$(\ )_{,xy}$	$\partial^2(\ )/\partial x \partial y$, etc.
$'$	denotes differentiation with respect to the variable
$\bar{}$	over-bar denotes a mean value except in Section D where it denotes system coordinates
$\bar{\bar{}}$	double over-bar denotes stiffness of system
$(\ )\|_x$	evaluated at x

Subscripts

$(\ )_c$	denotes curved
$(\ )_e$	denotes edge
$(\ )_f$	denotes flat
$_h(\ )$	denotes honeycomb

I - INTRODUCTION

Previous programs directed toward eliminating or reducing sonic fatigue effects from intense acoustical noise on flight vehicles have established design criteria and nomographs (presently available in Reference 1). The nomographs in Reference 1 were empirically derived from sonic fatigue tests of certain of the more popular structural designs. The tests were made generally using discrete frequency excitation, and the resulting fatigue data were converted to "random fatigue data" through the use of Miles' single-degree-of-freedom theory (Reference 2) and the Miner-Palmgren cumulative damage rule(Reference 3 and 4). The nomographs have been helpful in designing sonic-fatigue-resistant structure for present-day and near-future aircraft.

However, lightweight, sonic-fatigue-resistant flight vehicle structure is essential to high-performance aircraft. To meet these critical demands for weight reduction and increased resistance to sonic fatigue, existing design nomographs must be refined. These design nomographs, based on limited empirical data, have proven to be conservative and somewhat restricted in application. It is essential that the reliability of the available design nomographs be refined and extended in application by conducting additional sonic-fatigue tests using random noise excitation representative of power-plant noise environment. Initially, the refinement program would naturally involve the more commonly used structural configurations: skin-stringer and honeycomb sandwich.

The first step in the sonic-fatigue refinement program was accomplished by the research program reported here. A description of the theoretical and analytical studies is given in Section II; the experimental investigations are described in Section III; Section IV is a description of the correlation of the test results and theory; development of the design nomographs is given in Section V; and a description of the test facility, data collection and data reduction system and test procedure are described in detail in Appendices I and II.

II - THEORETICAL AND ANALYTICAL

A. Introduction

This research program was primarily experimental in nature. Consequently, one of the main objectives of the theoretical effort was to suggest the significant variables and the mathematical expressions governing skin-stringer and honeycomb sandwich structural response to acoustical excitation representative of in-service environment. Also, the utility of the design nomographs, very important end products of this program, depends upon simplicity, ease of use, and accurate representations of the test results from which they were derived. Therefore, the classical theory for the complete description of the response of a continuous structure such as an aircraft fuselage, wing flap, or control surface as described in Reference 5 is too complex for design purposes. Also, it will be shown in Section III that the majority of the structural response results from one predominant mode, usually the fundamental.

B. General Theory

From Reference 6 , it is shown that the mean-square displacement for single-mode response can be expressed as (for the i^{th} mode)

$$\overline{W}^2(t) = \frac{\pi F_i^2(x_1)}{2\omega_i^3 \eta_i M_i^2} \int_A \int_A F_i(x_A)\, F_i(x_B)\, G_p(x_A, x_B; \omega_i)\, dA\, dA \qquad (1)$$

where

$F_i(x)$	is the i^{th} mode shape
M_i	is the generalized mass
ω_i	is the undamped circular frequency
η_i	is the structural damping factor
$G_p(x_A, x_B; \omega_i)$	is the cross-spectral density function of the excitation pressure at x_A and x_B
i	is the predominant mode, usually the fundamental

Equation (1) describes the structure as a set of independent plates or panels responding in their first mode only.

To simplify Equation (1), it will be assumed that the excitation pressure is exactly in phase over the whole panel. The mean-square deflection response is then expressed as

$$\overline{W}^2(t) = \frac{\pi F_i^2(x_1)}{2\omega_i^3 \eta_i M_i^2} \left[\int_A F_i(x_A)\, dA \right]^2 G_p(\omega_i) \,. \qquad (2)$$

The static displacement, W_o, at x_1 due to a uniform static pressure of unit magnitude is

$$W_o = \frac{F_i(x_1)}{\omega_i^2 M_i} \int_A F_i(x_A)\, dA \qquad (3)$$

and Equation (2) can be expressed as

$$\overline{W}^2(t) = \frac{\pi}{2\eta_i} \omega_i G_p(\omega_i) W_o^2 \tag{4}$$

The expression commonly used, however, for the mean-square stress in terms of the viscous damping ratio, δ, and the frequency, f_i, in Hz. is

$$\overline{\sigma}^2(t) = \frac{\pi}{4\delta} f_i \Phi(f) \sigma_o^2 \tag{5}$$

where σ_o is the stress at the point of concern due to a uniform static pressure of unit magnitude, and $\Phi(f)$ is the mean-square pressure density function.

C. Skin-Stringer Construction

This subsection is a description of the analysis defining the response of a single bay of skin-stringer construction to an arbitrary acoustical excitation.

Most panels have edge conditions which, in practice, are between simply supported edges and clamped edges. The basic approach will be to determine panel response for both clamped edges and simply supported edges. These two edge conditions will provide a bound in the actual situation. The overall motion of the supporting structure will be presented in the next subsection.

1. Frequency Analysis

The Rayleigh energy method will be used below to obtain the response of a panel vibrating in its fundamental mode. The panel material is considered to be Hookean and isotropic, and the thickness remains constant before, during, and after deformation.

a. Clamped Edges - The strain energy expression for a thin elastic plate of length a and width b is

$$U = \frac{1}{2} D \int_o^a \int_o^b \left\{ \left(\frac{\partial^2 w}{\partial x^2} + \frac{\partial^2 w}{\partial y^2} \right)^2 - 2(1-\nu) \left[\frac{\partial^2 w}{\partial x^2} \frac{\partial^2 w}{\partial y^2} - \left(\frac{\partial^2 w}{\partial x \partial y} \right)^2 \right] \right\} dy dx \tag{6}$$

and the kinetic energy for the vibrating plate is

$$T = \frac{1}{2} \int_o^a \int_o^b \rho \left(\frac{\partial w}{\partial t} \right)^2 dx dy \tag{7}$$

where

ρ is the mass per unit area

$D = Et^3/12(1 - \nu^2)$

E is Young's Modulus

t is the panel thickness

ν is Poission's ratio

w is the transverse displacement

For clamped edges it is assumed that the mode shape is as shown in Figure 1.

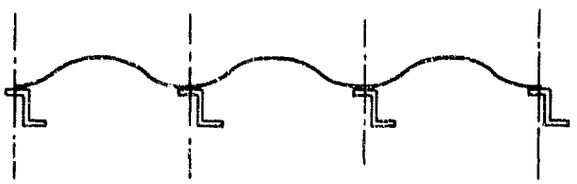

FIGURE 1. ASSUMED MODE SHAPE FOR A SKIN-STRINGER PANEL WITH CLAMPED EDGES

The first mode response is represented mathematically as

$$w(x, y, t) = \left[1 - \cos\ (2\pi\ x/a)\right]\left[1 - \cos (2\pi\ y/b)\right]\ \xi\ (t) \qquad (8)$$

When Equation (8) is substituted into Equations (6) and (7), the expressions for the kinetic energy and the strain energy becomes

$$T = \frac{1}{2}\rho \int_0^a \int_0^b \dot{\xi}^2 \left[1 - \cos\frac{2\pi x}{a}\right]^2 \left[1 - \cos\frac{2\pi y}{b}\right]^2 dy\,dx \qquad (9)$$

$$U = \frac{1}{2}D \int_0^a \int_0^b \xi^2 \left\{\left[\frac{4\pi^2}{a^2}\cos\frac{2\pi x}{a}\left(1 - \cos\frac{2\pi y}{b}\right) + \frac{4\pi^2}{b^2}\cos\frac{2\pi y}{b}\left(1 - \cos\frac{2\pi x}{a}\right)\right]^2 - 2(1-\nu)\left[\frac{16\pi^4}{a^2b^2}\cos\frac{2\pi x}{a}\cos\frac{2\pi y}{b}\left(1 - \cos\frac{2\pi x}{a}\right)\cdot\left(1 - \cos\frac{2\pi y}{b}\right) - \left(\frac{4\pi^2}{ab}\sin\frac{2\pi x}{a}\sin\frac{2\pi y}{b}\right)^2\right]\right\} dy\,dx \qquad (10)$$

After the change of variable is performed,

$\theta = 2\pi x/a$ $\qquad$ $\phi = 2\pi y/b$, Equations (9) and (10) become

$$T = \frac{1}{2} \rho \dot{\xi}^2 \frac{ab}{4\pi^2} \int_0^{2\pi} \int_0^{2\pi} (1 - \cos\theta)^2 (1 - \cos\phi)^2 \, d\theta \, d\phi \qquad (11)$$

$$U = \frac{1}{2} D \xi^2 \frac{ab}{4\pi^2} \int_0^{2\pi} \int_0^{2\pi} \left\{ \left[\frac{4\pi^2}{a^2} \cos\theta (1 - \cos\phi) + \frac{4\pi^2}{b^2} \cos\phi (1 - \cos\theta) \right]^2 - 2(1 - \nu) \left[\frac{4\pi^2}{a^2} \frac{4\pi^2}{b^2} \cdot \right. \right.$$

$$\left. \left. \cos\phi \cos\theta (1 - \cos\phi)(1 - \cos\theta) - \left(\frac{4\pi^2}{ab} \sin\phi \sin\theta \right)^2 \right] \right\} d\theta \, d\phi \qquad (12)$$

After the necessary algebraic manipulations and integrations are performed, the kinetic energy and the strain energy expressions become

$$T = \frac{1}{2} \left[\frac{9}{4} \rho ab \dot{\xi}^2 (t) \right] \qquad (13)$$

and

$$U = \frac{1}{2} \left[\frac{4\pi^4}{ab} DR \xi^2 (t) \right] \qquad (14)$$

where $R = 3(b/a)^2 + 3(a/b)^2 + 2$.

Basically, the kinetic energy and strain energy are expressed as

$$T = \frac{1}{2} M \dot{\xi}^2 (t) \qquad (15)$$

and

$$U = \frac{1}{2} K \xi^2 (t) \qquad (16)$$

where M is the modal mass
K is the modal stiffness constant.

The modal mass constant and the modal stiffness constant from Equations (13) through (16) are given by

$$M = \frac{\rho}{4} \rho ab \tag{17}$$

and

$$K = \frac{4\pi^4}{ab} DR \tag{18}$$

The natural circular frequency of the fundamental mode is

$$\omega^2 = \frac{K}{M} \tag{19}$$

and from Equations (17) and (18):

$$\omega^2 = \frac{16\pi^4 D}{9\rho a^2 b^2} R \tag{20a}$$

or in terms of the frequency in Hz:

$$f^2 = \frac{4\pi^2}{9 a^2 b^2} \frac{D}{\rho} R \tag{20b}$$

b. Simply Supported Edges - Using the same approach as in the previous subsection, the mode assumed for simple supports is of the form

$$w = \xi(t) \sin\left(\frac{\pi x}{a}\right) \sin\left(\frac{\pi y}{b}\right) \tag{21}$$

The modal mass, modal stiffness constant, and first mode frequency are

$$M = \frac{1}{4} \rho ab \tag{22}$$

$$K = \frac{\pi^4}{4} Dab \left[\frac{1}{a^2} + \frac{1}{b^2}\right]^2 \tag{23}$$

and

$$\omega^2 = \pi^4 \frac{D}{\rho} \left[\frac{1}{a^2} + \frac{1}{b^2}\right]^2 \tag{24a}$$

or

$$f^2 = \frac{\pi^2}{4} \frac{D}{\rho} \left[\frac{1}{a^2} + \frac{1}{b^2}\right]^2 \tag{24b}$$

2. Stress Response

The stress analysis of a single bay of a skin-stringer panel is based on the assumption that the elastic characteristics of the stiffeners produce negligible effect on the stress.

a. Clamped Edges - The expression for the stress, due to bending at the surface of a thin plate, is given by (see Reference 7).

$$\sigma_x = \frac{M_x}{z} \tag{25}$$

where z is the section modulus and

$$M_x = -D\left[\frac{\partial^2 w}{\partial x^2} + \nu \frac{\partial^2 w}{\partial y^2}\right] \tag{26}$$

The fundamental mode can be defined as

$$w = W_o\left(1 - \cos\left(\frac{2\pi x}{a}\right)\right)\left(1 - \cos\left(\frac{2\pi y}{b}\right)\right) \tag{27}$$

where W_o is the static displacement at the center of the bay due to a uniform static pressure of unit magnitude.

After substituting for w in Equation (26), the bending moment, M_x, is given as

$$M_x = 4\pi^2 D W_o\left[\frac{1}{a^2}\left(\cos\left(\frac{2\pi x}{a}\right)\right)\left(1 - \cos\left(\frac{2\pi y}{b}\right)\right) + \frac{\nu}{b^2}\left(\cos\left(\frac{2\pi y}{b}\right)\right)\left(1 - \cos\left(\frac{2\pi x}{a}\right)\right)\right] \tag{28}$$

Substitution of Equation (28) into Equation (25) yields the following expression for the stress:

$$\sigma_x = 24\frac{\pi^2 D}{t^2} W_o\left[\frac{1}{a^2}\cos\frac{2\pi x}{a}\left(1 - \cos\frac{2\pi y}{b}\right) + \frac{\nu}{b^2}\cos\frac{2\pi y}{b}\left(1 - \cos\frac{2\pi x}{a}\right)\right] \tag{29}$$

The point of interest on the panel is the center of the long side along the fastener row, where the moment is maximum, i.e., at $x = 0$, $y = b/2$, and $x = a$, $y = b/2$. At this point the stress is given by

$$\sigma_{x_{max}} = \frac{48\pi^2 D W_o}{a^2 t^2} \tag{30}$$

W_o is evaluated for this case as

$$W_o = F/K \tag{31}$$

where F is the generalized acoustic pressure force

$$F = \int_0^a \int_0^b P_o \left(1 - \cos\left(\frac{2\pi x}{a}\right)\right)\left(1 - \cos\left(\frac{2\pi y}{b}\right)\right) dx\, dy \tag{32}$$

and P_o is the acoustic pressure amplitude. By integrating Equation (32)

$$F = P_o ab \tag{33}$$

after substituting Equations (18) and (33) into Equation (31), W_o is evaluated as

$$W_o = \frac{a^2 b^2}{4\pi^4 R}\left(\frac{P_o}{D}\right) \tag{34}$$

By combining Equation (30) and Equation (34), the static stress due to a uniform static pressure of unit magnitude is obtained:

$$\sigma_{x_{max}} = \frac{12}{\pi^2}\left(\frac{b}{t}\right)^2 \frac{1}{R} \tag{35}$$

An estimate of the mean-square stress response of a lightly damped panel exposed to random noise excitation can be obtained by substituting Equation (35) into Equation (5)

$$\bar{\sigma}^2_{x_{max}} = \frac{36}{\pi^3}\left(\frac{b}{t}\right)^4 \frac{f_i \Phi(f)}{\delta R^2} \tag{36}$$

b. Simply Supported Edges - Assuming that the elastic characteristics of the supporting structure may be approximated by simply supported edges, the mean-square stress in a bay of skin-stringer construction is developed below, using the same general procedure as described in Section 2.a.

The fundamental mode for a simply supported panel is described as

$$w = W_o \sin\left(\frac{\pi x}{a}\right) \sin\left(\frac{\pi y}{b}\right) \tag{37}$$

Equations (37) and (26) are used to evaluate the bending moment. Substitution of this value into Equation (25) results in the expression for the stress. The maximum stress, of course, occurs at the center of the panel and is

$$\sigma_{x_{max}} = 6\pi^2 \frac{DW_o}{t^2}\left[\frac{1}{a^2} + \nu \frac{1}{b^2}\right] \tag{38}$$

The static deflection at the center of the panel due to a uniform static pressure of unit magnitude is

$$W_o = F/K \tag{39}$$

where $F = \int_0^a \int_0^b \sin\left(\frac{\pi x}{a}\right) \sin\left(\frac{\pi y}{b}\right) dy\, dx = \frac{4ab}{\pi^2}$

K is given by Equation (23).

The static deflection at the center of the simply supported panel due to a unit pressure becomes

$$W_o = \frac{16}{\pi^6 D \left[\frac{1}{a^2} + \frac{1}{b^2}\right]^2} \tag{40}$$

The maximum stress due to the uniform static pressure is

$$\sigma_{x_{max}} = \frac{96}{\pi^4 t^2} \frac{\left[\frac{1}{a^2} + \frac{\nu}{b^2}\right]}{\left[\frac{1}{a^2} + \frac{1}{b^2}\right]^2} \tag{41}$$

The mean-square stress response of a lightly damped bay of skin-stringer construction considered to be simply supported by the stiffeners and excited by a random acoustical noise is obtained by substituting $\sigma_{x_{max}}$ from Equation (41) for σ_o in Equation (5).

Hence, the mean-square stress response of a simply supported bay of skin-stringer construction is given as

$$\bar{\sigma}^2_{x_{max}} = \frac{2304}{\pi^7 t^4} \frac{f_i \Phi(f)}{\delta} \frac{\left[\frac{1}{a^2} + \frac{\nu}{b^2}\right]^2}{\left[\frac{1}{a^2} + \frac{1}{b^2}\right]^4} \tag{42}$$

D. Vibration Analysis of Supporting Structure using Finite Element Techniques

1. General Theory

The analytical model of the supporting structure was assumed to be a thin cover sheet supported by two parallel ribs and, perpendicular to the ribs, two parallel stringers, with the edges of the system completely restrained from movement. This choice was prompted by the design of the test panels used in the experimental phase of the program. The coordinate system and general arrangement for the stiffened panel is illustrated in Figure 2. The intersection points of the ribs and stringers were selected as grid points for measuring the deformation of the system. Each grid point has 3 degrees of freedom: two rotations and a translation. These coordinates were ordered as shown in Figure 2.

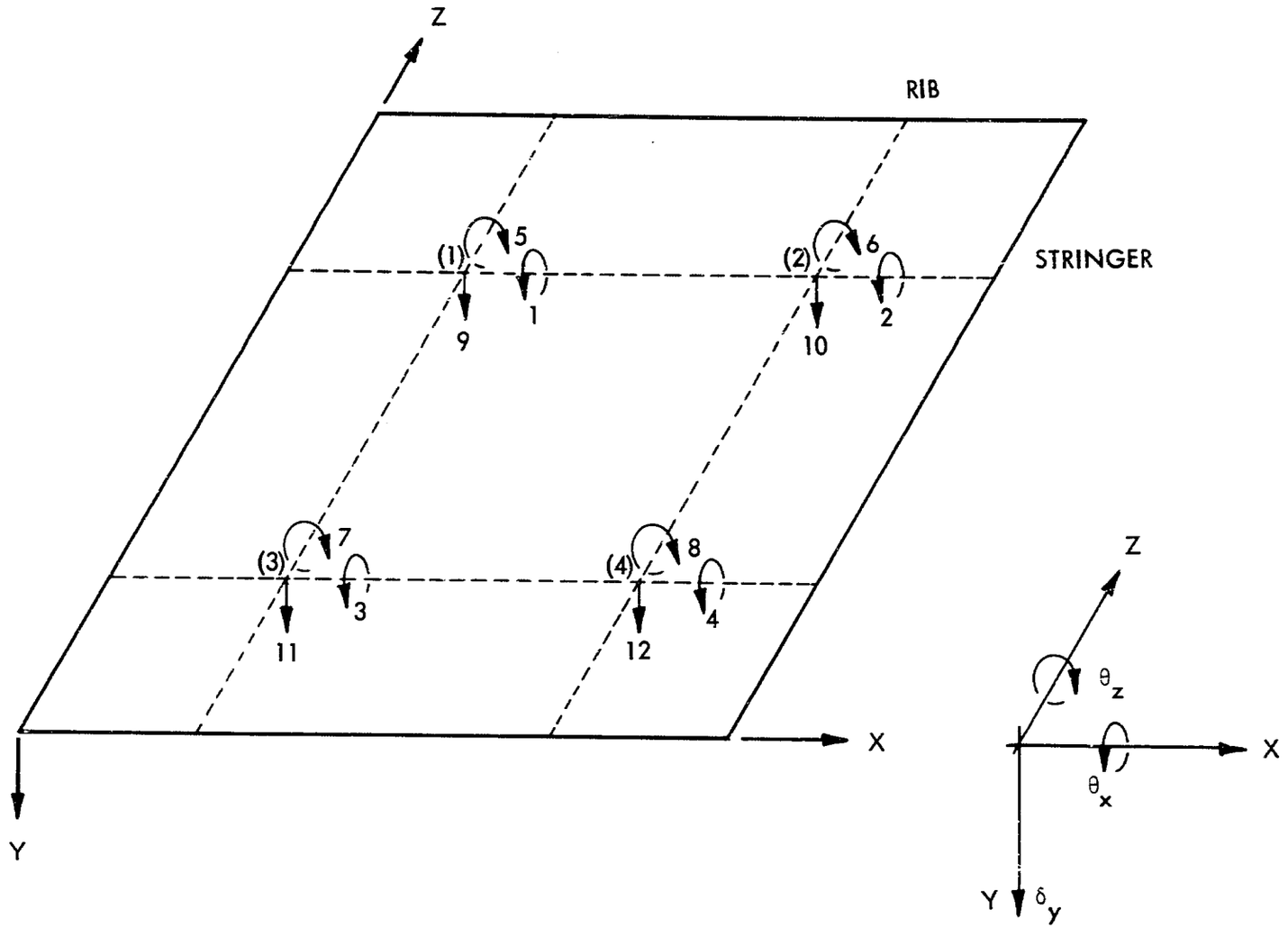

FIGURE 2. COORDINATE SYSTEM AND GENERAL ARRANGEMENT OF STIFFENED PANEL

The equations of motion represent a 12-degree-of-freedom, spring-mass system. These equations are of the form

$$\left[\begin{array}{c|c|c} I_{xx} & I_{xz} & I_{xy} \\ \hline I_{zx} & I_{zz} & I_{zy} \\ \hline I_{yx} & I_{yz} & I_{yy} \end{array}\right]\left[\begin{array}{c} \ddot{\theta}_x \\ \hline \ddot{\theta}_z \\ \hline \ddot{\delta}_y \end{array}\right] + \left[\begin{array}{c|c|c} K_{xx} & K_{xz} & K_{xy} \\ \hline K_{zx} & K_{zz} & K_{zy} \\ \hline K_{yx} & K_{yz} & K_{yy} \end{array}\right]\left[\begin{array}{c} \theta_x \\ \hline \theta_z \\ \hline \delta_y \end{array}\right] = \left[\begin{array}{c} 0 \\ \hline 0 \\ \hline 0 \end{array}\right] \tag{43}$$

for free vibrations. The above equations are the classical eigenvalue problem of linear algebra. Details of the formulation of the mass and stiffness characteristics and the solution of the above problem are given in the following sections.

2. Formulation of the Stiffness Matrix

a. Supporting Structure - The stiffness matrix for the system will be treated in two parts: supporting structure and cover plates. The supporting structure stiffness matrix will be synthesized as a network of beam elements. The stiffness characteristics of the system are developed using the equilibrium method. This method is well described in Reference 8 .

Beginning with the beam element shown in Figure 3, the load-deflection relation for the i^{th} element is

$$\left[\begin{array}{c} P_1 \\ \hline P_2 \end{array}\right]_i = \left[\begin{array}{c|c} K_{11} & K_{12} \\ \hline K_{21} & K_{22} \end{array}\right]_i \left[\begin{array}{c} d_1 \\ \hline d_2 \end{array}\right]_i \tag{44}$$

where at station j on the element

$$\left[P_j\right]_i = \left[\begin{array}{c} M_{xj} \\ P_{yj} \\ M_{zj} \end{array}\right]_i, \quad \left[d_j\right]_i = \left[\begin{array}{c} \theta_{xj} \\ \delta_{yj} \\ \theta_{zj} \end{array}\right] \tag{45a}$$

$$\left[K_{11}\right]_i = \left[\begin{array}{ccc} \tau_i & 0 & 0 \\ 0 & 12\beta_i & 6\beta_i L_i \\ 0 & 6\beta_i L_i & 4\beta_i L_i^2 \end{array}\right] \qquad \begin{array}{l} \tau_i = (GJ/L)_i \\ \beta_i = (EI/L^3)_i \end{array} \tag{45b}$$

$$\left[K_{12}\right]_i = \left[\begin{array}{ccc} -\tau_i & 0 & 0 \\ 0 & -12\beta_i & 6\beta_i L_i \\ 0 & -6\beta_i L_i & 2\beta_i L_i^2 \end{array}\right] = \left[K_{21}\right]^T_i \tag{45c}$$

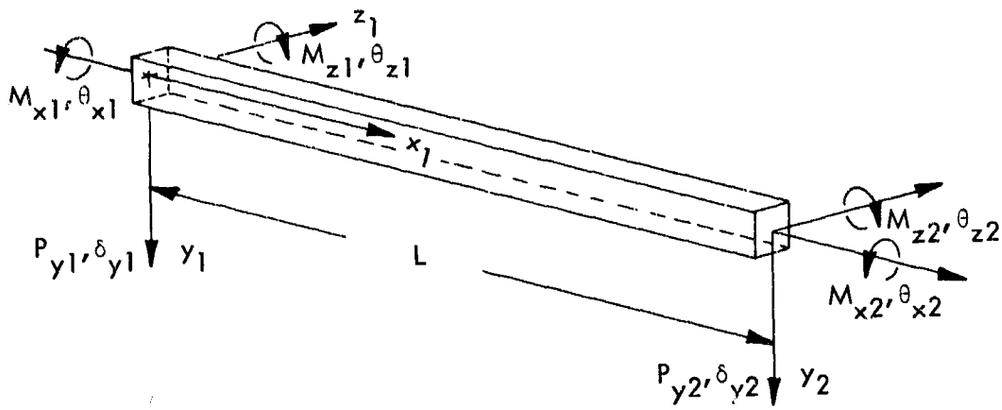

FIGURE 3. BEAM ELEMENT AND COORDINATES

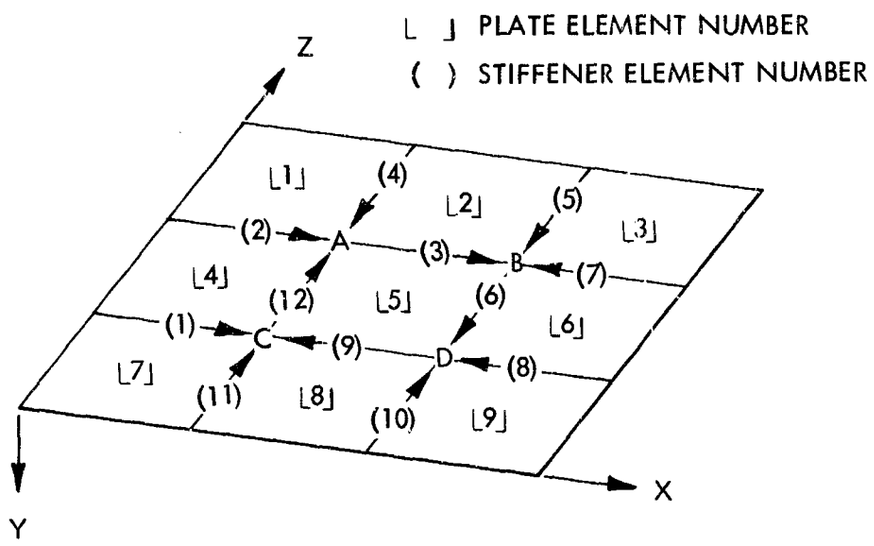

FIGURE 4. ELEMENT NOMENCLATURE

$$\left[K_{22}\right]_i = \begin{bmatrix} \tau_i & 0 & 0 \\ 0 & 12\beta_i & -6\beta_i L_i \\ 0 & -6\beta_i L_i & 4\beta_i L_i^2 \end{bmatrix} \tag{45d}$$

For simplicity, it was assumed here that there was no coupling between the bending-torsion coordinates of the beam element.

The elements were ordered as shown in Figure 4 , and it is necessary to rotate the coordinates of the elements to match the system coordinates. Such a transformation is easily accomplished, and is represented as

$$\left[\bar{K}_{ir}\right]_i = \left[T\right]_i \left[K_{ir}\right]_i \left[T\right]_i^T \tag{46}$$

for the i^{th} member, where the overbar denotes the element stiffness in system coordinates and the transformation matrix $\left[T\right]_i$ is

$$\left[T\right]_i = \begin{bmatrix} \cos\alpha_i & 0 & -\sin\alpha_i \\ 0 & 1 & 0 \\ \sin\alpha_i & 0 & \cos\alpha_i \end{bmatrix} \tag{47}$$

for the coordinate transformation, as illustrated in Figure 5.

As shown in Figure 4, the elements are oriented by the direction of an arrow which points from station 1 to station 2 for each element. Equations (48a) through (48d) are the compatibility equations for grid points A through D, respectively (system coordinates are denoted by an overbar):

$$\left[\bar{d}\right]_A = \left[d_2\right]_2 = \left[d_1\right]_3 = \left[d_2\right]_4 = \left[d_2\right]_{12} \tag{48a}$$

$$\left[\bar{d}\right]_B = \left[d_2\right]_3 = \left[d_2\right]_5 = \left[d_1\right]_6 = \left[d_2\right]_7 \tag{48b}$$

$$\left[\bar{d}\right]_C = \left[d_2\right]_1 = \left[d_2\right]_9 = \left[d_2\right]_{11} = \left[d_1\right]_{12} \tag{48c}$$

$$\left[\bar{d}\right]_D = \left[d_2\right]_6 = \left[d_2\right]_8 = \left[d_1\right]_9 = \left[d_2\right]_{10} \tag{48d}$$

The boundary conditions for clamped edges are given by

$$\left[\bar{d}_1\right]_r = \left[0\right] \tag{49}$$

for $r = 1, 2, 4, 5, 7, 8, 10, 11$.

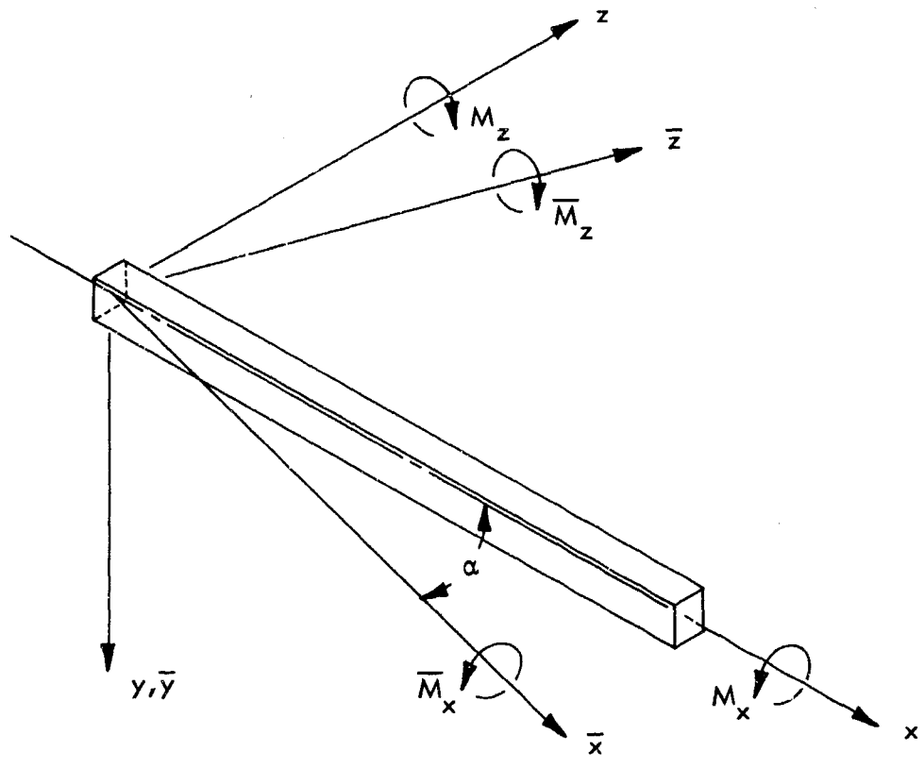

FIGURE 5 COORDINATE TRANSFORMATION OF BEAM ELEMENT

For equilibrium of forces at each grid point the following equations are obtained:

$$\left[\bar{P}\right]_A = \left[\bar{P}_2\right]_2 + \left[\bar{P}_1\right]_3 + \left[\bar{P}_2\right]_4 + \left[\bar{P}_2\right]_{12} \tag{50a}$$

$$\left[\bar{P}\right]_B = \left[\bar{P}_2\right]_3 + \left[\bar{P}_2\right]_5 + \left[\bar{P}_1\right]_6 + \left[\bar{P}_2\right]_7 \tag{50b}$$

$$\left[\bar{P}\right]_C = \left[\bar{P}_2\right]_1 + \left[\bar{P}_2\right]_9 + \left[\bar{P}_2\right]_{11} + \left[\bar{P}_1\right]_{12} \tag{50c}$$

$$\left[\bar{P}\right]_D = \left[\bar{P}_2\right]_6 + \left[\bar{P}_2\right]_8 + \left[\bar{P}_1\right]_9 + \left[\bar{P}_2\right]_{10} \tag{50d}$$

where the load-deflection relations for the i^{th} element in the system coordinates are

$$\begin{bmatrix} \bar{P}_1 \\ \hline \bar{P}_2 \end{bmatrix}_i = \begin{bmatrix} \bar{K}_{11} & \bar{K}_{12} \\ \hline \bar{K}_{21} & \bar{K}_{22} \end{bmatrix}_i \begin{bmatrix} d_1 \\ \hline d_2 \end{bmatrix}_i \tag{51}$$

After combining the compatibility equations (48a-d), the boundary conditions (49), and the load-deflection equation (51), the equilibrium equations (50a-d) become

$$\left[\bar{P}\right]_A = \left[\bar{\bar{K}}_{11}\right]\left[\bar{d}\right]_A + \left[\bar{\bar{K}}_{12}\right]\left[\bar{d}\right]_B + \left[\bar{\bar{K}}_{13}\right]\left[\bar{d}\right]_C \tag{52a}$$

$$\left[\bar{P}\right]_B = \left[\bar{\bar{K}}_{21}\right]\left[\bar{d}\right]_A + \left[\bar{\bar{K}}_{22}\right]\left[\bar{d}\right]_B + \left[\bar{\bar{K}}_{24}\right]\left[\bar{d}\right]_D \tag{52b}$$

$$\left[\bar{P}\right]_C = \left[\bar{\bar{K}}_{31}\right]\left[\bar{d}\right]_A + \left[\bar{\bar{K}}_{33}\right]\left[\bar{d}\right]_C + \left[\bar{\bar{K}}_{34}\right]\left[\bar{d}\right]_D \tag{52c}$$

$$\left[\bar{P}\right]_D = \left[\bar{\bar{K}}_{42}\right]\left[\bar{d}\right]_B + \left[\bar{\bar{K}}_{43}\right]\left[\bar{d}\right]_C + \left[\bar{\bar{K}}_{44}\right]\left[\bar{d}\right]_D \tag{52d}$$

where

$$\left[\bar{\bar{K}}_{11}\right] = \left[\bar{K}_{22}\right]_2 + \left[\bar{K}_{11}\right]_3 + \left[\bar{K}_{22}\right]_4 + \left[\bar{K}_{22}\right]_{12} \tag{53a}$$

$$\left[\bar{\bar{K}}_{12}\right] = \left[\bar{K}_{12}\right]_3 \tag{53b}$$

$$\left[\bar{\bar{K}}_{13}\right] = \left[K_{21}\right]_{12} \tag{53c}$$

$$\left[\bar{\bar{K}}_{22}\right] = \left[\bar{K}_{22}\right]_3 + \left[\bar{K}_{22}\right]_5 + \left[\bar{K}_{11}\right]_6 + \left[\bar{K}_{22}\right]_7 \tag{53d}$$

$$\left[\bar{\bar{K}}_{24}\right] = \left[\bar{K}_{12}\right]_6 \tag{53e}$$

$$\left[\bar{\bar{K}}_{33}\right] = \left[\bar{K}_{22}\right]_1 + \left[\bar{K}_{22}\right]_9 + \left[\bar{K}_{22}\right]_{11} + \left[\bar{K}_{11}\right]_{12} \tag{53f}$$

$$\left[\bar{\bar{K}}_{34}\right] = \left[\bar{K}_{21}\right]_9 \tag{53g}$$

$$\left[\bar{\bar{K}}_{44}\right] = \left[\bar{K}_{22}\right]_6 + \left[\bar{K}_{22}\right]_8 + \left[\bar{K}_{11}\right]_9 + \left[\bar{K}_{22}\right]_{10} \tag{53h}$$

and, of course, the symmetry condition

$$\left[\bar{\bar{K}}_{ij}\right] = \left[\bar{\bar{K}}_{ij}\right]^T \tag{53i}$$

After grouping the coordinates as implied by Equation (43) where

$$\left[\theta_x\right] = \begin{bmatrix} \theta_{xA} \\ \theta_{xB} \\ \theta_{xC} \\ \theta_{xD} \end{bmatrix}, \left[\theta_z\right] = \begin{bmatrix} \theta_{zA} \\ \theta_{zB} \\ \theta_{zC} \\ \theta_{zD} \end{bmatrix}, \text{ and } \left[\delta_y\right] = \begin{bmatrix} \delta_{yA} \\ \delta_{yB} \\ \delta_{yC} \\ \delta_{yD} \end{bmatrix} \tag{54}$$

and after dropping the overbars, the stiffness matrix for the supporting structure becomes

$$\left[K_{xx}\right] = \begin{bmatrix} (\tau_2 + \tau_3 + 4\left[(\beta L^2)_4 + (\beta L^2)_{12}\right]) & (-\tau_3) & (2(\beta L^2)_{12}) & (0) \\ (-\tau_3) & (\tau_3 + \tau_7 + 4\left[(\beta L^2)_5 + (\beta L^2)_6\right]) & (0) & (2(\beta L^2)_6) \\ (2(\beta L^2)_{12}) & (0) & (\tau_1 + \tau_9 + 4\left[(\beta L^2)_{11} + (\beta L^2)_{12}\right]) & (-\tau_9) \\ (0) & (2(\beta L^2)_6) & (-\tau_9) & (\tau_8 + \tau_9 + 4\left[(\beta L^2)_6 + (\beta L^2)_{10}\right]) \end{bmatrix} \tag{55a}$$

$$\left[K_{xz}\right] = \left[0\right] \tag{55b}$$

$$\left[K_{xy}\right] = \begin{bmatrix} (6\left[(\beta L)_{12} - (\beta L)_4\right]) & (0) & (-6(\beta L)_{12}) & (0) \\ (0) & (6\left[(\beta L)_6 - (\beta L)_5\right]) & (0) & (-6(\beta L)_6) \\ (6(\beta L)_{12}) & (0) & (6\left[(\beta L)_{11} - (\beta L)_{12}\right]) & (0) \\ (0) & (6(\beta L)_5) & (0) & (6\left[(\beta L)_{10} - (\beta L)_6\right]) \end{bmatrix} \tag{55c}$$

$$\left[K_{zz}\right] = \begin{bmatrix} (\tau_4 + \tau_{12} + 4[(\beta L^2)_2 + (\beta L^2)_3]) & (2(\beta L^2)_3) & (-\tau_{12}) & (0) \\ (2(\beta L^2)_3) & (\tau_5 + \tau_6 + 4[(\beta L^2)_3 + (\beta L^2)_7]) & (0) & (-\tau_6) \\ (-\tau_{12}) & (0) & (\tau_{11} + \tau_{12} + 4[(\beta L^2)_1 + (\beta L^2)_9]) & (2(\beta L^2)_9) \\ (0) & (-\tau_6) & (2(\beta L^2)_9) & (\tau_6 + \tau_{10} + 4[(\beta L^2)_8 + (\beta L^2)_9]) \end{bmatrix} \tag{55d}$$

$$\left[K_{zy}\right] = \begin{bmatrix} (6[(\beta L)_3 - (\beta L)_2]) & (-6(\beta L)_3) & (0) & (0) \\ (6(\beta L)_3) & (6[(\beta L)_7 - (\beta L)_3]) & (0) & (0) \\ (0) & (0) & (6[(\beta L)_9 - (\beta L)_1]) & (-6(\beta L)_9) \\ (0) & (0) & (6(\beta L)_9 & (6[(\beta L)_8 - (\beta L)_9]) \end{bmatrix} \tag{55e}$$

$$\left[K_{yy}\right] = \begin{bmatrix} (12[\beta_2 + \beta_3 + \beta_4 + \beta_{12}]) & (-12\beta_3) & (-12\beta_{12}) & (0) \\ (-12\beta_3) & (12[\beta_3 + \beta_5 + \beta_6 + \beta_7]) & (0) & (-12\beta_6) \\ (-12\beta_{12}) & (0) & (12[\beta_1 + \beta_9 + \beta_{11} + \beta_{12}]) & (-12\beta_9) \\ (0) & (-12\beta_6) & (-12\beta_9) & (12[\beta_6 + \beta_8 + \beta_9 + \beta_{10}]) \end{bmatrix} \tag{55f}$$

und the symmetry condition

$$\left[K_{ij}\right] = \left[K_{ij}\right]^T \tag{55g}$$

b. Cover Plates – The approached used for deriving the stiffness matrix of a cover plate element is given in Reference 9, and a brief derivation is given in the appendix for completeness. For the coordinates in Equation (43) and the nomenclature in Figure 5, the stiffness matrix for the complete cover sheet is

$$\left[K_{xx}\right] = \begin{bmatrix} (2[\alpha_1+\alpha_2+\alpha_4+\alpha_5]) & (0) & (\alpha_4+\alpha_5) & (0) \\ (0) & (2[\alpha_2+\alpha_3+\alpha_5+\alpha_6]) & (0) & (\alpha_5+\alpha_6) \\ (\alpha_4+\alpha_5) & (0) & (2[\alpha_4+\alpha_5+\alpha_7+\alpha_8]) & (0) \\ (0) & (\alpha_5+\alpha_6) & (0) & (2[\alpha_5+\alpha_6+\alpha_8+\alpha_9]) \end{bmatrix} \qquad (56a)$$

$$\left[K_{xy}\right] = \begin{bmatrix} (\rho_1+\rho_2-\rho_4-\rho_5) & (30[(\delta/b)_5-(\delta/b)_2])(\sigma_4+\sigma_5) & (-6(\delta/b)_4) \\ (30[(\delta/b)_5-(\delta/b_2)])(\rho_2+\rho_3-\rho_5-\rho_6) & (-6(\delta/b)_5)(\sigma_5+\sigma_6) & \\ -(\sigma_4+\sigma_5) & (6(\delta/b)_5) & (\rho_4+\rho_5-\rho_7-\rho_8)\ (30[(\delta/b)_8-(\delta/b)_5]) \\ (6(\delta/b)_5)-(\sigma_5+\sigma_6) & (30[(\delta/b)_8-(\delta/b)_5]) & (\rho_5+\rho_6-\rho_8-\rho_9) \end{bmatrix} \qquad (56b)$$

$$\left[K_{zz}\right] = \begin{bmatrix} (2[\beta_1+\beta_2+\beta_4+\beta_5]) & (\beta_2+\beta_5) & (0) & (0) \\ (\beta_2+\beta_5) & (2[\beta_2+\beta_3+\beta_5+\beta_6]) & (0) & (0) \\ (0) & (0) & (2[\beta_4+\beta_5+\beta_7+\beta_8]) & (\beta_5+\beta_8) \\ (0) & (0) & (\beta_5+\beta_8) & (2[\beta_5+\beta_6+\beta_8+\beta_9]) \end{bmatrix} \qquad (56c)$$

$$\left[K_{zy}\right]=\begin{bmatrix} (\chi_2+\chi_5-\chi_1-\chi_4) & (-\tau_2-\tau_5) & (30[(\delta/a)_4-(\delta/a)_5]) & (6(\delta/a)_5) \\ (\tau_2+\tau_5) & (\chi_3+\chi_6-\chi_2-\chi_5) & (-6(\delta/a)_5) & (30[(\delta/a)_5-(\delta/a)_6]) \\ (30[(\delta/a)_4-(\delta/a)_5])(6(\delta/a)_5) & (\chi_5+\chi_8-\chi_4-\chi_7) & (-\tau_5-\tau_8) & \\ (-6(\delta/a)_5) & (30[(\delta/a)_5-(\delta/a)_6]) & (\tau_5+\tau_8) & (\chi_6+\chi_9-\chi_5-\chi_8) \end{bmatrix} \quad (56d)$$

$$\left[K_{yy}\right]=\begin{bmatrix} (\kappa_1+\kappa_2+\kappa_4+\kappa_5) & (-\lambda_2-\lambda_5) & (-\mu_4-\mu_5) & (\gamma_5+72(\delta/ab)_5) \\ (-\lambda_2-\lambda_5) & (\kappa_2+\kappa_3+\kappa_5+\kappa_6) & (\gamma_5+72(\delta/ab)_5) & (-\mu_5-\mu_6) \\ (-\mu_4-\mu_5) & (\gamma_5+72(\delta/ab)_5) & (\kappa_4+\kappa_5+\kappa_7+\kappa_8) & (-\lambda_5-\lambda_8) \\ (\gamma_5+72(\delta/ab)_5) & (-\mu_5-\mu_6) & (-\lambda_5-\lambda_8) & (\kappa_5+\kappa_6+\kappa_8+\kappa_9) \end{bmatrix} \quad (56e)$$

where for the i^{th} panel element

$$D_i=\left(\frac{Et^3}{12(1-\nu^2)}\right)_i \quad (57)$$

$$\alpha_i = D_i (b/a)_i \qquad \gamma_i = 2\left(\frac{(1-\nu)D}{a \cdot b}\right)_i$$

$$\beta_i = D_i (a/b)_i \qquad \delta_i = \frac{1}{16}(\nu D)_i$$

$$\rho_i = 3\,(\alpha/a)_i + 10(\delta/b)_i$$

$$\sigma_i = 3\,(\alpha/a)_i + 2(\delta/b)_i$$

$$\chi_i = 3\,(\beta/b)_i + 10(\delta/a)_i \qquad (58)$$

$$\tau_i = 3\,(\beta/b)_i + 2(\delta/a)_i$$

$$\kappa_i = \gamma_i + 72(\delta/ab)_i + 6(\alpha/a^2)_i + 6(\beta/b^2)_i$$

$$\lambda_i = \gamma_i + 72(\delta/ab)_i + 6(\beta/b^2)_i$$

$$\mu_i = \gamma_i + 72(\delta/ab)_i + 6(\alpha/a^2)_i$$

3. Inertia Matrix

The inertia characteristics of the system is derived below by considering the rigid body motion of a patch of structure as shown in Figure 6. The displacement of a point in the surface of the patch at a point (x,z) is

$$y(t) = \delta_y(t) + x\theta_z(t) - z\theta_x(t) \qquad (59)$$

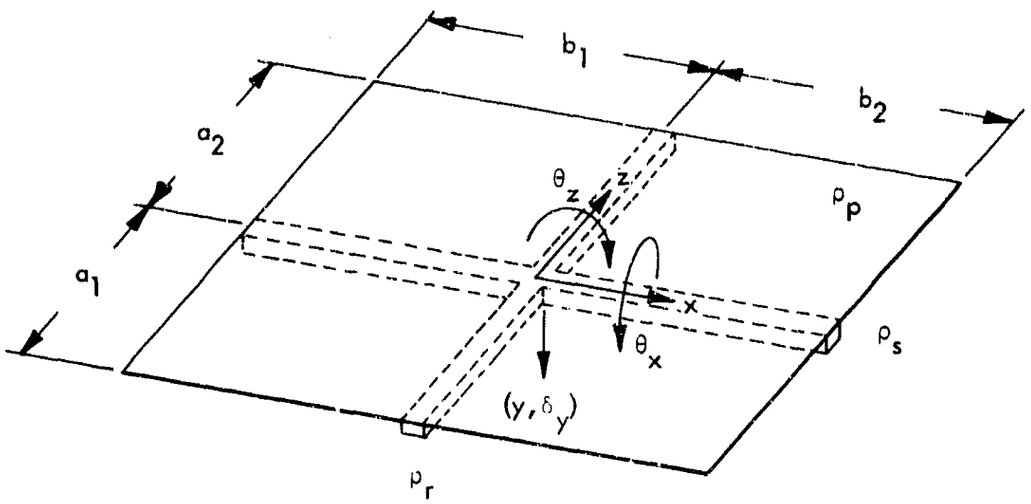

FIGURE 6. ELEMENT FOR INERTIA CHARACTERISTICS

The kineric energy of the patch of structure is

$$T = \frac{1}{2} \int_{-a_1}^{a_2} \int_{-b_1}^{b_2} \rho_p \dot{y}^2 \, dx\, dz + \frac{1}{2} \int_{-a_1}^{a_2} \rho_R \dot{y}_R^2 \, dz + \frac{1}{2} \int_{-b_1}^{b_2} \rho_S \dot{y}_S^2 \, dx \tag{60}$$

where

$y_R(t) = \delta_y(t) - z\theta_x(t)$ – displacement of rib

$y_S(t) = \delta_y(t) + x\theta_z(t)$ – displacement of stringer

ρ_P – mass per unit area of the plate

ρ_R – mass per unit length of the rib

ρ_S – mass per unit length of the stringer.

By integrating the expression for the kinetic energy one obtains

$$T = \frac{1}{2}\left[(m_p + m_R + m_S)\dot{\delta}_y^2 + \frac{1}{3}P_1(m_p + m_S)\dot{\theta}_z^2 + \frac{1}{3}P_2(m_p + m_R)\dot{\theta}_x^2 + P_3(m_p + m_S)\dot{\delta}_y\dot{\theta}_z - P_4(m_p + m_R)\dot{\delta}_y\dot{\theta}_x - \frac{1}{2}m_p P_3 P_4 \dot{\theta}_x\dot{\theta}_z\right] \tag{61}$$

where

$m_p = \rho_p(a_1 + a_2)(b_1 + b_2)$ mass of plate element

$m_R = \rho_R(a_1 + a_2)$ mass of rib element

$m_S = \rho_S(b_1 + b_2)$ mass of stringer element

$P_1 = b_1^2 - b_1 b_2 + b_2^2$

$$P_2 = a_1^2 - a_1 a_2 + a_2^2$$

$$P_3 = b_2 - b_1$$

$$P_4 = a_2 - a_1$$

From Equation (61), it follows that the inertia forces at the coordinates are

$$M_x = \frac{1}{3} P_2 (m_p + m_R) \ddot{\theta}_x - \frac{1}{4} m_p P_3 P_4 \ddot{\theta}_z - \frac{1}{2} P_4 (m_p + m_R) \ddot{\delta}_y \tag{62a}$$

$$M_z = -\frac{1}{4} m_p P_3 P_4 \ddot{\theta}_x + \frac{1}{3} P_1 (m_p + m_S) \ddot{\theta}_z + \frac{1}{2} P_3 (m_p + m_S) \ddot{\delta}_y \tag{62b}$$

$$P_y = -\frac{1}{2} P_4 (m_p + m_R) \ddot{\theta}_x + \frac{1}{2} P_3 (m_p + m_S) \ddot{\theta}_z + (m_p + m_R + m_S) \ddot{\delta}_y \tag{62c}$$

Then, with reference to Equation (43) and Figure 5, the inertia matrix is

$$\begin{bmatrix} I_{xx} \end{bmatrix} = \begin{bmatrix} \frac{1}{3} (P_2 (m_p + m_R))_i \end{bmatrix} \tag{63a}$$

$$\begin{bmatrix} I_{xz} \end{bmatrix} = \begin{bmatrix} -\frac{1}{4} (m_p P_3 P_4)_i \end{bmatrix} = \begin{bmatrix} I_{zx} \end{bmatrix} \tag{63b}$$

$$\begin{bmatrix} I_{xy} \end{bmatrix} = \begin{bmatrix} -\frac{1}{2} (P_4 (m_p + m_R))_i \end{bmatrix} = \begin{bmatrix} I_{yx} \end{bmatrix} \tag{63c}$$

$$\begin{bmatrix} I_{zz} \end{bmatrix} = \begin{bmatrix} \frac{1}{3} (P_1 (m_p + m_S))_i \end{bmatrix} \tag{63d}$$

$$\begin{bmatrix} I_{zy} \end{bmatrix} = \begin{bmatrix} \frac{1}{2} (P_3 (m_p + m_S))_i \end{bmatrix} = \begin{bmatrix} I_{yz} \end{bmatrix} \tag{63e}$$

$$\left[I_{yy} \right] = \left[(m_p + m_R + m_S)_i \right] \tag{63f}$$

where i = 1, 2, 3, 4 denotes grid points A, B, C, and D, respectively.

4. Method of Solution

The general method of solution of the equations of motion (43) is presented below. Beginning with the equations of free undamped motion of a spring-mass system

$$\left[M \right]\left[\ddot{X} \right] + \left[K \right]\left[X \right] = \left[0 \right] , \tag{64}$$

one obtains the classic eigenvalue problem of linear algebra, upon assuming simple harmonic motion

$$\left[X \right] = e^{i\omega t} \left[\bar{X} \right] . \tag{65}$$

The relation (65) is substituted into the equations of motion (64), and the eigenvalue problem is obtained in the form

$$\left[K \right]\left[\bar{X} \right] = \omega^2 \left[M \right]\left[\bar{X} \right] \tag{66}$$

From a computational standpoint, it is advantageous to solve an eigenvalue problem of the form

$$\left[Q \right]\left[Z \right] = \lambda \left[Z \right] \tag{67}$$

where $\left[Q \right]$ is a real symmetric matrix - that is, it is advantageous to transform Equation (66) to the form of Equation (67) before solving the eigenvalue problem (66) directly.

The following method is used to perform the above mentioned transformation. The eigenvalues, $\left[\bar{M} \right]$, and the eigenvectors, $\left[\Phi_m \right]$, of the mass matrix are computed. The mass matrix, $\left[M \right]$ is then expressed in terms of its eigenvalues and eigenvectors with form

$$\left[M \right] = \left[\Phi_m \right]\left[\bar{M} \right]\left[\Phi_m \right]^T \tag{68}$$

$\left[M \right]$ from Equation (68) is substituted into Equation (66), and the eigenvalue problem becomes

$$\left[K \right]\left[\bar{X} \right] = \omega^2 \left[\Phi_m \right]\left[\bar{M} \right]\left[\Phi_m \right]^T \left[\bar{X} \right] \tag{69}$$

After premultiplying Equation (69) by $\left[\Phi_m \right]^T$, letting

$$\left[H \right] = \left[\Phi_m \right]^T \left[K \right]\left[\Phi_m \right] \tag{70}$$

and making the transformation

$$\left[\bar{Y} \right] = \left[\Phi_m \right]^T \left[\bar{X} \right] \tag{71}$$

the eigenvalue problem (69) becomes

$$\left[H \right]\left[\bar{Y} \right] = \omega^2 \left[\bar{M} \right]\left[\bar{Y} \right] \quad . \tag{72}$$

Now, by expressing the eigenvalues, $\left[\bar{M} \right]$, of the mass matrix, $\left[M \right]$, as

$$\left[\bar{M} \right] = \left[G \right]\left[G \right] \tag{73}$$

where, obviously, $G_{ii} = \sqrt{\bar{M}_{ii}}$, Equation (72) becomes

$$\left[H \right]\left[\bar{Y} \right] = \omega^2 \left[G \right]\left[G \right]\left[\bar{Y} \right] \tag{74}$$

or

$$\left[G \right]^{-1} \left[H \right]\left[G \right]^{-1} \left[G \right]\left[\bar{Y} \right] = \omega^2 \left[G \right]\left[\bar{Y} \right] \tag{75}$$

Finally, after making the transformation

$$\left[Z \right] = \left[G \right]\left[\bar{Y} \right] \tag{76}$$

the final form of the eigenvalue problem (64) is

$$\left[G \right]^{-1} \left[H \right]\left[G \right]^{-1} \left[Z \right] = \omega^2 \left[Z \right]. \tag{77}$$

The eigenvalue problem (77) is solved by the Jacobi method, and the resulting eigenvectors are transformed back to the original problem (Equation 64) by the relation

$$\left[\bar{X} \right] = \left[\Phi_m \right]\left[G \right]^{-1} \left[Z \right]. \tag{78}$$

Of course, the eigenvalues of Equation (77) are invariant under the above transformations. It should be noted that

$$\left[G \right]^{-1} \left[H \right]\left[G \right]^{-1} = \left[G \right]^{-1} \left[\Phi_m \right]^T \left[K \right] \left[\Phi_m \right]\left[G \right]^{-1} \tag{79}$$

is indeed, a symmetric matrix. A more detailed discussion of the above theory is given in Reference 10. The above problem is programmed for the IBM Remote Access Computing System. The program is written in IBM System/360 Basic Fortran IV Language. The coordinates are numbered as shown in Figure 2 and the elements are numbered as shown in Figure 4. Use is made of the IBM furnished subroutines "LOC", "EIGEN", and "NROOT". The subroutines are described in detail in Reference 11. The program accepts basic input data and fills the inertia and stiffness matrix directly. The output format consists of natural frequencies and the corresponding mode shapes. As shown in Figure 7, the mode shapes are ordered as

$$\begin{array}{cccc} \theta_{xA} & \theta_{xB} & \theta_{xC} & \theta_{xD} \\ \theta_{zA} & \theta_{zB} & \theta_{zC} & \theta_{zD} \\ \delta_{yA} & \delta_{yB} & \delta_{yC} & \delta_{yD} \end{array}$$

where

θ_{xi} – rotation about the x axis at the i^{th} grid point

```
 VIBRATION ANALYSIS OF A STIFFENED PANEL
FREQUENCY=  0.11396D 04 HZ.
MODE SHAPE
 0.11095D 00-0.11095D 00 0.11095D 00-0.11095D 00
-0.17247D-01-0.17247D-01 0.17247D-01 0.17247D-01
 0.48723D 00-0.48723D 00-0.48723D 00 0.48723D 00
FREQUENCY=  0.11372D 04 HZ.
MODE SHAPE
 0.11170D 00 0.11170D 00 0.11170D 00 0.11170D 00
-0.18050D-01 0.18050D-01 0.18050D-01-0.18050D-01
 0.48703D 00 0.48703D 00-0.48703D 00-0.48703D 00
FREQUENCY=  0.69184D 03 HZ.
MODE SHAPE
-0.22019D 00 0.22019D 00 0.22019D 00-0.22019D 00
-0.21795D-01-0.21795D-01-0.21795D-01-0.21795D-01
 0.44837D 00-0.44838D 00 0.44837D 00-0.44838D 00
FREQUENCY=  0.69161D 03 HZ.
MODE SHAPE
-0.22328D 00-0.22328D 00 0.22328D 00 0.22328D 00
-0.23746D-01 0.23746D-01-0.23746D-01 0.23746D-01
 0.44675D 00 0.44674D 00 0.44675D 00 0.44674D 00
FREQUENCY=  0.62562D 03 HZ.
MODE SHAPE
-0.16472D 00 0.16472D 00-0.16472D 00 0.16472D 00
-0.22050D-01-0.22050D-01 0.22050D-01 0.22050D-01
 0.47157D 00-0.47157D 00-0.47157D 00 0.47157D 00
FREQUENCY=  0.62380D 03 HZ.
MODE SHAPE
-0.16341D 00-0.16341D 00-0.16341D 00-0.16341D 00
-0.24644D-01 0.24644D-01 0.24644D-01-0.24644D-01
 0.47190D 00 0.47190D 00-0.47190D 00-0.47190D 00
FREQUENCY=  0.33671D 03 HZ.
MODE SHAPE
-0.86286D-01 0.86286D-01 0.86286D-01-0.86286D-01
 0.21824D-01 0.21824D-01 0.21824D-01 0.21824D-01
-0.49201D 00 0.49201D 00-0.49201D 00 0.49201D 00
FREQUENCY=  0.33091D 03 HZ.
MODE SHAPE
 0.85412D-01 0.85412D-01-0.85412D-01-0.85412D-01
-0.33122D-01 0.33122D-01-0.33122D-01 0.33122D-01
 0.49154D 00 0.49154D 00 0.49154D 00 0.49154D 00
FREQUENCY=  0.16951D 03 HZ.
MODE SHAPE
 0.30746D-02-0.30747D-02 0.30758D-02-0.30758D-02
-0.49972D 00-0.49972D 00 0.49968D 00 0.49968D 00
-0.17019D-01 0.17019D-01 0.17010D-01-0.17010D-01
FREQUENCY=  0.16836D 03 HZ.
MODE SHAPE
 0.12446D-01-0.12446D-01-0.12445D-01 0.12445D-01
 0.49066D 00 0.49067D 00 0.49071D 00 0.49071D 00
 0.95241D-01-0.95241D-01 0.95243D-01-0.95242D-01
FREQUENCY=  0.13569D 03 HZ.
MODE SHAPE
-0.82224D-02-0.82224D-02-0.82224D-02-0.82224D-02
 0.49676D 00-0.49676D 00-0.49676D 00 0.49676D 00
 0.56253D-01 0.56252D-01-0.56252D-01-0.56253D-01
FREQUENCY=  0.12830D 03 HZ.
MODE SHAPE
-0.39885D-01-0.39885D-01 0.39885D-01 0.39885D-01
-0.40557D 00 0.40557D 00-0.40557D 00 0.40557D 00
-0.28970D 00-0.28970D 00-0.28970D 00-0.28970D 00
```

FIGURE 7. TYPICAL COMPUTER OUTPUT

θ_{zi} – rotation about the z axis at the i^{th} grid point

δ_{yi} – deflection in the y direction of the i^{th} grid point

i = 1, 2, 3, 4 denotes A, B, C, D, respectively.

The mode shapes are normalized to the length of the eigenvector so that

$$\sum_{i=1}^{4} (\theta_{xi}^2 + \theta_{zi}^2 + \delta_{yi}^2) = 1.0 \qquad (80)$$

In Figures 8a through 8l the mode shapes for a typical stiffened panel are sketched with the deformations highly exaggerated. It is seen that three modes will respond to normal forcing i.e., Figures 8d, 8h, and 8l. These modes represent rib-bending stringer-torsion, rib-torsion stringer bending, and coupled rib-stringer-bending, respectively. It is difficult to state which mode will be the most responsive to excitation, since the panel modes described in Section C must also be taken into account. However, the analysis does explain some of the coupling effects which arise due to the substructure motion. If the stiffeners are uniform and equally spaced, the rib-torsion stringer-bending mode will probably be the most responsive of the substructure modes. In any event, the computer program included in Appendix IV should yield the substructure modes for any particular design. It should be noted that any element may be deleted from the model by setting its modulus of elasticity to zero in the input data.

E. Honeycomb Sandwich Construction

For design purposes, a somewhat simplified method is proposed to relate the stress response to panel parameters and acoustical excitation. In other words, simple plate theory can be used to suggest the significant panel parameters and their mathematical arrangement in the empirical development of the design nomographs. The applicability of simple panel theory is demonstrated by the correlation between measured and computed frequencies and stress response. Also, tests conducted by Ballentine (Reference 12), Sweers (Reference 13) and Mead (Reference 14) indicate that core shear does not affect the first mode response of flat honeycomb panels, provided that the core has a specific weight of 2 lb/ft^3 or greater.

The analysis to be presented in this section is based on a theoretical model of the honeycomb sandwich panel edge, as shown in Figure 9. This theoretical model is compared with the actual edge geometry. Although the edge taper is reduced to a step-discontinuity in thickness, it is believed that this effect will be negligible.

Physically, the honeycomb sandwich panel model is replaced by a simple plate with equivalent stiffness. This approach presents analysis of the flat honeycomb panel on the basis of simple plate theory. To idealize the model, several simplifying assumptions are introduced as follows:

- The panels are flat and rectangular.
- The edge condition corresponds to clamped and/or simply supported edges.
- The panels behave as thin plates. (Restoring force is due to bending rather than membrane action.)

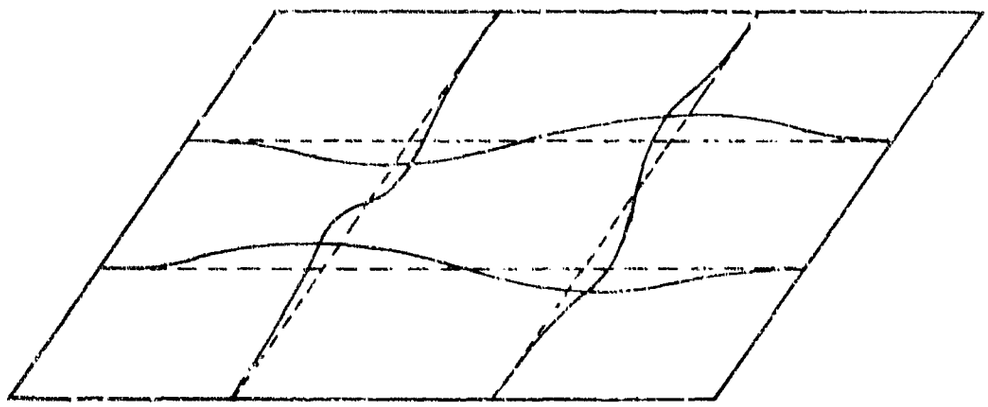

a. f = 1139.6 Hz

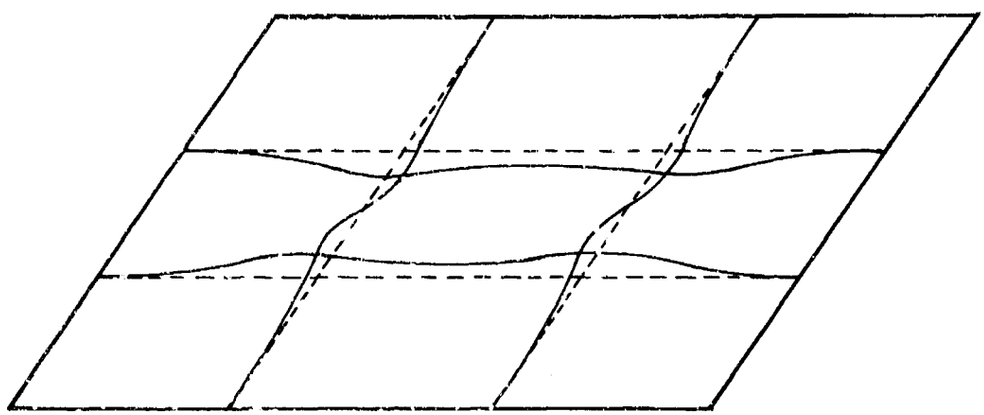

b. f = 1137.2 Hz

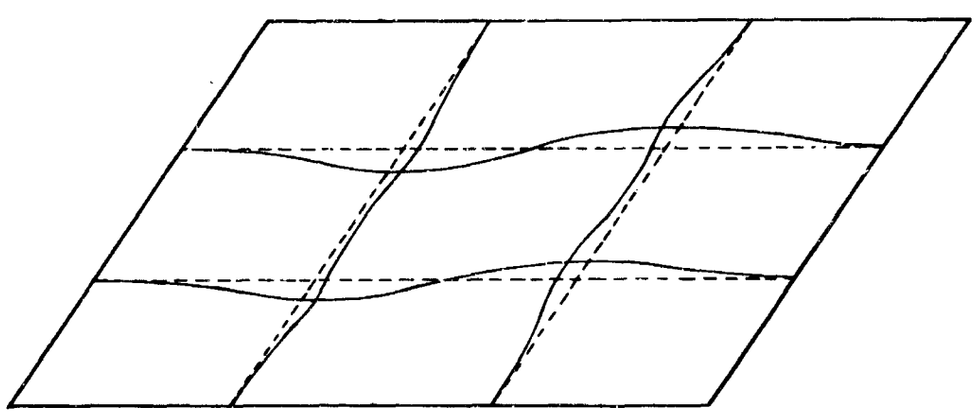

c. f = 691.8 Hz

FIGURE 8. MODE SHAPES FROM COMPUTER OUTPUT (CONTINUED)

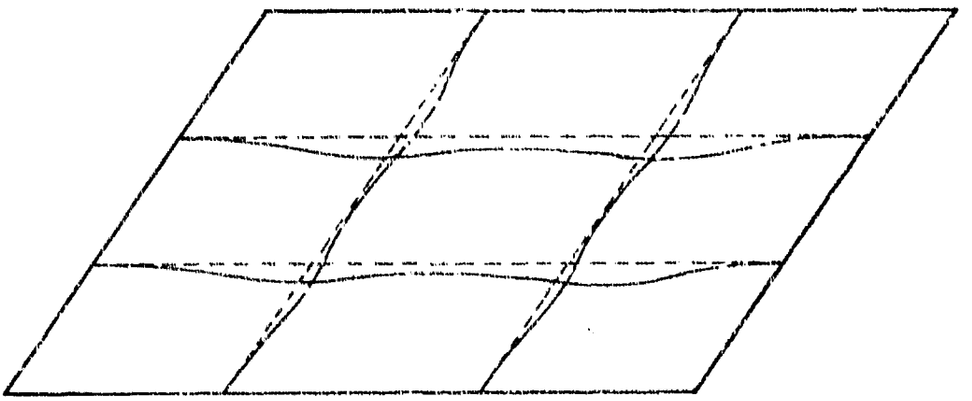

d. f = 691.0 Hz

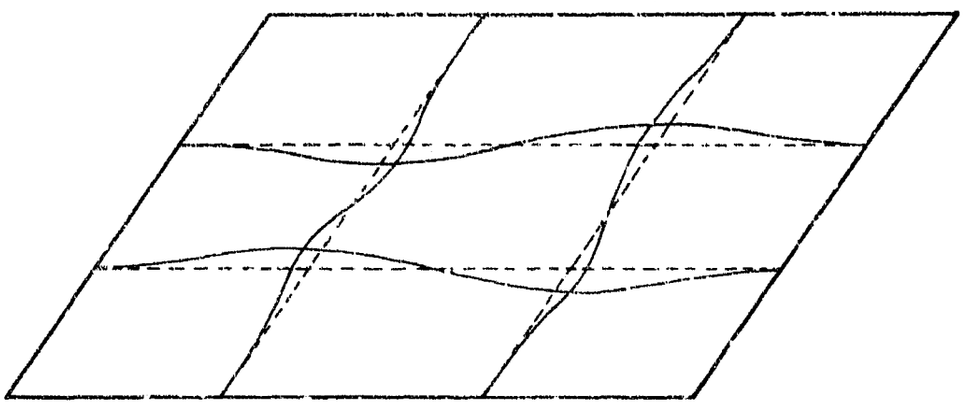

e. f = 625.6 Hz

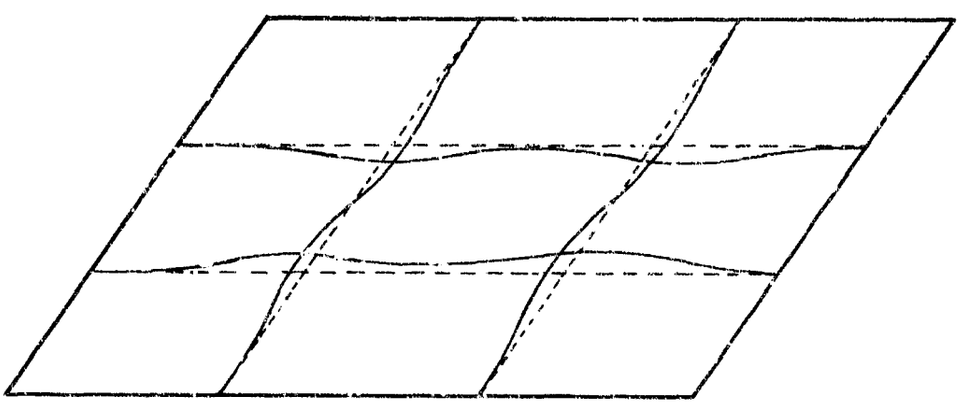

f. f = 623.8 Hz

FIGURE 8 (CONTINUED)

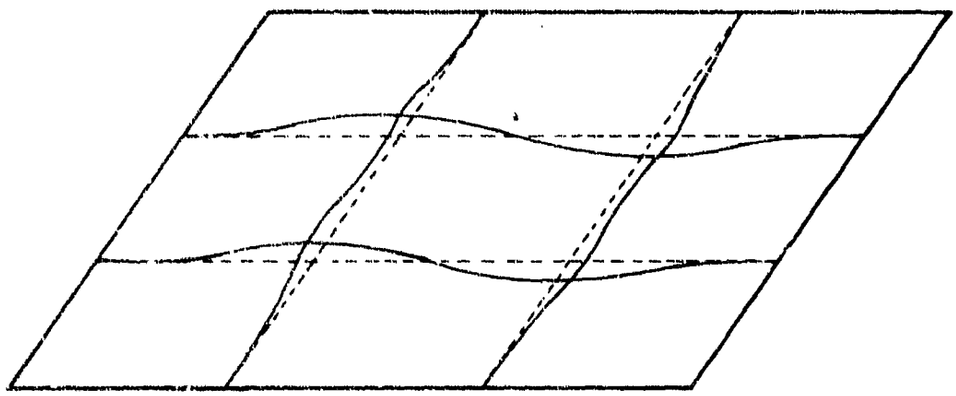

g. f = 336.7 Hz

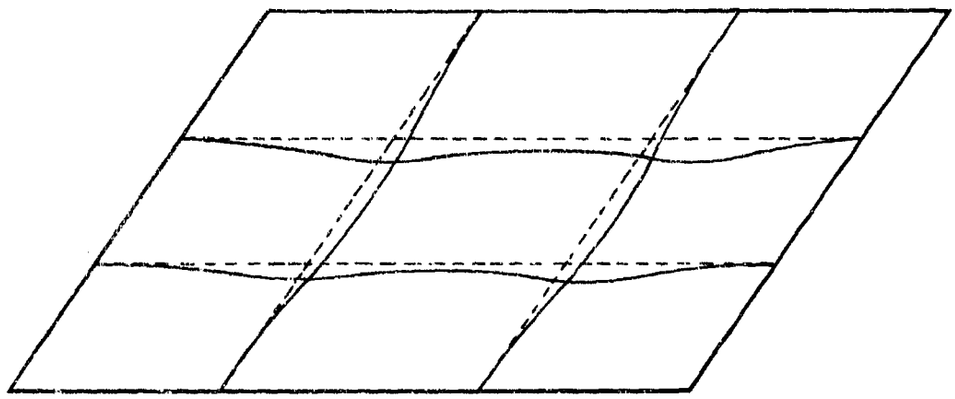

h. f = 330.9 Hz

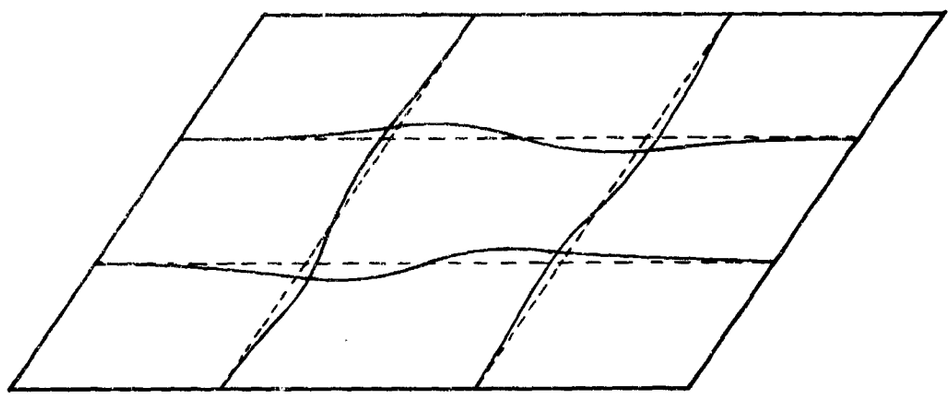

i. f = 169.5 Hz

FIGURE 8 (CONTINUED)

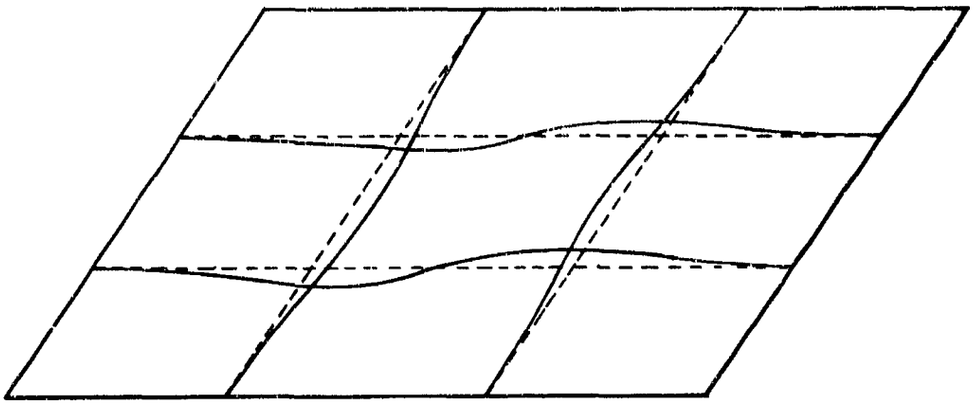

j. f = 168.4 Hz

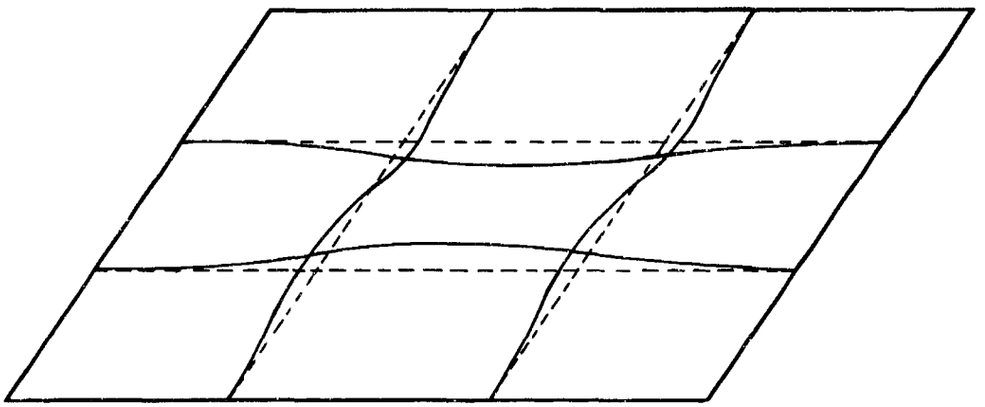

k. f = 135.7 Hz

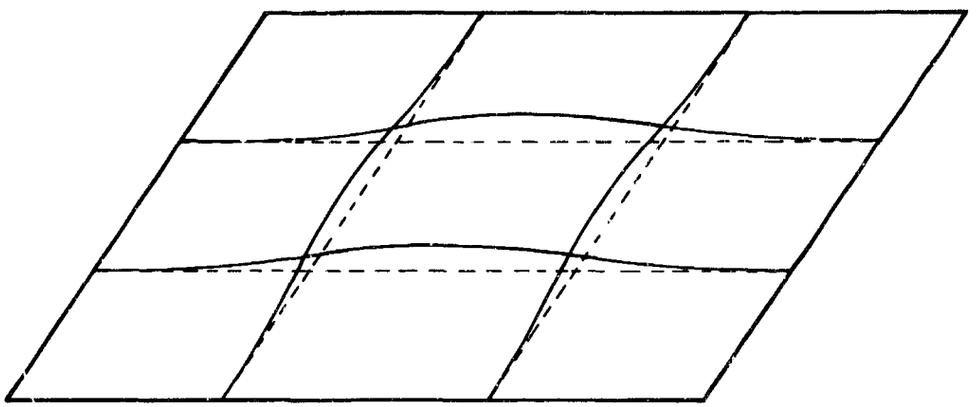

1. f = 128.3 Hz

FIGURE 8. MODE SHAPES FROM COMPUTER OUTPUT (CONCLUDED)

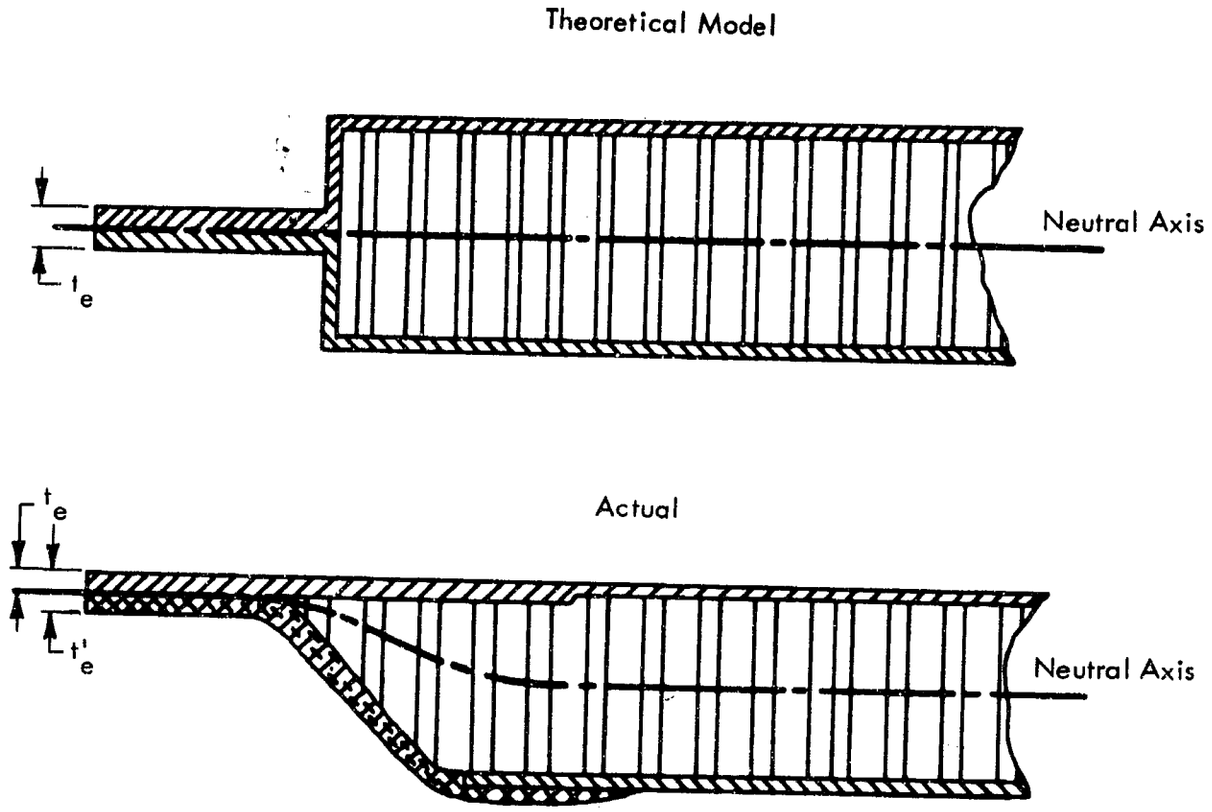

t'_e IS THE EDGE THICKNESS ONLY WHEN METAL PAN IS USED.

FIGURE 9 THEORETICAL AND ACTUAL MODELS OF TAPERED EDGE GEOMETRY

- The panel stiffness is derived from the facing sheet only.
- The panel responds to random excitation only in the first mode.

1. Frequency Analysis

Estimation of the first mode vibrational frequency for clamped edge panels will be considered first, with simply supported panels presented subsequently.

a. Clamped Edges - By changing the flexural rigidity only, Equations (20a) and (20b) are modified to obtain an estimate of the first mode frequency of flat clamped-edge honeycomb sandwich panels with thin facing sheets, i.e.,

$$D = \frac{Eth^2}{2\lambda} \tag{81}$$

where h is the core thickness
t is the minimum facing sheet thickness
λ is $(1 - \nu^2)$

and

$$_h(f^2) = \frac{4}{9}\left(\frac{\pi}{ab}\right)^2 \frac{Eth^2}{2\lambda\rho} R \tag{82}$$

b. Simply Supported Edges - Equations (24a) and (24b) are modified by replacing the flexural rigidity of a plate with that of a honeycomb sandwich panel with thin facing sheets to provide an estimate of the first mode frequency for simply supported edges. From Equation (24b) the fundamental frequency is

$$_h(f^2) = \frac{\pi^2}{4} \frac{Eth^2}{2\lambda\rho}\left[\frac{1}{a^2} + \frac{1}{b^2}\right]^2 \tag{83}$$

2. Stress Response

Estimations of the dynamic stresses at the edges and in the facing sheets of flat honeycomb sandwich panels when exposed to random acoustical noise is presented below for clamped and simply supported edges.

a. Clamped Edges - Equations (25) through (35), modified to reflect the honeycomb sandwich parameters, are used to estimate the maximum stresses at the edges of the honeycomb sandwich panels. Equation (25) is rewritten as

$$_h(\sigma_x) = \frac{6 M_x}{t_e^2} \tag{84}$$

where t_e is the metal edge thickness of the flat honeycomb panel (see Figure 9). Equation (35) then becomes

$$_h(\sigma_x)_{max} = \frac{12}{\pi^2}\left(\frac{b}{t_e}\right)^2 \frac{1}{R} \tag{85}$$

for the maximum edge stress resulting from a uniformly distributed static pressure of unit magnitude.

The mean-square edge stress response, considering light damping, for a honeycomb panel exposed to random acoustical noise excitation is, by combining Equations (5) and (85),

$$h(\overline{\sigma^2})_e = \frac{36}{\pi^3}\left(\frac{b}{t_e}\right)^4 \frac{f_i\,\Phi(f)}{\delta R^2} \tag{86}$$

An estimate of the maximum facing sheet stress is obtained from Equations (25) and (28) evaluated at the center of the panel ($x = a/2$, $y = b/2$). The resulting expression for the facing sheet stress is

$$h(\sigma)_f = \frac{8\,\pi^2 D}{thb^2}\, W_o \left[\left(\frac{b}{a}\right)^2 + \nu\right] \tag{87}$$

Equation (34) is an applicable expression for W_o. Therefore, the maximum facing sheet static stress resulting from a uniform static load of unit magnitude is

$$h(\sigma)_f = \frac{2\,a^2}{\pi^2 ht} \frac{\left[(b/a)^2 + \nu\right]}{R} \tag{88}$$

and the mean-square facing sheet stress response for a lightly damped panel exposed to random acoustic excitation is

$$h(\overline{\sigma^2})_f = \frac{36\,f_i\,a^4\,\Phi(f)}{\pi^3\,\delta\,h^2 t^2} \frac{\left[(b/a)^2 + \nu\right]^2}{R^2} \tag{89}$$

b. Simply Supported Edges - It can be shown that an estimate of the facing sheet stress response can be obtained from Equations (25), (26), and (37), evaluated at $x = a/2$, $y = b/2$, as follows:

$$h(\sigma)_f = \frac{\pi^2 D\, W_o}{th\, b^2} \left[(b/a)^2 + \nu\right] \tag{90}$$

where W_o is evaluated using Equation (40).

The maximum static facing sheet stress resulting from a uniform static pressure of unit magnitude is obtained by combining Equations (40) and (90) as

$$h(\sigma)_{f_{max}} = \frac{16\,b^2\left[(b/a)^2 + \nu\right]}{\pi^4\, th\left[(b/a)^2 + 1\right]^2} \tag{91}$$

An estimate of the mean-square stress response in the facing sheet for a lightly damped, flat honeycomb sandwich panel exposed to random acoustic pressure excitation can be obtained from Equations (5) and (91). The result is

$$h(\bar{\sigma})_f^2 = \frac{64\, b^4\, f_i\, \Phi(f) \left| (b/a)^2 + \nu \right|^2}{\pi^7\, t^2\, h^2\, \delta \left| (b/a)^2 + 1 \right|^4} \tag{92}$$

F. Curvature Effects

1. Introduction

Based on both theoretical and experimental evidence, it has been shown that curvature greatly influences the dynamic response characteristics and fatigue resistance of aircraft structure. Hence, curvature effects on dynamic response and fatigue applications are very important in the analysis of flight vehicle structure.

Considerable analytical work has been done for this research program, and where possible, the object has been to provide design information. The effects of curvature on the natural frequencies and stress response of skin-stringer and honeycomb sandwich cylindrical panels have been studied. The relations developed and reported herein, for estimating natural frequencies and stress response, must be considered as the first step in a long-range program to accurately determine curvature effects. A combined theoretical program to extend the ideas presented here and an experimental program involving a number of test specimens of various configurations and radii of curvature is required to obtain an accurate definition of the dynamic response characteristics for both skin-stringer and honeycomb sandwich construction.

2. Cylindrical Skin-Stringer Panels

a. Frequency Analysis - Much work has been done in the past few years in the area of shell dynamics (Reference 15). Little, if any, of this work is capable of providing preliminary design information (i.e., without extensive mathematical analysis and computing faculties) in the response of cylindrical panels to acoustic excitation. Indeed, the calculation of frequencies is no simple task for any set of specified boundary conditions. The basic approach has been to use a Rayleigh-Ritz technique to estimate the fundamental frequency of a thin cylindrical panel with clamped boundaries. Assumptions are introduced in order to provide an estimate suitable for design use. Also, several analytical methods are compared in order to illustrate the effect of boundary conditions on the fundamental frequency.

The approach used to estimate the fundamental frequency of a clamped cylindrical panel is the same as described in Reference 12 . The characteristic equation is determined from the equations

$$\begin{bmatrix} G_{11} - \lambda^2 J_{11} & G_{12} & G_{13} \\ G_{21} & G_{22} - \lambda^2 J_{22} & G_{23} \\ G_{31} & G_{32} & G_{33} - \lambda^2 J_{33} \end{bmatrix} \begin{bmatrix} U_{mn} \\ V_{mn} \\ W_{mn} \end{bmatrix} = \begin{bmatrix} 0 \\ 0 \\ 0 \end{bmatrix} \tag{93}$$

For flat panels or shallow cylindrical panels, the frequency of flexural vibration is approximated by

$$G_{33} - \lambda^2 J_{33} = 0. \tag{94}$$

After substituting the expressions for G_{33} and J_{33}, the frequency parameter, λ , is expressed as

$$\lambda^2 = \frac{\rho a b^3 (1 - \nu^2)}{t^2 E} \omega^2_{mn} = \frac{M_3(m)\, N_1(n)}{12} A + \frac{M_2(m)\, N_2(n)}{6A} + \frac{M_1(m)\, N_1(n)\, L^2 \phi^2}{A} + \frac{M_1(m)\, N_3(n)}{12A^3} \tag{95}$$

where

a	is the panel arch length
b	is the panel length
t	is the panel thickness
ρ	is the panel mass density
E	is Young's modulus
ν	is Poission's ratio
r	is the panel radius of curvature

$$A = \frac{a}{b}, \quad L = \frac{b}{t}, \quad \phi = \frac{a}{r}$$

The curved panel coordinate system is shown in Figure 10. The M's and N's are defined in Table I for both clamped and simply supported edges. Values for the M's and N's are given in Table II for both boundary conditions.

Substitution of the values from Table II for the fundamental clamped modes yields

$$\lambda^2 = 41.7A + (25.2 + L^2 \phi^2)/A + 41.7/A^3 \tag{96}$$

b. Stress Response - The stresses in the panel are (Reference 15).

$$\left.\begin{aligned}
\sigma_{xx} &= \frac{E}{1-\nu^2}\left\{\frac{\partial u}{\partial x} + \nu\left(\frac{\partial v}{\partial y} - \frac{w}{r}\right) + z\left[\frac{\partial^2 w}{\partial x^2} + \nu\left(\frac{1}{r}\,\frac{\partial v}{\partial y} + \frac{\partial^2 w}{\partial x^2}\right)\right]\right\} \\
\sigma_{yy} &= \frac{E}{1-\nu^2}\left\{\frac{\partial v}{\partial y} - \frac{w}{r} + \nu\,\frac{\partial u}{\partial x} + z\left[\frac{1}{r}\,\frac{\partial v}{\partial y} + \frac{\partial^2 w}{\partial y^2} + \nu\,\frac{\partial^2 w}{\partial x^2}\right]\right\} \\
\tau_{xy} &= \frac{E}{2(1+\nu)}\left\{\frac{\partial u}{\partial y} + \frac{\partial v}{\partial x} + 2z\left(\frac{1}{r}\,\frac{\partial v}{\partial x} + \frac{\partial^2 w}{\partial x\, \partial y}\right)\right\}
\end{aligned}\right\} \tag{97}$$

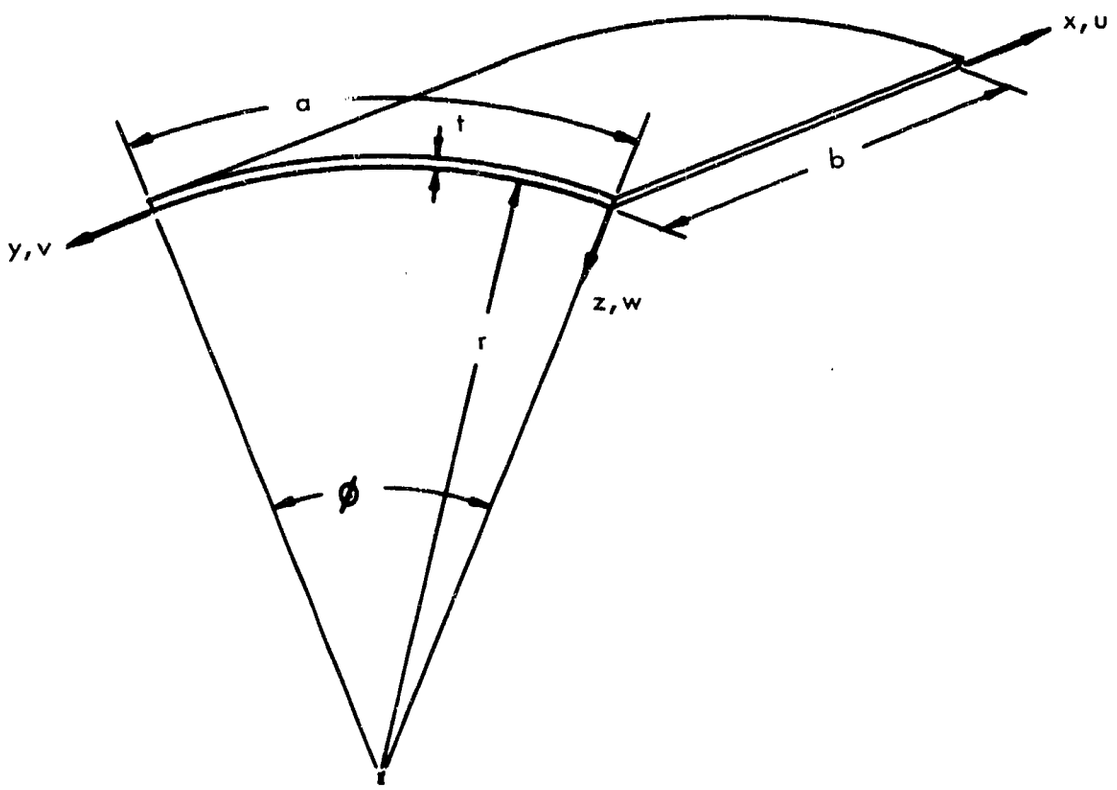

FIGURE 10 CURVED PANEL COORDINATE SYSTEM

TABLE I

DEFINITIONS OF M_i AND N_i

	Clamped	Simply Supported
$M_1(m)$	1	1/2
$M_2(m)$	$\alpha_m \beta_m b (\alpha_m \beta_m b - 2)$	$(\beta_m b)^2/2$
$M_3(m)$	$(\beta_m b)^4$	$(\beta_m b)^4/2$
$N_1(n)$	1	1/2
$N_2(n)$	$\theta_n \gamma_n a (\theta_n \gamma_n a - 2)$	$(\gamma_n a)^2/2$
$N_3(n)$	$(\gamma_n a)^4$	$(\gamma_n a)^4/2$

TABLE II

NUMERICAL VALUES OF M_i & N_i

m, n	$M_2(m)$, $N_2(n)$		$M_3(m)$, $N_3(m)$	
	Clamped	S.S.	Clamped	S.S.
1	12.303	4.93	500	48.6
2	46.050	19.72	3,800	778
3	98.905	44.4	14,618	3930
4	171.586	78.9	39,943	12,430
5	263.998	123.1	89,135	30,350

The displacement functions u, v, and w have been approximated in this analysis by

$$\begin{aligned} u &= \sum\sum U_{mn} X'_m(x) Y_n(y) \\ v &= \sum\sum V_{mn} X_m(x) Y'_n(y) \\ w &= \sum\sum W_{mn} X_m(x) Y_n(y) \end{aligned} \tag{98}$$

For clamped edges the assumed modes are

$$\left.\begin{aligned} X_m(x) &= \cosh(\beta_m x) - \cos(\beta_m x) - \alpha_m \left[\sinh(\beta_m x) - \sin(\beta_m x) \right] \\ Y_n(y) &= \cosh(\gamma_n y) - \cos(\gamma_n y) - \theta_n \left[\sinh(\gamma_n y) - \sin(\gamma_n y) \right] \end{aligned}\right\} \tag{99}$$

For skin-stringer construction, stresses are highest at the center of the longer edge. This stress is normal to the edge direct stress. In the case where the straight edge is the long side, the maximum stress, σ_y, is

$$\sigma_y = \frac{E}{1-\nu^2} \left[\frac{\partial v}{\partial y} + \frac{t}{2} \frac{\partial^2 w}{\partial y^2} \right] \tag{100}$$

After substituting for v and w from Equations (98) and (99) and after evaluating at the center of the long side, the following expression for the maximum stress is obtained:

$$\sigma_y = \frac{Et}{(1-\nu^2)} \gamma_n^2 X_m(b/2) W_{mn} \left[\frac{2K}{\gamma_n t} - 1 \right] \tag{101}$$

where V_{mn} is determined from the frequency Equation (93) in terms of W_{mn}, as given below:

$$V_{mn} = \frac{\left[G_{21}G_{13} - G_{23}(G_{11} - \lambda^2_{mn} J_{11}) \right]}{(G_{11} - \lambda^2_{mn} J_{11})(G_{22} - \lambda^2_{mn} J_{22}) - G_{21} G_{12}} W_{mn} = K W_{mn} \tag{102}$$

The term $2K/(\gamma_n t)$ can be defined in terms of the dimensionless ratios A, L, and ϕ as

$$\frac{2K}{\gamma_n t} = \frac{2KAL}{\gamma_n a} \tag{103}$$

The root mean square response to an arbitrary acoustic input at resonance is taken from Reference 12 and is

$$\bar{W}_{mn} = \left[\frac{\bar{Q}^2_{mn}}{2M^2_{mn}\ \delta_{mn}\ \omega^3_{mn}} \right]^{1/2} \tag{104}$$

where

$\bar{Q}^2_{mn}$ is the mean square generalized acoustic force

M_{mn} is the generalized mass

δ_{mn} is the viscous damping ratio

ω_{mn} is the natural frequency.

The ratio of curved panel to flat panel root mean-square stress is

$$\frac{\bar{\sigma}_{yc}}{\bar{\sigma}_{yf}} = \frac{\left(\frac{E_c t_c}{1 - \nu_c^2} \right) \gamma_{nc}^2 X_{mc} (b/2) \bar{W}_{mnc} \left[\frac{2K_c AL}{(\gamma_n a)_c} - 1 \right]}{\left(\frac{E_f t_f}{1 - \nu_f^2} \right) \gamma_{nf}^2 X_{mf} (b/2) \bar{W}_{mnf} \left[\frac{2K_f AL}{(\gamma_n a)_f} - 1 \right]} \tag{105}$$

The parameters which are affected by curvature in Equation (105) are ω_{mn} and K (K = 0 for a flat panel). Hence, the stress ratio reduces to

$$\frac{\bar{\sigma}_{yc}}{\bar{\sigma}_{yf}} = \frac{\bar{W}_{mnc}}{\bar{W}_{mnf}} \left[1 - \frac{2K_c AL}{\gamma_n a} \right] \tag{106}$$

From Equation (104), for root mean-square response, the response ratio reduces to

$$\frac{\bar{W}_{mnc}}{\bar{W}_{mnf}} = \left(\frac{\omega_{mnf}}{\omega_{mnc}} \right)^{3/2} \tag{107}$$

when it is assumed that damping and input force are identical for both configurations, and that the generalized mass is unaffected by small curvature. The stress ratio now becomes

$$\frac{\bar{\sigma}_{yc}}{\bar{\sigma}_{yf}} = \left(\frac{\omega_{mnf}}{\omega_{mnc}} \right)^{3/2} \left[1 - \frac{2K_c AL}{\gamma_n a} \right] \tag{108}$$

The frequency ratio, using the results of Equation (96), for the first damped mode is

$$\left(\frac{\omega_{mnf}}{\omega_{mnc}} \right)^{3/2} = \left[\frac{1}{1 + \frac{0.024\, AL\emptyset^2}{A^4 + 0.61\, A^2 + 1}} \right]^{3/4} \tag{109}$$

Data from tests described in Reference 12 show that the analytically determined constant 0.024 in Equation (109) should be 0.006 to match the test frequencies. This difference is attributed to the fact that the test panel boundaries were not completely clamped.

An approximate solution to Equation (102) for the first mode is

$$\frac{2KAL}{\gamma_n{}^a} = C_1 \left[\frac{A^2 + 0.0336}{A^4 + 9.62\, A^2 + 1} \right] A\emptyset L \tag{110}$$

and the final result for the stress ratio is obtained by substituting Equations (109) and (110) into Equations (108):

$$\frac{\bar{\sigma}_{yc}}{\bar{\sigma}_{yf}} = \left[1 + \frac{C_2 (A\emptyset L)^2}{A^4 + 0.61 A^2 + 1} \right]^{-3/4} \left[1 + C_1 \left(\frac{A^2 + 0.0336}{A^4 + 9.62 A^2 + 1} \right) A\emptyset L \right] \tag{111}$$

c. Effect of Boundary Conditions

Several methods of analysis were compared in order to calculate the natural frequencies of a cylindrical panel with various boundary conditions. Figure 11 presents a comparison of three different methods of solution for the completely clamped panel, illustrates the analogy of the arch to the panel, and presents the exact solution for the simply supported panel (from Reference 12). The methods used for the clamped edges were (1) a double-finite Fourier transform solution, (2) a Galerkin-Fourier transform solution, and (3) a Rayleigh-Ritz solution. The panel parameters for this example were selected to match available experimental data (Reference 12). Figure 11 clearly illustrates the relative importance of clamping along the length as opposed to clamping the arc. The experimental points in Figure 11 are for an ideally clamped panel. Clearly, the analytical methods leave much to be desired when compared to the experiment. After much study, it is felt that this discrepancy is due to imperfect restraint of the inplane motion of the clamped edges in the circumferential direction. The importance of this relaxed restraint will now be investigated.

The approach used is a one term Rayleigh-Ritz analysis with a free parameter, ξ, included with the assumed mode for the inplane motion, v, which is selected so as to make the fundamental frequency a minimum.

The expression for the kinetic energy and the strain energy are given below for the classical cylindrical panel; however, an additional strain energy term is required to include the elastic effects of the edge. The kinetic energy is

$$T = \frac{1}{2} \int_0^a \int_0^b \rho t \left[\dot{u}^2(x,s,t) + \dot{v}^2(x,s,t) + \dot{w}^2(x,s,t) \right] dx ds \tag{112}$$

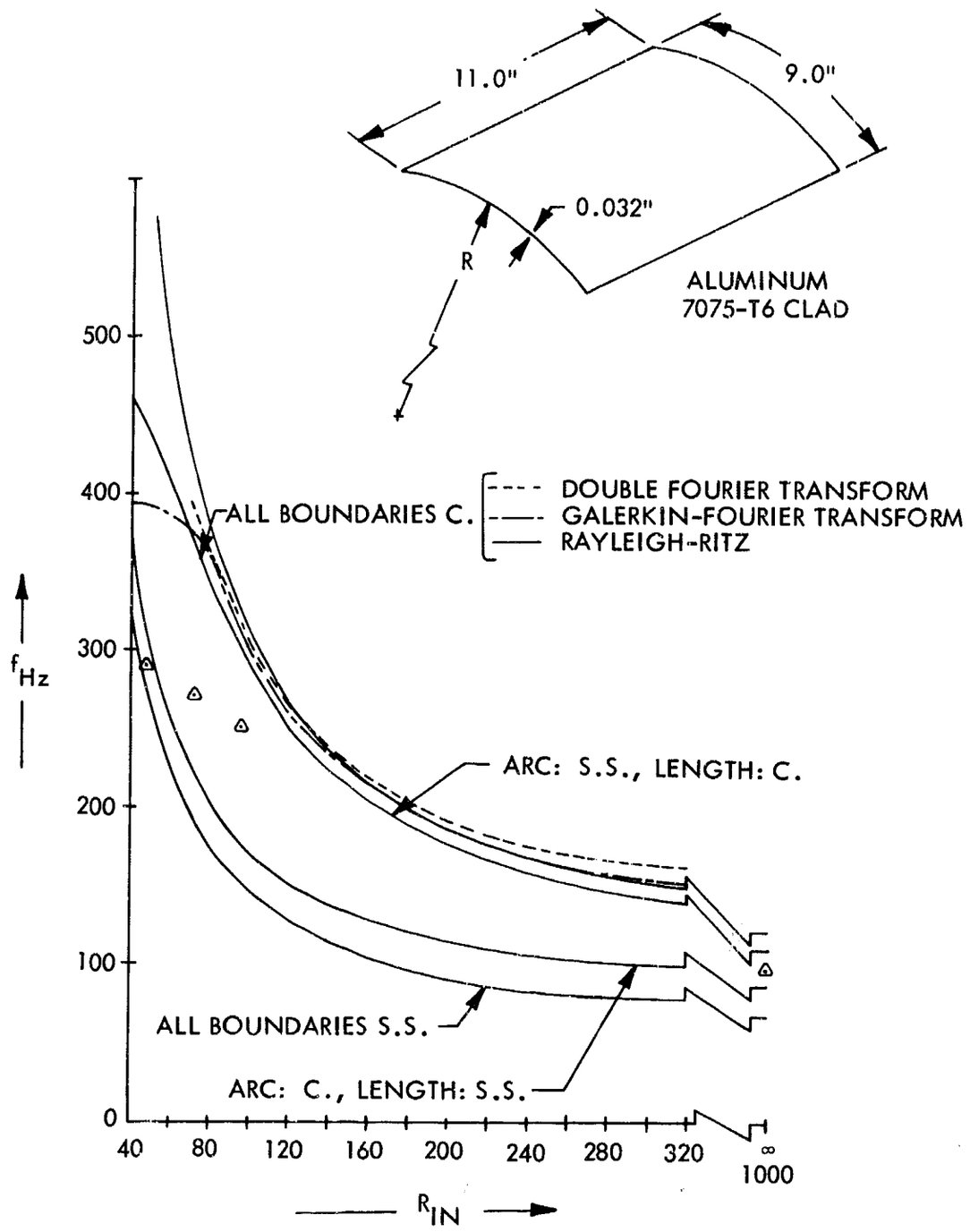

FIGURE 11. STUDIES OF THE FUNDAMENTAL FREQUENCY VERSUS THE RADIUS OF CURVATURE OF A PANEL UNDER VARIOUS BOUNDARY CONDITIONS

the shell strain energy is

$$U_s = \frac{1}{2} \int_o^a \int_o^b \left\{ D \left[w_{,xx}^2 + (w_{,ss} + \frac{1}{r} v_{,s})^2 + 2\nu w_{,xx} (w_{,ss} + \frac{1}{r} v_{,s}) \right.\right.$$

$$\left. + 2(1 - \nu) (w_{,xs} + \frac{1}{r} v_{,x})^2 \right] + C \left[u_{,x}^2 + (v_{,s} - \frac{1}{r} w)^2 + 2\nu u_{,x} (v_{,s} - \frac{1}{r} w) \right.$$

$$\left.\left. + \frac{1}{2}(1 - \nu) (v_{,x} + u_{,s})^2 \right] \right\} dxds \qquad (113)$$

and the strain energy of the edge member is

$$U_e = \frac{1}{2} \int_o^b K v^2(x,o)\, dx + \frac{1}{2} \int_o^b K v^2(x,a)\, dx \qquad (114)$$

where

$$D = \frac{Et^3}{12(1 - \nu^2)}, \quad C = \frac{Et}{(1 - \nu^2)}, \text{ and}$$

K is the inplane spring constant

Assuming harmonic motion, conservation of energy yields the relation

$$\int_o^a \int_o^b (U_{max} - T_{max})\, dxdy = 0 \qquad (115)$$

The boundary conditions for clamped edges with relaxed circumferential restraint along the length of the panel are

$$w(o,y) = w(b,y) = w(x,o) = w(x,a) = 0$$

$$w_{,x}(o,y) = w_{,x}(b,y) = w_{,y}(x,o) = w_{,y}(x,a) = 0 \qquad (116)$$

$$u(o,y) = u(b,y) = u(x,o) = u(x,a) = 0$$

$$v(o,y) = v(b,y) = 0$$

A solution, in the form presented below, is assumed:

$$u(x,y) = \sum\sum \frac{1}{\beta}_{m} U_{mn} X_m'(x)\, Y_n(y)$$

$$v(x,y) = \sum\sum \frac{1}{\gamma}_{n} V_{mn} X_m(x)\, Y_n^{*\prime}(y) \qquad (117)$$

$$w(x,y) = \sum\sum W_{mn} X_m(x)\, Y_n(y)$$

where

$X_m(x)$ & $Y_n(y)$ are given by Equation (99) and

$$Y_n^*(y) = (1 - \xi)\sin\left(\frac{\pi y}{a}\right) + \xi\, Y_n(y) \qquad (118)$$

ξ is a factor proportional to the degree of inplane restraint, $o \leq \xi \leq 1$

After assuming a one term solution for u, v, and w in Equations (117) substituting this into Equation (115), evaluating the integrals, and differentiating as indicated below

$$\frac{\partial}{\partial u}\left\{\int_o^a \int_o^b (U_{max} - T_{max})\, dxds\right\} = 0$$

$$\frac{\partial}{\partial v}\left\{\int_o^a \int_o^b (U_{max} - T_{max})\, dxds\right\} = 0 \qquad (119)$$

$$\frac{\partial}{\partial w}\left\{\int_o^a \int_o^b (U_{max} - T_{max})\, dxds\right\} = 0$$

yields a system of linear algebraic equations. The integrals in Equations (119) are evaluated for the most part in Reference 16. The system of algebraic equations has the form

$$\begin{bmatrix} A_{11} & A_{12} & A_{13} \\ A_{12} & A_{22} & A_{23} \\ A_{13} & A_{23} & A_{33} \end{bmatrix} \begin{bmatrix} U_{11} \\ V_{11} \\ W_{11} \end{bmatrix} = \begin{bmatrix} 0 \\ 0 \\ 0 \end{bmatrix} \qquad (120)$$

where

$$A_{11} = \beta^2 ab + \frac{1}{2}(1-\nu)\frac{\alpha}{\beta}(\alpha\beta b - 2)\alpha\gamma(\alpha\gamma a - 2)$$

$$A_{12} = \frac{\nu}{\beta\gamma}\alpha\beta(2 - \alpha\beta b) \int_0^a Y(y)\, Y^{*'''}(y)dy$$

$$+\frac{1}{2}(1-\nu)\frac{\alpha}{\gamma}(\alpha\beta b - 2) \int_0^a Y'(y)\, Y^{*'}(y)\, dy$$

$$A_{13} = \frac{\nu a}{r}\alpha(\alpha\beta b - 2)$$

$$A_{22} = \frac{1}{\gamma^2} b \int_0^a Y^{*''}(y)\, dy + \frac{1}{2}(1-\nu)\alpha\beta(\alpha\beta b - 2) \int_0^a (Y^{*''}(y))^2\, dy$$

$$+\frac{1}{12}\left(\frac{t}{r\gamma}\right)^2\left[b\int_0^a (Y^{*''}(y))^2\, dy + 2(1-\nu)\alpha\beta(\alpha\beta b - 2)\int_0^a Y^{*'}(y)\, dy\right]$$

$$+2b\left(\frac{Ka}{C}\right)\left[\frac{\pi^2(1-\xi)}{\gamma a}\right]\frac{1}{a}$$

$$A_{23} = \frac{t^2}{12 r\gamma}\left[b\int_0^a Y''(y)\, Y^{*''}(y)\, dy + \nu\alpha\beta(2 - \alpha\beta b)\int_0^a Y(y)\, Y^{*''}(y)\, dy\right.$$

$$\left.+2(1-\nu)\alpha\beta(\alpha\beta b - 2)\int_0^a Y'(y)\, Y^{*'}(y)\, dy\right] - \frac{b}{r\gamma}\int_0^a Y(y)\, Y^{*''}(y)\, dy$$

$$A_{33} = \frac{ab}{r^2} + \frac{t^2}{12}\left[(\gamma^4 + \beta^4)ab + 2\alpha\beta(\alpha\beta b - 2)\alpha\gamma(\alpha\gamma a - 2)\right] - \frac{(1-\nu^2)}{E}\rho ab\omega^2$$

and the integrals are evaluated as

$$\int_0^a Y(y)\, Y^{*\prime\prime}(y)\, dy = \xi\, a\, \gamma\, (2 - a\gamma a) - \frac{(1-\xi)\, 4\gamma^2 (\pi/a)^3}{\gamma^4 - (\pi/a)^4}$$

$$\int_0^a Y'(y)\, Y^{*\prime}(y)\, dy = \xi\, a\, \gamma\, (a\gamma a - 2) + \frac{(1-\xi)\, 4\gamma^2 (\pi/a)^3}{\gamma^4 - (\pi/a)^4}$$

$$\int_0^a \left[Y^{*\prime}(y) \right]^2 dy = \frac{\pi}{2a}^2 (1-\xi)^2 + \frac{8\xi(1-\xi)\, \gamma^2 (\pi/a)^3}{\gamma^4 - (\pi/a)^4} + \xi^2 a\gamma\, (a\gamma a - 2)$$

$$\int_0^a \left[Y^{*\prime\prime}(y) \right]^2 dy = \frac{\pi}{2} \left(\frac{\pi}{a}\right)^3 (1-\xi)^2 + \frac{8\xi(1-\xi)\, \gamma^2 (\pi/a)^5}{\gamma^4 - (\pi/a)^4} + \xi^2\, \gamma^4\, a$$

$$\int_0^a Y''(y)\, Y^{*\prime\prime}(y)\, dy = \xi \gamma^4 a + (1-\xi)(\pi/a)^2 \frac{4\gamma^2 (\pi/a)^3}{\gamma^4 - (\pi/a)^4}$$

The eigenvalue problem (120) is solved by selecting ω^2 for specified ξ so that the determinant of the coefficient matrix vanishes. The edge restraint parameter, ξ, is selected so that ω^2 is a minimum. The dimensionless inplane spring constant, (Ka/C), is difficult to determine in practice, but its affect on the fundamental frequencies of the previous example (Figure 11) is illustrated in Figure 12 where

$$\Omega^2 = \frac{\rho a b^3 (1-\nu^2)}{Et^2}\, \omega^2 \qquad (121)$$

The referenced experimental data in comparison with the various analytical studies indicates that aircraft-type panel construction does not realize the degree of in-plane restraint represented in the classical clamped panel analysis. An analytical solution that more nearly determines the fundamental frequency of an aircraft-type curved panel is obtained by relaxing the in-plane restraint along the length through appropriate changes in the energy representation and the assumed mode shapes.

Having compared available experimental data, a fundamental frequency estimate for a curved panel clamped on one side to a frame with screws or rivets is obtained by assuming a value for Kb/C of zero. If the panel is clamped between two frames with screws or rivets, Kb/C = 1.0 gives the best frequency estimate. A more rigidly clamped panel, of course, requires a higher assumed spring constant.

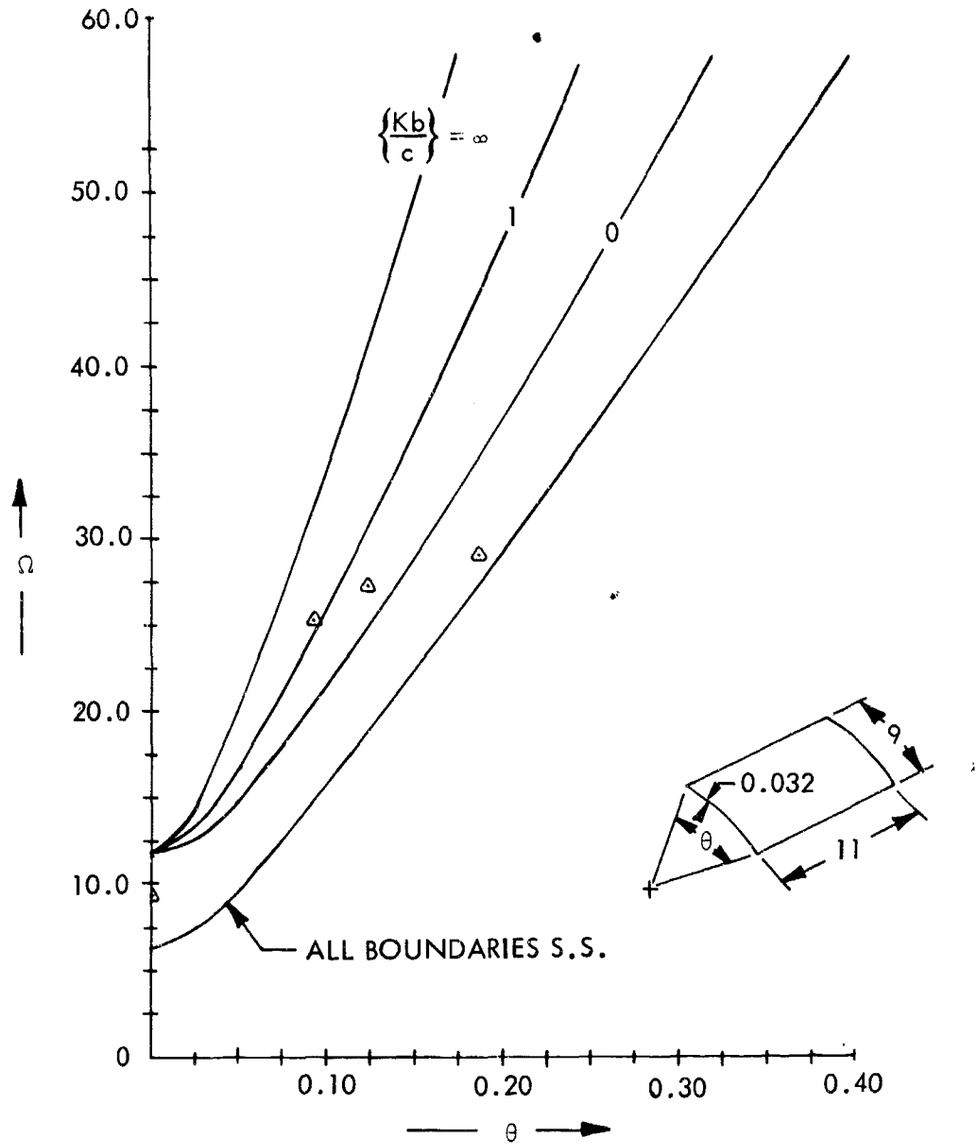

FIGURE 12. NON-DIMENSIONAL FREQUENCY SOLUTION FOR CLAMPED PANEL WITH RELAXED IN-PLANE RESTRAINT FOR VARIOUS CURVATURES VERSUS AIRCRAFT-TYPE TEST VALUES (REFERENCE 12)

3. Cylindrical Honeycomb Sandwich Panels

The curved honeycomb sandwich panel design techniques used in this study relied almost entirely upon analytical methods. The stress data for the curved sandwich panel design presented in Reference 12 were used where possible.

Plumblee (Reference 12) analyzed the curved sandwich panel with clamped boundaries using a Rayleigh-Ritz method. The flexural modes were of primary concern; however, the in-plane and shearing motion was also included. Wallace (Reference 17) used Donnell's method (Reference 18) for including shear deformation of elastic panels to derive the natural frequencies of simply supported sandwich panels. Face sheet stress was calculated and conclusions were drawn that the maximum facing sheet stress occurs at the center of the panel. The maximum shear stress, for simply supported edges, that occurs at the middle of the largest boundary was calculated.

Experience shows that fatigue failure of curved sandwich panels must be considered to occur in the thin edge member or in the facing sheets. Hence, the effect of edge member restraint, and thus stress, can only be taken into account if clamped or elastic boundary conditions are used. Also, for design purposes, only a ratio of the change in edge stress due to changes in curvature will be investigated. This approach will yield trends which indicate the effect of panel parameters on fatigue life due to acoustic excitation.

The above reasoning allows use of the vibration analysis of a cylindrically curved honeycomb sandwich panel with clamped edges, as reported in Reference 12 . This analysis, though too complex for design purposes, provides a basis for a simplified solution and also an accurate check for this simplified solution. In essence, the analysis is a free vibration analysis of a curved sandwich panel. The basic assumptions are that the materials, including the core, are linearly elastic, homogeneous, and orthotropic. The radial (or normal) displacement does not vary through the shell thickness. Normals to the middle surface before deformation remain normal to the middle surface after deformation (i.e., the core shear displacement is linear). The facing sheets are thin and resist only membrane stresses. The core resists only transverse shear stresses. The original analysis (Reference 12) included in-plane and rotatory inertias; however, only transverse inertia will be included in this analysis.

A typical curved sandwich panel is shown in Figure 13. The actual panel is modeled as a panel of uniform thickness in order to avoid complications in the analysis due to the tapered edges used in practice. The sandwich panel configuration, coordinate system, and shell element reactions are shown in Figures 14 and 15. While the actual frequencies calculated for sandwich panels using this method may be high, the ratio of curved panel to flat panel frequencies will be sufficiently accurate to provide reliable design information.

a. Frequency Analysis - The Rayleigh-Ritz method is used for the frequency analysis of the clamped cylindrical honeycomb panel described above. The strain energy in each layer of the panel is expressed in terms of the midsurface displacements and rotations. Mode shapes which satisfy the clamped boundary conditions are introduced, and finally the energy density is integrated over the volume of the body.

The strain energy density in the r^{th} layer of the sandwich panel is

$$ {}_rU_o = \frac{1}{2} \left\lfloor {}_r\sigma_i \right\rfloor \left[{}_r\epsilon_i \right] = \frac{1}{2} \left\lfloor {}_r\epsilon_i \right\rfloor \left[{}_rC_{ij} \right] \left[{}_r\epsilon_i \right] \qquad (122) $$

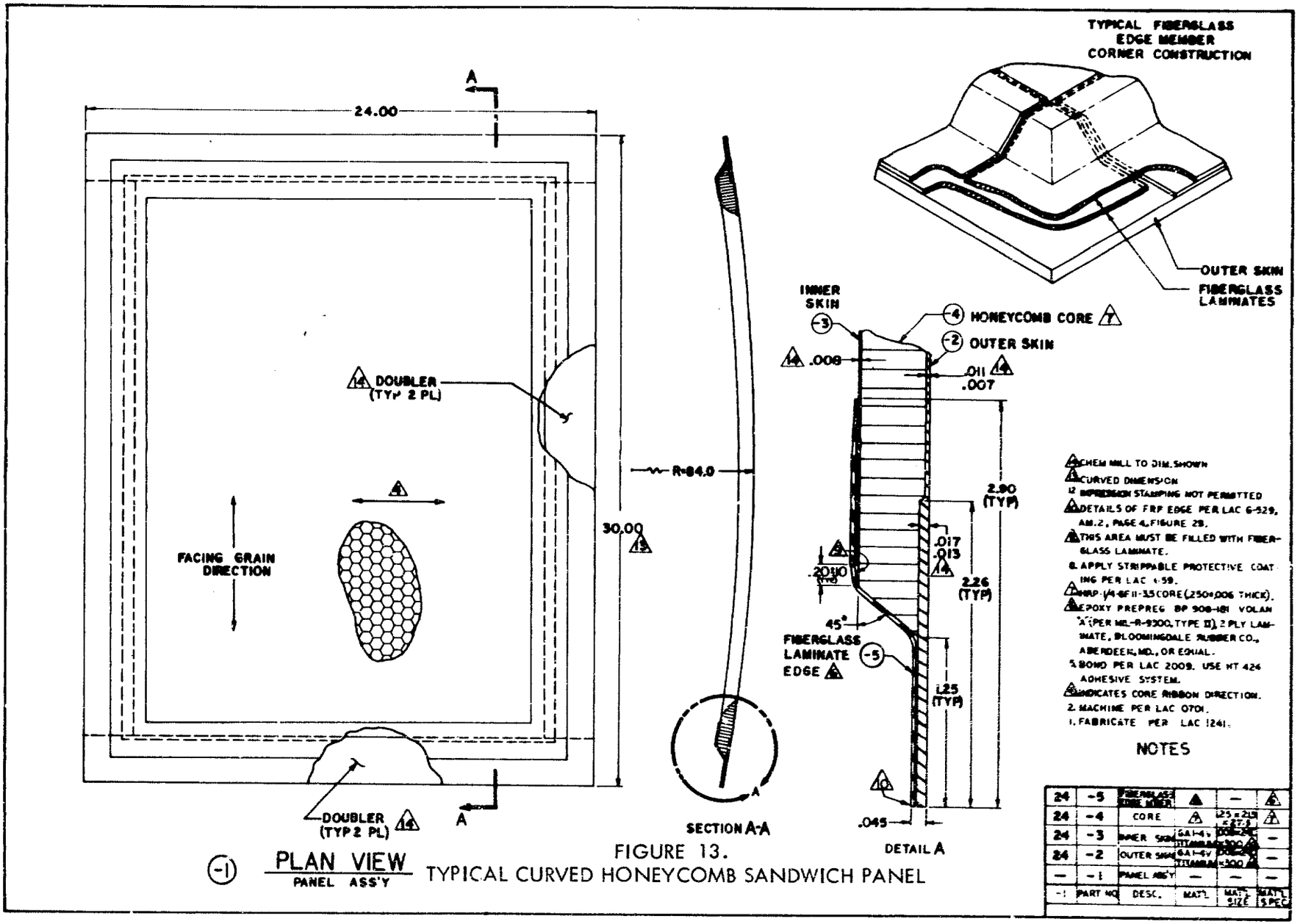

FIGURE 13. TYPICAL CURVED HONEYCOMB SANDWICH PANEL

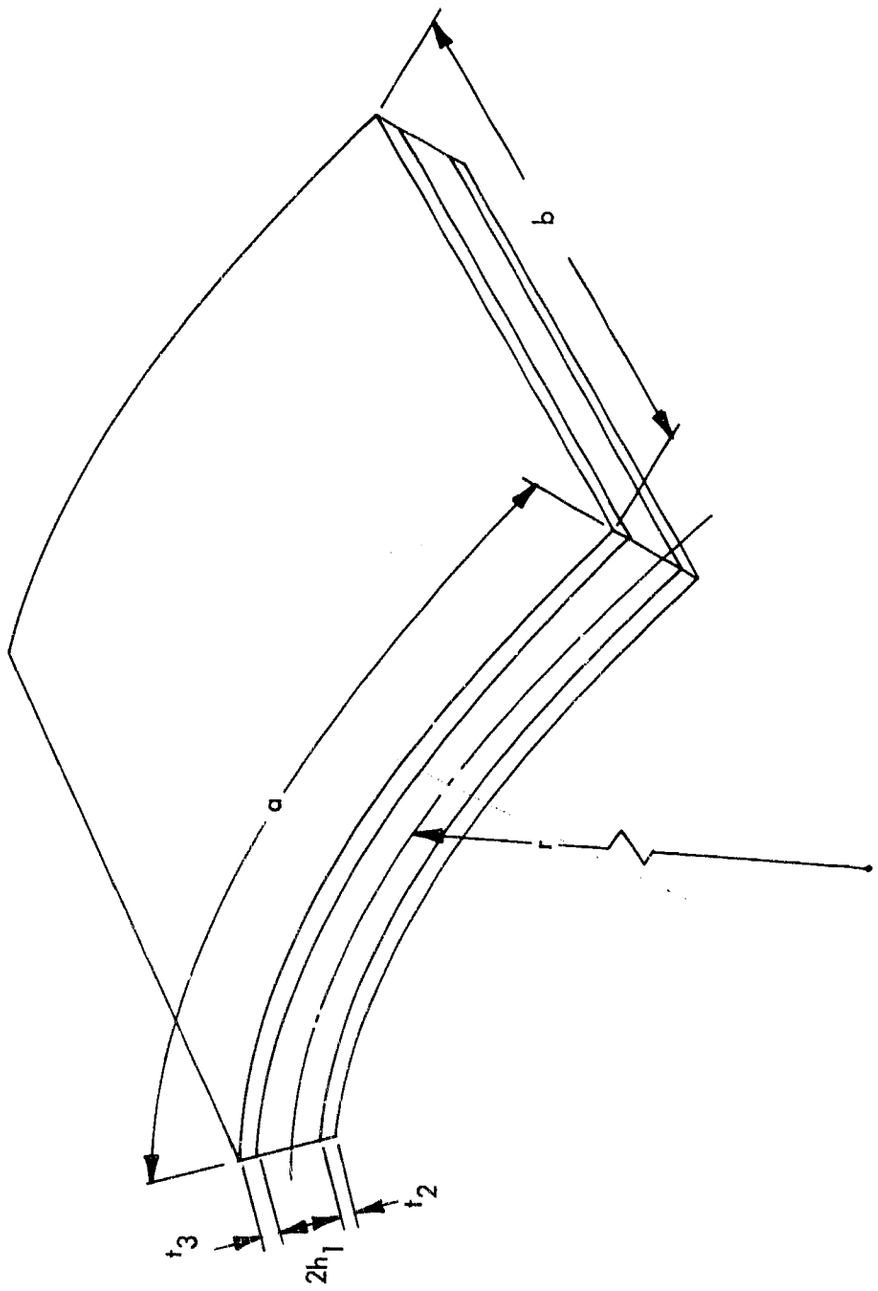

FIGURE 14. CURVED SANDWICH PANEL CONFIGURATION

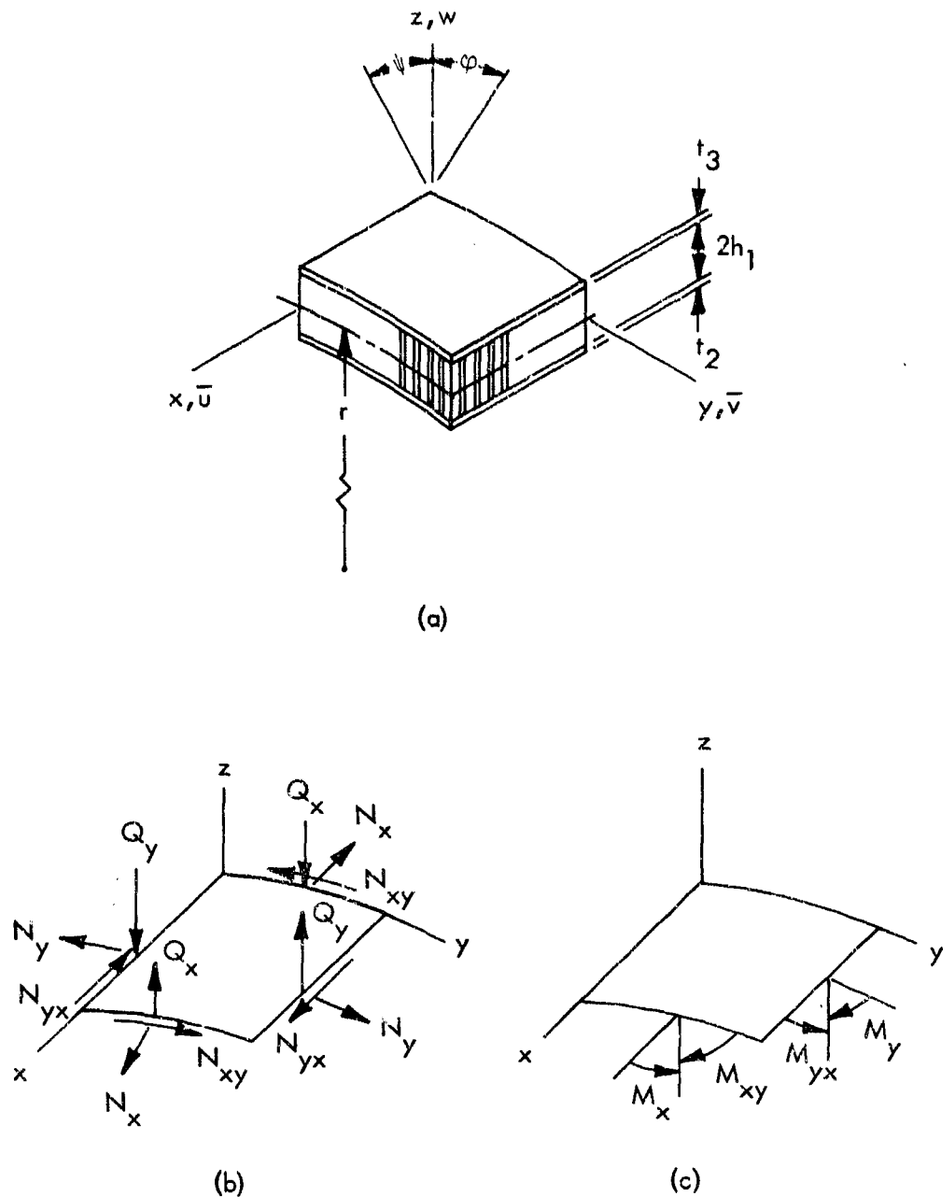

FIGURE 15. SANDWICH PANEL COORDINATE SYSTEM SHOWING THE SHELL FORCES AND MOMENTS

The convention adopted for the stress nomenclature is from Reference 12. The strain-displacement relations used are

$$\epsilon_1 = \frac{\partial u}{\partial x} + \frac{z}{h_1}\frac{\partial(h_1\psi)}{\partial x}$$

$$\epsilon_2 = \frac{w}{r} + \frac{\partial v}{\partial y} + \frac{z}{h_1}\frac{\partial(h_1\phi)}{\partial y}$$

$$\epsilon_3 = 0$$

$$\epsilon_4 = \frac{\partial w}{\partial y} + \frac{(h_1\phi)}{h_1} \tag{123}$$

$$\epsilon_5 = \frac{\partial w}{\partial x} + \frac{(h_1\psi)}{h_1}$$

$$\epsilon_6 = \frac{\partial v}{\partial x} + \frac{\partial u}{\partial y} + \frac{z}{h_1}\left(\frac{\partial(h_1\phi)}{\partial x} + \frac{\partial(h_1\psi)}{\partial y}\right)$$

In the facing sheets, z in Equations (123) is replaced by h_1 (it is assumed that there is no rotation in the face sheets).

In matrix form the strain-displacement relations are represented as

$$\left[{}_r\epsilon_i \right] = \left[{}_rA_{ik} \right]\left[u_k \right] \tag{124}$$

where u_k represents the displacements (i.e.; $u_1 = u$, $u_2 = v$, $u_3 = w$, $u_4 = h\psi$, $u_5 = h_1\phi$) and $\left[{}_rA_{ik} \right]$ is an operator matrix for the r^{th} layer.

In Reference 12 the mode shape was assumed to be a series of clamped - clamped beam functions, and it is shown that only one term is necessary to accurately predict the fundamental frequency. The displacement functions for the $(m,n)^{th}$ mode are

$$u = U_{mn}(t)\, X'_m(x)\, Y_n(y)/\beta_m$$

$$v = V_{mn}(t)\, X_m(x)\, Y'_n(y)/\gamma_n$$

$$w = W_{mn}(t) X_m(x)\, Y_n(y)$$

$$\psi = \Psi_{mn}(t) X'_m(x)\, Y_n(y)/\beta_m \tag{125}$$

$$\phi = \Phi_{mn}(t) X_m(x)\, Y'_n(y)/\gamma_n$$

where $X_m(x)$ and $Y_n(y)$ are given by Equation (99). The prime denotes a derivative with respect to the variable. The assumed displacements are written in matrix form as

$$\left[u_K \right] = \left[B_{mnk} \right] \left[q_{mnk} \right] \tag{126}$$

The strain energy density in terms of the generalized coordinates is obtained by substituting Equation (126) into Equation (124) and then using Equation (122).

The strain energy density for each layer is integrated over the layer thickness and the contributions summed. Finally, the integration over the panel area is performed.

For the core the elastic constants are

$$ {}_1C_{44} = G_{yz} \qquad {}_1C_{55} = G_{xz} \tag{127}$$

and all others are zero. The facing sheets are assumed to be isotropic and of the same material. The elastic constants are

$$\begin{aligned} {}_2C_{11} &= {}_3C_{11} = {}_2C_{22} = {}_3C_{22} = E/(1-\nu^2) \\ {}_2C_{12} &= {}_3C_{12} = {}_2C_{21} = {}_3C_{21} = \nu E/(1-\nu^2) \\ {}_2C_{66} &= {}_3C_{66} = E/2(1+\nu) \end{aligned} \tag{128}$$

where it has been assumed that $t_2 = t_3$.

The stiffness matrix resulting from using the strain energy expression and Castigliano's theorem is presented in terms of the following dimensionless parameters

$$\begin{aligned} \theta &= a/r & g &= t/h \\ L &= b/h & s &= (1-\nu^2)G_{yz}/E \\ A &= a/b & c &= G_{xy}/G_{yz} \end{aligned} \tag{129}$$

The number of variables that must be considered, when the parameters (129) are used, is reduced by two.

The kinetic energy, neglecting the core mass is

$$T = \rho\, t_2\, ab\, \dot{w}^2 \tag{130}$$

The eigenvalue problem is then cast in the form

$$\begin{bmatrix} L_{11} & L_{12} & L_{13} & 0 & 0 \\ L_{12} & L_{22} & L_{23} & 0 & L_{25} \\ L_{13} & L_{23} & L_{33}-\Omega^2 & L_{34} & L_{35} \\ 0 & 0 & L_{34} & L_{44} & L_{45} \\ 0 & L_{25} & L_{35} & L_{45} & L_{55} \end{bmatrix} \begin{bmatrix} U_{mn} \\ V_{mn} \\ W_{mn} \\ h_1 \psi_{mn} \\ h_1 \phi_{mn} \end{bmatrix} = \begin{bmatrix} 0 \\ 0 \\ 0 \\ 0 \\ 0 \end{bmatrix} \tag{131}$$

For completeness, the elements in the stiffness matrix are listed below

$$L_{11} = A(\beta_m b)^2 + \frac{(1-\nu)}{2A} \frac{M_2(m)\, N_2(n)}{(\beta_m b)^2}$$

$$L_{12} = \frac{(1+\nu)}{2} \frac{M_2(m)\, N_2(n)}{(\beta_m b)(\gamma_n a)}$$

$$L_{13} = -\nu\theta \frac{M_2(m)}{\beta_m b}$$

$$L_{14} = L_{15} = 0$$

$$L_{22} = \frac{(\gamma_n a)^2}{A} + sg \frac{\theta^2}{A} \frac{N_2(n)}{(\gamma_n a)^2} + \frac{(1-\nu)}{2A} \frac{M_2(m)\, N_2(n)}{(\gamma_n a)^2}$$

$$L_{23} = \frac{\theta}{A}(1 + scg) \frac{N_2(n)}{(\gamma_n d)}$$

$$L_{24} = 0$$

$$L_{25} = -sL\theta \frac{N_2(n)}{(\gamma_n a)^2}$$

$$L_{33} = \frac{\theta}{A} + \frac{sg}{A} N_2(n) + scg\, A\, M_2(m)$$

$$L_{34} = scLA \frac{M_2(m)}{(\gamma_n a)}$$

$$L_{35} = \frac{sL\, N_2(n)}{(\gamma_n a)}$$

$$L_{44} = A(\beta_m b)^2 + \frac{scL^2 A}{g} \frac{M_2(m)}{(\beta_m b)^2} + \frac{(1-\nu)}{2A} \frac{M_2(m)\, N_2(n)}{(\beta_m b)^2}$$

$$L_{45} = \frac{(1+\nu)}{2} \frac{M_2(m)}{(\beta_m b)} \frac{N_2(n)}{(\gamma_n a)}$$

$$L_{55} = \frac{(\gamma_n a)^2}{A} + \frac{sL^2 A}{g} \frac{N_2(n)}{(\gamma_n a)^2} + \frac{(1-\nu)}{2} \frac{M_2(m)\, N_2(n)}{(\gamma_n a)^2}$$

The nondimensional frequency, Ω, is related to the natural frequency by the relation

$$\Omega^2 = \frac{\rho a b (1 - \nu^2)}{E} \omega^2 \tag{132}$$

The nondimensional terms $M_2(m)$ and $N_2(n)$ are given in Tables I and II, and for the fundamental mode

$$(\beta_1 b) = (\gamma_1 a) = 4.73$$

b. Stress Response - It is possible to solve the eigenvalue problem and obtain stress in terms of the generalized coordinates. Then by using the generalized damping force, the generalized acoustic forcing function, and the generalized mass in LaGrange's equations of motion, the actual stresses can be obtained. Experience, however, implies that this method is not an extremely accurate indicator of stress response. But in cases where no better method is available these equations must be used. Since there is only a limited amount of experimental data available for acoustically induced core shear, then the core shear stress must be calculated using this method. A solution for the fundamental frequency is first necessary to obtain the stresses.

It is recognized that, for a flat panel ($\theta = 0$), the eigenvalue matrix uncouples into a 2 x 2 matrix and a 3 x 3 matrix from examination of Equation(131). The 3 x 3 matrix contains the coupling terms between w, ψ and ϕ while the 2 x 2 matrix contains the coupling between ϕ and v, the in-plane motions. For small angles, the u-w, v-w, and v-ϕ coupling is small and does not significantly affect the frequency. This has been verified numerically. Therefore, for small angles the frequency can be determined from the 3 x 3 (w, ψ, ϕ) matrix. After eliminating higher order terms, the first mode frequency of a shallow cylindrical curved sandwich panel with clamped edges is

$$\Omega^2 = \frac{\theta^2}{A} + \frac{(\beta b)^4 g^2}{A^3 L^2} \frac{S_1}{S_2}$$

$$S_1 = 1 + A^4 + 40.7 \frac{g}{scL^2} (1 + cA^2) \tag{133}$$

$$S_2 = 1 + 40.7 \frac{g}{scL^2} \left(1 + \frac{c}{A^2}\right) + 1655. \left(\frac{g}{scL^2}\right)^2 \frac{c}{A^2}$$

Restrictions on the use of this equation are

$\theta \leq .35$ radians
$g \geq 10$
$s \leq .01$
$L \geq 100$

If these limits are exceeded, the results will not be reliable.

In order to determine stress or stress ratio, it is necessary to determine the generalized coordinates U_{mn}, V_{mn}, Φ_{mn}, and Ψ_{mn} in terms of W_{mn}. Some simplication is necessary so

that these coordinates can be expressed in fairly simple terms. The nature of the generalized coordinates was studied as the pertinent parameters were varied. Table III shows the variation of the generalized coordinates and natural frequency with variation in the subtended angle θ for a given panel configuration. For angles less than 0.35 radian, ψ and ϕ are relatively unchanged, indicating an independence of the shell rotation angles with panel curvature. Also, the variation of u and v is nearly linear with θ, for $\theta \leq 0.3$ radian. These observations aid considerably in the evaluation of the generalized coordinates.

TABLE III

EFFECT OF SUBTENDED ANGLE ON THE GENERALIZED COORDINATES

θ	W_{11}	$h_1\Psi_{11}$	$h_1\Phi_{11}$	V_{11}	U_{11}	Ω
0.0	.994	-.0244	-.0119	0.0	0.0	.04430
0.05	.994	-.0244	-.0119	.00329	.00051	.04464
0.1	.9945	-.02445	-.01197	.006605	.001017	.04566
0.2744	.9965	-.02418	-.01225	.01888	.002693	.05339
0.5	.9969	-.02444	-.01291	.03819	.004319	.06985
1.0	.7075	-.01689	-.01294	.09857	-.00102	.09899

$A = a/b = 1.3939$
$L = b/h = 1031.25$
$g = t/h = 11.625$
$s = \dfrac{(1-\nu^2)G_{yz}}{E} = .0005007$
$c = Gxz/Gyz = 1.98895$

When evaluating Ψ and Φ in terms of W, all coupling with U and V can be neglected as demonstrated in the above example. The expressions for Ψ and Φ are found to be

$$h_1\Psi = -3.51 \frac{g}{ALS_2}\left[1 + 40.7\frac{g}{scL^2}\left(1 - \frac{c}{5}\right)\right]W = K_2W \qquad (134)$$

$$h_1\Phi = -3.51 \frac{g}{LS_2}\left[1 + 40.7\frac{g}{sA^2L^2}\left(1 - \frac{1}{5c}\right)\right]W = K_4W$$

In this evaluation, ν was assumed to be 0.33 and is representative of most metals and metal alloys used in the fabrication of flight vehicle honeycomb sandwich structure.

With the evaluation of Ψ and Φ complete, the first two expressions of Equation (131) are used to determine U and V. The following relationships were determined:

$$V = \frac{0.085\,\theta\,W}{1 + 0.1A^2} = K_1 W$$

$$U = \frac{0.01740W}{A(1 + 0.1A^2)} = K_3 W \qquad (135)$$

The expressions for stress in terms of displacement are determined by substituting Equation (124) into Equation (122). In expanded form the face sheet tensile stress and core transverse shear stresses are

$$\sigma_y = \frac{E}{1 - \nu^2}\left[\frac{w}{r} + \frac{\partial v}{\partial y} + \frac{\nu\,\partial u}{\partial x} + z\left(\frac{\partial \phi}{\partial y} + \frac{\nu\,\partial \psi}{\partial x}\right)\right]$$

$$\sigma_x = \frac{E}{1 - \nu^2}\left[\frac{\partial u}{\partial x} + \nu\left(\frac{w}{r} + \frac{\partial v}{\partial y}\right) + z\left(\frac{\partial \psi}{\partial x} + \frac{\nu\,\partial \phi}{\partial y}\right)\right]$$

$$\tau_{xz} = Gxz\left[\frac{\partial w}{\partial x} + \psi\right] \qquad (136)$$

$$\tau_{yz} = Gyz\left[\frac{\partial w}{\partial y} + \phi\right]$$

Substituting the mode shapes of Equation (125) into Equation (136) gives the stresses in terms of the generalized coordinate W, the panel physical parameters, and the assumed mode shape. These generalized stress response equations are

$$\sigma_y = 5.32\,E\,\frac{XY''}{a}\,W\left[\frac{0.212\,Y\,\theta}{Y''} + K_1 + \frac{AK_3}{3}\,\frac{X''Y}{XY''} + \frac{z}{h_1}\left(K_2 + \frac{AK_4X''Y}{3XY''}\right)\right]$$

$$\sigma_x = 5.32\,E\,\frac{X''Y}{b}\,W\left[0.0635\,\frac{X\theta}{X''A} + K_3 + \frac{K_1}{3A}\,\frac{XY''}{X''Y} + \frac{z}{h_1}\left(K_4 + \frac{K_2}{3A}\,\frac{XY''}{X''Y}\right)\right] \qquad (137)$$

$$\tau_{xz} = 4.73\,G_{xz}\,\frac{X'Y}{b}\,W\left[1 + 0.212\,\frac{L}{g}\,K_4\right]$$

$$\tau_{yz} = 4.73\,G_{yz}\,\frac{XY'}{a}\,W\left[1 + 0.212\,\frac{AL}{g}\,K_2\right]$$

where the primed variables are derivatives with respect to the argument. The conclusion to be drawn from this analysis is that there are two regions which are tensile stress critical: the center of the panel and the panel edges. For a flat panel with some edge fixity, the maximum edge stress occurs at the center of the long boundary. Generalizations of this type are not possible with curved panels. The stresses in Equation (137) are only for sandwich panels with uniform thickness. An approximation must be made in the determination of stress at the edges for designs of the type shown in Figure 9.

The change in tensile stress at the center of the panel, caused by curvature in the y direction is evaluated as

$$\frac{\sigma_{yc}}{\sigma_{yf}} = \frac{W_c}{W_f}\left[\frac{-.276\theta + K_1 + .33AK_3 + K_2 + .33AK_4}{K_2 + .33AK_4}\right] \tag{138}$$

Later in this section, it is shown that, for sinusoidal excitation,

$$\frac{W_c}{W_f} = \left(\frac{\Omega_f}{\Omega_c}\right)^2 \tag{139}$$

From Equation (133) the ratio of frequencies is

$$\left(\frac{\Omega_c}{\Omega_f}\right)^2 = 1 + 0.002\,\frac{S_2}{S_1}\left(\frac{AL\theta}{g}\right)^2 \tag{140}$$

Substitution of Equations (134), (135), and (140) into Equation (138) results in

$$\left.\frac{\sigma_{yc}}{\sigma_{yf}}\right|_{\substack{z=h_1\\y=a/2\\x=b/2}} = \frac{1 + .0527\left[(1 + .049A^2)\;S_2/S_3\left(\frac{AL\theta}{g}\right)\right]}{1 + .002\;\frac{S_2}{S_1}\left(\frac{AL\theta}{g}\right)^2} \tag{141}$$

where $S_3 = 1 + 0.33A^2 + \frac{38.0g}{scL^2}(1 + 0.143c)$.

Similarly the ratio of σ_{xc}/σ_{xf} is

$$\left.\frac{\sigma_{xc}}{\sigma_{xf}}\right|_{\substack{z=h_1\\y=a/2\\x=b/2}} = \frac{1 + 0.0396\,(1 + 0.103A^2)\,\frac{AL\theta}{g}\;S_2/S_4}{1 + 0.002\;\left(\frac{AL\theta}{g}\right)^2 S_2/S_1} \tag{142}$$

The ratio of σ_y to σ_x for the curved panel is given as

$$\left.\frac{\sigma_y}{\sigma_x}\right|_{\substack{z=h_1\\ y=a/2\\ x=b/2}} = .387\left[\frac{(1+.049A^2)(\frac{AL\theta}{g})+.649\ S_3/S_2}{(1+.0285A^2)(\frac{AL\theta}{g})+.754\ S_4/S_2}\right] \tag{143}$$

where $S_4 = 1 + 3A^2 + \frac{16.3g}{scL^2}\quad(1+7c)$

Another item of iterest in structural design is the ratio of stress in the outer facing sheet to the stress in the inner facing sheet. This ratio is

$$\left.\frac{\sigma_y}{\sigma_{y,}}\right|_{\substack{z=h_1\\ y=a/2\\ x=b/2}} = -\left[\frac{1+0.0527(1+0.049A^2)\ \frac{S_2}{S_3}(\frac{AL\theta}{g})}{1-0.0527(1+0.049A^2)\ \frac{S_2}{S_3}(\frac{AL\theta}{g})}\right] \tag{144}$$

In order to obtain a first order evaluation of the effect of curvature on edge stress, the effect of curvature for a simple panel is examined. In Reference 12, the ratio of stress in a curved panel to stress in a flat panel was found to be, assuming sinusoidal excitation,

$$\frac{\sigma_{yc}}{\sigma_{yf}} = \left[1+\frac{.445\,(A^2+.108)\,AL_e\theta}{A^4+9.62A^2+1}\right]\left(\frac{\Omega f}{\Omega c}\right)^2 \tag{145}$$

If the frequency ratio of the sandwich panel is used, then the ratio of stresses becomes

$$\frac{\sigma_{yc}}{\sigma_{yf}} = \frac{1+\frac{.445\,(A^2+.108)\,AL\theta}{A^4+9.62A^2+1}}{1+.002\frac{S_2}{S_1}\,(\frac{AL\theta}{g})^2} \tag{146}$$

In examining the transverse shear stress, it is determined that the maximum value of τ_{xz} occurs at $y = a/2$, $x \approx 0.22b$ and $x \approx 0.78b$. These coordinates were determined by calculating the x and y which produce maxima in X' and Y. The maximum in τ_{yz} occurs at $x = b/2$, $y \approx 0.22b$ and $y \approx 0.78b$. For clamped edges, the transverse shear is zero at the center of the panel and along its boundaries. Actually the greatest transverse shear occurs somewhere between the edge and 22 percent of the span as evidenced by the core fatigue failure experienced by HC-15A. (See Table X, Section III.) It should be pointed out that

because of the type loads resisted by the honeycomb core, panel curvature does not affect transverse shear stress. Only the natural frequency is changed. Therefore, for sinusoidal loading

$$\frac{\tau_{xzc}}{\tau_{xzf}} = \frac{\tau_{yzc}}{\tau_{yzf}} = \left(\frac{\Omega_f}{\Omega_c}\right)^2 \tag{147}$$

It is necessary to determine the generalized response to an acoustic forcing function before estimates of stress magnitude can be determined. Lagrange's equation which describes the motion of the generalized coordinate, W_{mn}, is

$$\ddot{W}_{mn} + 2\,\delta_{mn}\,\Omega_{mn}\,\dot{W}_{mn} + \Omega^2_{mn}\,W_{mn} = \frac{Q_{mn}(t)}{M_{mn}} \tag{148}$$

For sinusoidal excitation, the response is

$$W_{mn} = \frac{Q_{mn}}{2\,\delta_{mn} M_{mn}\,\Omega^2_{mn}} \tag{149}$$

If the forcing function is random acoustical noise (or if the bandwidth of the forcing function is at least three times the bandwidth of the system at resonance) then the response is

$$\bar{W}_{mn} = \sqrt{\frac{\pi}{2}\,\frac{Q^2_{omn}}{\delta_{mn}\,\Omega^3_{mn}\,M^2_{mn}}} \tag{150}$$

For the case of sinusoidal response, the ratio of W_{mnc} to W_{mnf} becomes

$$\frac{W_{mnc}}{W_{mnf}} = \frac{Q_{mnc}}{2\,\delta_{mnc} M_{mnc}\,\Omega^2_{mnc}} \times \frac{2\,\delta_{mnf} M_{mnf}\,\Omega^2_{mnf}}{Q_{mnf}} = \left(\frac{\Omega_{mnf}}{\Omega_{mnc}}\right)^2 \tag{151}$$

The generalized force and modal mass do not change with frequency of the mode and it is a valid assumption that the modal damping ratio remains essentially constant for small changes in frequency. In the same manner, the generalized displacement ratio for random excitation is

$$\frac{\bar{W}_{mnc}}{\bar{W}_{mnf}} = \left(\frac{\Omega_{mnf}}{\Omega_{mnc}}\right)^{3/2} \tag{152}$$

The generalized force for the case of sinusoidal plane wave excitation at normal incidence is

$$Q_{mn} = \int_0^b \int_0^a P(x, y, t)\, Xm(x)\, Yn(y)\, dx\, dy \tag{153}$$

while the generalized force for random acoustical noise excitation is

$$Q^2_{omn} = \int_0^b \int_0^a \bar{P}o^2(x, y, t)\, Xm(x)\, Yn(y)\, dx\, dy \tag{154}$$

where $\bar{P}^2_o$ is in units of $(psi)^2/Hz$.

For uniform pressure distribution

$$Q_{11} = 0.691\, a\, b\, P \tag{155}$$

Then

$$Q_{o11} = 0.691\, a\, b\, \bar{P}_o$$

The modal mass for the sandwich panel with clamped edges, assuming contribution from the face sheets only, is

$$M_{mn} = 2\, \rho\, t_2\, a\, b \tag{156}$$

Substitution of Equations (156) and (155) into Equation (150) gives an expression for rms modal response to a random normally incident pressure wave. The result is

$$\bar{W}_{mn} = 0.432\, \frac{\bar{P}o}{\rho t_2}\, \delta_{mn}^{-1/2}\, \Omega_{mn}^{-3/2} \tag{157}$$

The stress response can be estimated by combining Equations (157), (133), (134), (135), and (137).

The equations are useful only for the full depth honeycomb sandwich portion of the panel (i.e., the equations are not to be used for the thin tapered edge).

III - EXPERIMENTAL

A. Introduction

The objectives of the experimental investigation were:

- To increase the accuracy of existing skin-stringer and honeycomb sandwich design nomographs.
- To extend the range of application of existing skin-stringer and honeycomb sandwich design nomographs.

To accomplish the intent of the investigation, high-intensity, random-noise, sonic fatigue tests of 120 specimens were conducted. Tests were made on 30 skin-stringer designs and 30 honeycomb sandwich designs, 2 each to check repeatability. The test specimen design covered a wide range of parameters. The skin-stringer design parameter limits were:

skin thickness	0.020 to 0.100 inch
rib thickness	0.027 to 0.125 inch
rib spacing	3.00 to 10.00 inches
aspect ratio	1.50 to 3.00

Honeycomb sandwich parameter limits were:

facing sheet thickness	0.008 to 0.040 inch
doubler thickness	0.015 to 0.090 inch
core thickness	0.25 to 0.82 inch
edge thickness	0.025 to 0.115 inch
overall size	21 x 21 inches to 37 x 61 inches
aspect ratio	1.0 to 1.7

A description of the test specimens, test procedure, skin-stringer tests, and honeycomb sandwich tests is given in the following subsections.

B. Test Specimen Design

Detailed drawings of the test specimens are presented in Appendix Vi; however, a brief description of them is given here. A few photographs and line drawings are also presented.

The test specimens were designed using the applicable design nomographs in Reference 1. Fastener edge distances, etc., were selected in accordance with accepted aircraft standards. Standard manufacturing techniques and processes were used in test specimen fabrication. All ribs and stringers were aluminum alloy extrusions. In a few instances, chemical milling was required to obtain the desired flange and web thickness. Bonding and finishing processes were checked against process standards. Quality control procedures were used at all times. All test specimens were made of 7075-T6 clad aluminum alloy.

1. Skin-Stringer

The skin-stringer test specimens were designed as shown in Figure 16, with the details shown in Table IV. The number of ribs and stringers on each test specimen was determined by the stringer spacing and aspect ratio of each bay. For example, Figure 17 is a photograph of a typical nine-bay test specimen showing the skin side and the stringer and rib side.

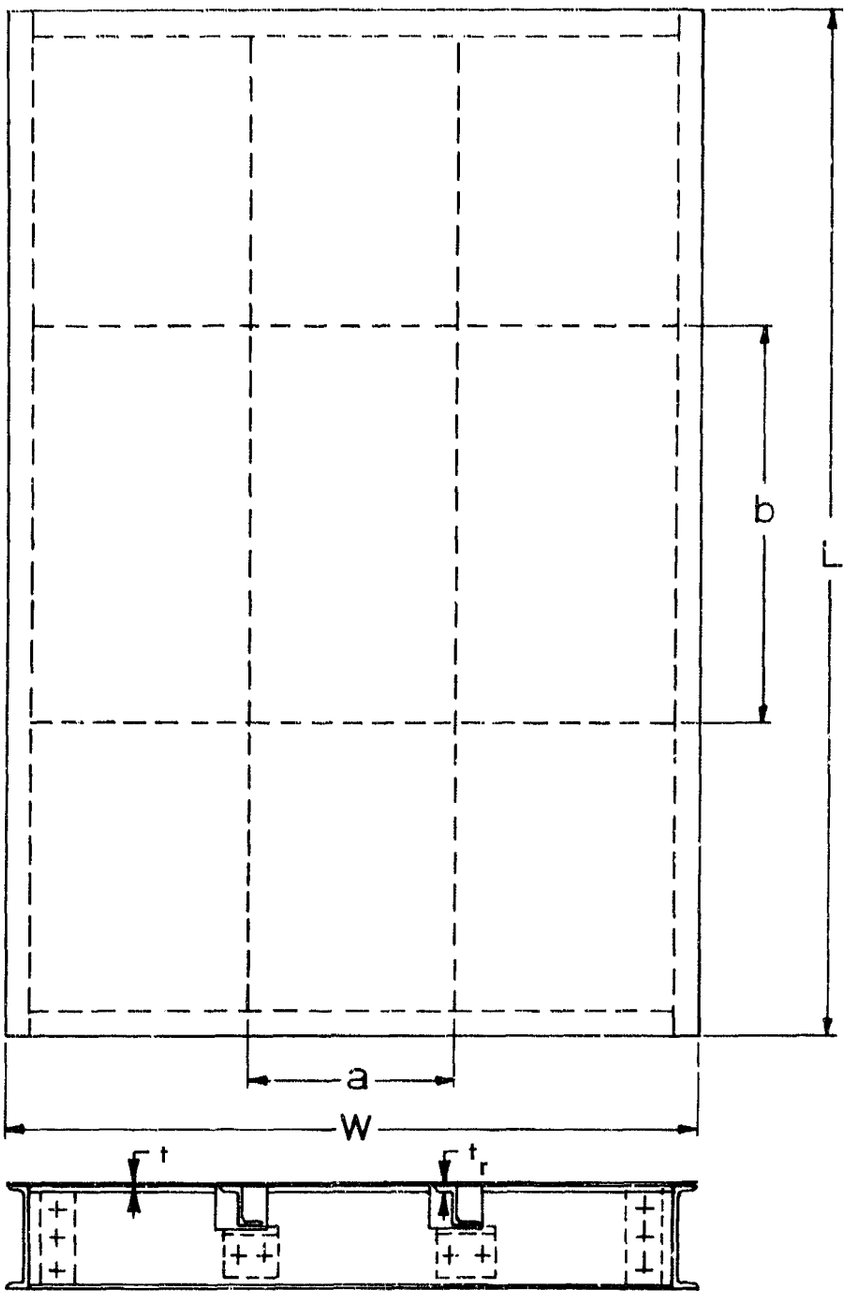

FIGURE 16. SKIN-STRINGER TEST SPECIMEN DRAWING

TABLE IV

SKIN-STRINGER TEST SPECIMEN DETAILS

Designation	Quantity	No. Bays	Dimensions*							Remarks
			L	W	a	b	r	t_r	b/a	
STR-1	2	9	30	20	6.00	12.00	.032	.040	2.0	lipped stringer
STR-2	2	9	30	20	6.00	12.00	.032	.040	2.0	
STR-3	2	9	30	20	6.00	12.00	.032	.040	2.0	
STR-4	2	12	30	20	4.00	8.00	.032	.050	2.0	
STR-5	2	9	30	20	5.00	10.00	.050	.071	2.0	
STR-6	2	9	30	20	9.00	18.00	.071	.071	2.0	
STR-7	2	9	30	20	5.00	10.00	.020	.027	2.0	
STR-8	2	9	30	20	6.00	12.00	.100	.125	2.0	
STR-9	2	9	30	20	9.00	18.00	.040	.040	2.0	
STR-10	2	9	30	20	6.00	9.00	.032	.040	1.5	
STR-11	2	9	30	20	8.00	16.00	.032	.032	2.0	
STR-12	2	9	30	20	5.00	10.00	.025	.032	2.0	
STR-13	2	12	30	20	4.00	8.00	.020	.032	2.0	
STR-14	2	9	30	20	9.00	18.00	.050	.050	2.0	
STR-15	2	12	30	20	3.00	6.00	.025	.040	2.0	
STR-16	2	9	30	20	5.00	10.00	.040	.050	2.0	
STR-17	2	9	30	20	7.00	14.00	.050	.063	2.0	
STR-18	2	12	30	20	4.00	8.00	.040	.063	2.0	
STR-19	2	9	30	20	6.00	12.00	.063	.080	2.0	
STR-20	2	9	30	20	10.00	20.00	.090	.090	2.0	
STR-21	2	9	30	20	6.00	12.00	.032	.040	2.0	same as STR-3
STR-22	2	9	30	20	5.00	10.00	.051	.070	2.0	same as STR-5
STR-23	2	12	30	20	6.00	9.00	.032	.040	1.5	redesign of STR-10
STR-24	2	9	30	20	9.00	18.00	.040	.040	2.0	
STR-25	2	12	30	20	4.00	6.00	.040	.063	1.5	
STR-26	2	9	30	20	6.00	9.00	.063	.080	1.5	
STR-27	2	12	30	20	4.00	12.00	.040	.063	3.0	
STR-28	2	9	30	20	6.00	18.00	.063	.080	3.0	
STR-29	2	9	30	20	5.00	10.00	.032	.050	2.0	
STR-30	2	9	30	20	8.00	16.00	.050	.064	2.0	

*Letters representing test specimen dimensions refer to Figure 16, Skin-Stringer Test Specimen Drawing.

FIGURE 17. TYPICAL SKIN-STRINGER TEST SPECIMEN SHOWING SKIN AND BACK-UP STRUCTURE SIDES

Each test specimen was designed in accordance with Figure 31, Reference 1. MS20426AD rivets were sized and spaced as specified by the design nomograph for fasteners, Figure 35, Reference 1.

2. Honeycomb Sandwich

The honeycomb sandwich test specimens were designed using Figure 41, Reference 1. Figure 18 is a drawing showing test specimen details. Figure 19a is a photograph showing the general appearance of a typical honeycomb sandwich test specimen. An enlarged photograph of crushed honeycomb core as it appeared at the edge closure of test specimen HC-29 is shown in Figure 19b. Table V is a listing of the design details for all thirty designs. There were four test specimen sizes, 21" x 21", 21" x 25", 25" x 37", and 37" x 61", and four edge configurations, fiberglass closure pan, aluminum alloy closure pan, crushed core edges, and tapered doubler.

Doubler widths were determined at first using a conservative rule of thumb based on static test results. After testing four honeycomb sandwich beams described in Section III.D, a rule of thumb for designing to meet sonic fatigue requirements was established at about the half-way point in the test program. Specimen configuration HC-15 and all subsequent doubler widths were established from the new rule of thumb.

Honeycomb core densities were determined using the core shear design nomograph in Section V.C.

C. General Test Procedure

The various tests were conducted using the following procedure:

1. Modal Frequency Studies

Mode shapes for each test specimen design were determined at the beginning of the program. The test specimen to be observed was fastened to a picture frame mounting fixture. This mounting fixture was then placed over two electromechanical speakers arranged as shown in Figure 20. Cork particles were sprinkled on the surface of the vibrating test specimen to produce a Chladni pattern for each mode of concern. See Figure 21. When possible, mode shapes for each test specimen design were determined through the (3,3) mode.

2. Test Specimen Instrumentation

After a thorough study of test specimen response characteristics, strain gage locations were selected. Figure 22 shows typical uniaxial gages mounted on skin-stringer test specimens. Typical uniaxial gages mounted on honeycomb sandwich test specimens are presented in Figure 23.

A strain gage rosette was mounted at the center of one of the honeycomb sandwich test specimens to estimate the direction and value for the maximum principal stress. See Figure 24 for strain rosette location.

TYPICAL FIBERGLAS
EDGE MEMBER
CORNER CONSTRUCTION

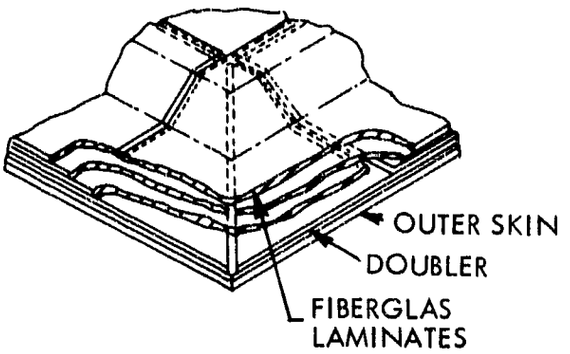

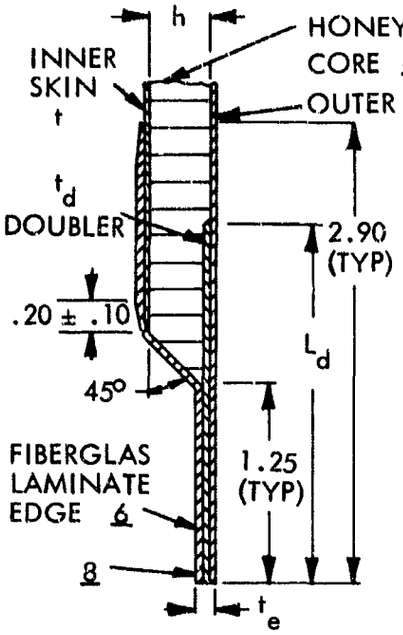

DETAIL A

NOTES:

1. Fabricate per LAC 1241.
2. Machine per LAC 0701.
3. Bevel to be accomplished by machining, except HC-28 which is to be crush formed.
4. Indicates core direction.
5. Bond per LAC 2009. Use HT 424.
6. Epoxy prepreg BP 908-181 Volan "A" 4 ply laminate.
7. 3.4-3/16-15N(5052H39) core.
8. Aluminum alloy metal edge HC-27 and HC-29.
9. Material to be 7075-T6 clad.

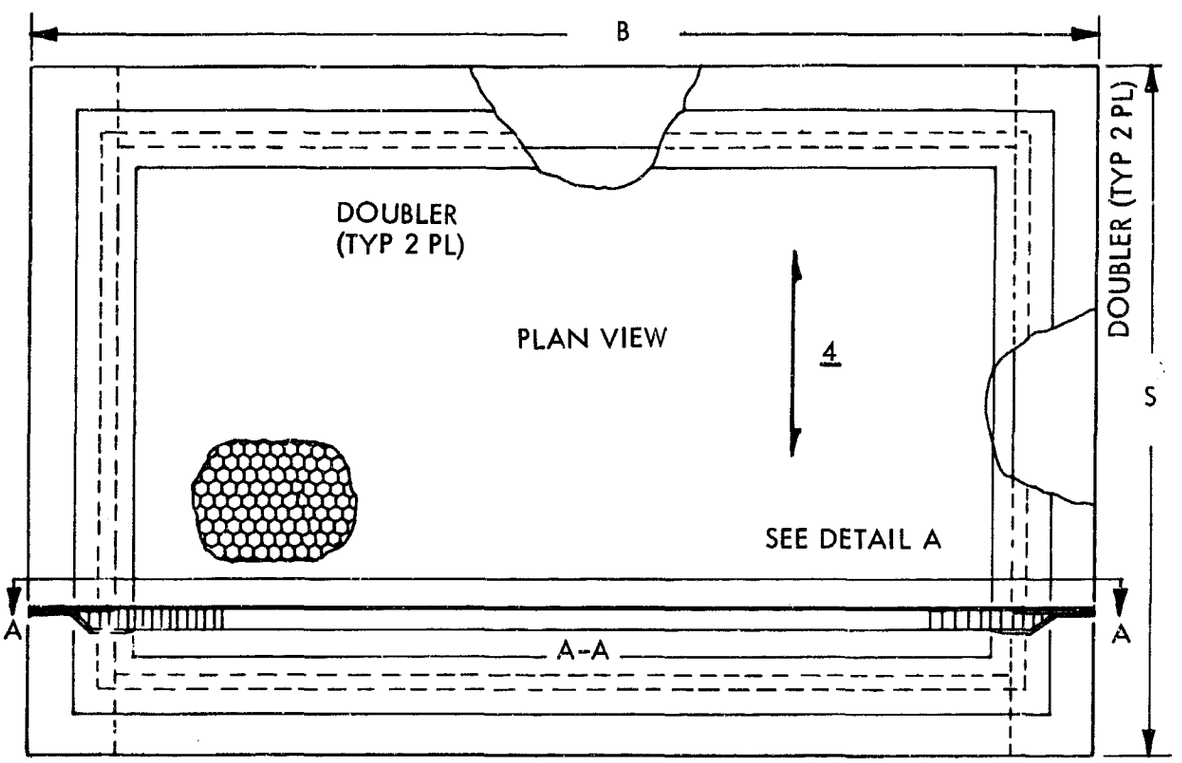

FIGURE 18. ALUMINUM HONEYCOMB SANDWICH TEST SPECIMEN DETAILS

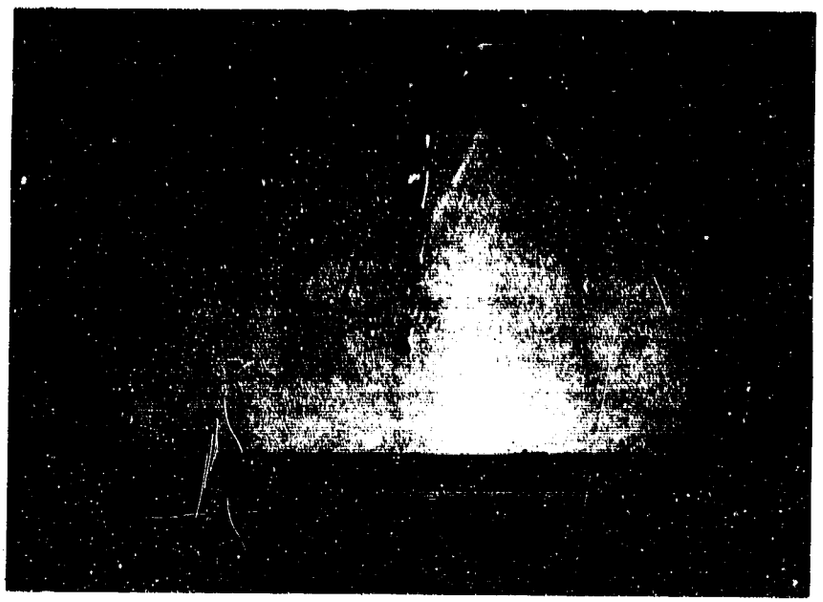

(a) Typical Test Specimen

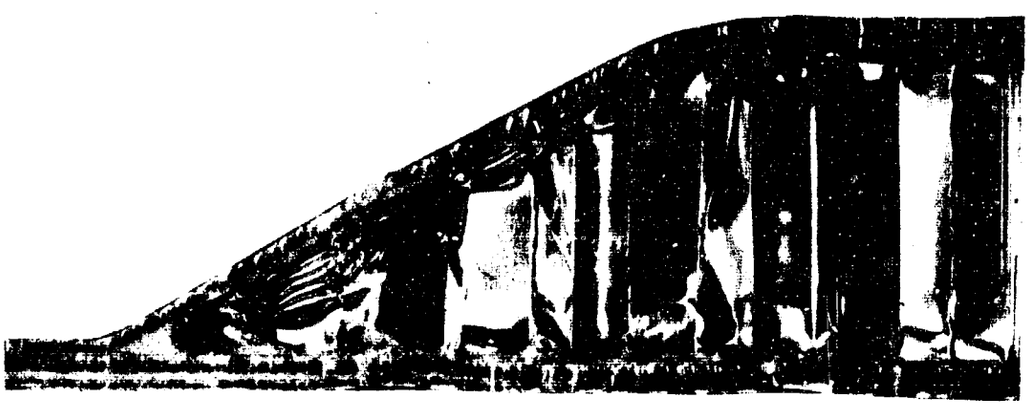

(b) Crushed Honeycomb Core - At Edge Closure of HC-29

FIGURE 19. HONEYCOMB SANDWICH TEST SPECIMEN

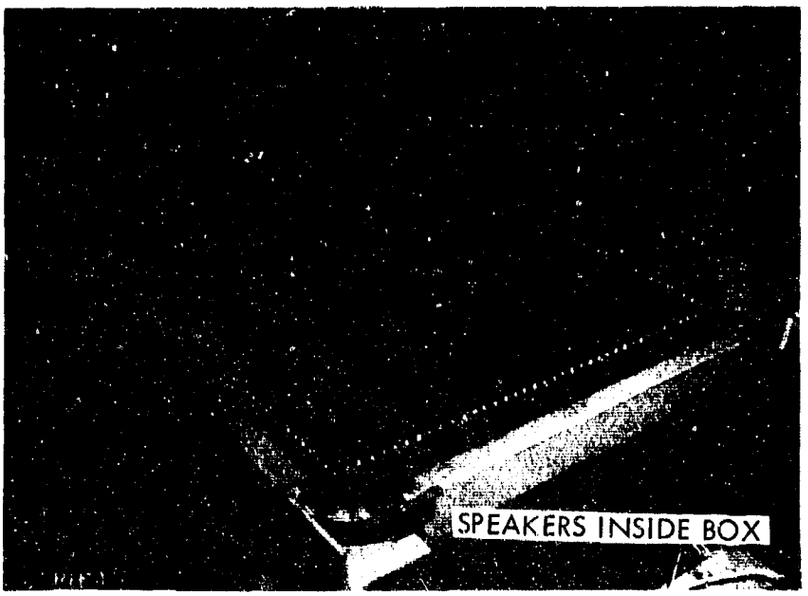

FIGURE 20. TEST SPECIMEN MOUNTED FOR MODAL FREQUENCY STUDY

FIGURE 21. CHLADNI PATTERN DEVELOPED FOR (1,3) MODE, STR-6

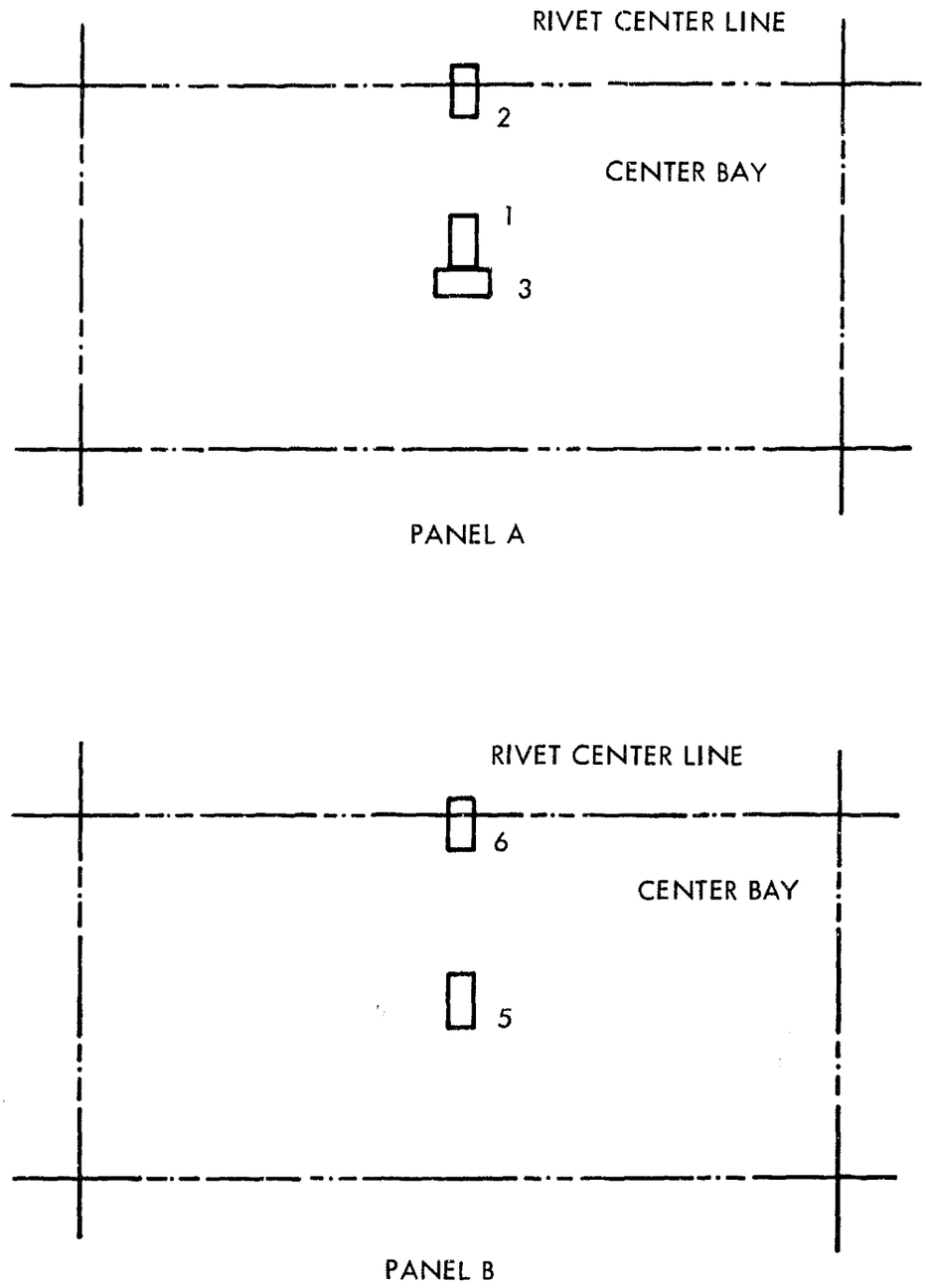

FIGURE 22. STRAIN GAGE LOCATIONS FOR SKIN-STRINGER PANELS

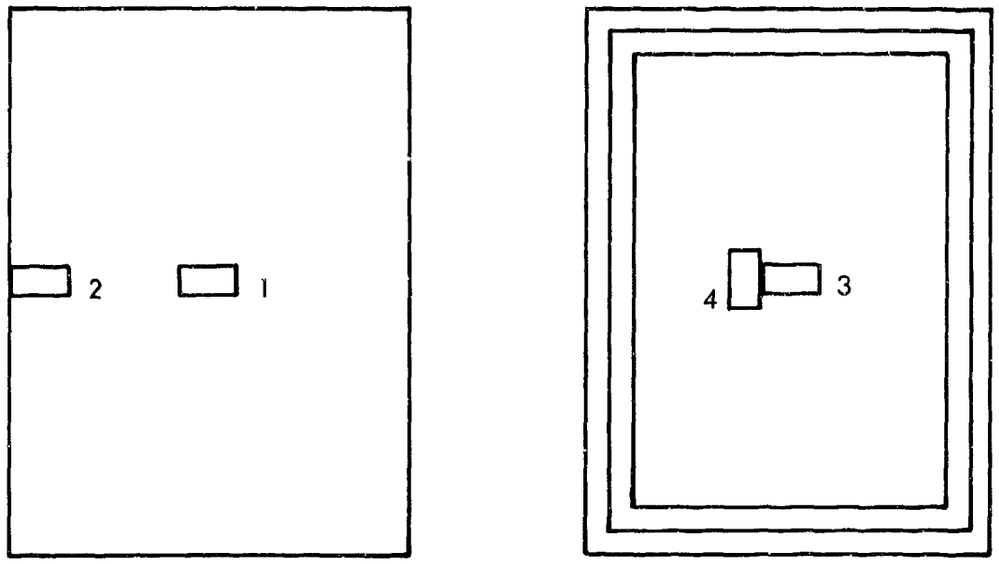

PANEL A

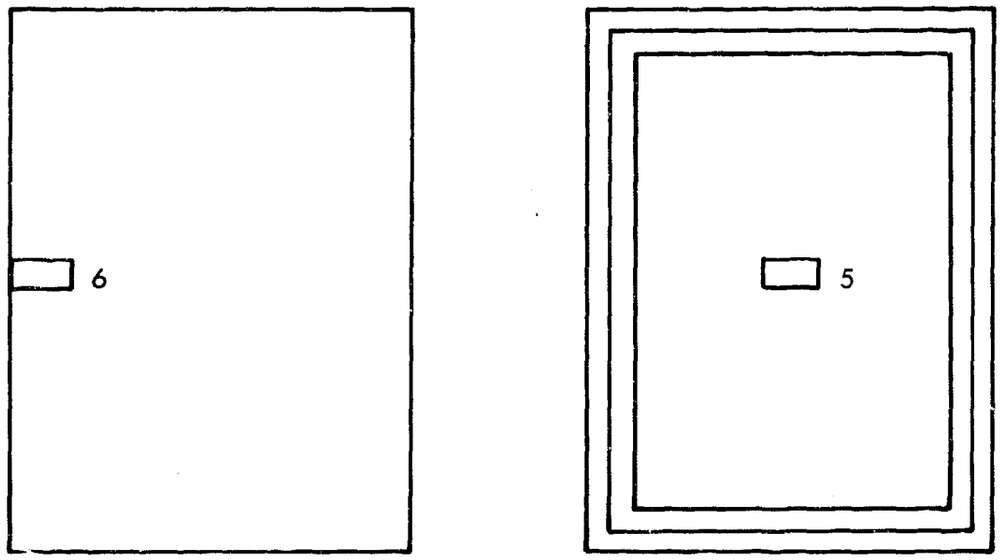

PANEL B

FIGURE 23a. STRAIN GAGE LOCATIONS FOR RECTANGULAR HONEYCOMB SANDWICH PANELS

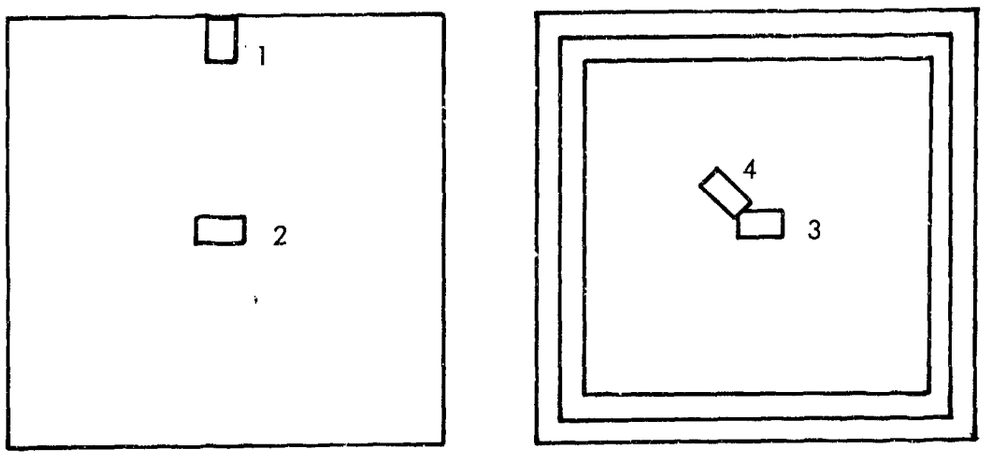

PANEL A

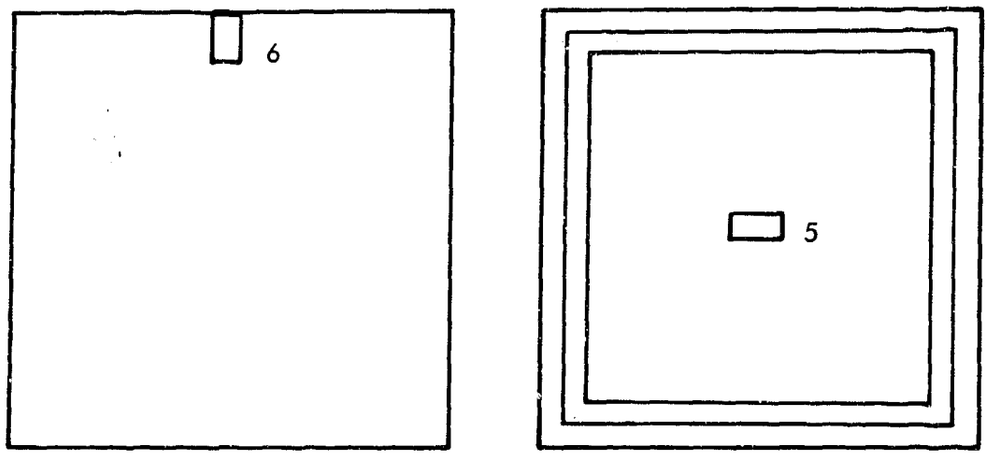

PANEL B

FIGURE 23b.
STRAIN GAGE LOCATIONS FOR SQUARE HONEYCOMB SANDWICH PANELS

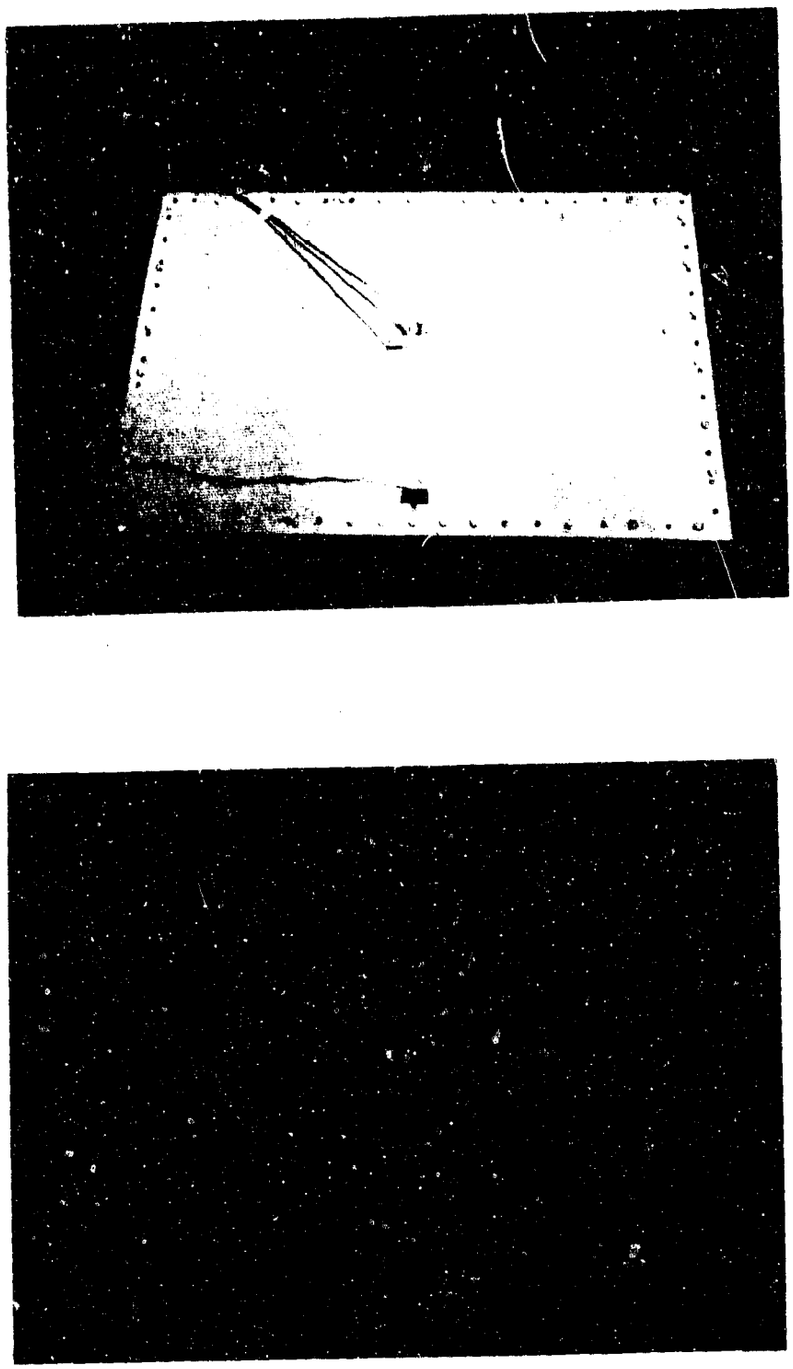

FIGURE 24. HONEYCOMB SANDWICH PANELS SHOWING STRAIN GAGE ROSETTES

TABLE V

HONEYCOMB SANDWICH TEST SPECIMEN DESIGN DETAILS

Description	Quantity	Dimensions B	S	h	t_1 & t_2	t_d	L_d	t_e	Aspect Ratio* b/a
HC-1	2	25	21	.27	.025	.025	2.16	.050	1.2
HC-2	2	25	21	.38	.016	.025	2.39	.041	1.2
HC-3	2	25	21	.38	.016	.025	2.39	.041	1.2
HC-4	2	25	21	.31	.040	.030	2.18	.070	1.2
HC-5	2	25	21	.27	.010	.015	2.16	.025	1.2
HC-6	2	25	21	.27	.016	.020	2.16	.036	1.2
HC-7	2	25	21	.38	.025	.032	2.39	.057	1.2
HC-8	2	25	21	.82	.010	.015	3.71	.025	1.2
HC-9	2	21	21	.25	.025	.025	2.00	.050	1.0
HC-10	2	31	21	.29	.025	.025	2.12	.050	1.5
HC-11	2	25	21	.27	.025	.080	2.16	.105	1.2
HC-12	2	25	21	.38	.016	.090	2.39	.106	1.2
HC-13	2	25	21	.38	.016	.072	2.39	.089	1.2
HC-14	2	25	21	.31	.032	.072	2.18	.104	1.2
HC-15	2	25	21	.27	.010	.064	2.16	.074	1.2
HC-16	2	25	21	.27	.016	.072	1.79	.088	1.2
HC-17	2	25	21	.38	.025	.090	2.01	.115	1.2
HC-18	2	25	21	.82	.010	.090	2.89	.100	1.2
HC-19	2	21	21	.25	.025	.072	1.75	.097	1.0
HC-20	2	31	21	.29	.025	.080	1.83	.105	1.5
HC-21	2	25	21	.42	.008	.064	2.09	.072	1.2
HC-22	2	25	21	.27	.010	.015	1.79	.025	1.2
HC-23	2	21	21	.42	.008	.064	2.09	.072	1.0
HC-24	2	21	21	.27	.010	.015	1.79	.025	1.0
HC-25	2	25	21	.27	.016	.072	1.79	.088	1.2
HC-26	2	37	25	.50	.016	.025	2.25	.041	1.5
HC-27[1]	2	37	25	.63	.012	.032	2.51	.069	1.5
HC-28[2]	2	37	25	.50	.016	.025	2.25	.041	1.5
HC-29[3]	2	37	25	.63	.012	.040	2.51	.082	1.5
HC-30	2	61	37	.75	.016	.040	2.75	.056	1.7

* Aspect ratio computed using fastener line dimensions.

1. .025" aluminum pan closing member.
2. Core crushed at edges to accomplish taper.
3. .030" aluminum pan closing member and tapered doubler.

3. Damping Studies

An average damping ratio, δ, was determined for first mode response. In every case the test specimen used was equipped with four strain gages. The first mode was excited using the electromechanical speaker arrangement described previously. Decaying strain oscillations were used to determine δ by the log-decrement method.

4. Sinusoidal Frequency Sweeps

Test specimen A and test specimen B of a given design, strain gaged as described above, were mounted to a picture frame mounting fixture. The complete assembly was then mounted on the progressive wave test section of the High Intensity Structural Test Facility. Figures 25 and 26 present a typical test arrangement.

Grazing incidence sinusoidal frequency sweeps in the range of 50 - 2000 Hz were made at a sound pressure level of 140 db to determine the test specimen strain response. Strains from all six gages were monitored. They were then studied and used to shape the broad-band acoustical excitation for the fatigue tests.

5. Broad-Band Acoustical Noise Test Spectra

The test specimen picture-frame assembly was removed from the progressive wave test section and replaced by a one-inch thick plywood panel. The test sound pressure spectrum was then shaped out of the presence of the vibrating test specimens and in accordance with the strain responses obtained from the sinusoidal sweeps. Spectrum shaping was necessary to concentrate the acoustical energy in a desired range of frequencies.

The plywood panel was removed when the desired spectrum level and shape were obtained.

6. Fatigue Tests

The test specimen and its picture frame mounting assembly were reinstalled on the progressive wave test section ready for fatigue testing to take place. Inspections were made following test segments ranging from five minutes at the beginning to one hour after ten hours of total exposure to acoustical excitation.

A detailed description of the test procedures, test facilities, data collection and reduction systems, and modal frequency study test setup is given in Appendix I.

D. Test Results

Results of the skin-stringer and honeycomb sandwich panel tests are described in the following subsections.

1. Skin-Stringer Test Results

a. Modal Frequency Studies - Mode shapes for each skin-stringer design were determined, when possible, through the 3,3 mode. A summary of these studies is presented in Table VI.

b. Damping Ratios - In order to obtain an average damping, several decaying strain oscillations of the type shown in Figures 27a and 27b were recorded for each design. An arithmetic average of the damping ratio was calculated for each design. Table VII is a listing of these average damping ratios determined by the log-decrement method.

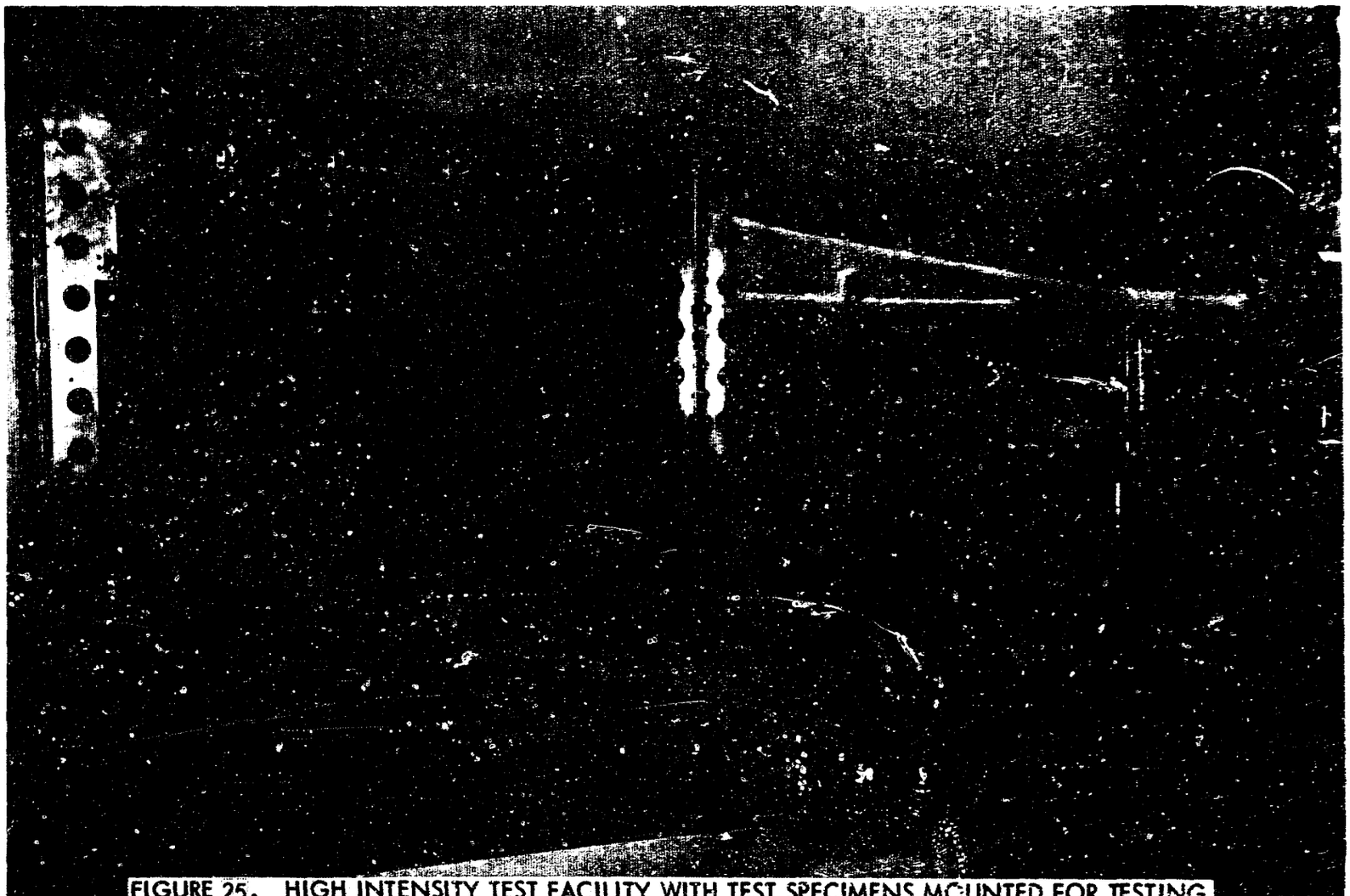

FIGURE 25. HIGH INTENSITY TEST FACILITY WITH TEST SPECIMENS MOUNTED FOR TESTING

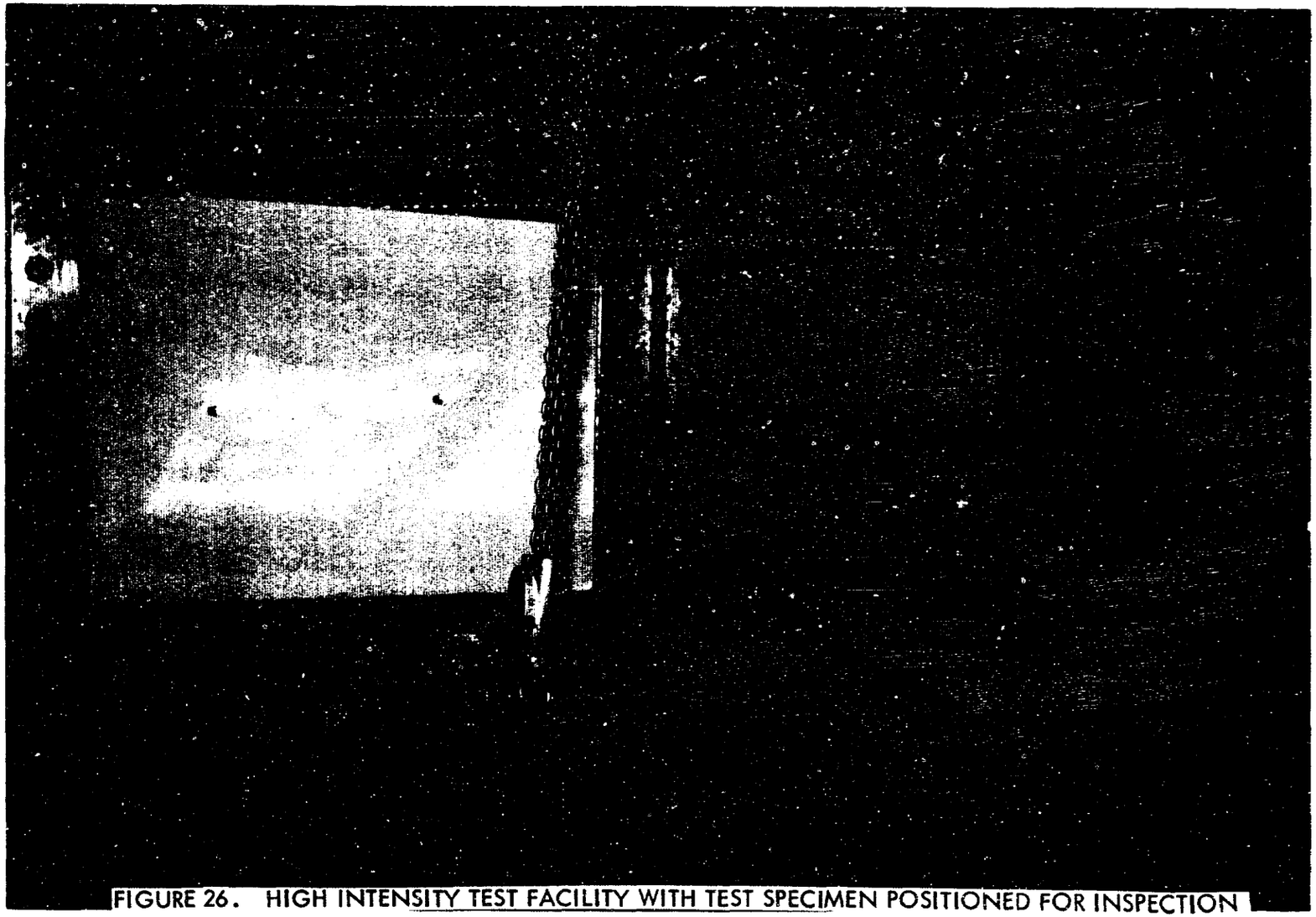

FIGURE 26. HIGH INTENSITY TEST FACILITY WITH TEST SPECIMEN POSITIONED FOR INSPECTION

TABLE VI

SUMMARY OF SKIN-STRINGER MODAL FREQUENCY INVESTIGATION

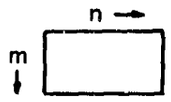

DESIGNATION	m,n	Modal Frequency - Hz							
	1,1	1,2	1,3	2,1	2,2	2,3	3,1	3,2	3,3
STR-1, STR-2, STR-3, STR-21	142	249	358	417	526	637	777	941	1071
STR-4	375	521	743	1006	1196	1445	1638	2056	2349
STR-5, STR-22	328	481	716	892	1121	-	-	-	-
STR-6	133	194	300	346	455	633	528	876	1032
STR-7	156	249	313	357	481	564	709	830	918
STR-8	468	776	1092	1331	1683	2050	-	-	-
STR-9, STR-24	162	192	384	268	326	-	500	535	876
STR-10, STR-23	198	320	470	428	513	679	711	905	1068
STR-11	113	169	238	264	320	381	527	563	640
STR-12	220	331	417	531	641	774	846	1184	1267
STR-13	245	348	-	642	798	-	1054	1282	-
STR-14	139	192	277	310	344	501	628	690	812
STR-15	540	750	1160	930	1700	2211	-	-	-
STR-16	230	361	507	613	715	910	1056	1320	1670
STR-17	183	287	396	451	611	739	811	-	1235
STR-18	290	435	615	705	863	1122	1311	1571	1910
STR-19	310	461	633	715	931	1242	1337	1682	2100
STR-20	154	236	322	439	509	633	-	-	-
STR-25	335	571	706	815	992	1390	1903	1811	2250
STR-26	360	500	745	813	1071	1405	1480	-	2443
STR-27	260	385	546	637	781	1025	1150	-	1778
STR-28	285	437	604	966	855	-	1296	1647	1950
STR-29	216	320	445	507	643	852	960	1131	1505
STR-30	143	216	302	351	428	656	763	-	-

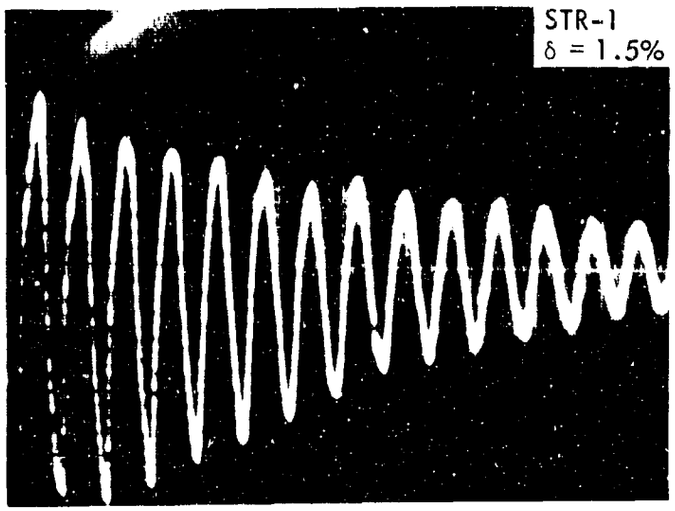

(a) Decaying Strain Oscillations, STR-1

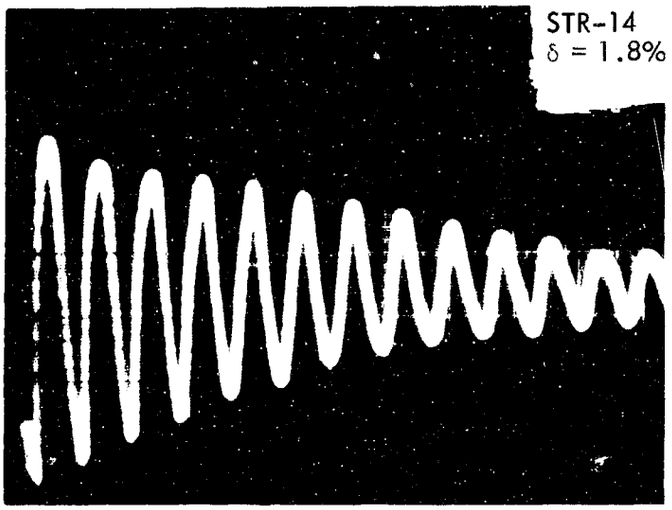

(b) Decaying Strain Oscillations, STR-14

FIGURE 27. LOG-DECREMENT DAMPING-SKIN-STRINGER

TABLE VII

SUMMARY OF SKIN-STRINGER DAMPING RATIOS

Test Specimen Configuration	Average Damping Ratio, %
STR-1	1.5
STR-2	1.8
STR-3	1.4
STR-4	1.0
STR-5	1.3
STR-6	1.0
STR-7	1.6
STR-8	1.7
STR-9	1.7
STR-10	1.8
STR-11	1.1
STR-12	1.3
STR-13	1.7
STR-14	1.8
STR-15	1.5
STR-16	1.8
STR-17	1.7
STR-18	1.3
STR-19	1.4
STR-20	1.3
STR-21	1.5
STR-22	1.3
STR-23	1.2
STR-24	1.5
STR-25	1.3
STR-26	1.7
STR-27	1.5
STR-28	1.2
STR-29	1.4
STR-30	1.3

c. Frequency Sweeps - Figures 28 through 30 are plots of strain response to sinusoidal excitation at 140 db. These frequency sweep plots are representative of the strain responses for all the rib-stringer designs.

d. Broad-Band Acoustical Test Spectra - The acoustical noise test spectra were shaped such that the bandwidth of the excitation was at least three times the bandwidth of the test specimen response. Figures 31 through 33 are representative test spectra for single mode response. Figure 32 is typical for a multimode stress response.

e. Fatigue Tests - Sixty skin-stringer test specimens, 2 each of 30 designs, were fatigue tested until one or more cracks formed in the center bay of the test specimen. Table VIII is a summary of the test results. Figure 34 shows the relationship between overall nominal rms stress along the panel fastener row and the number of positive crossings (cycles roughly) to failure. Ninety-five percent confidence limits were computed as described in Appendix II and as shown in Figure 34.

Magnetic tape recordings were made of the signals from the strain gages positioned along the fastener row. These strain data were analyzed using a narrow band filter (nominal 2Hz.) to determine the characteristics of the strain response to the acoustical excitation. Figures 35 through 38 are the narrow band analyses of typical single modes and multi-modal responses.

In addition to the narrow band analysis, a 10-second sample of the fastener row strain was analyzed using a probability analyzer to determine the probability density of instantaneous strain and probability distribution of strain peaks. Figures 39 through 42 are typical results of the statistical analyses.

2. Honeycomb Sandwich Fatigue Tests

a. Mode Shapes - Results of the modal frequency studies are listed in Table IX. It can be seen that very few of the modes above the (2,1) mode could be excited. Honeycomb panel rigidity coupled with the insufficient driving force from the electromechanical speaker system is believed to be reasons why the higher modes were not detected.

b. Damping Ratios - Damping ratios for the first mode were determined as described for the skin-stringer test specimens. Typical decaying strain oscillations are shown on Figure 43. Arithmetic average damping ratios are listed in the last column of Table IX.

c. Frequency Sweeps - Each test specimen was subjected to frequency sweeps made at a discrete frequency sound pressure level of 145 db. These sweeps were accomplished to determine test specimen strain response characteristics. Typical strain response curves for the honeycomb sandwich test specimens are presented, Figures 44 through 46, to show that a majority of the strain was concentrated in the first mode.

d. Broad-Band Acoustical Noise Test Spectra - Broad-band acoustical noise test spectra were shaped to fit the discrete frequency sweep strain response. Typical spectra are shown in Figures 47 through 49.

e. Fatigue Tests - Sixty flat honeycomb sandwich test sepcimens (designs are described in Table V) were exposed to high-intensity, broad-band noise until a fatigue crack was formed. Table X is a summary of the results of the test. Figure 50 shows the overall rms nominal stress along the fastener row at the edge of the panel and the number of crossings to failure. Figure 51 is a fatigue curve for facing sheet cracking determined in a manner similar to that for the panel edges. Ninety-five-and fifty-percent confidence limits were calculated for both fatigue curves to show the residual variance about the regression line.

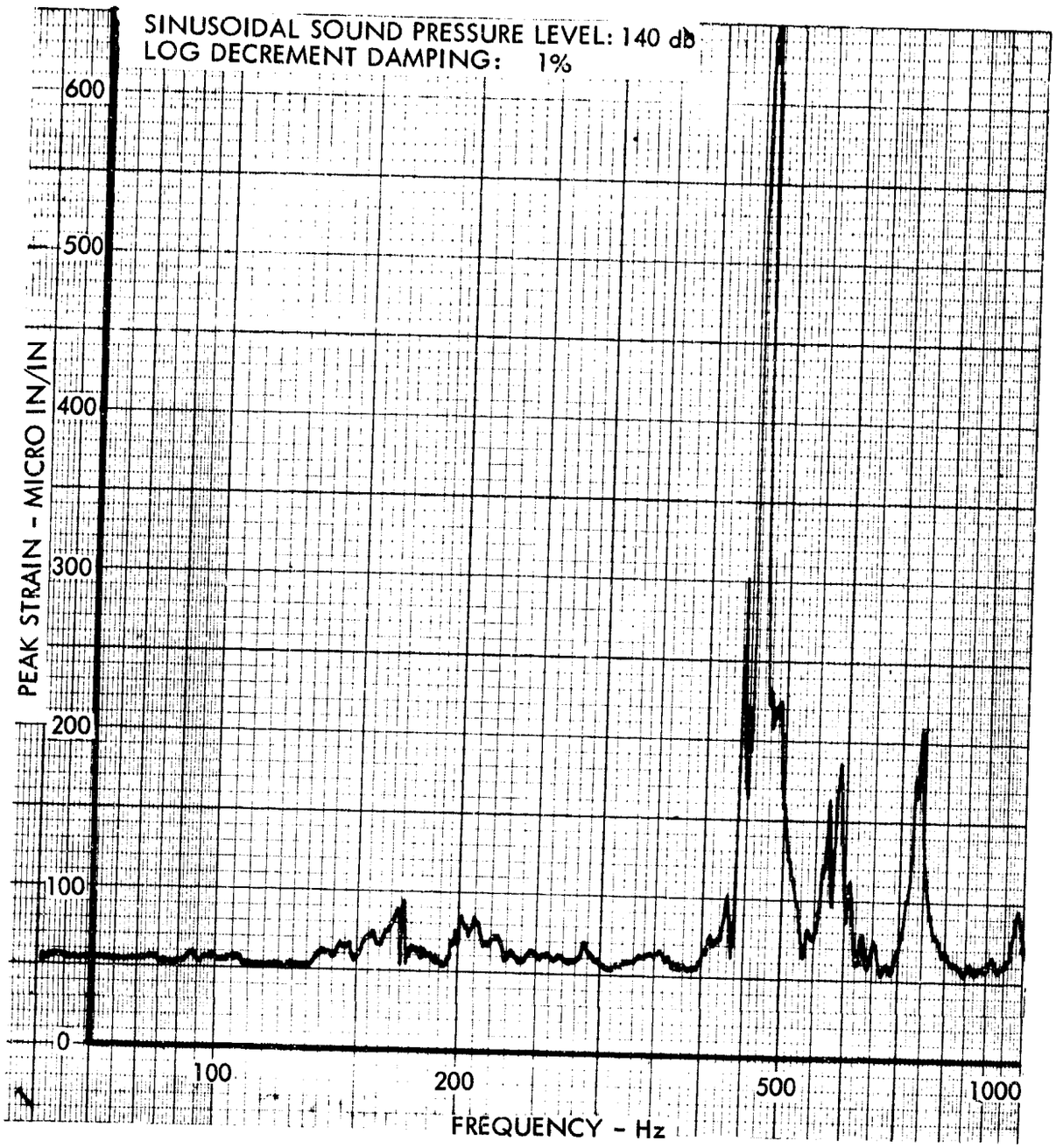

FIGURE 28. SINE-SWEEP EXCITATION - STR 4B

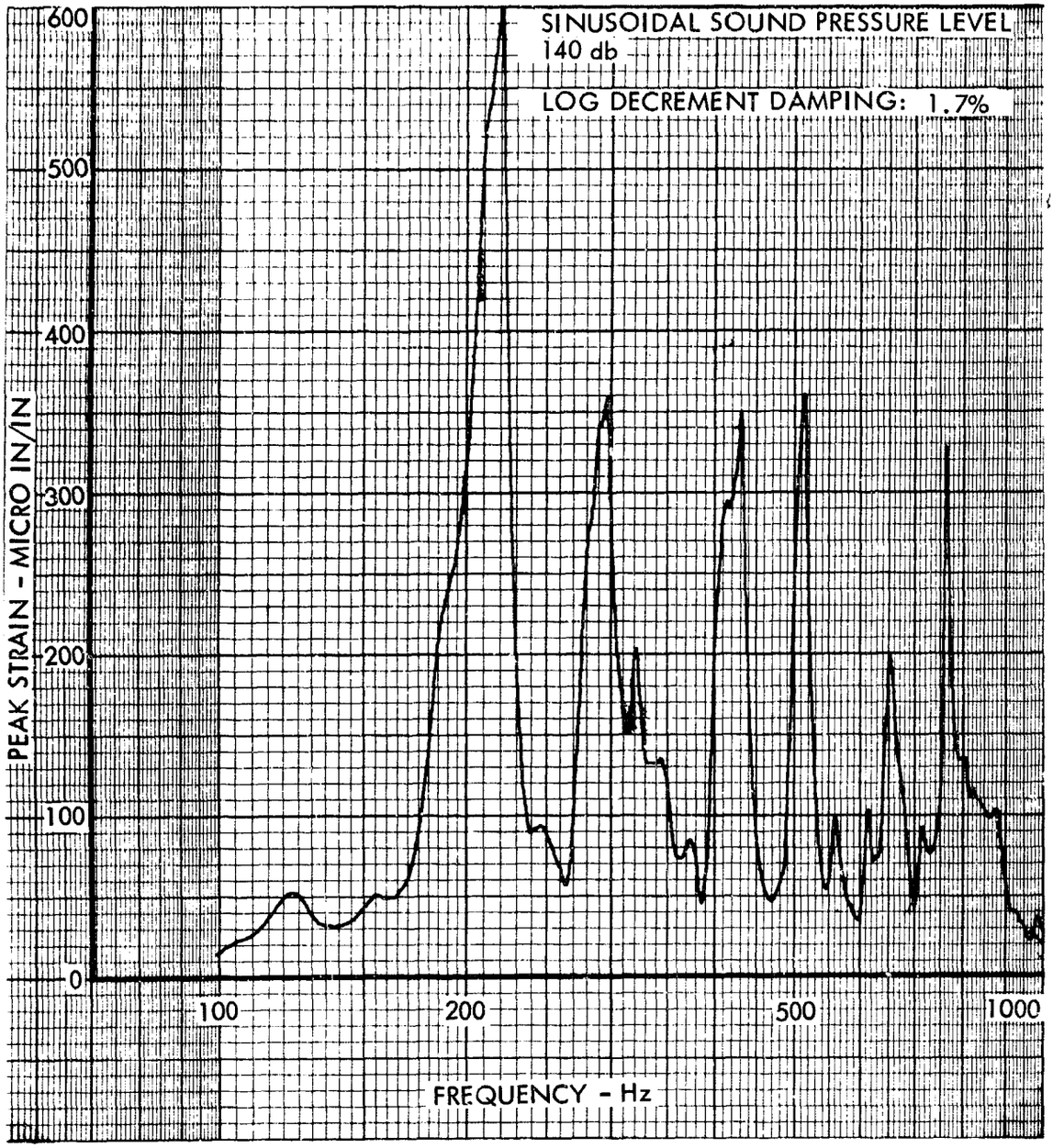

FIGURE 29. SINE-SWEEP EXCITATION - STR 17A

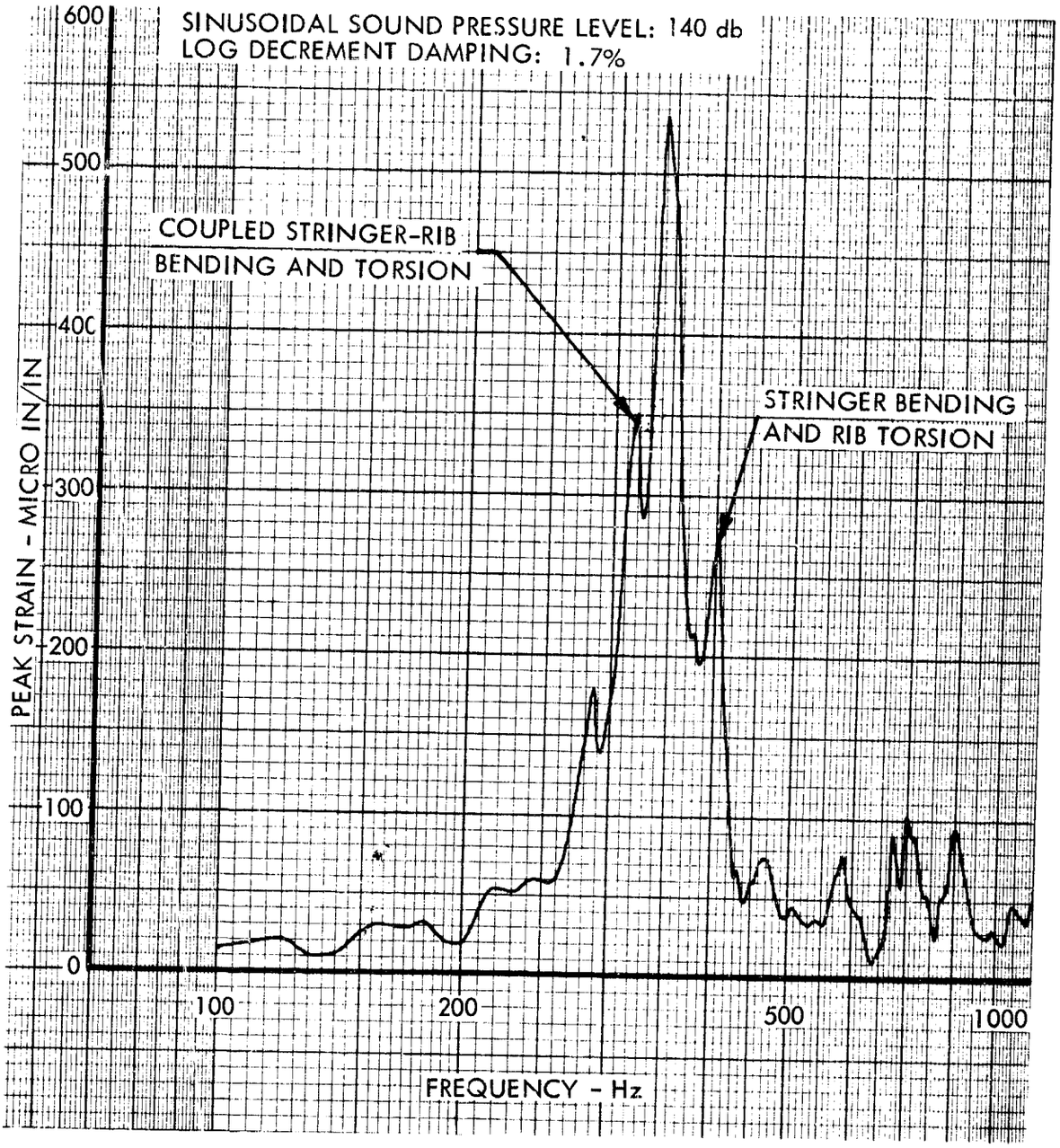

FIGURE 30. SINE-SWEEP EXCITATION - STR 26A

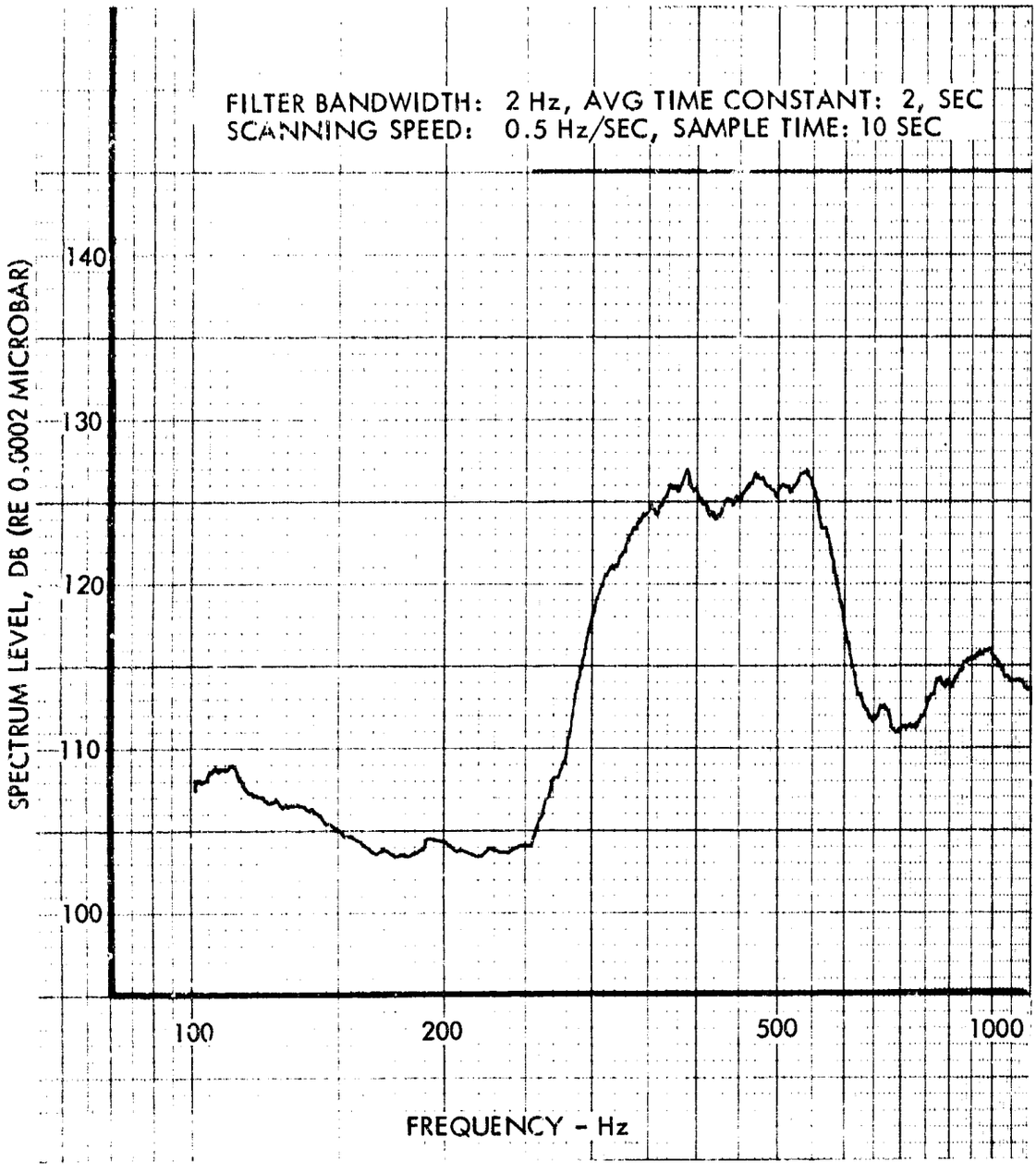

FIGURE 31. BROAD-BAND TEST SPECTRUM - STR 4B

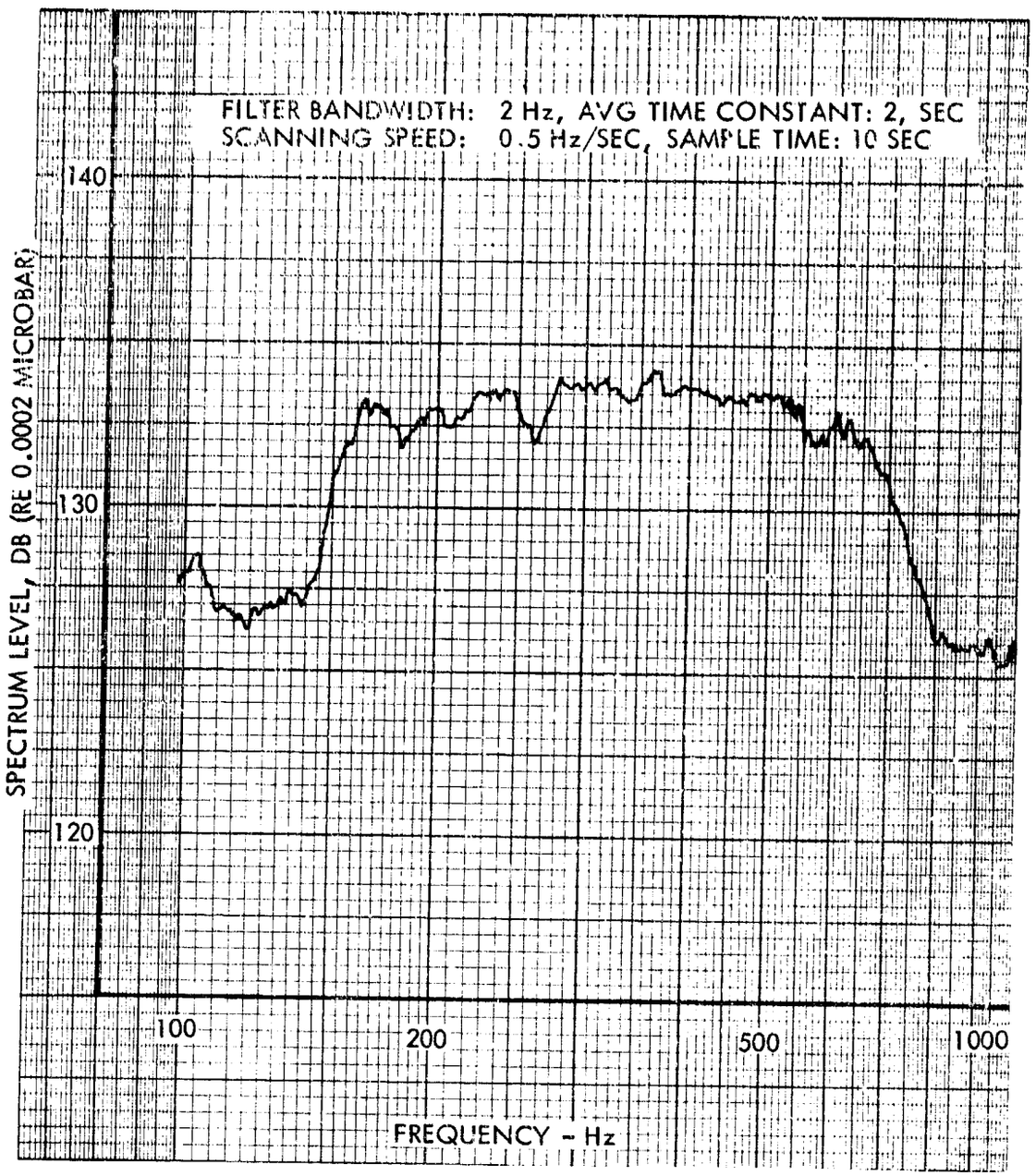

FIGURE 32. BROAD-BAND TEST SPECTRUM - STR 17A

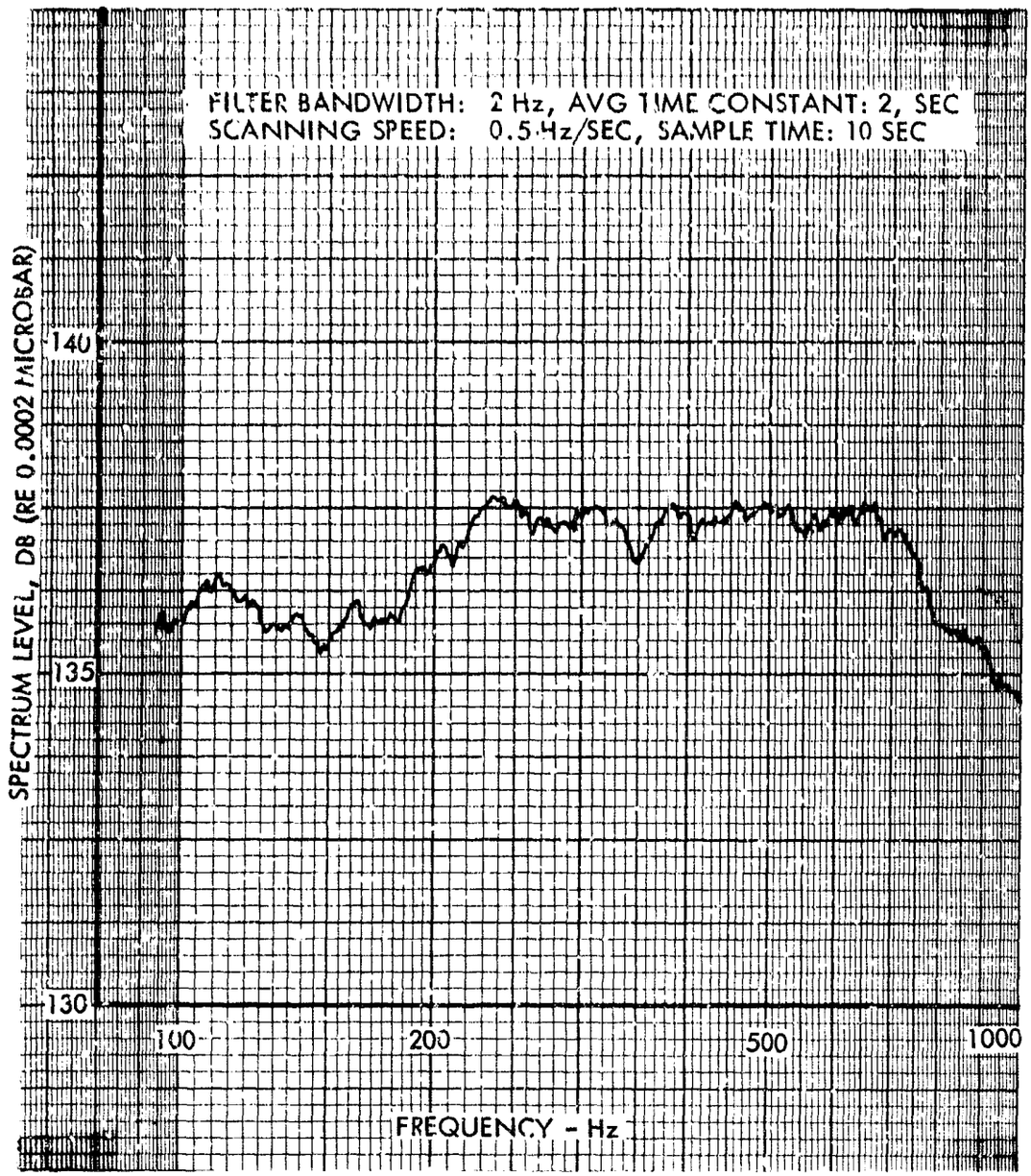

FIGURE 33. BROAD-BAND TEST SPECTRUM - STR 26A

TABLE VIII

SUMMARY OF SKIN-STRINGER FATIGUE TESTS

Designation	Test spectrum level, db	Response frequency, Hz.	Number of crossings to failure, Nc x 10-6	Overall Nominal rms stress, ksi	Remarks
STR-1A	123	200	17.50	5.22	lipped z type stringer
B	122	185	9.10	4.91	
STR-2A	123	125	13.50	4.53	
B	122	125	11.30	4.00	
STR-3A	119	245	27.00	5.05	1,2 mode response
B	117	230	16.00	4.10	
STR-4A	127	350	12.00	5.23	
B	126	460	27.00	5.81	
STR-5A	131	305	1.70	5.50	
B	129	275	10.00	4.71	
STR-6A	130	185	3.65	6.40	
B	128	180	3.00	6.74	
STR-7A	118	225	21.50	4.00	1,2 mode response
B	118	210	20.20	3.35	
STR-8A	140	490	9.70	5.11	
B	138	460	11.60	3.81	
STR-9A	120	150	1.61	6.20	
B	120	150	1.51	6.52	
STR-10A	123	220	1.20	-	results questionable
B	121	280	1.20	-	
STR-11A	119	195	21.60	4.41	1,2 mode response
B	118	200	22.00	5.10	
STR-12A	123	250	21.50	5.10	
B	121	270	23.80	4.07	
STR-13A	123	260	28.00	5.22	
B	122	300	33.00	4.80	
STR-14A	128	130	12.40	4.15	
B	126	150	14.90	5.05	
STR-15A	123	575,750	210.00	3.25	
B	122	575,750	208.00	2.90	
STR-16A	133	270	10.00	6.10	
B	131	250	9.70	6.88	
STR-17A	134	220,290	5.50	6.21	
B	133	240,310	6.00	5.81	
STR-18A	137	300	1.90	7.65	
B	135	340	3.10	8.45	
STR-19A	138	340	4.40	7.35	
B	137	360	4.50	7.17	
STR-20A	137	165	4.50	6.85	
B	135	175	4.70	4.85	
STR-21A	125	220	21.70	3.82	1,2 mode response
B	125	220	23.00	3.92	
STR-22A	131	270	19.00	3.05	
B	129	275	24.00	3.01	

TABLE VIII (Cont'd)

Designation	Test spectrum level, db	Response frequency, Hz.	Number of crossings to failure, Nc x 10^{-6}	Overall Nominal rms stress, ksi	Remarks
STR-23A	123	260	17.00	3.75	
B	121	240	15.50	3.41	
STR-24A	120	150	14.50	3.62	
B	119	145	16.20	4.61	
STR-25A	133	350,600	18.50	5.52	
B	132	350,600	21.60	4.75	
STR-26A	137	345	14.00	4.27	
B	135	390	13.00	6.10	
STR-27A	137	240,400	11.50	5.45	
B	136	240,400	29.00	6.88	
STR-28A	137	310	10.00	6.61	
B	137	290	13.00	6.61	
STR-29A	130	220	9.20	6.91	
B	129	240	8.10	7.10	
STR-30A	140	165	100.00	3.15	
B	138	165	145.00	2.80	

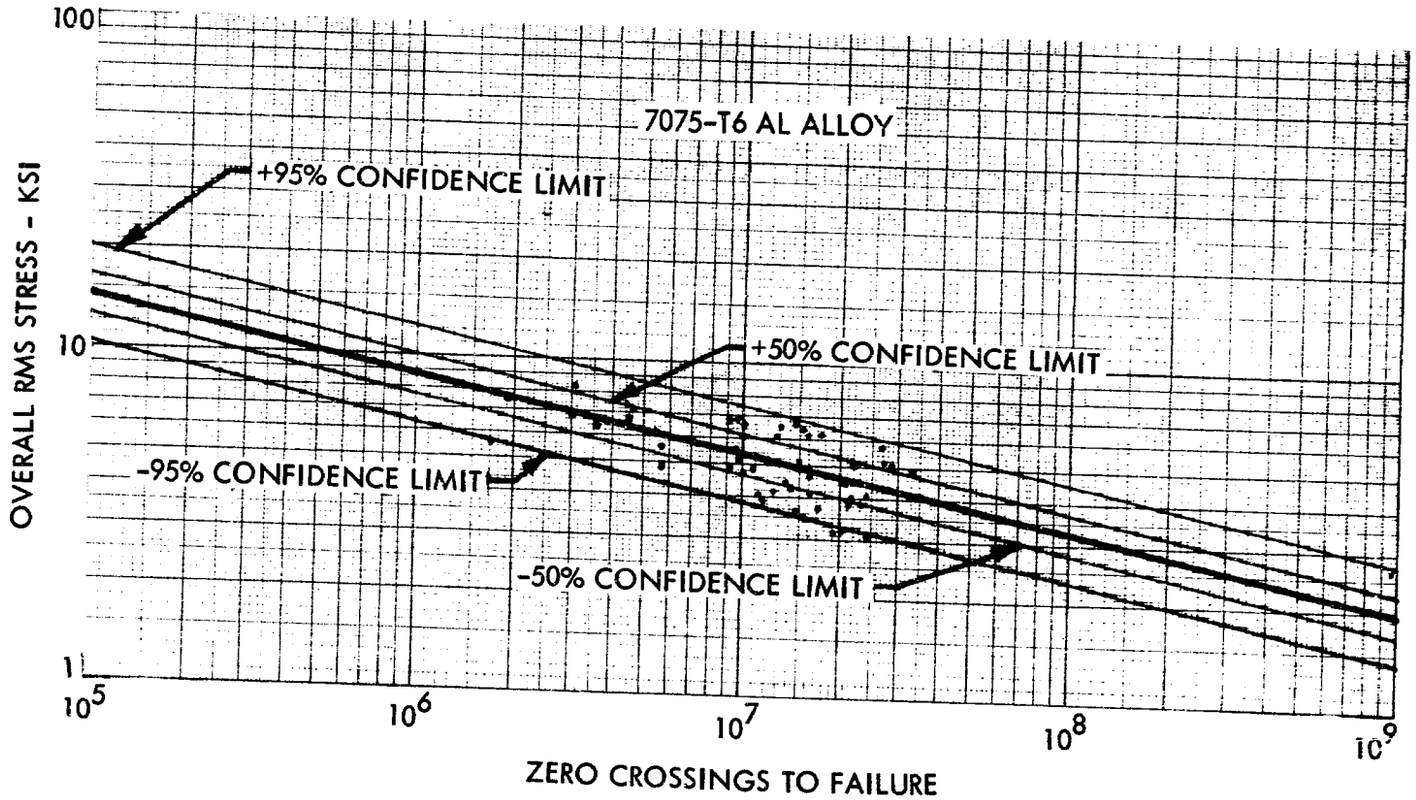

FIGURE 34. SKIN-STRINGER PLATING FATIGUE CURVE

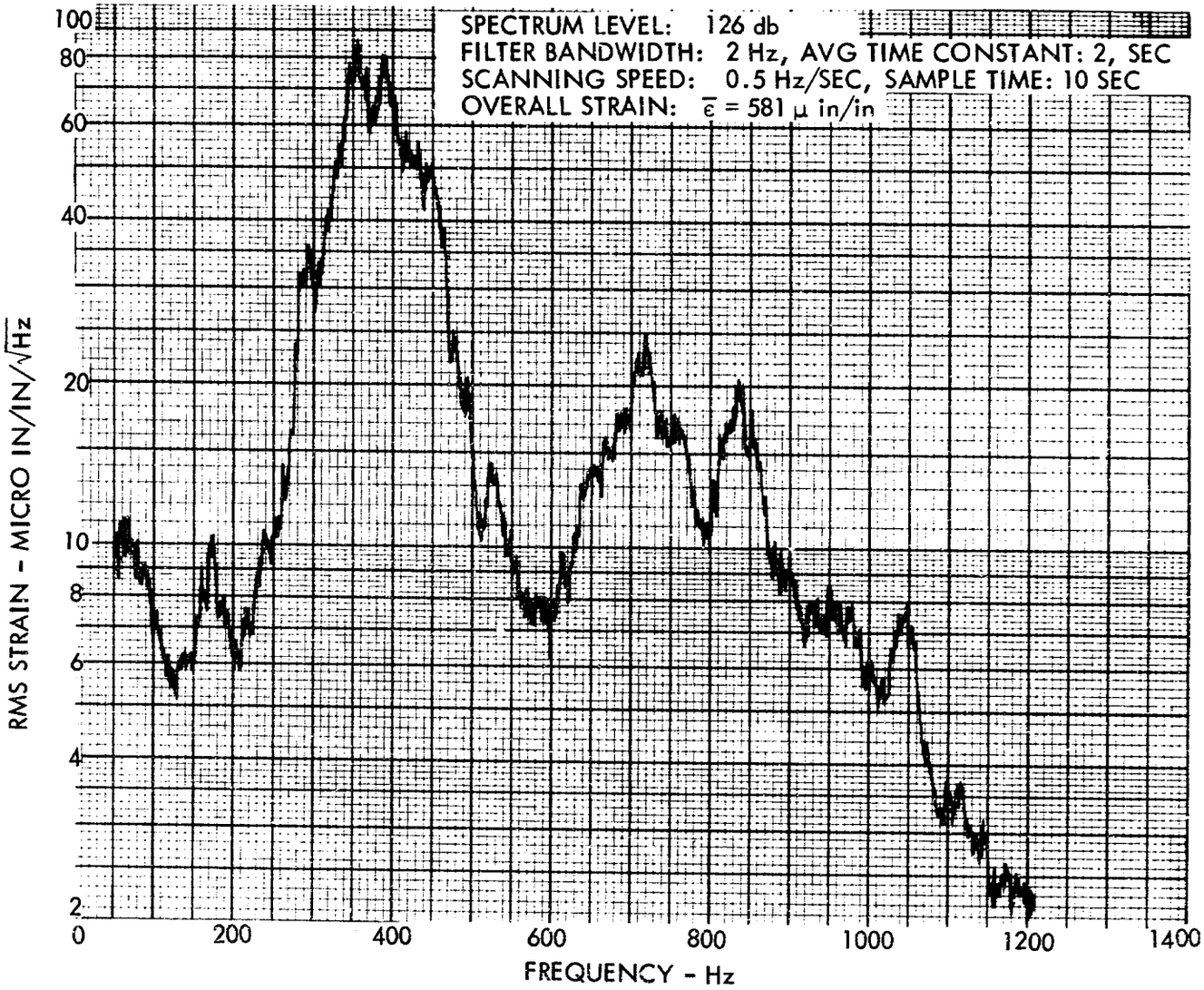

FIGURE 35. NARROW-BAND STRAIN ANALYSIS - STR 4B

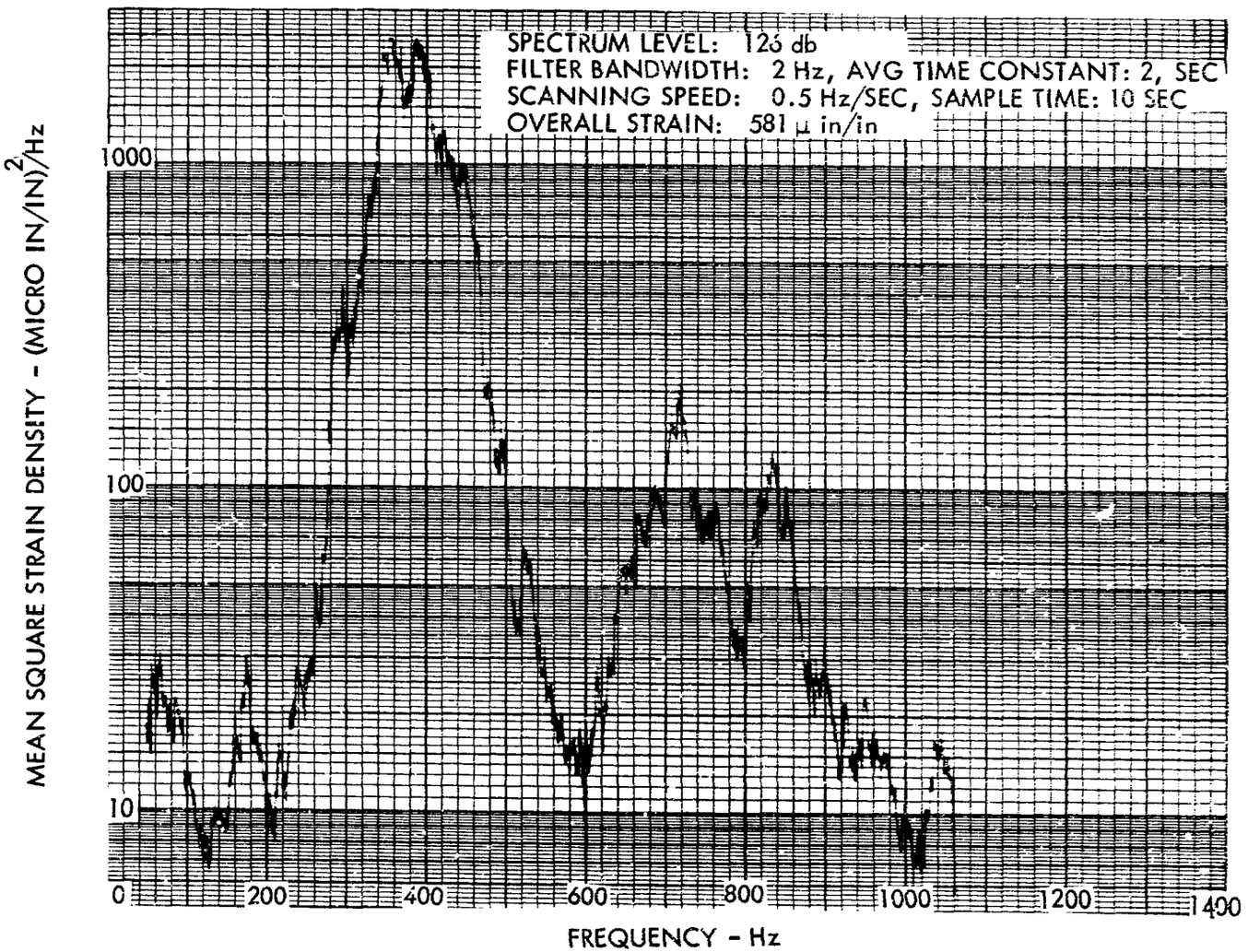

FIGURE 36. PSD STRAIN ANALYSIS - STR 4B

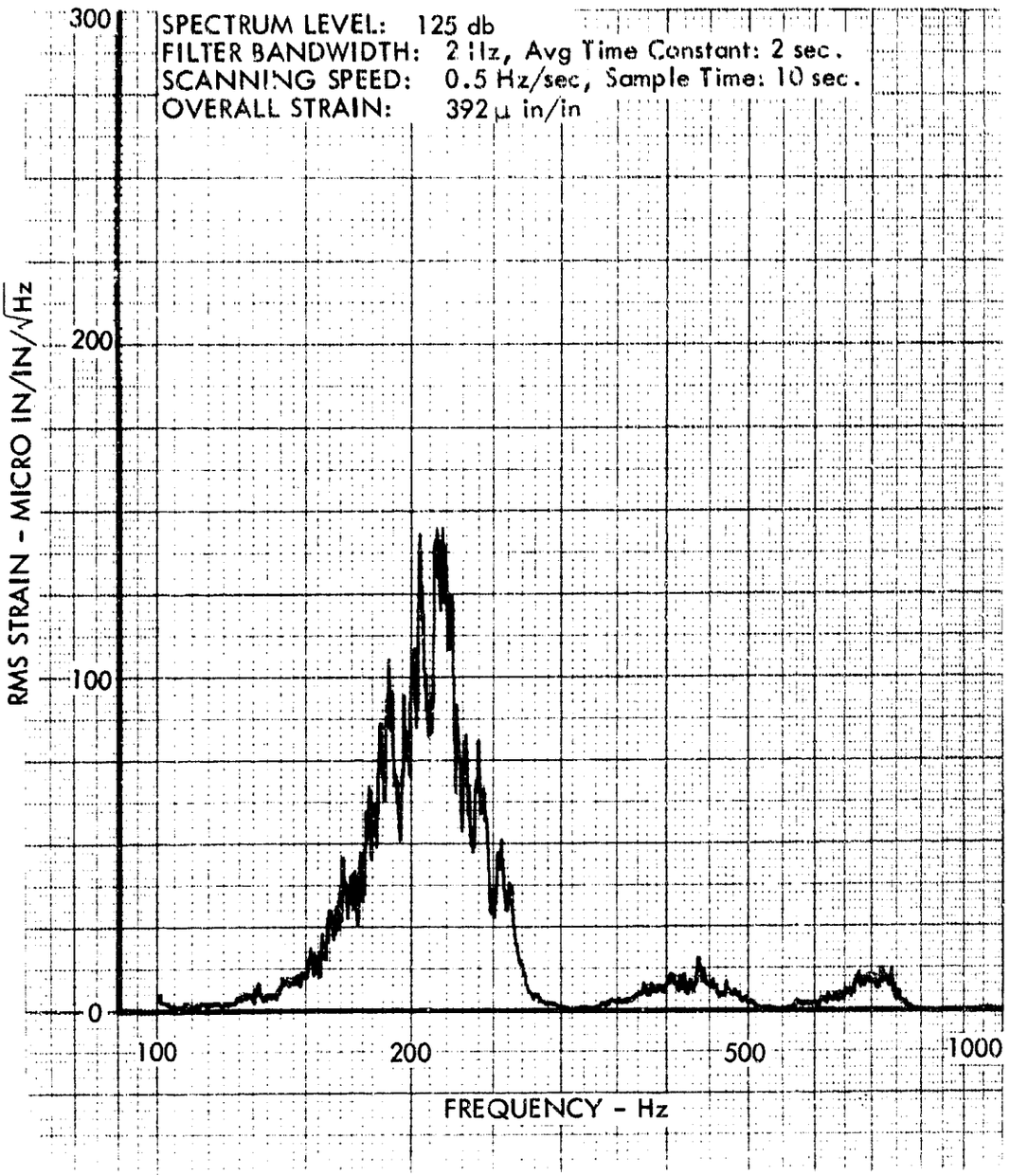

FIGURE 37. NARROW-BAND STRAIN ANALYSIS - STR 21B

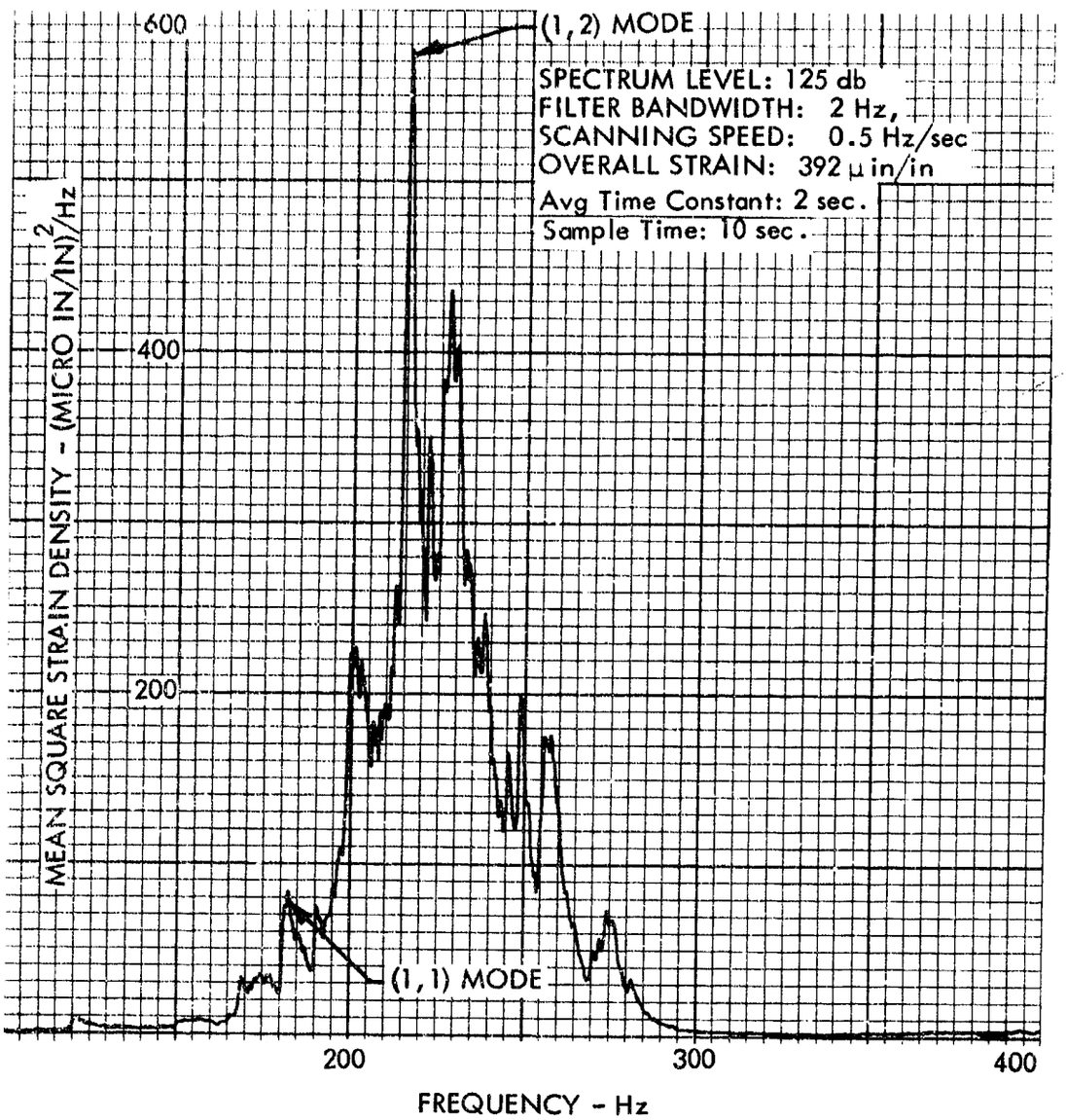

FIGURE 38. PSD STRAIN ANALYSIS - STR 21B

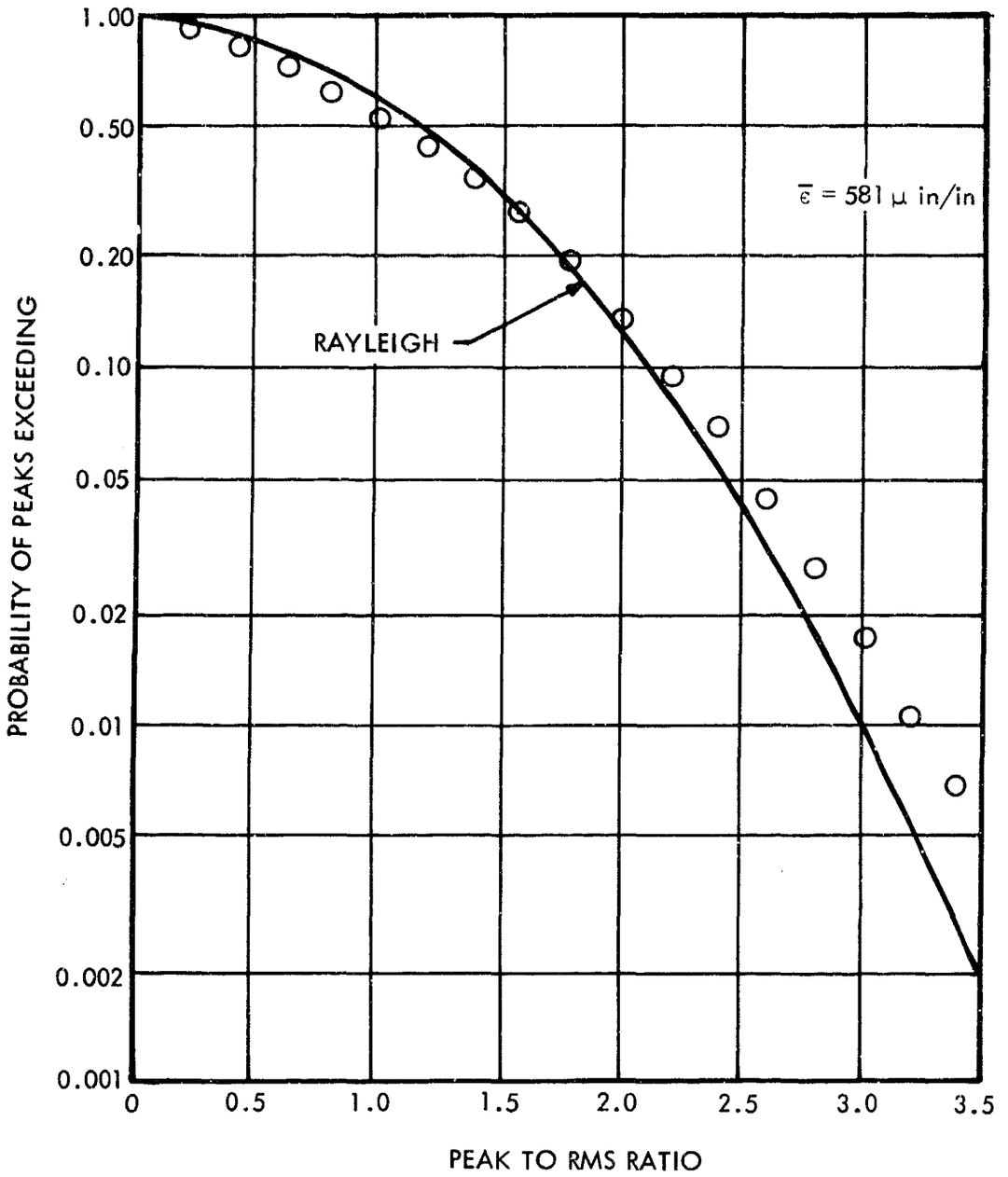

FIGURE 39. PROBABILITY DISTRIBUTION OF STRAIN PEAKS - STR-4B

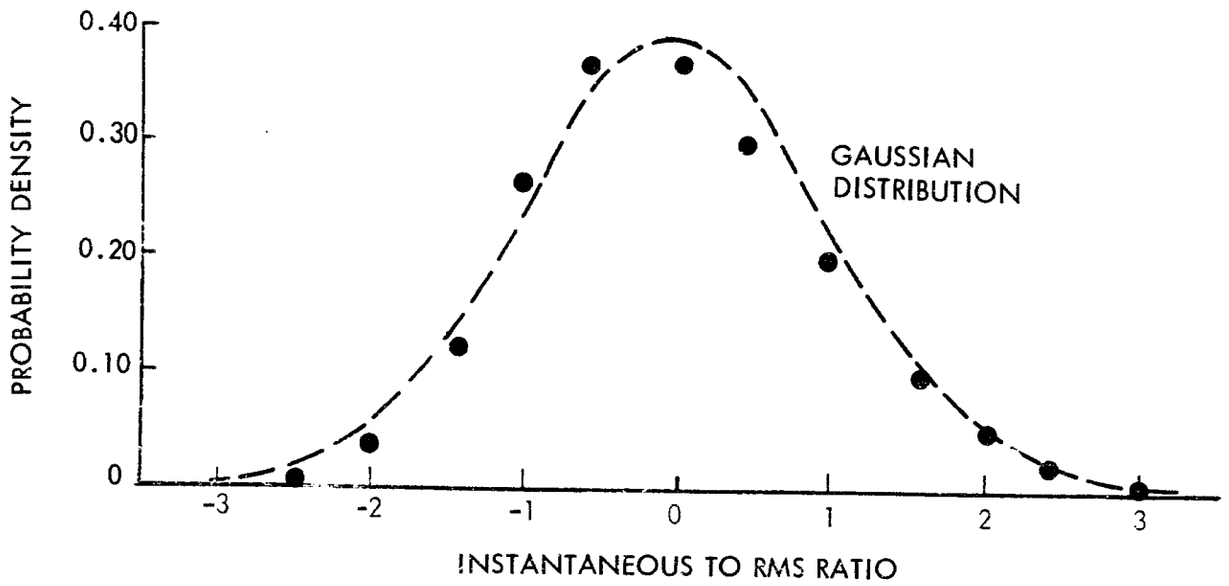

FIGURE 40. AMPLITUDE DISTRIBUTION OF STRAIN - STR-4B

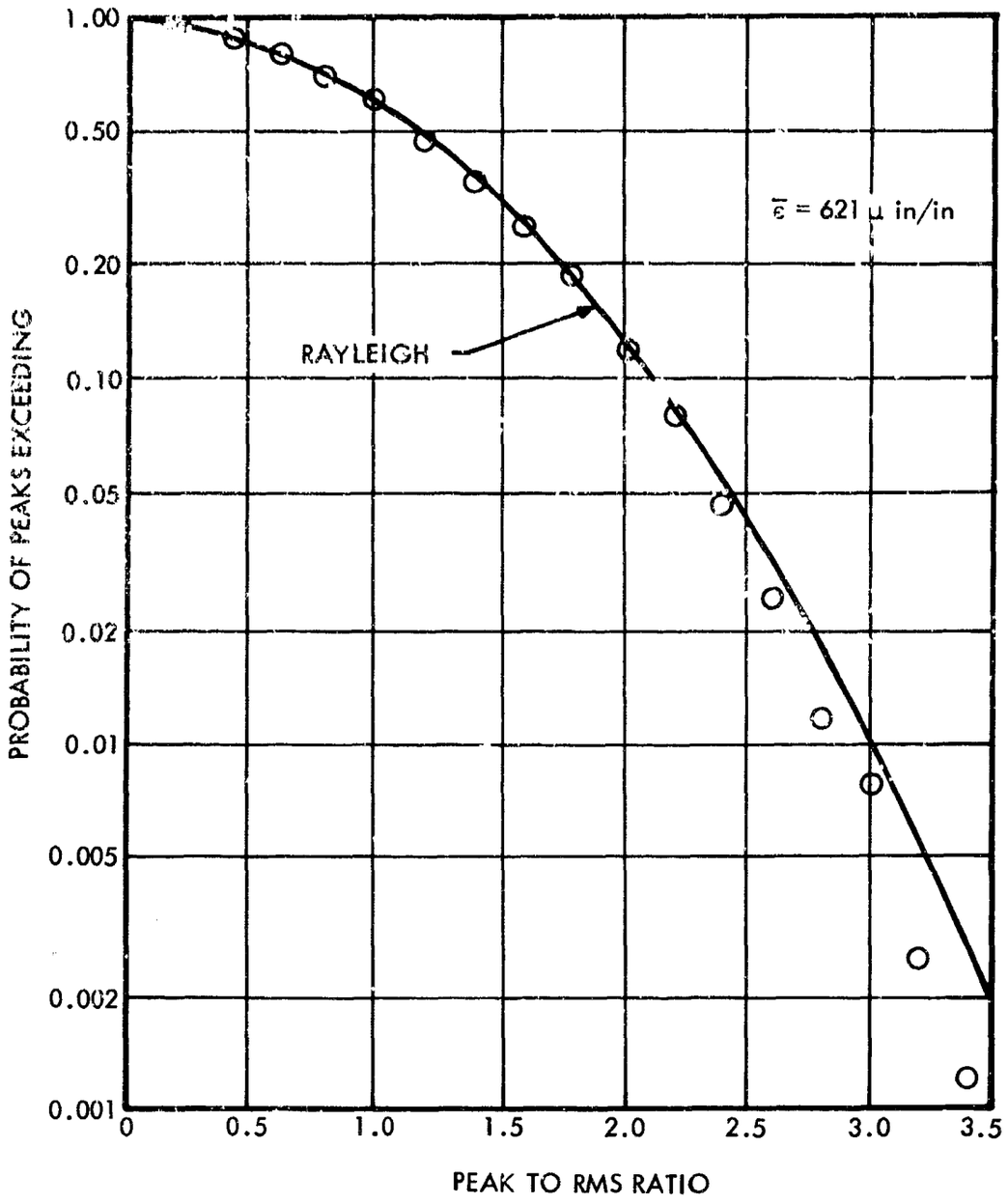

FIGURE 41. PROBABILITY DISTRIBUTION OF STRAIN PEAKS - STR-17A

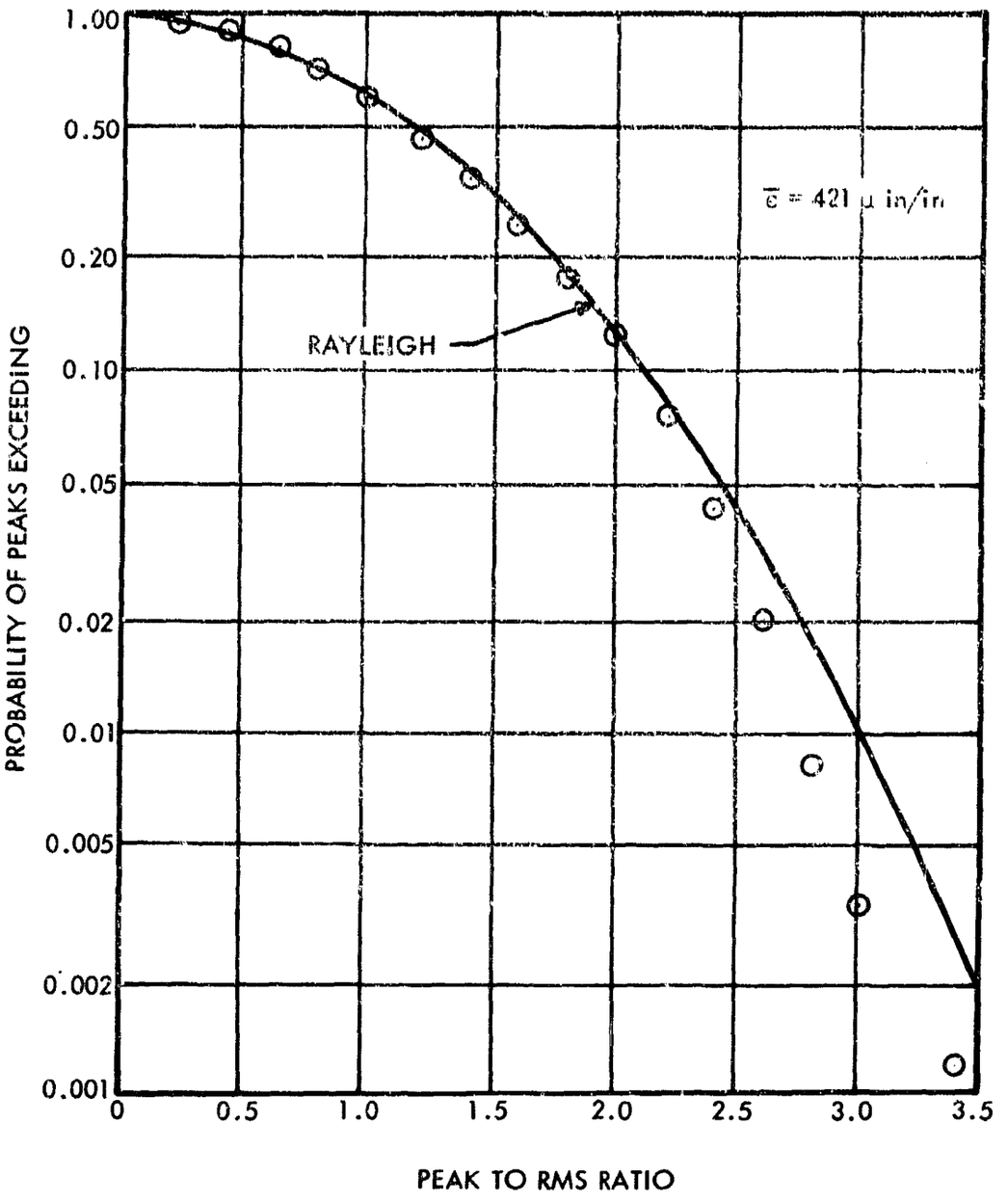

FIGURE 42. PROBABILITY DISTRIBUTION OF STRAIN PEAKS - STR-26A

TABLE IX

SUMMARY OF HONEYCOMB SANDWICH MODAL FREQUENCY AND DAMPING INVESTIGATION

Designation	Modal frequency,* Hz 1,1	1,2	1,3	2,1	Average damping for (1,1) mode, %
HC-1	229	451	925	632	1.5
	150				
HC-2, HC-3	250	521	-	-	1.8-2.1
HC-4	230	439	895	677	1.3
HC-5, HC-22	205	416	863	550	2.4
	145				
HC-6	190	335	780	536	1.5
HC-7	255	475	-	-	1.5
HC-8	515	-	-	-	1.7
HC-9	240	452	816	692	1.5
HC-10	275	359	900	-	1.6
	215				
HC-11	197	366	785	605	1.8
HC-12	282	635	-	-	2.6
	195				
HC-13	256	503	1015	705	2.4
HC-14	248	513	950	715	1.6
HC-15	201	425	805	576	2.0
HC-16, HC-25	233	535	935	637	1.8
HC-17	206	417	885	582	1.9
HC-18	493	-	-	-	2.7
HC-19	277	464	-	-	2.0
HC-20	262	397	702	-	1.5
	202				
HC-21	246	509	1120	711	1.5
HC-23	286	-	-	-	2.2
HC-24	213	480	905	595	2.2
HC-26, HC-28	191	312	647	610	2.2
HC-27	213	413	722	635	1.3
HC-29	217	405	742	682	1.7
HC-30	118	165	-	-	1.9
	95				

*Modes higher than (1,3) could not be excited.

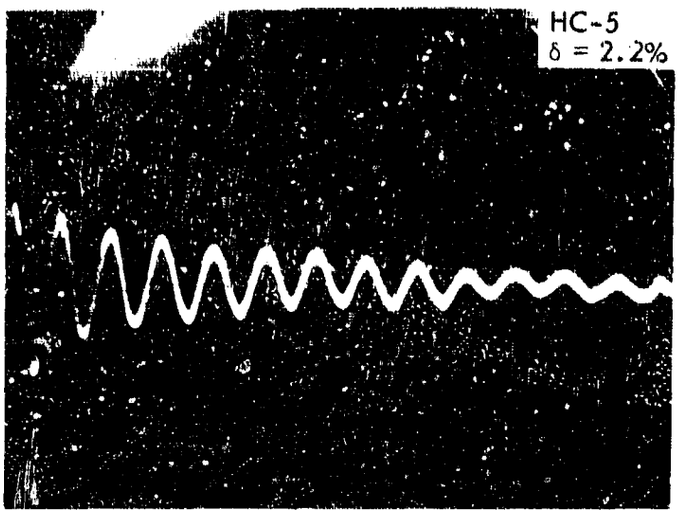

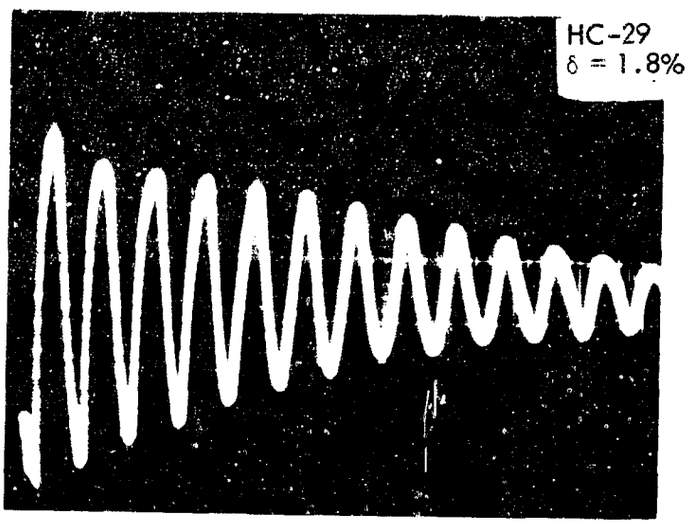

FIGURE 43. DECAYING STRAIN OSCILLATIONS FOR LOG-DECREMENT DAMPING, HC-5 AND HC-29

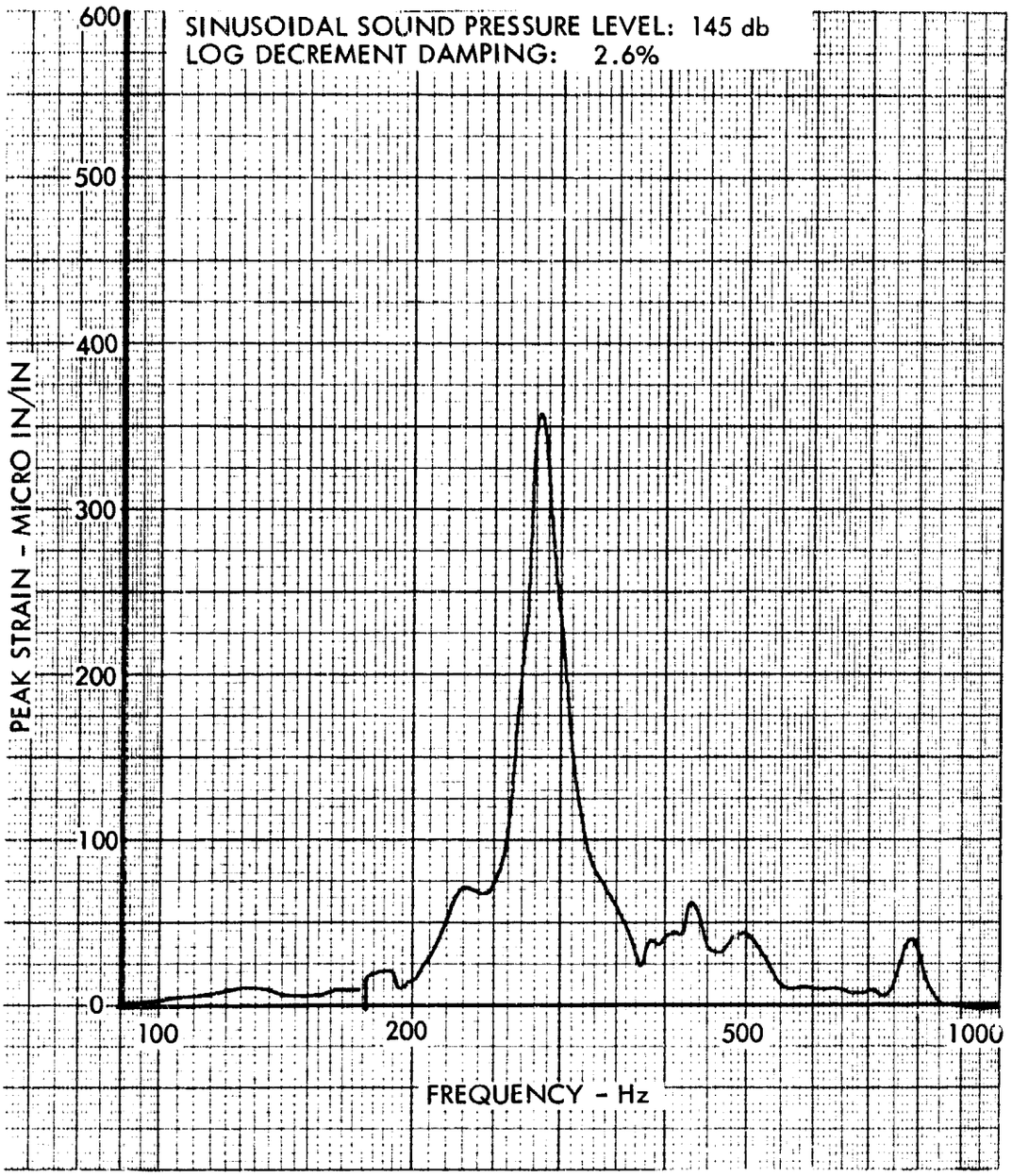

FIGURE 44. SINE-SWEEP EXCITATION - HC 12B

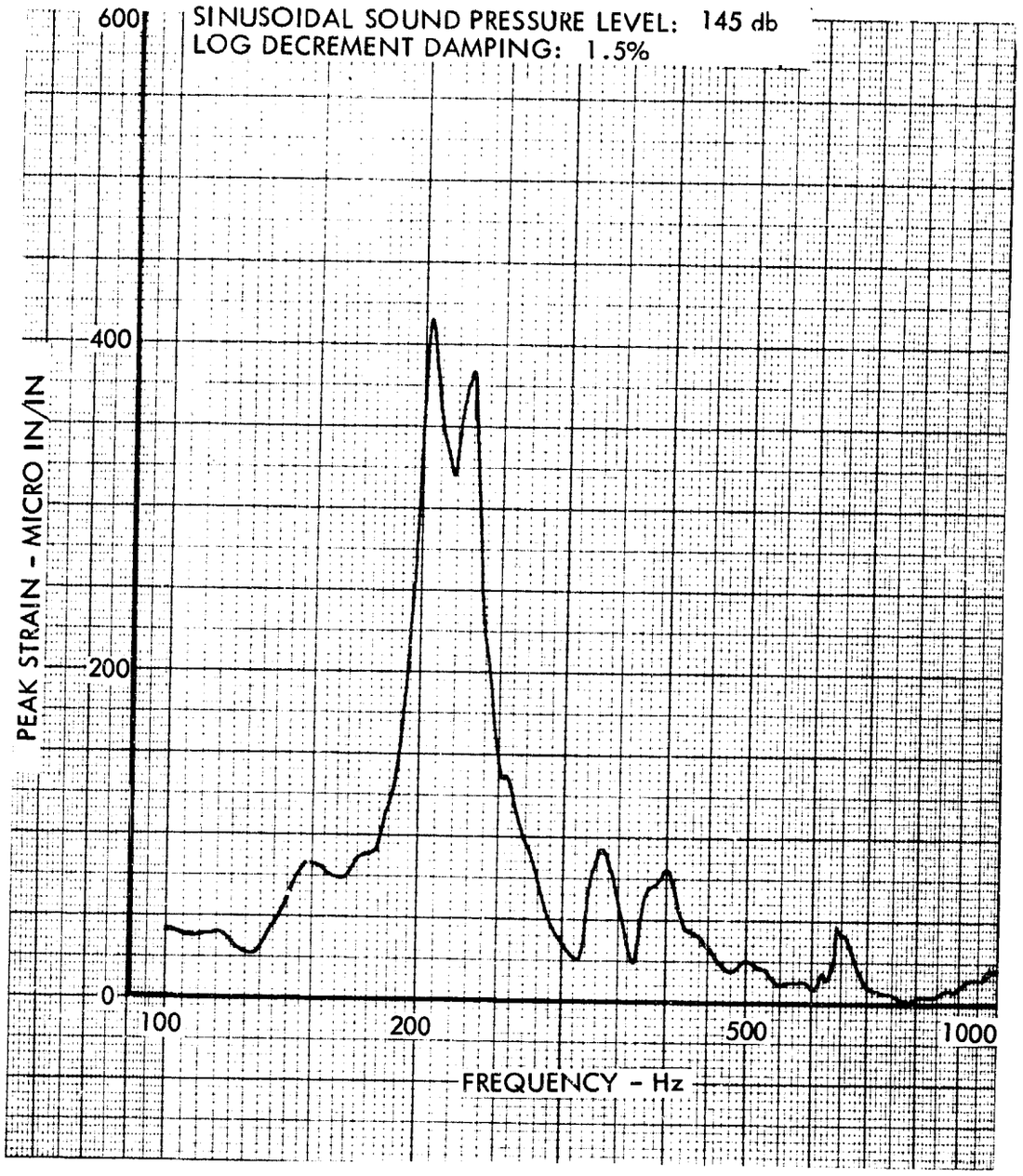

FIGURE 45. SINE-SWEEP EXCITATION - HC 20A

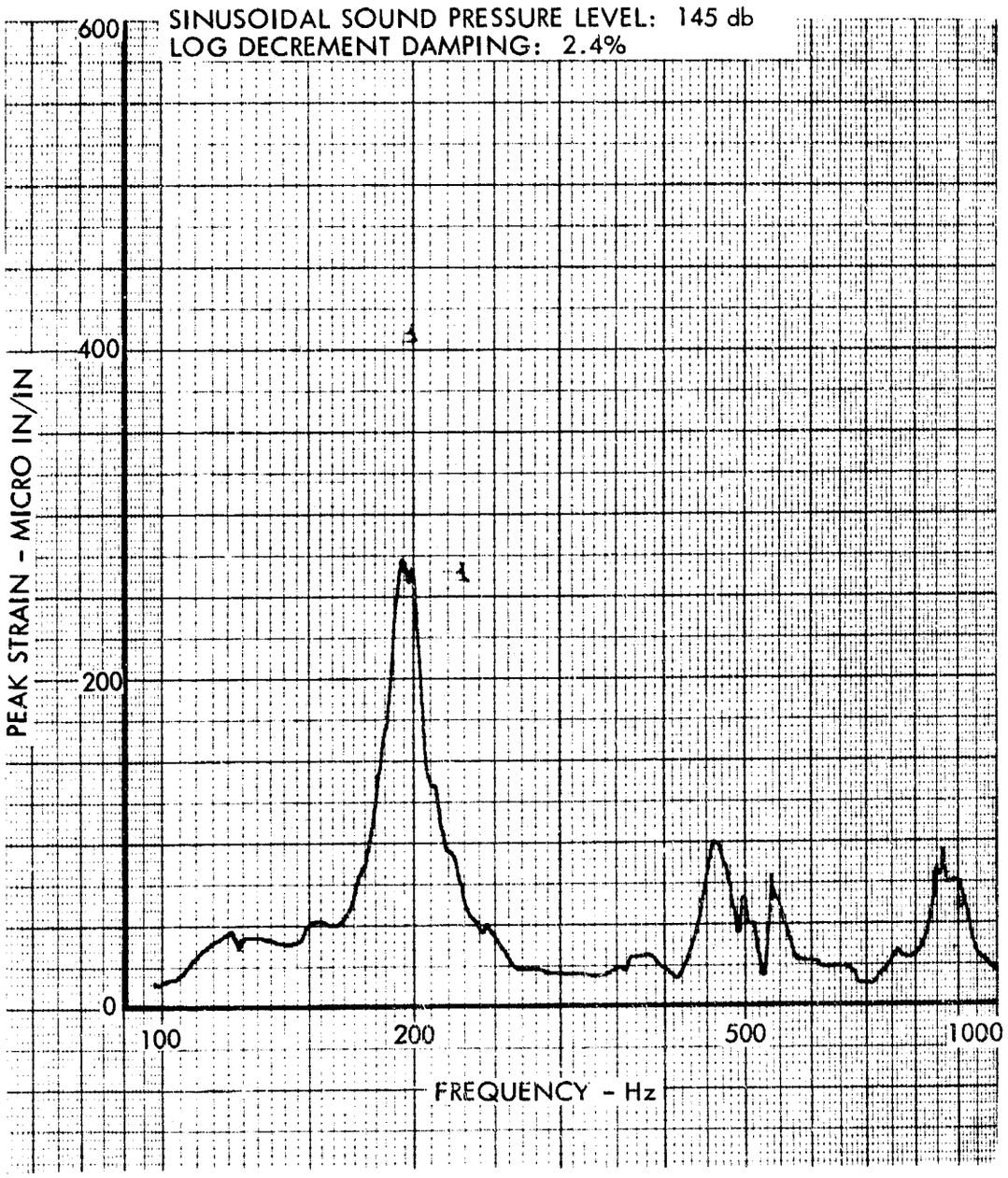

FIGURE 46. SINE-SWEEP EXCITATION - HC 22A

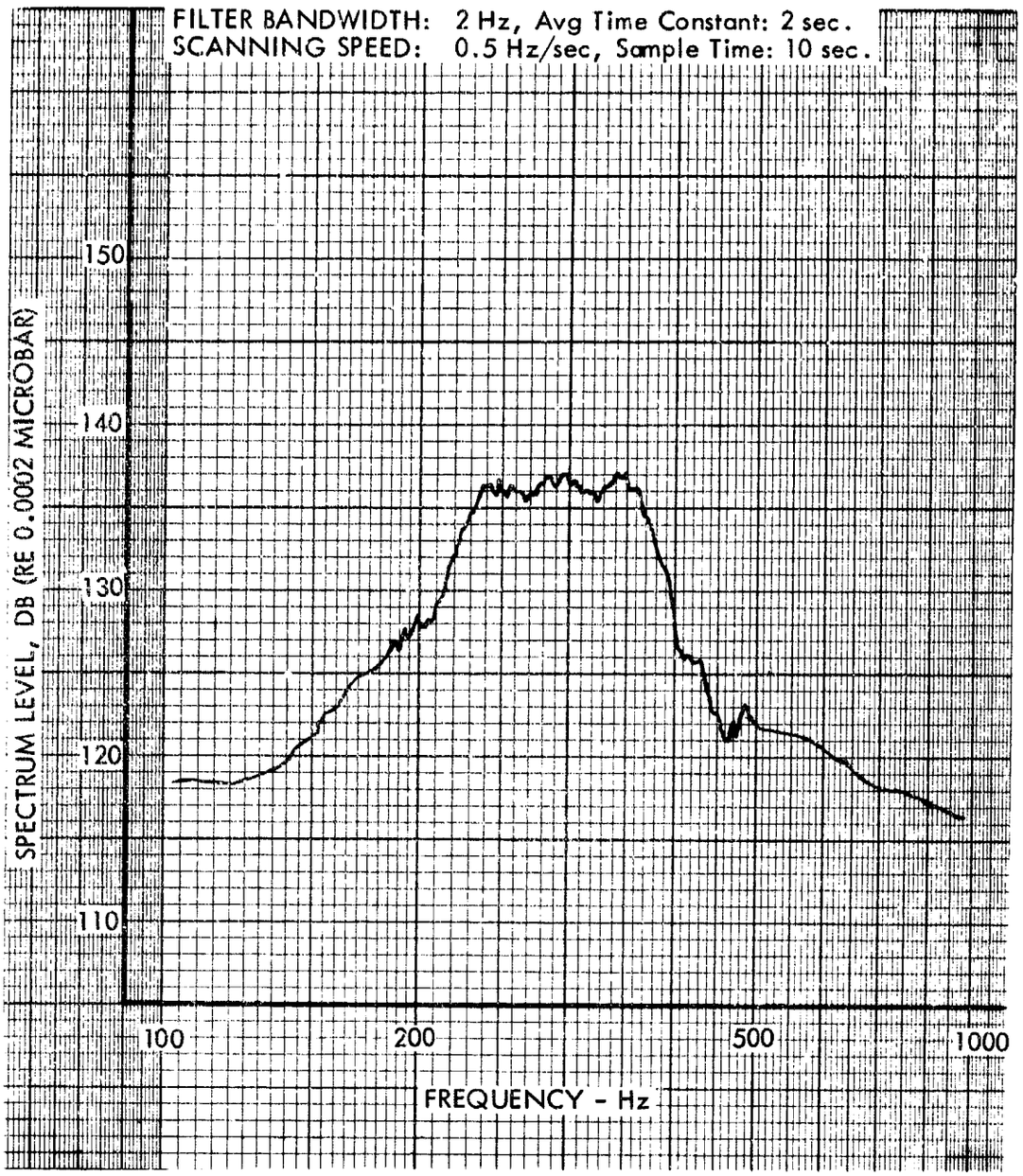

FIGURE 47. BROAD-BAND TEST SPECTRUM - HC 12B

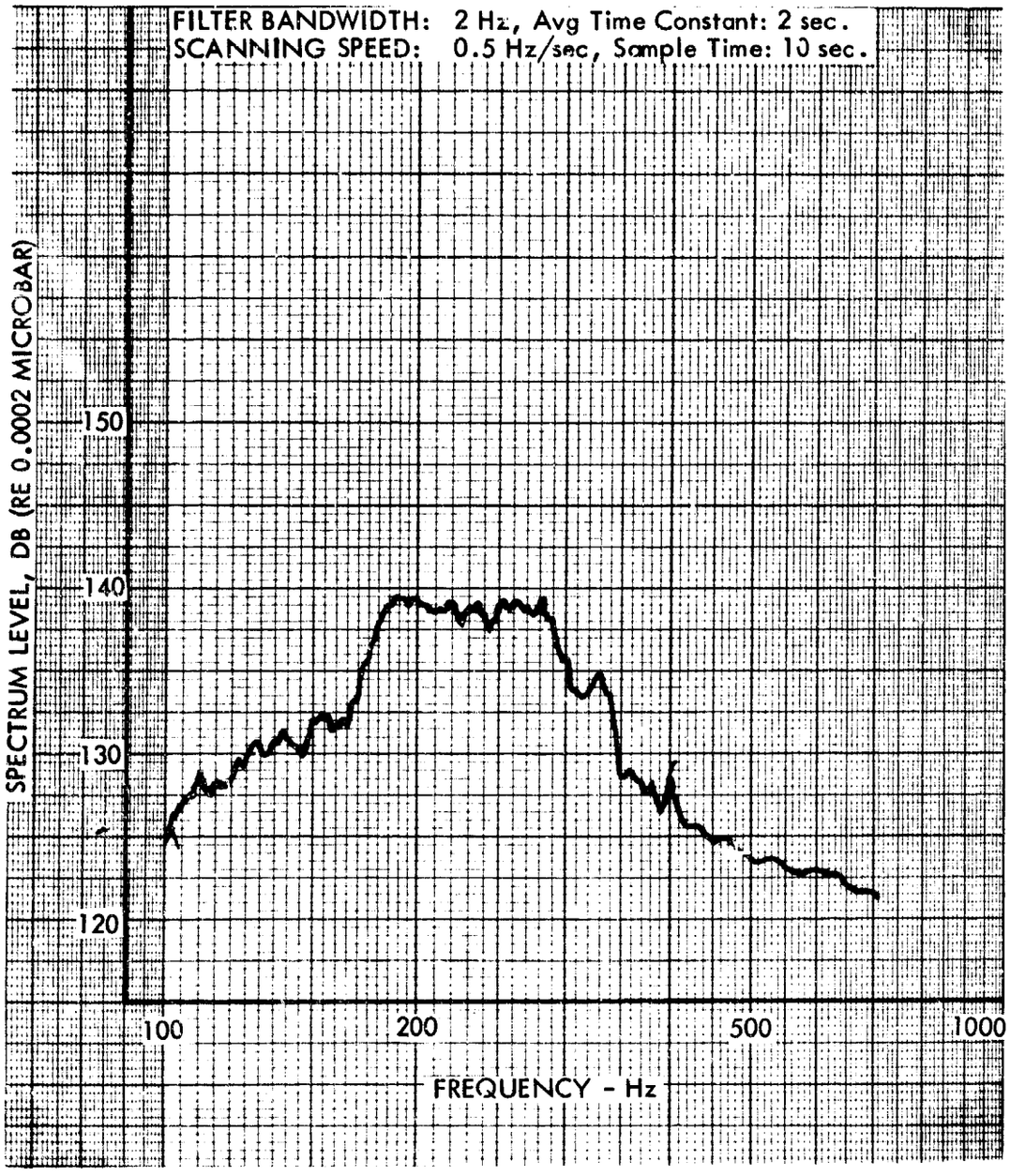

FIGURE 48. BROAD-BAND TEST SPECTRUM - HC 20A

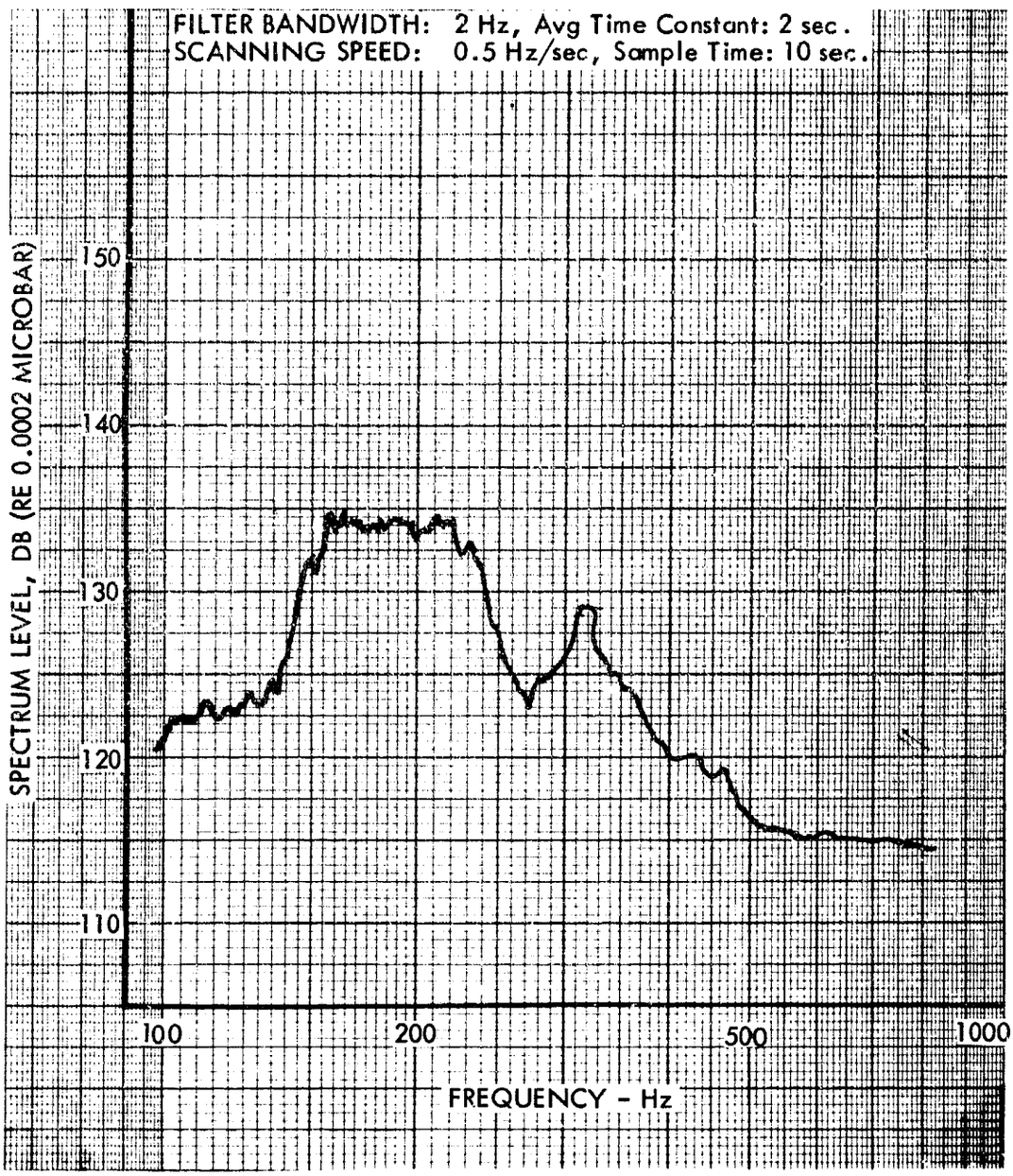

FIGURE 49. BROAD-BAND TEST SPECTRUM - HC 22A

TABLE X

SUMMARY OF HONEYCOMB SANDWICH FATIGUE TESTS

Designation		Test spectrum level, db	Response frequency, Hz	No. of crossings to failure, Nc x 10 $^{-6}$	Overall rms stress at failure point ksi	Remarks
HC-1	A	138	230	0.83	6.12	edge crack
	B	136	240	0.87	5.98	edge crack
HC-2	A	138	250	1.80	7.21	edge crack
	B	137	250	1.80	5.45	edge crack
HC-3	A	134	270	1.90	5.36	edge crack
	B	134	270	1.90	5.11	edge crack
HC-4	A	134	240	18.60	2.72	edge crack
	B	132	250	14.20	3.21	edge crack
HC-5	A	133	210	0.37	8.35	edge crack
	B	131	220	0.39	7.25	edge crack
HC-6	A	134	200	0.54	7.35	edge crack
	B	134	200	0.72	6.81	edge crack
HC-7	A	140	270	5.80	4.61	edge crack
	B	139	280	6.00	4.12	edge crack
HC-8	A	138	470	14.40		edge crack
	B	136	500	13.50		edge crack
HC-9	A	140	250	4.50	3.82	edge crack
	B	138	240	4.30	4.55	edge crack
HC-10	A	138	220	0.27	8.23	edge crack
	B	138	230	0.28	8.11	edge crack
HC-11	A	138	195	11.50	5.75	facing sheet crack
	B	137	190	11.80	4.25	facing sheet crack
HC-12	A	138	290	18.20	4.50	facing sheet crack
	B	137	290	17.20	5.35	facing sheet crack
HC-13	A	140	250	11.70	6.80	facing sheet crack
	B	139	265	14.30	5.10	facing sheet crack
HC-14	A	140	255	29.50	5.80	facing sheet crack
	B	138	260	29.50	5.00	facing sheet crack
HC-15	A	140	200	1.08	10.79	core shear failure
	B	140	200	1.90	10.50	facing sheet crack
HC-16	A	140	220	1.60	8.00	data not valid
	B	138	240	17.00	6.25	facing sheet crack
HC-17	A	140	210	17.40	5.00	facing sheet crack
	B	138	210	18.10	5.15	facing sheet crack
HC-18	A	138	260	11.40	5.50	facing sheet crack
	B	137	285	13.40	5.05	facing sheet crack
HC-19	A	140	290	22.50	4.10	facing sheet crack
	B	139	260	20.50	4.00	facing sheet crack
HC-20	A	138	210, 220	6.80	5.50	facing sheet crack
	B	138	210, 220	13.60	5.15	facing sheet crack
HC-21	A	131	220	16.20	5.50	facing sheet crack
	B	129	220	16.20	6.05	facing sheet crack
HC-22	A	134	270	3.78	7.61	edge crack
	B	132	275	4.80	7.33	edge crack

TABLE X (Cont'd)

Designation	Test spectrum level, db	Response frequency, Hz	No. of crossings to failure $N_c \times 10^{-6}$	Overall rms stress at failure point ksi	Remarks
HC-23 A	136	260	13.00	6.20	facing sheet crack
B	136	250	18.00	5.95	facing sheet crack
HC-24 A	136	150	3.45	8.12	edge crack
B	134	145	3.96	7.53	edge crack
HC-25 A	138	350,600	6.50	6.50	facing sheet crack
B	137	350,600	14.70	4.80	facing sheet crack
HC-26 A	137	345	1.38	8.15	edge crack
B	135	390	1.11	8.36	edge crack
HC-27 A	138	240, 400	6.70 & 8.70	5.81 & 4.90	edge crack - facing sheet crack
B	137	240, 400	5.70 & 7.70	5.15 & 5.03	edge crack - facing sheet crack
HC-28 A	138	310	1.10	8.42	edge crack
B	137	290	1.44	7.65	edge crack
HC-29 A	137	220	10.20	3.13	edge crack
B	135	240	11.20	2.76	edge crack
HC-30 A	133		1.30	6.18	edge crack
B	130		1.00	6.32	edge crack

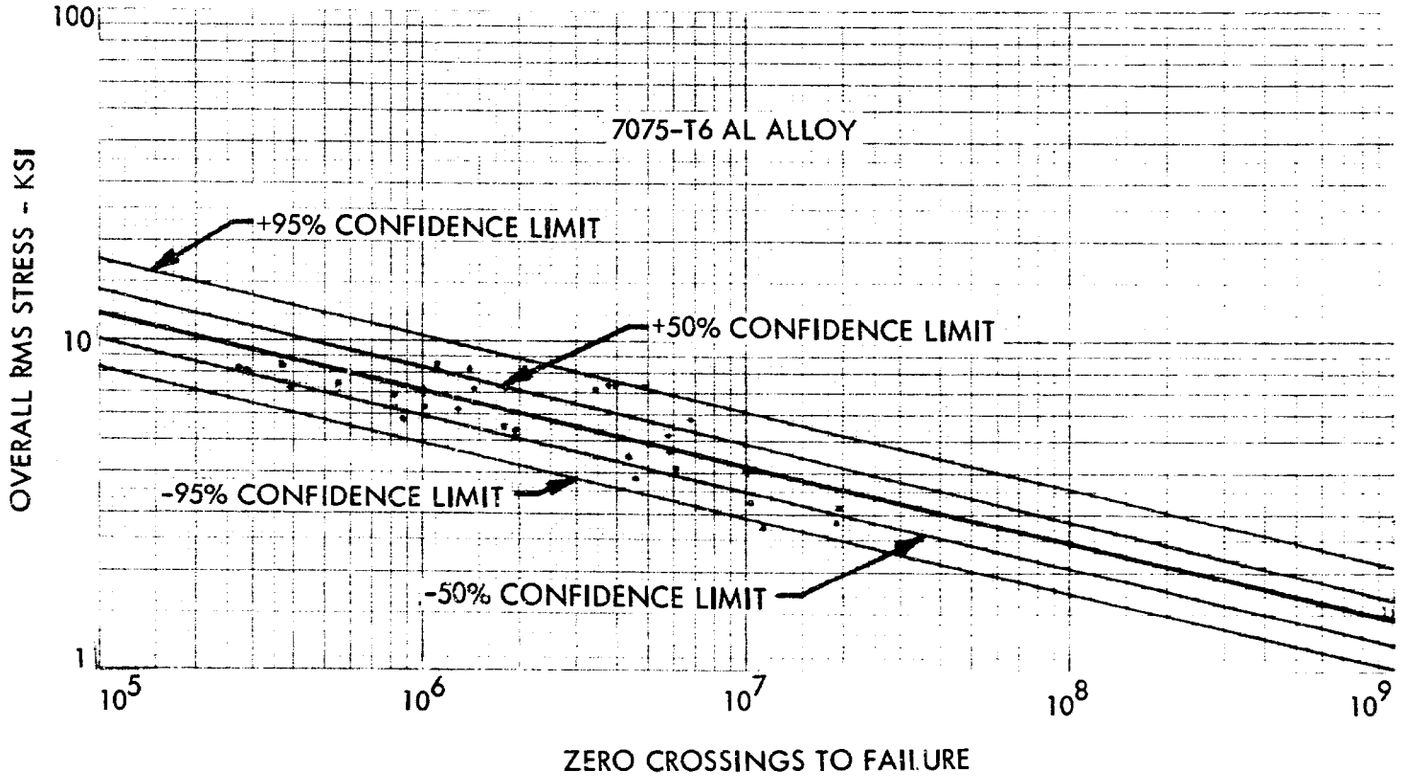

FIGURE 50 HONEYCOMB SANDWICH EDGE MEMBER FATIGUE CURVE

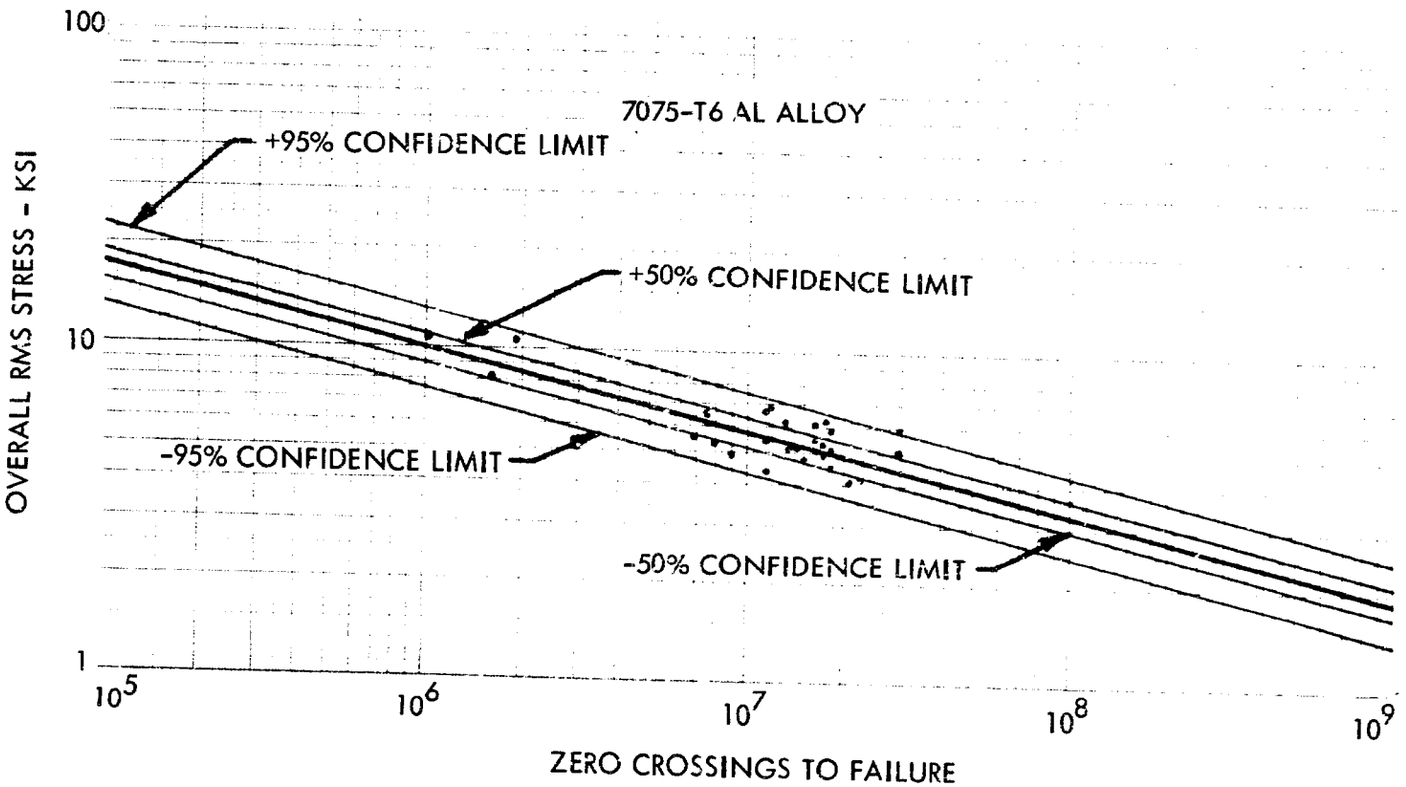

FIGURE 51. HONEYCOMB SANDWICH FACING SHEET FATIGUE CURVE

A number of selected tape recorded strain gage signals were analyzed to determine the nature of their statistical properties. Figures 52 through 55 present the statistical analysis of edge strains and facing sheet strains. Probability density of instantaneous strain and probability distribution of strain peaks are included.

Edge and facing sheet strain recordings were analyzed with a 2-Hz bandwidth filter to determine the characteristics of the strain response to the random acoustical excitation. The narrow-band analyses were also compared with the discrete frequency sweeps. Figures 56 through 59 are typical analyses.

f. Edge Doubler Tests - The edge of a honeycomb sandwich panel is generally comprised of a facing sheet thickness, a doubler, and a closing member, sometimes called a pan. The doubler is necessary to maintain the required strength at the edges where the load in the smaller facing sheet is transferred to the larger facing sheet. Obviously, the width of the doubler is dependent upon the portion of the panel span required to transfer load across the full depth core. The length of span required to transfer this load is a function of the bevel angle of the core. It is very important that a minimum width doubler be used since it contributes significantly to the total panel weight. It is believed that rules of thumb based on static tests have been used heretofore to establish doubler width.

A set of simple experiments were made in an attempt to determine what width doubler should be used for a given core bevel angle. Four simple beams of the configuration shown in Figure 60 were fabricated and tested. Strain gages were attached to the facing sheets and were spaced one half inch apart at the ends and one inch apart elsewhere along the centerline of the beam to measure bending strain. Figures 61a and 61b show a typical beam before and after strain gage installation. The beams were mounted one at a time over the electro-mechanical speaker system used for modal frequency studies, with the speaker producing discrete frequency sound tuned to the fundamental frequency of each beam. Strain measurements were recorded at two arbitrarily selected sound pressure levels, 140 and 145 db.

Figure 62 is a plot of the strain distribution of all configurations normalized to the maximum strain magnitude recorded at zero percent span of Configuration A (1.25-inch wide doubler).

The strain distributions shown in Figure 62 indicate that the doubler significantly influences the spanwise strain distribution. The greatest influence occurs at the end of the doubler, a very critical spot where fatigue cracks frequently form. Also, it should be noted that the strain experiences a change of sign (tension to compression or vice versa) near the line where the thin edge ends and the beveled core begins. Also in this same region, the strain was reduced approximately 32 percent with the 2.15-inch doubler as compared to the 1.25-inch doubler. The 2.60-inch doubler only reduced the strain 36 percent as compared to the 1.25-inch doubler, however. In every case, the strain experiences a minimum at 16.3 percent of the span.

The curves, Figure 62, indicate that the design with the 2.15-inch doubler was almost as effective as the design with the 2.60-inch doubler. As a result it was decided that narrow doublers would be used on test specimens HC-15 through HC-30. These test specimens were subsequently tested with no observable reduction in fatigue resistance, but with a significant reduction in weight. Therefore, it is recommended that the doubler width for design be established as shown in Figure 63.

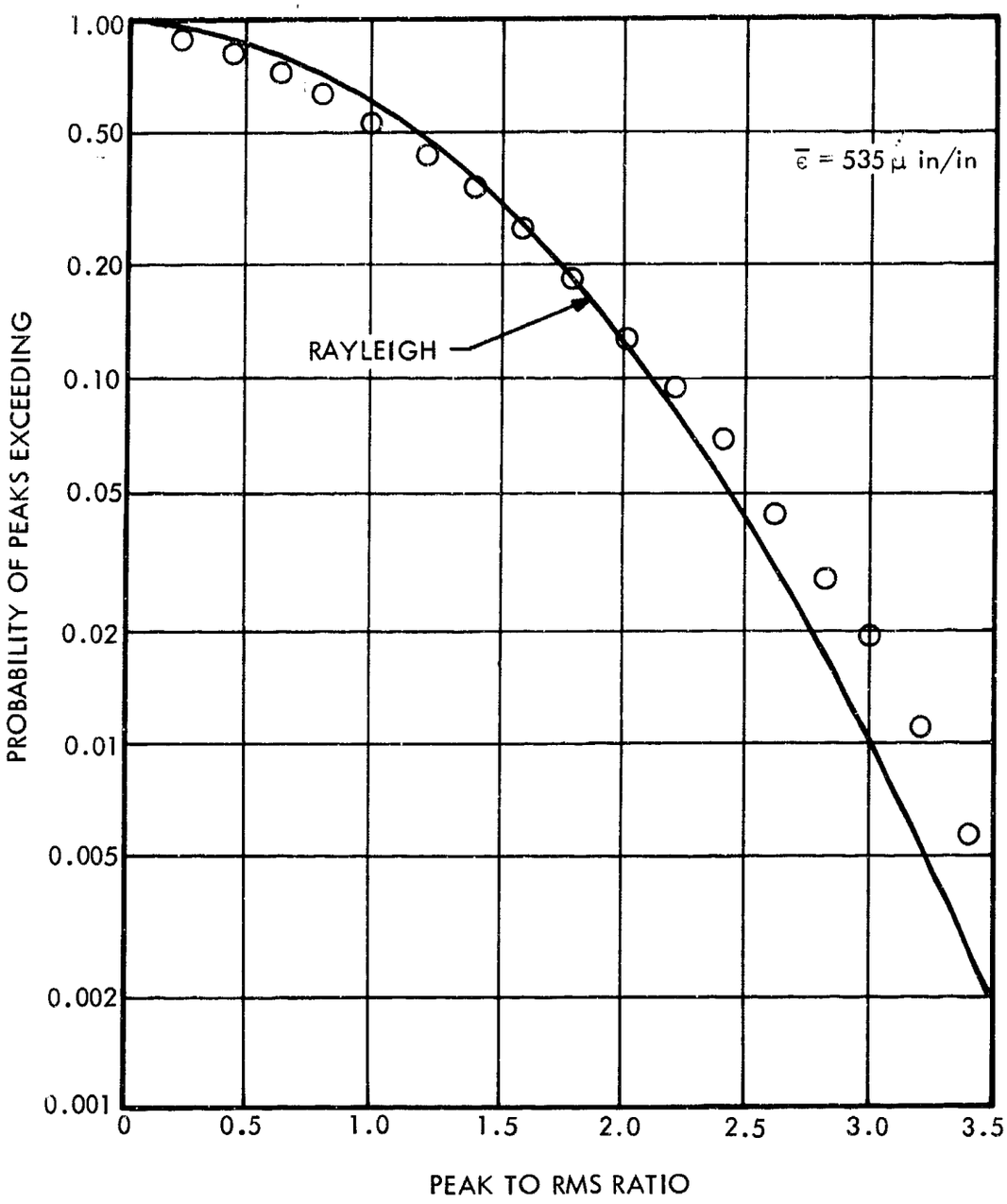

FIGURE 52. PROBABILITY DISTRIBUTION OF STRAIN PEAKS - HC-12B

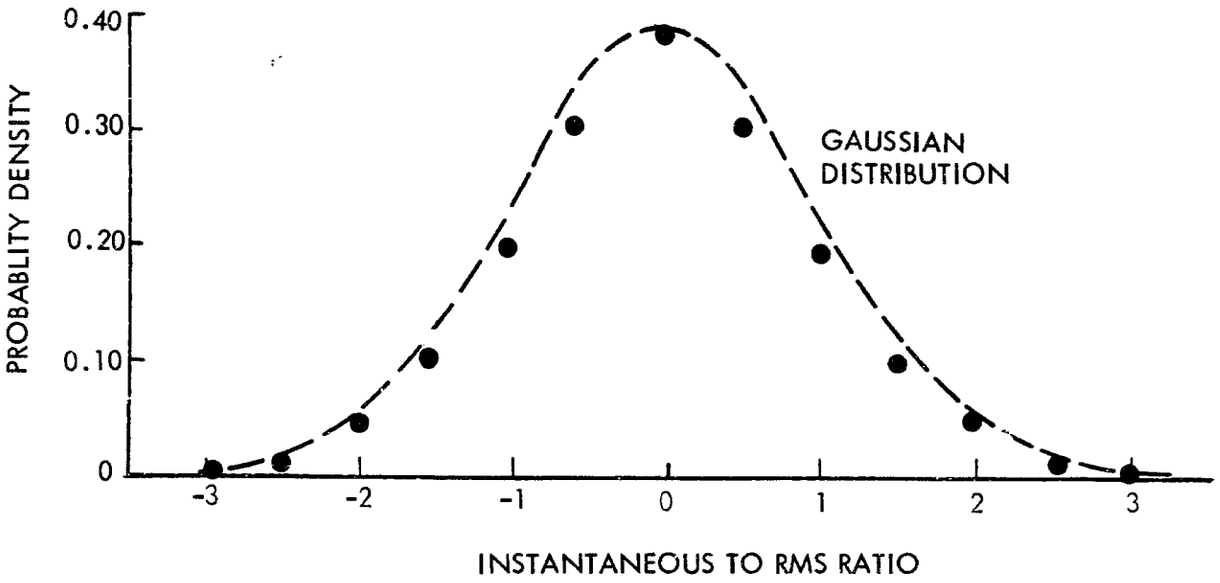

FIGURE 53. AMPLITUDE DISTRIBUTION OF STRAIN - HC-12B

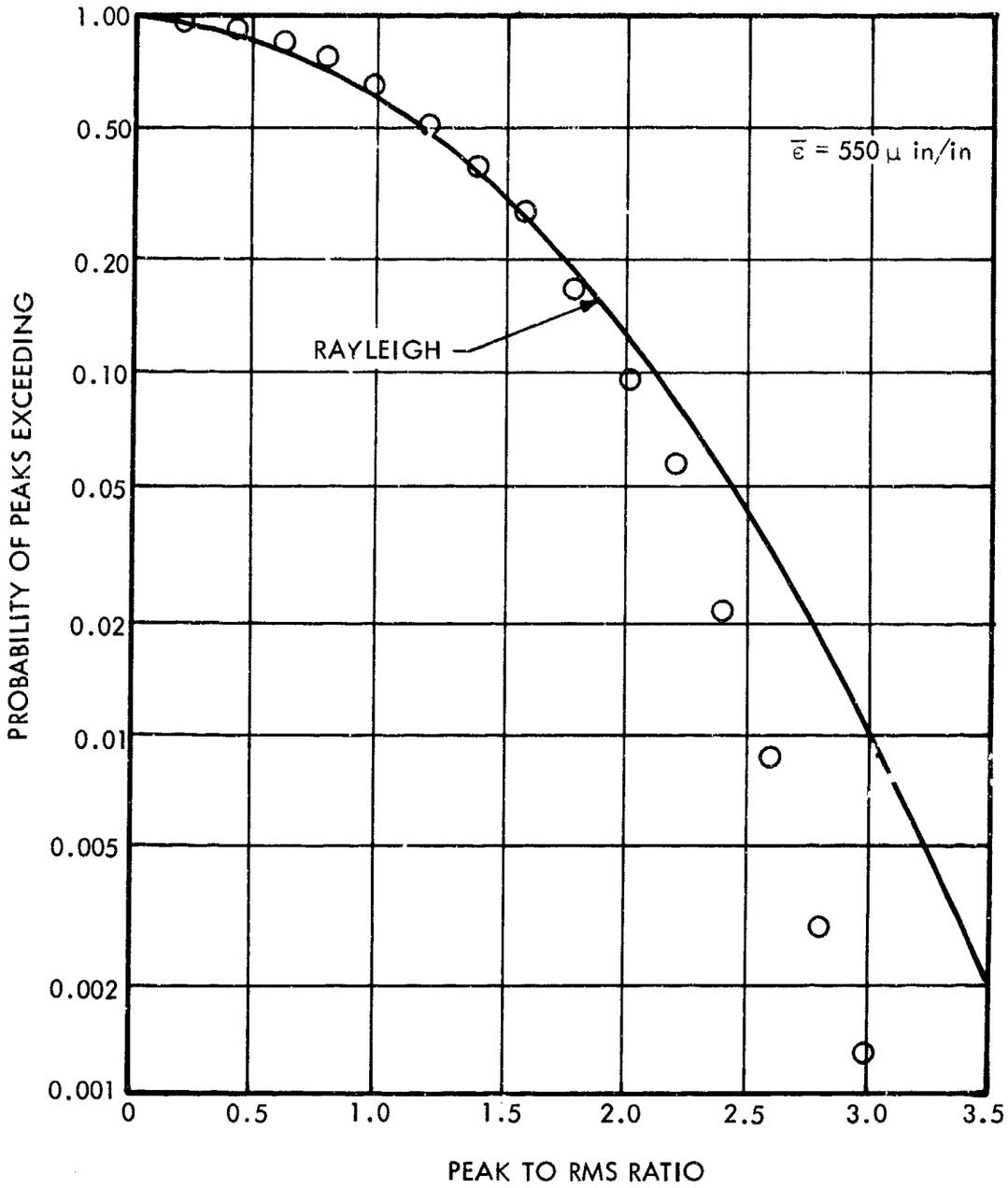

FIGURE 54. PROBABILITY DISTRIBUTION OF STRAIN PEAKS - HC-20A

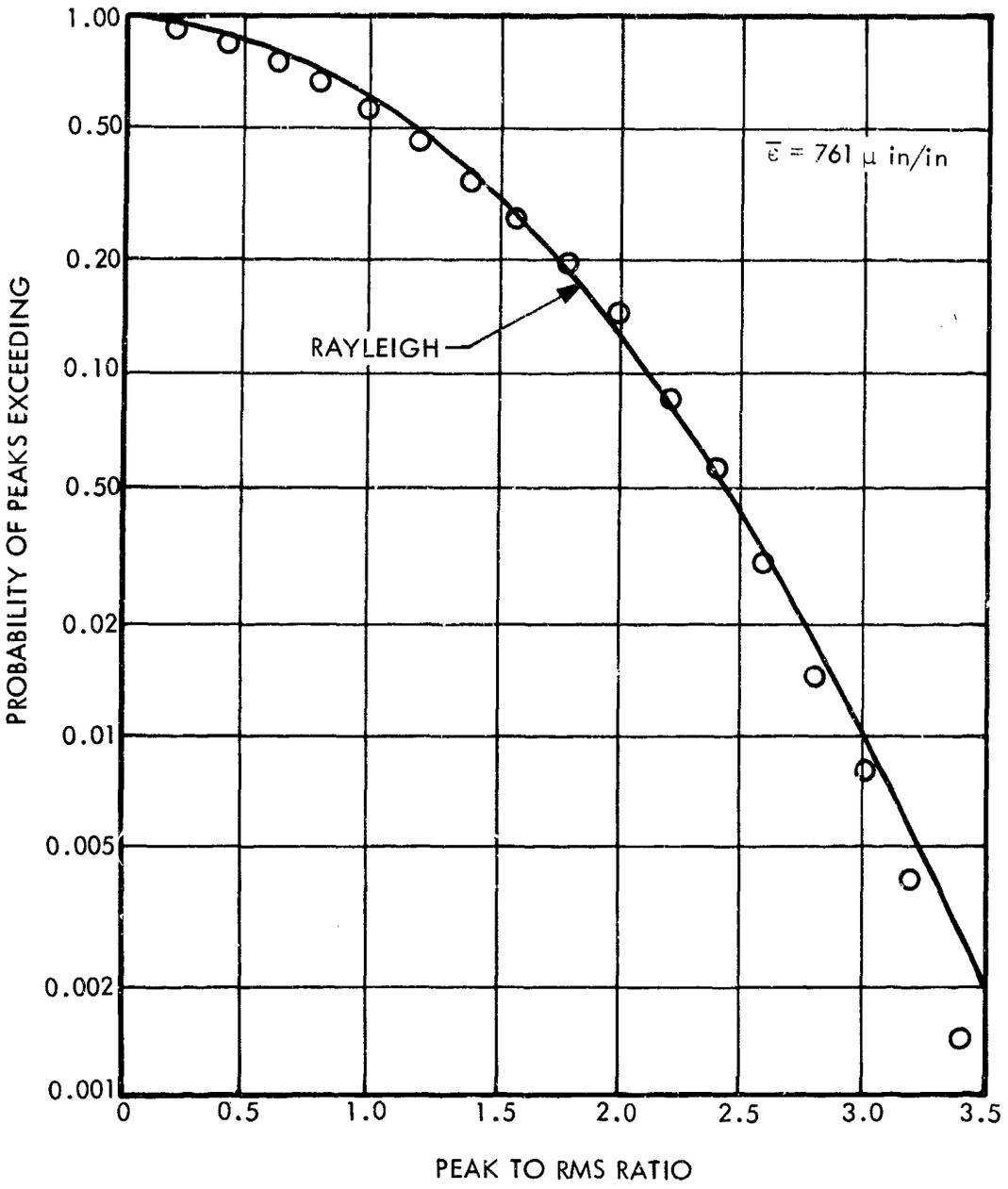

FIGURE 55. PROBABILITY DISTRIBUTION OF STRAIN PEAKS - HC-22A

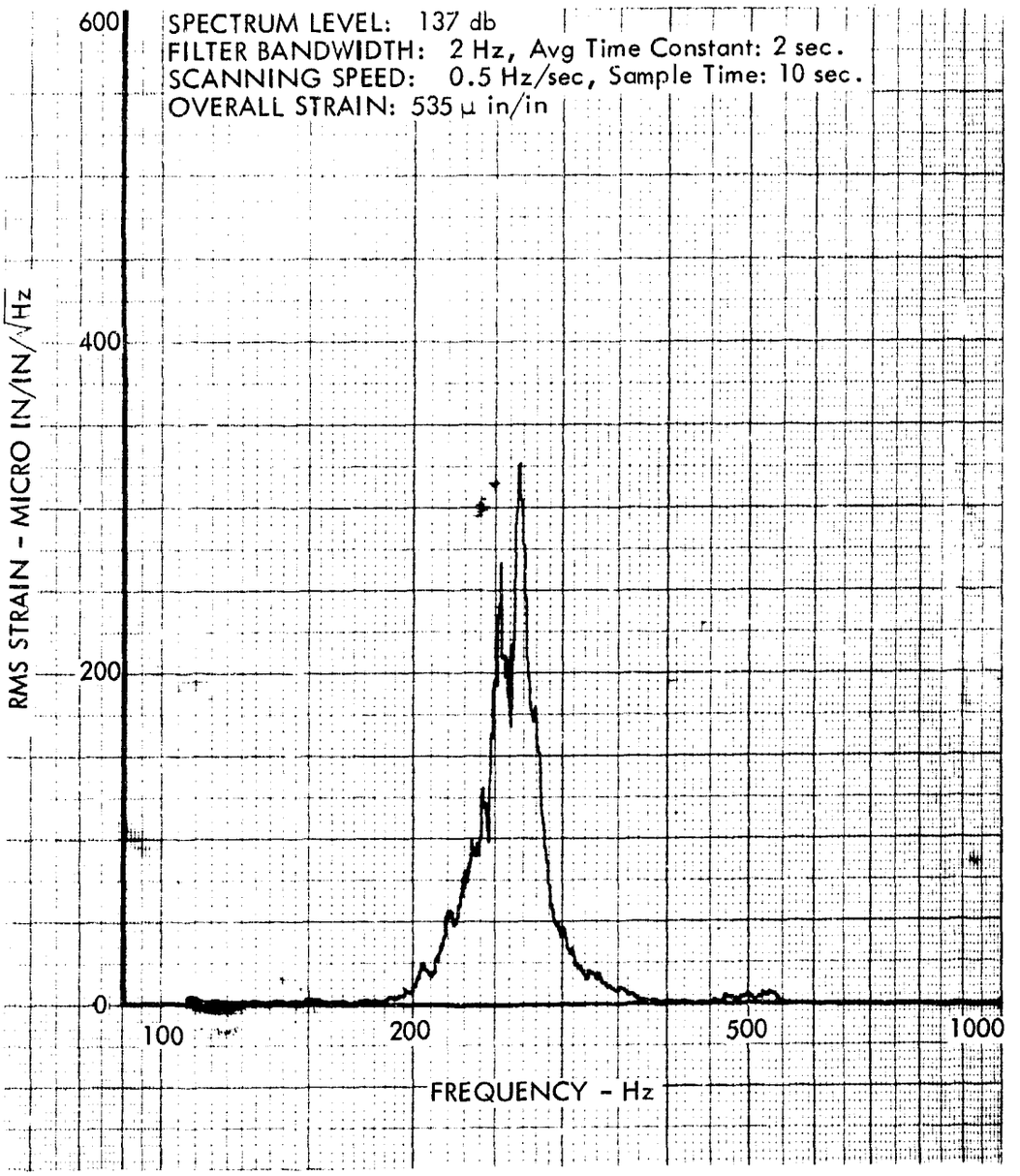

FIGURE 56. NARROW-BAND STRAIN ANALYSIS - HC 12B

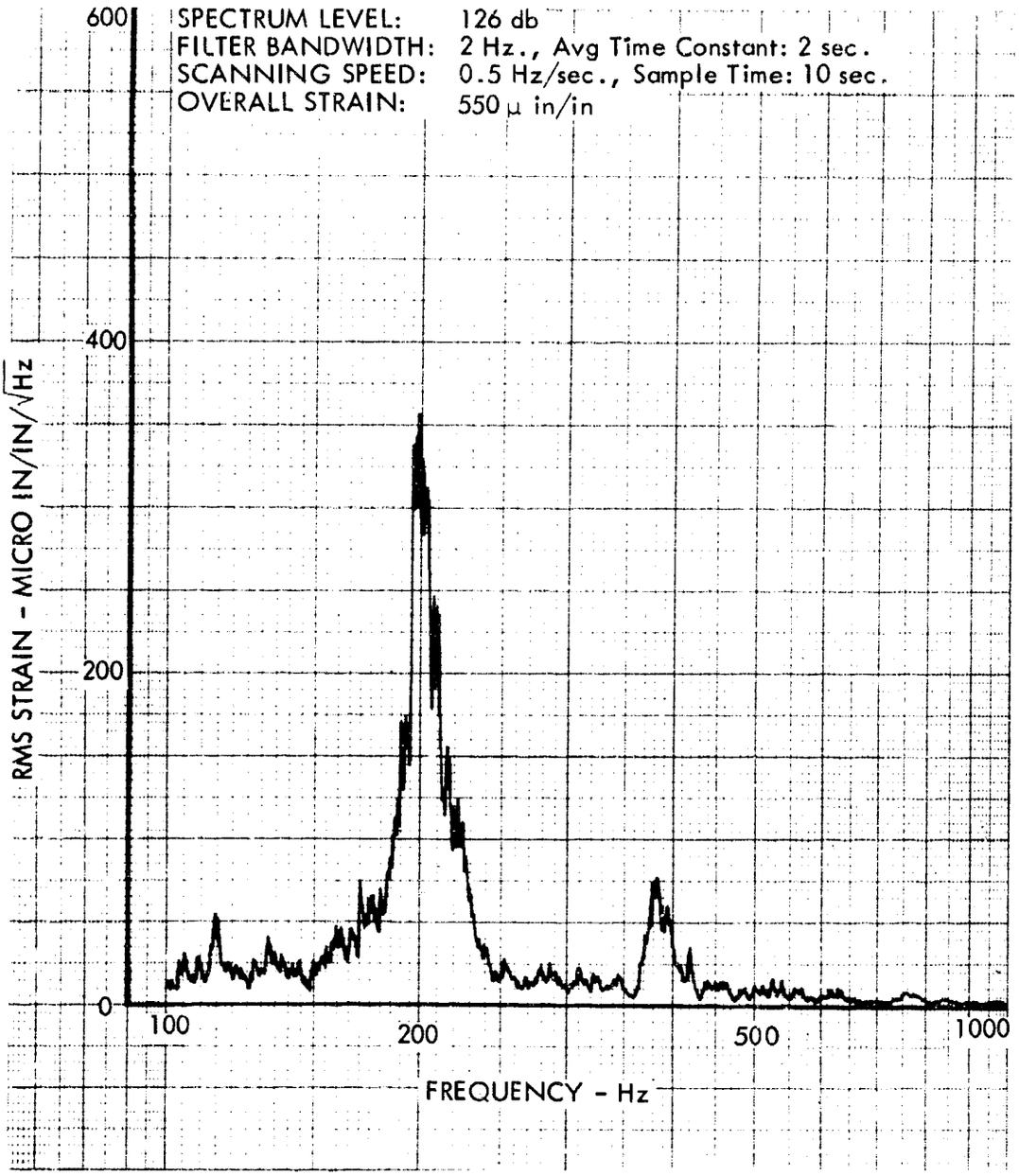

FIGURE 57. NARROW-BAND STRAIN ANALYSIS - HC 20A

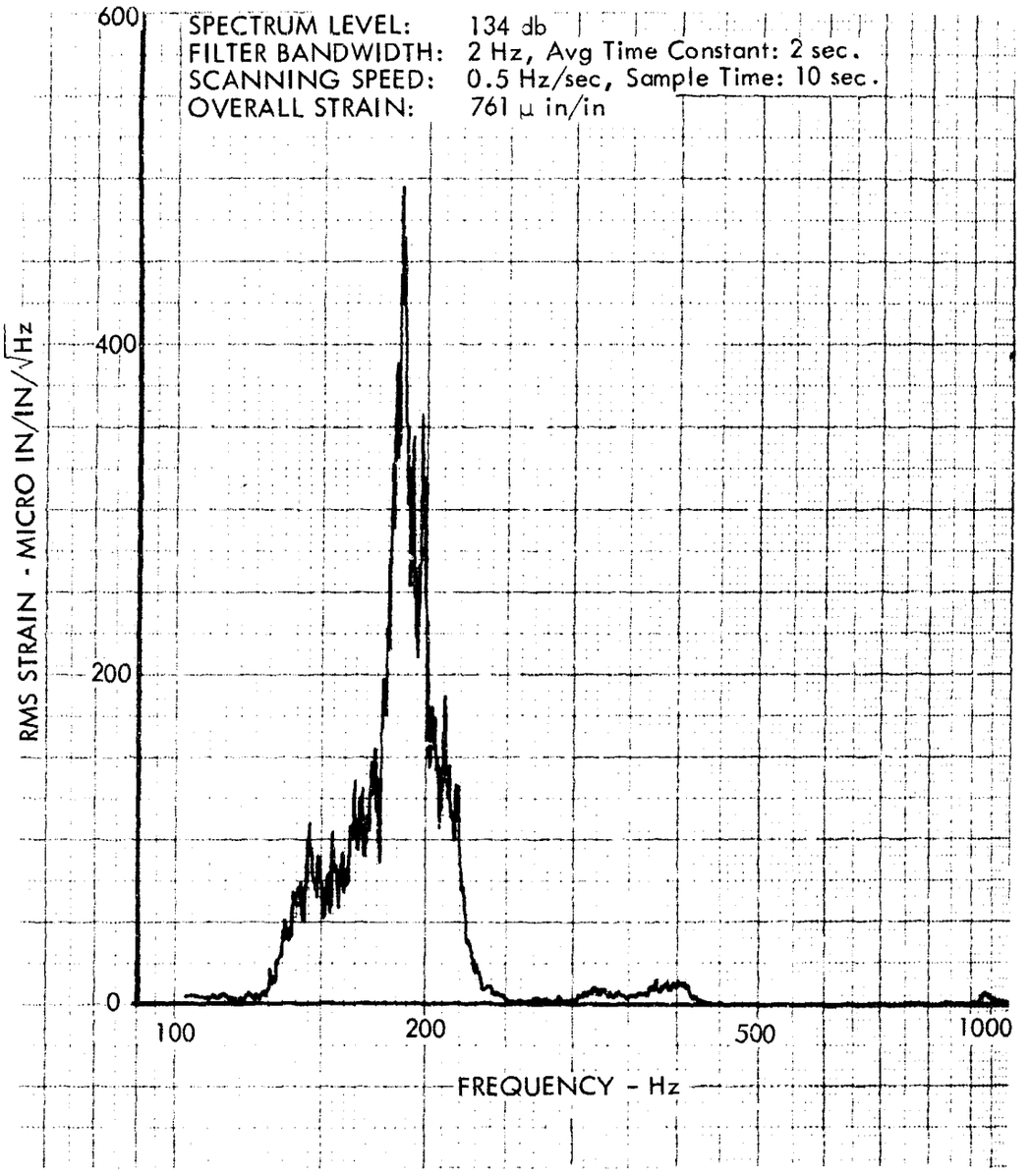

FIGURE 58. NARROW-BAND STRAIN ANALYSIS - HC 22A

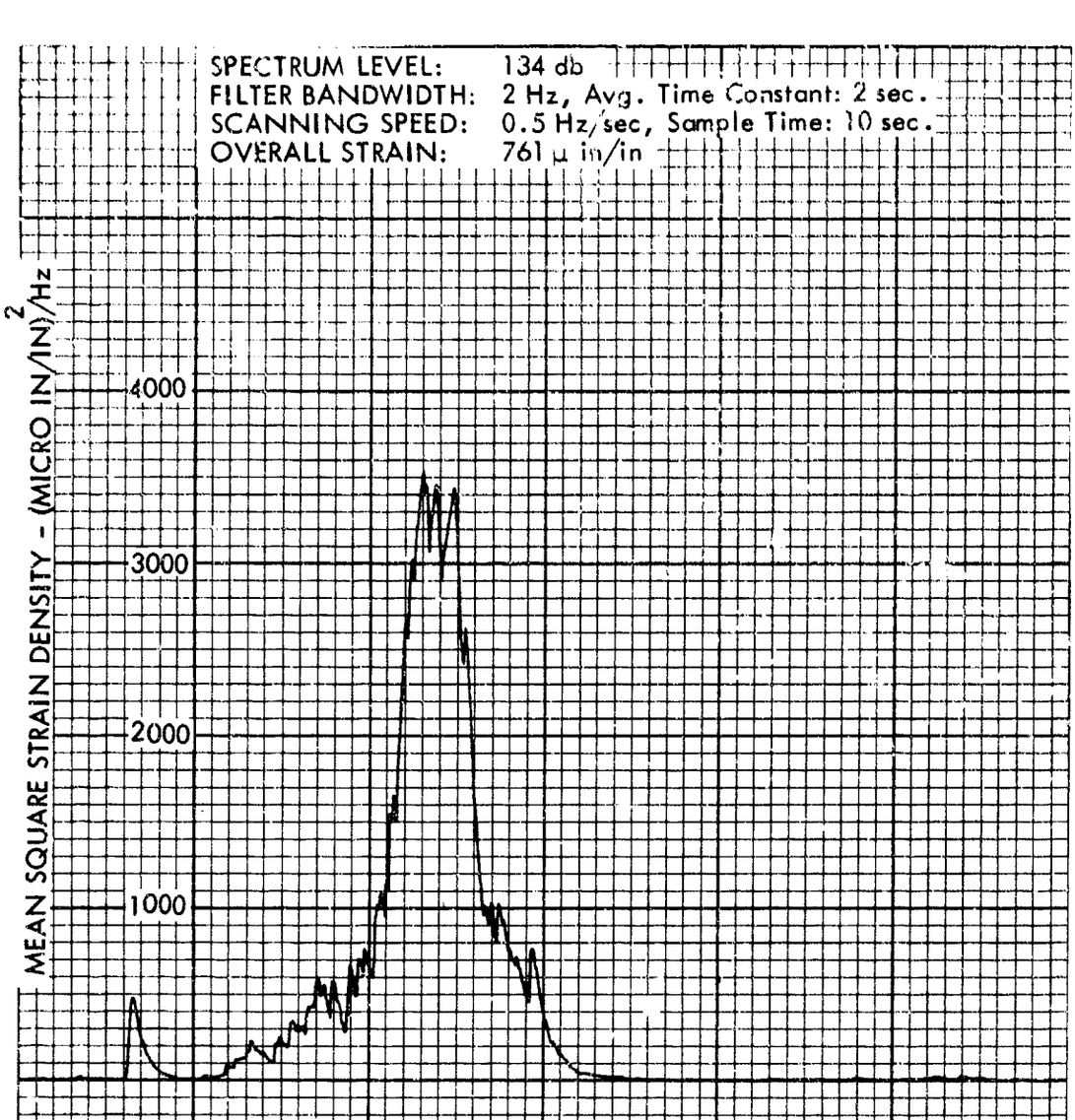

FIGURE 59. PSD STRAIN ANALYSIS - HC 22A

DESIGN DETAILS

Config.	Length, in.	Width, in.	t_p	A	B	C	Core density lb/ft^3
I	21.0	4.0	4 ply 181 Fiber-glass	1.25	1.25	1.00	3.4
II	21.0	4.0		1.70	1.25	1.00	3.4
III	21.0	4.0		2.15	1.25	1.00	3.4
IV	21.0	4.0		2.60	1.25	1.00	3.4

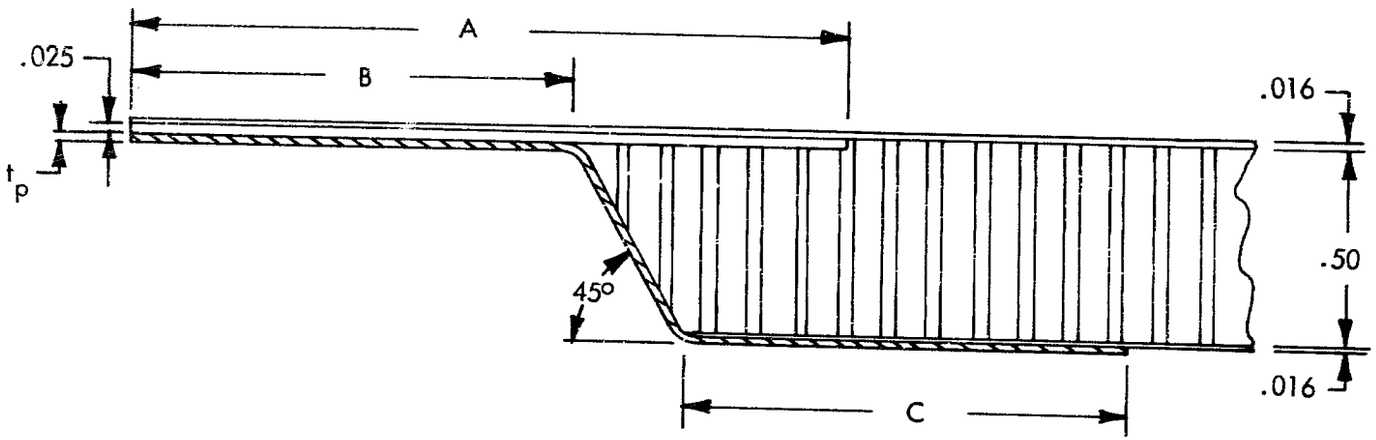

FIGURE 60. HONEYCOMB SANDWICH BEAMS FOR INVESTIGATING SPANWISE STRAIN DISTRIBUTION

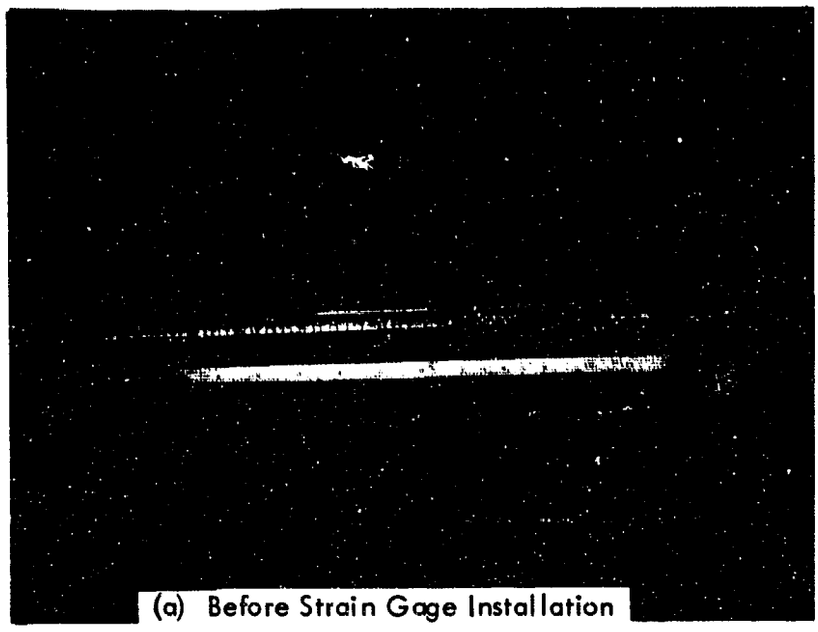

(a) Before Strain Gage Installation

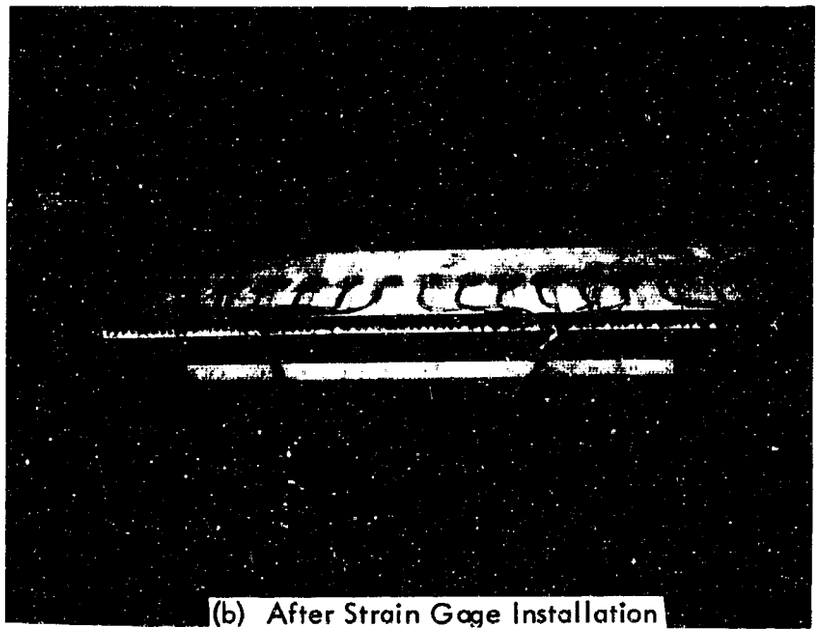

(b) After Strain Gage Installation

FIGURE 61. TYPICAL HONEYCOMB SANDWICH BEAM FOR DOUBLER INVESTIGATION

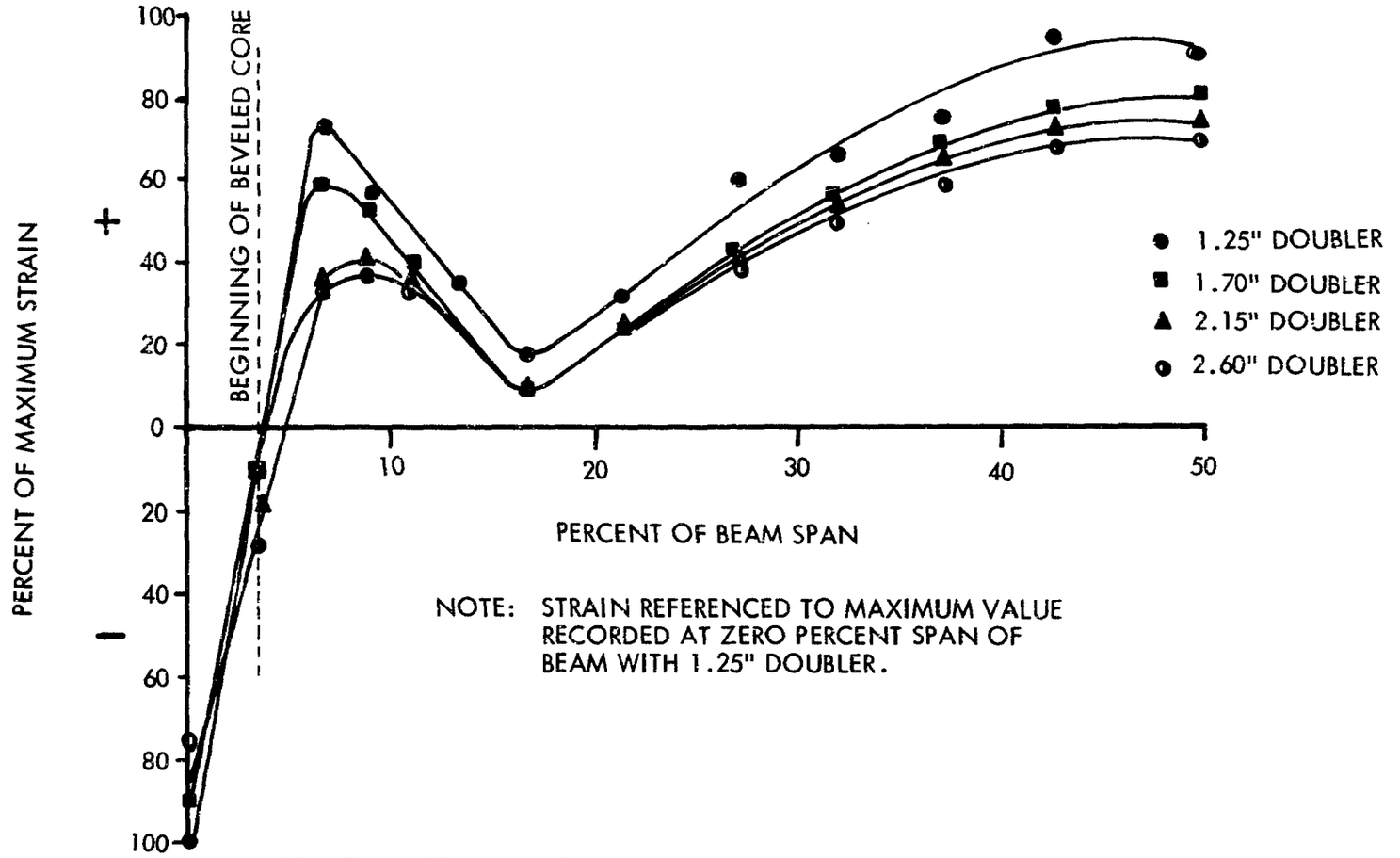

FIGURE 62. SPANWISE STRAIN FOR HONEYCOMB SANDWICH BEAM

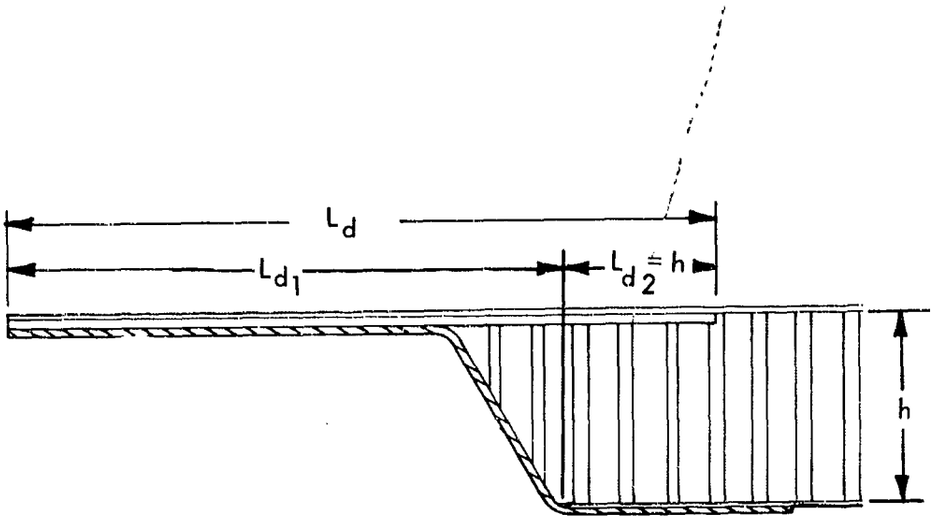

$$L_d = L_{d_1} + L_{d_2}$$

WHERE L_d IS THE WIDTH OF DOUBLER NECESSARY.

L_{d_1} IS THE WIDTH OF DOUBLER FROM THE EDGE OF THE PANEL TO BEGINNING OF FULL DEPTH CORE.

L_{d_2} IS THE ADDITIONAL WIDTH NEEDED AND EQUAL TO THE CORE THICKNESS.

FIGURE 63. SKETCH OF RECOMMENDED DOUBLER WIDTH TO MEET SONIC FATIGUE REQUIREMENTS

E. Discussion of Test Results

1. Skin-Stringer

a. Mode Shapes - Some of the modes could not be excited. From Table VI, it can be seen that the (2, 3), (3, 1), (3, 2) and (3, 3) modes were unresponsive in a number of instants. The lack of response is attributed to the inability of the electro-mechanical speakers to supply sufficient excitation energy at the higher frequencies.

A comparison of the skin-stringer modal frequencies determined for the modal frequency investigation and the frequencies resulting from the frequency sweeps show that the frequencies for the first mode do not correlate too well. It is believed that the differences can be attributed to ambient temperature differences. The temperature of the test specimens was approximately 70°F during the modal frequency investigation, which was conducted in a well-insulated anechoic room. Test specimen temperature during frequency sweeps was measured to be as low as 58°F and as high as 70°F, depending on the test chamber ambient temperature and the mass flow of air through the progressive wave test section. It is well known that modal frequencies for thin plates can vary greatly with small changes of temperature.

b. Frequency Sweeps - Strain activity above the first mode was less than originally expected. All but seven of the skin-stringer designs showed only one significant mode above the fundamental, usually the (1, 2) mode. Figure 29, the sweep response for STR-17A, is an illustration of strain response occurring in a number of modes. STR-26A demonstrated a response similar to that of STR-17A.

As described above, significant frequencies found during the modal frequency studies did not accurately compare with the frequency sweeps. This lack of correlation is attributed to dissimilar ambient temperature.

In some instances, stringer and rib torsion and stringer and rib bending influenced the response of the skin. Figure 30 presents the stringer and rib torsion and bending and rib influence on skin response for STR-26A.

c. Fatigue Tests - Three types of failures are commonly experienced by skin-stringer construction. The most common failure is the formation of fatigue cracks. These generally form around the fasteners where stress raisers exist. The cracks propagate, if the acoustical excitation is allowed to persist, until they include a number of fasteners. Figure 64a is a photograph of this type of fatigue crack which grew quite rapidly with continued exposure to the random acoustical excitation.

The prying action of the attached stringer or rib flange on the fasteners induces high stresses in them, and fastener fatigue and popped heads result. This type of failure was also experienced during the sonic fatigue tests. Figure 64b is a photograph of fastener fatigue and popped rivet heads typical of this type of fatigue failure.

The prying action of the attached flange on the fasteners also cause stresses in the attached flange, which may be critical if the stiffener thickness is smaller than the skin thickness, or if the flange is quite wide with a large bend radius. This type of fatigue failure was not experienced at anytime during the test program, indicating that stringer and rib flange thicknesses determined from Figure 31, Reference 1 , result in conservative designs.

Table VIII, the summary of skin-stringer fatigue tests, shows that the test spectrum was not the same for specimens A and B in every case. Average sound pressure level measurements

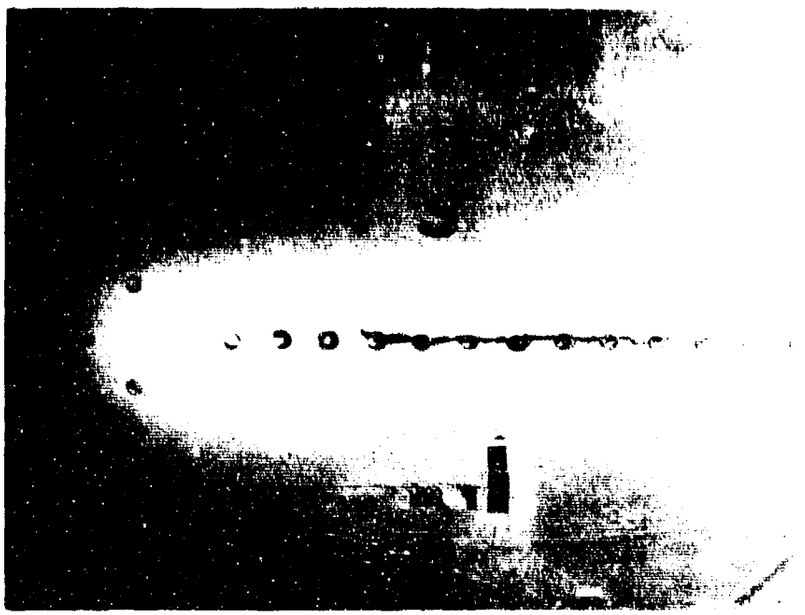

(a) Typical Fatigue Crack

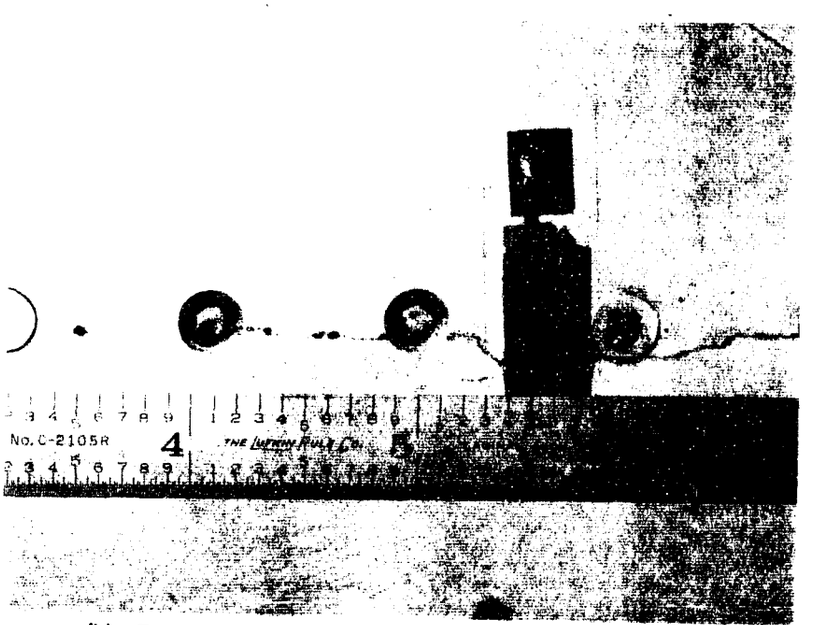

(b) Typical Fatigue Crack and Popped Rivet Heads

FIGURE 64. SKIN-STRINGER FATIGUE FAILURES

made during the tests showed a maximum variation of 2 decibels. A 1 decibel difference was common. The difference of sound pressure at specimens A and B was probably due to the normal modes of the progressive wave test section.

Four of the skin-stringer configurations showed predominant strain response in the (1, 2) mode, instead of the (1, 1) mode. The (1, 1) mode strain response of STR-3, STR-7, STR-11 and STR-21 was considerably less than the (1, 2) mode strain. A stroboscope was used in each case to determine which mode was predominant. The stroboscope study confirmed the belief that the (1, 2) mode was the strongest in each case. No explanation is offered as to why this happened, except possibly the (1, 1) mode damping was more than the (1, 2) mode damping. Figure 37, a narrow-band analysis of panel strain from the fastener line of STR-21B, is an illustration of this type response.

The number of positive crossings to failure was determined from unfiltered oscillograph traces. Ten-second samples of the type shown on Figure 65 were used to determine the number of positive crossings per second.

The fatigue curve, Figure 34, shows the characteristic data scatter, especially above 10^7 crossings to failure. Between the ±95-percent confidence limits, the scatter factor bounded by the ±95-percent confidence limits is 17.85.

The fatigue curve for the skin-stringer tests should be compared to fatigue curves for similar material, loading and stress raisers. Royal Aeronautical Society fatigue data, Reference 19 , were selected for the comparison. Table XI is a summary of the comparison.

TABLE XI

COMPARISON OF RAS FATIGUE DATA WITH SKIN-STRINGER FATIGUE DATA

Description	Inverse negative slope of fatigue curve	Regression line rms stress, ksi			Scatter factor bounded by ±95% conf. limits
		10^6	10^7	10^8	
RAS	4.59	8.95	5.39	3.24	23.10
Skin-Stringer Plating	4.55	8.80	5.25	3.18	17.85

The data tabulated above indicate that the skin-stringer fatigue data and RAS fatigue data compare favorably.

Ninety-five-percent confidence limits were established for the mean fatigue curve of the skin-stringer design nomograph, Figure 31, Reference 1. This was done by assuming that the fatigue curve of Figure 31, Reference 1, had the same mean stress and standard deviation as the fatigue curve for reversed bending across a rivet line contained in Reference 20. This assumption may not have been extremely accurate, but it was the only known way of getting an indication of the 95-percent confidence limits. The confidence limits were needed to establish a go/no-go test for determining whether or not additional sets of a given design should be tested to establish structural reliability.

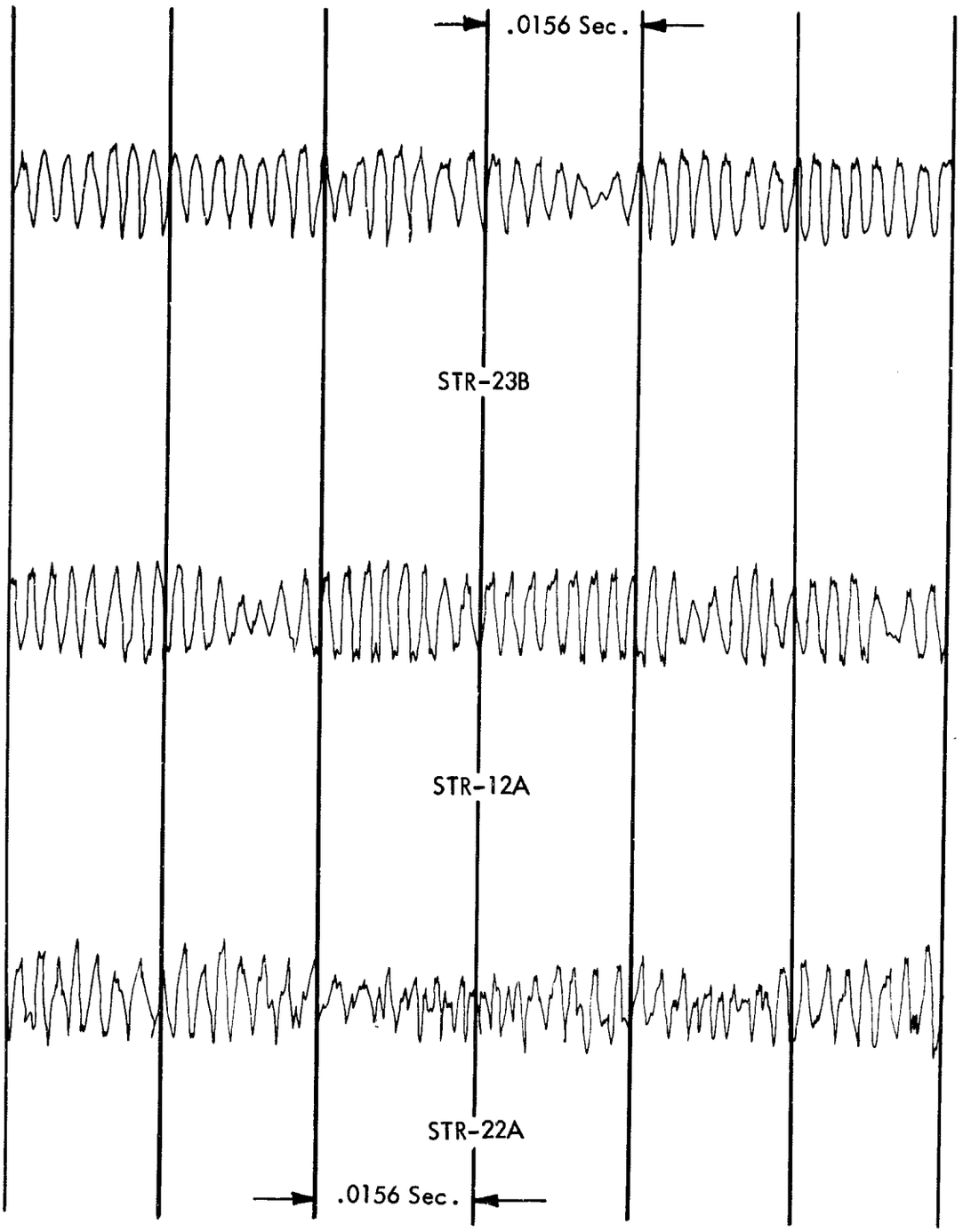

FIGURE 65. TYPICAL SKIN-STRINGER STRAIN TIME HISTORIES

The rule established was that if one of the two specimens tested at a given condition exhibit a life which fell outside the ±95-percent confidence limits, the status of the test results relative to the design nomograph was no-go. The fatigue life of both replicates had to fall within the ±95-percent confidence limits for the status to be go. Only 4 of the 30 designs fell in the go category. In fact, only 15 percent of the test specimens tested had lives which fell in the ±95-percent confidence limits. Furthermore, 6.65 percent of the 60 test specimens tested fell below the lower 95-percent confidence limit and 78.4 percent were above the 95-percent confidence limit. These results indicate that the design nomograph for skin-stringer construction in Reference 1 is conservative in the range of test conditions reported herein.

STR-1 and STR-2 were identical designs except the stringers on STR-2 had bent flanges. They were tested under the same conditions to determine if the added stringer flange stiffness influenced the fatigue resistance of the design. Apparently it did not since the fatigue life in each case was about the same (see Table VIII).

STR-3 design was retested as STR-21 because the first test resulted in one specimen falling in the go category and the other specimen in the no-go category. STR-21 tests decided the issue and placed the design into the go category; both STR-21A and STR-21B demonstrated lives which fell within the ±95-percent confidence interval described above.

STR-5 was retested as STR-22 because the fatigue life of STR-5B was approximately ten times that of STR-5A. The tests of STR-22 showed conclusively that the time to failure experienced by STR-5A was not representative of the fatigue resistance of the design.

The results of the tests involving STR-10 were questionable due to poor test specimen design. This design should have had a greater fatigue resistance than STR-1, STR-2, and STR-3. It did not! The adjacent bays of the test specimen were slightly larger than the most important center bay. It is believed the adjacent bays were excited in their first mode because the bandwidth of the sound pressure excitation was wide enough to develop their full (1,1) mode response. The cracks which formed on the fastener lines probably resulted from the vibration of the slightly larger adjacent bays. STR-23 was designed as a retest of STR-10. The adjacent bays of STR-23 were the same size as the center bay. STR-23 test results showed that the STR-10 specimen design was poor. The time to failure was comparable to STR-1, STR-2, and STR-3, within acceptable scatter of fatigue data.

The experimentally determined probability distribution of fastener line instantaneous strain and strain peaks, Figures 39 through 42, show that both probability distributions for each of the designs deviate somewhat from the Gaussian and Rayleigh. The deviation from the theoretical distributions is attributed to nonlinear response and multimodal influences.

2. Honeycomb Sandwich

a. Mode Shapes - From Table IX it can be seen that, in general, modes above the (2,1) were unresponsive. In some instances the (1,3) mode could not be detected by the cork particles. The lack of response is attributed to insufficient excitation energy from the electromechanical speakers at the higher frequencies where the generalized force is reduced.

HC-1, HC-5 and HC-22, HC-10, HC-12, HC-20, and HC-30 showed two (1,1) mode Chladni patterns at two frequencies. This is attributed to the tapered edge design, because at the lower frequency the mode lines formed very close to the fastener row. At the higher frequency, the mode lines formed near the shoulder of the bevel where the tapered edge begins. Apparently the two (1,1) Chladni patterns are the result of this relative stiffness phenomenon.

A comparison of the first mode frequencies from the modal studies with the frequency sweeps shows that the correlation is much better for the honeycomb sandwich panels than it was for the skin-stringer test specimens. Vibration response of honeycomb sandwich is less sensitive to ambient temperature changes than thin skin-stringer designs.

b. Frequency Sweeps - Significant strain response activity above the first mode was negligible. HC-20A, however, showed a two-peak response with the frequencies about 20 Hz apart (see Figure 45). This two-peak type response was detected more during the modal frequency studies than at any other time.

c. Fatigue Tests - Three types of sonic fatigue failures were experienced by the honeycomb sandwich test specimens. The most common was fatigue cracks which formed around the fastener holes. Figure 66 is a photograph of a typical fatigue crack of this type. This type of failure occurred in 56.8 percent of the specimens.

Facing sheet cracks occurred at the center of a panel. The cracks were found to occur for the most part at the midspan of the long dimension of the panel. Figure 67 is a photograph of this type failure. This type of failure occurred in 43.4 percent of ths specimens.

Core shear fatigue was the third type of failure that was experienced. This type occurred near the edge (20-30% of short span) of HC-15A where the core shearing stress was the greatest. Figures 68a and 68b are photographs of this core shear fatigue failure.

Bubbling-mode failures and facing sheet to core bonding failures were not detected.

As discussed previously, the test spectrum level was not always the same for specimens A and B. The variation seemed to be a function of test specimen frequency and test specimen size. However, the maximum variation in level was 3 db, experienced by the large 37-inch by 61-inch panels. One to two db variations were common.

Like the skin-stringer tests, a go/no-go test was set up for checking the honeycomb sandwich design nomograph in Reference 1 against the test results. Honeycomb sandwich fatigue data from Reference 21 were used to establish the ±95-percent confidence limits.

Three of the thirty designs fell in the go category. Ten percent of all specimens tested fell in the go category. Only 6.7 percent of all the specimens tested fell below the lower 95-percent confidence limit and 81.7 percent were above the upper 95-percent confidence limit, indicating that the design nomograph in Reference 1 is conservative in the range of test conditions reported here.

HC-16A was damaged when the test fixture broke. The results from this test specimen were omitted from all analyses.

HC-27 was designed with an aluminum alloy pan 0.025-inch thick instead of fiberglass. There were no outstanding increases in fatigue resistance or response characteristics as compared to the fiberglass closure.

HC-29 was designed with an aluminum alloy pan 0.030-inch thick and a tapered doubler. Like HC-27, there were no outstanding changes observed in fatigue life and response characteristics as compared to the conventional doubler and fiberglass closure.

HC-28 was made with the honeycomb core crushed to form the beveled edge instead of the conventional machined edge. There were no observable changes in dynamic response characteristics or differences in fatigue life as compared to the test specimens with

FIGURE 66. TYPICAL HONEYCOMB SANDWICH EDGE FATIGUE CRACKS

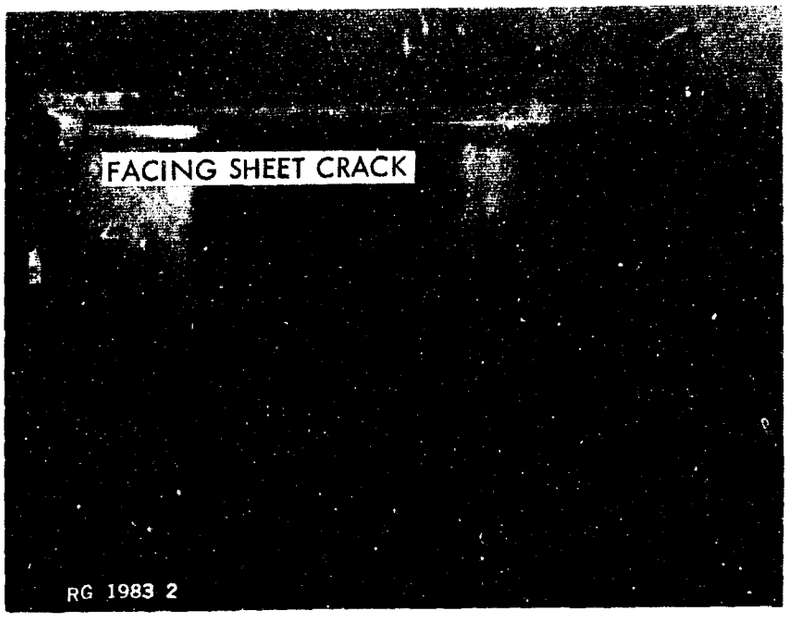

FIGURE 67. TYPICAL HONEYCOMB SANDWICH FACING SHEET FATIGUE CRACK

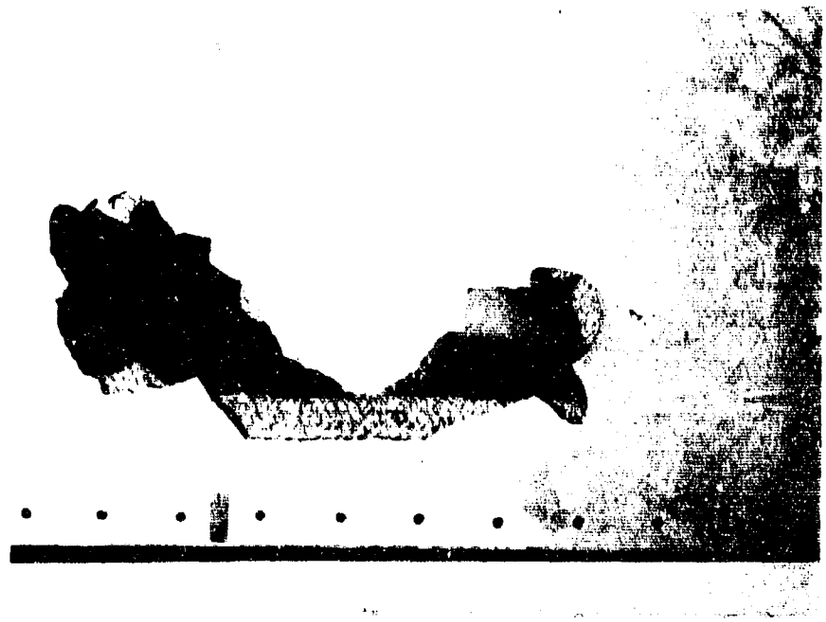

(a) Typical CORE Shear Fatigue Failure

(b) Section of Honeycomb Panel Showing Core Shear Fatigue

FIGURE 68. HONEYCOMB CORE SHEAR FATIGUE FAILURES

machined beveled edges. The test specimens were sectioned in a number of places to examine the crushed core for shear fatigue. The examinations showed that the integrity of the core had not been altered by crushing it.

IV - CORRELATION OF TEST DATA AND DYNAMIC STRESS RESPONSE PARAMETERS

A. Introduction

The theoretical and analytical material presented in Section II suggests ways of correlating the test data contained in Section III and dynamic stress response parameters for the two types of aircraft structure relevant to this research program. For example, the first mode response was observed to be the most active and most fatigue damaging for both types of structure. Also, the location and type of fatigue cracks experienced in the experimental phase of the program suggest there are bending moments at the edges of the panels, or along the fastener line in the case of the skin-stringer configuration. Modal frequency studies and frequency sweep investigations indicate strongly that both the skin-stringer and honeycomb sandwich panel edge fixity lies intermediate of fully clamped and simply supported. See Figures AV-1 and AV-2, Appendix V.

It is the purpose of this section to show the correlation of test data with the dynamic stress response parameters as suggested by the theory presented in Section III.

B. Skin-Stringer Construction

In aircraft structure, the individual bays (panels) are connected to adjacent bays or support structure at their boundaries and have elastic restraints at their edges. As shown in Section II.D, a combination of stringer torsion and bending, rib torsion and bending, and phasing among adjacent bays can result in a very complicated dynamic system. For this analysis, however, the significant mode of response is considered to be that of a plate having an edge fixity someplace between fully clamped and simply supported; the fixity to be determined empirically.

Intuitively, Equation (36) contains the significant parameters for describing the skin stress response of a bay of skin-stringer structure. This will be tested as follows:

First, Equation (36) can be written in terms of root-mean-square (rms) stress as

$$\frac{{}_s(\bar{\sigma})_e}{\left[f_i \Phi_{(f)}\right]^{1/2}} = K_1 \left(\frac{b}{t}\right)^2 \frac{1}{R\delta}^{1/2} \qquad (36a)$$

where K_1 is a proportionality constant.

Second, the first mode frequency for clamped edges, Equation (20b), can be expressed as

$$f_i = K_2 \left[\frac{gE}{\gamma}\right]^{1/2} \frac{t}{ab} R^{1/2} \qquad (20c)$$

where K_2 is a proportionality constant dependent upon the edge fixity.

Third, Equation (20c) is substituted into Equation (36a) to obtain two dimensionless groups as follows:

$$\frac{{}_s(\bar{\sigma})_e}{\left(\frac{gE}{\gamma}\right)^{1/4}\left(\frac{t}{ab}\right)^{1/2}\Phi_{(f)}^{1/2}} = K_3\frac{\left(\frac{b}{t}\right)^2}{R^{3/4}\delta^{1/2}} \qquad (36b)$$

where K_3 is a proportionality constant.

Equation (36b) suggests that nominal overall stresses measured at the point of maximum stress on the fastener line where the fatigue cracks developed should be divided by the groupings $(gE/\gamma)^{1/4}$, $(t/ab)^{1/2}$, and $\Phi_{(f)}^{1/2}$ and plotted versus the dimensionless group $(b/t)^2/(R^{3/4}\delta^{1/2})$ to empirically determine K_3. This was accomplished. Table XII is the tabulated results and Figure 69 is a rectangular coordinate plot of the data.

The regression lines drawn through the data points of Figure 69 were determined by the method of least squares described in Appendix II. A correlation coefficient, a measure of the "goodness of fit" of the equation to the test data was computed to be 0.86 for the linear equation and 0.88 for the exponential equation. From a table of correlation coefficients in Reference 22, it was determined that the probability of getting correlation coefficients of the magnitudes described above in the absence of any correlation is less than 1 in 1,000.

The exponential regression line equation for the data plotted in Figure 69 is

$$\bar{\sigma} = 1.62 \times 10^{-4}\left[\frac{Eg}{\gamma}\right]^{1/4}\frac{a^{1.25}}{t^{1.75}}\frac{\Phi_{(f)}^{1/2}}{\delta^{0.56}}F(ar) \qquad (36c)$$

where $F(ar) = (b/a)^{1.75}/R^{0.84}$.

For aluminum alloy, $(Eg/\gamma)^{1/4} \approx 443$ and Equation (36c) becomes

$$\bar{\sigma} = 0.072\frac{a^{1.25}}{t^{1.75}}\frac{\Phi_{(f)}^{1/2}}{\delta^{0.56}}F(ar) \qquad (36d)$$

The regression lines from the physical viewpoint should pass through the origin of the axes. It did not in the case of the linear equation because of test data scatter and possible response non-linearities.

The arrangement of parameters suggested by the simply supported edge equations, Equations (24b) and (42), was also analyzed as described above because the edge fixity lies between clamped and simply supported. The correlation coefficients for these regression lines were significantly lower: 0.54 for the linear fit and 0.58 for the exponential fit.

Comparing the correlation coefficient, it is apparent that Equation (36d) should be used to develop the design nomograph for aluminum alloy skin-stringer plating.

TABLE XII

DATA FOR CORRELATING SKIN-STRINGER PANEL RESPONSE PARAMETERS WITH MEASURED STRESS

Designation	Dimensionless group $\frac{\left(\frac{b}{t}\right)^2}{R^{3/4}\,\delta^{1/2}} \times 10^{-3}$	Dimensionless group $\frac{\bar{\sigma}}{\left(\frac{qE}{\gamma}\right)^{1/4}\left(\frac{t}{ab}\right)^{1/2}\Phi_{(f)}^{1/2}} \times 10^{-1}$
1A	15.25	13.62
B	15.25	14.36
2A	13.93	11.82
B	13.93	11.70
3A	15.79	20.58
B	15.79	21.30
4A	8.30	5.74
B	8.30	7.15
5A	4.66	3.85
B	4.66	4.10
6A	8.54	7.50
B	8.54	9.95
7A	26.26	19.62
B	26.26	16.43
8A	1.47	1.07
B	1.47	1.00
9A	20.64	30.70
B	20.64	32.28
11A	31.67	24.20
B	31.67	31.64
12A	18.65	12.55
B	18.65	12.22
13A	16.30	11.49
B	16.30	12.03
14A	12.83	7.30
B	12.83	11.18
16A	6.19	3.74
B	6.19	5.38
17A	7.99	4.25
B	7.99	4.46
18A	4.66	2.38
B	4.66	3.31

TABLE XII (Continued)

DATA FOR CORRELATING SKIN-STRINGER PANEL RESPONSE PARAMETERS WITH MEASURED STRESS

Designation	Dimensionless group $\frac{\left(\frac{b}{t}\right)^2}{R^{3/4}\delta^{1/2}} \times 10^{-3}$	Dimensionless group $\frac{\bar{\sigma}}{\left(\frac{gE}{\gamma}\right)^{1/4}\left(\frac{t}{ab}\right)^{1/2}\Phi_{(f)}^{1/2}} \times 10^{-1}$
19A	4.07	2.41
B	4.07	2.67
20A	5.75	3.55
B	5.75	3.16
21A	15.26	7.89
B	15.26	8.10
22A	4.48	2.11
B	4.48	2.67
23A	12.76	8.48
B	12.76	9.41
24A	21.97	17.92
B	21.97	25.46
25A	3.49	2.35
B	3.49	2.26
26A	2.77	1.38
B	2.77	2.47
27A	5.83	2.08
B	5.83	2.95
28A	5.91	3.01
B	5.91	3.01
29A	10.97	6.70
B	10.97	7.72
30A	11.93	1.24
B	11.93	1.39

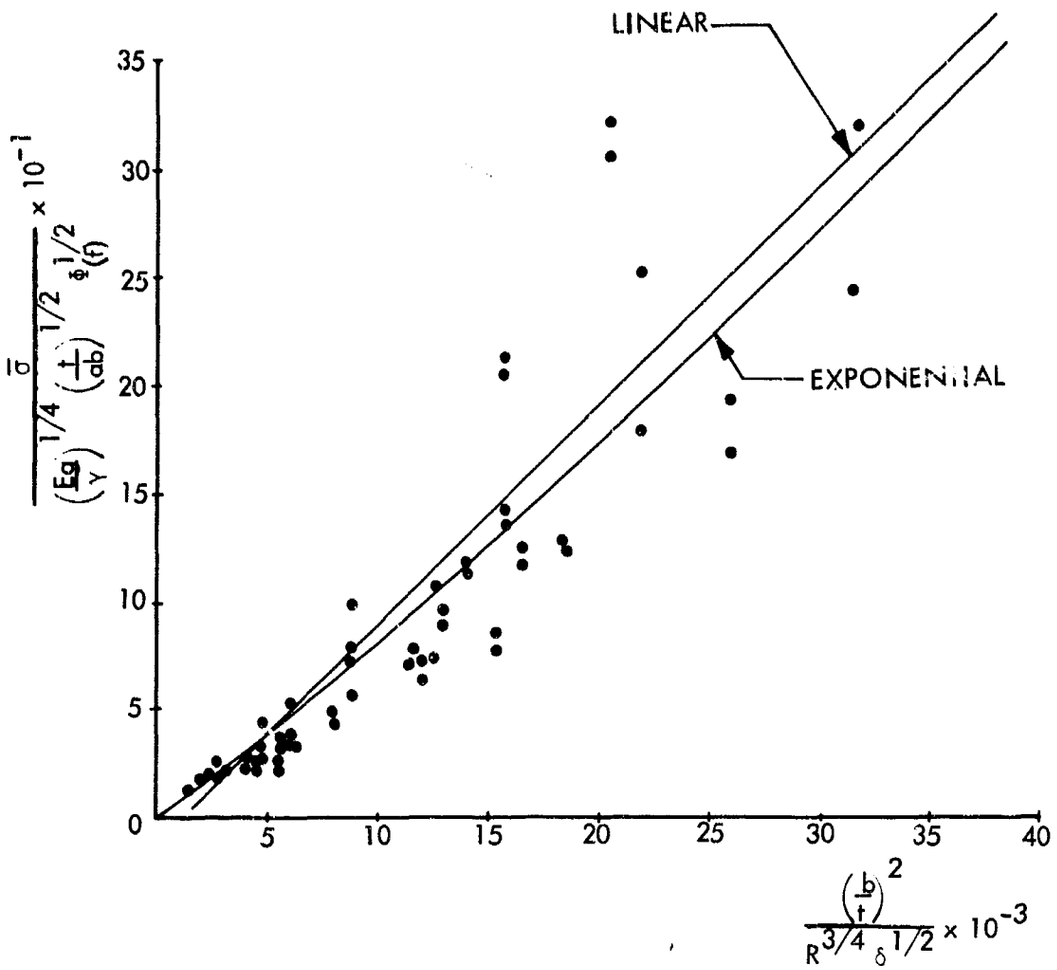

FIGURE 69.

PLOT OF $\frac{\bar{\sigma}}{\left(\frac{Eg}{\gamma}\right)^{1/4}\left(\frac{t}{ab}\right)^{1/2}\Phi_{(f)}^{1/2}}$ VS. $\frac{\left(\frac{b}{t}\right)^2}{R^{3/4}\,\delta^{1/2}}$

C. Honeycomb Sandwich Construction

Facing sheet and edge fatigue cracks are by far the most common failure in honeycomb sandwich construction. Core shear fatigue is considered to be secondary. All three of the potential failure modes were investigated from the test data correlation point of view.

1. Edge Stress Correlation

The observed response characteristics of the flat honeycomb sandwich panels were those of a panel having edge fixity between fully clamped and simply supported. Therefore, the arrangement of parameters suggested by Equations (82) and (86) was intuitively believed to be the arrangement which would show the better correlation. These equations were arranged into two dimensionless groups as described in the previous section, with the end result as follows:

$$\frac{h(\bar{\sigma})_e}{\left(\frac{Eg}{\gamma}\right)^{1/4}\left(\frac{h}{ab}\right)^{1/2}\Phi_{(f)}^{1/2}} = K_e \frac{\left(\frac{b}{t_e}\right)^2}{R^{3/4}\,\delta^{1/2}} \tag{86a}$$

where ρ in Equation (82) was approximated by $2t\gamma/g$, γ being the specific weight of the facing sheet material.

Table XIII is a tabulation of the values computed as suggested by Equation (86a) and Figure 70 is a plot of the data. The regression lines shown on Figure 70 were determined by the method of least squares. The correlation coefficients for the linear equation and the exponential equation are 0.86 and 0.88, respectively.

The arrangement of dimensionlss groups suggested by the combination of Equations (83) and (92) for simply supported edges was also studied. Correlation coefficients were computed to be 0.56 for the linear fit and 0.59 for the exponential fit. These are considerably less significant than the coefficients for fixed edges.

Consequently, the most accurate empirically determined regression line equation for honeycomb sandwich edge stress design is

$$\bar{\sigma} = 1.46 \times 10^{-3}\left(\frac{Eg}{\gamma}\right)^{1/4} \frac{a^{0.51}}{t_e^{1.51}} \frac{\left[h\,\Phi_{(f)}\right]^{1/2}}{\delta^{0.38}} F(ar) \tag{86b}$$

where $F(ar) = (b/a)^{1.01}/R^{0.57}$.

For aluminum alloy, Equation (86b) becomes

$$\bar{\sigma} = 0.65 \frac{a^{0.51}}{t_e^{1.51}} \frac{\left[h\,\Phi_{(f)}\right]^{1/2}}{\delta^{0.38}} F(ar) \tag{86c}$$

The above equation will be used in Section V to develop the design nomograph.

TABLE XIII

DATA FOR CORRELATING HONEYCOMB SANDWICH PANEL EDGE STRESS RESPONSE PARAMETERS WITH MEASURED STRESS

Designation	Dimensionless group $\frac{\left(\frac{b}{te}\right)^2}{R^{3/4}\,\delta^{1/2}} \times 10^{-5}$	Dimensionless group $\frac{\bar{\sigma}}{\left(\frac{gE}{\gamma}\right)^{1/4}\left(\frac{h}{ab}\right)^{1/2}\phi_{(f)}^{1/2}} \times 10^{-1}$
1A	4.15	2.65
B	4.15	5.50
2A	5.63	2.63
B	5.63	2.22
3A	5.21	4.30
B	5.21	4.10
4A	2.27	2.41
B	2.27	2.92
5A	13.12	8.06
B	13.12	7.20
6A	8.00	6.99
B	8.00	6.48
7A	3.19	1.33
B	3.19	1.33
9A	3.03	1.25
B	3.03	1.87
10A	2.93	3.15
B	2.93	3.10
22A	13.12	7.24
B	13.12	7.18
24A	10.00	6.84
B	10.00	6.56
26A	9.81	3.84
B	9.81	7.64
27A	4.50	2.18
B	4.50	2.31
28A	9.81	3.55
B	9.81	3.60
29A	2.79	1.31
B	2.79	2.25
30A	14.01	7.43
B	14.01	8.52

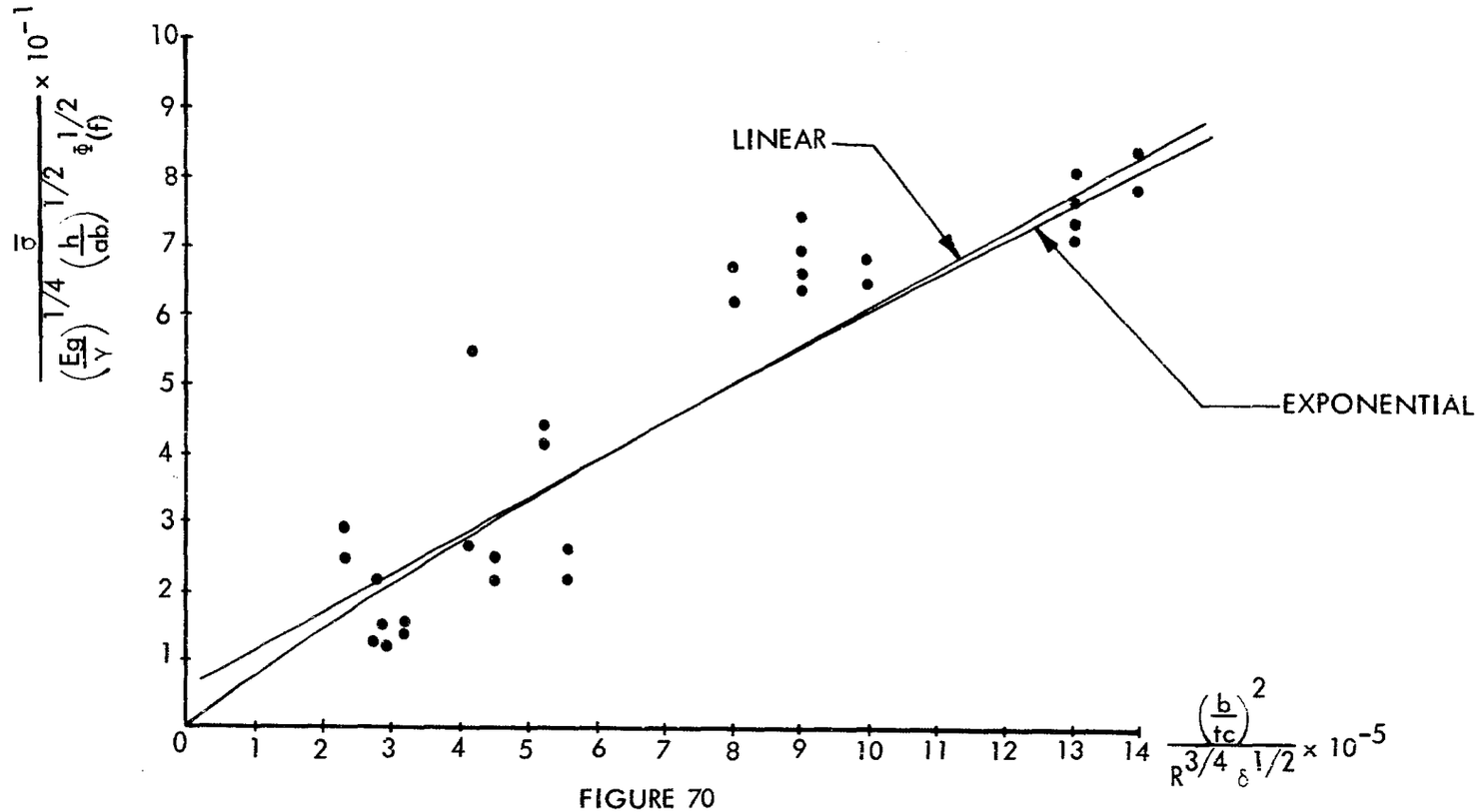

FIGURE 70

PLOT OF $\frac{\bar{\sigma}}{\left(\frac{Eg}{\gamma}\right)^{1/4}\left(\frac{h}{ab}\right)^{1/2}\Phi_{(f)}^{1/2}}$ VS. $\frac{\left(\frac{b}{te}\right)^2}{R^{3/4}\delta^{1/2}}$

2. Facing Sheet Stress Correlation

Equations for simply supported and fully clamped edges were considered in the correlation of the facing sheet stresses and flat panel stress response parameters. The arrangement of parameters suggested by Equations (83) and (92) and arranged in two dimensionless groups as described previously demonstrated the better correlation coefficients. These were 0.86 for the linear equation and 0.87 for the exponential equation. Correlation coefficients computed for the arrangement of parameters suggested by the combination of Equations (82) and (89) were considerably less significant than those listed above.

A combination of Equations (83) and (92) produces the following equation:

$$\frac{h(\bar{\sigma})_f}{\left(\frac{Eg}{\gamma}\right)^{1/4}\left(\frac{h}{a^2}\right)^{1/2}\Phi_{(f)}^{1/2}} = K_o \frac{a^2 f(ar)}{th\,\delta^{1/2}} \tag{92a}$$

where K_o is a proportionality constant and

$$f(ar) = \frac{\left(\frac{b}{a}\right)\left[\left(\frac{b}{a}\right)^2 + \nu\right]}{\left[\left(\frac{b}{a}\right)^2 + 1\right]^{3/2}}$$

Table XIV is a summary of the values computed as suggested by the above equation. Figure 71 is a plot of these data which resulted in the following exponential regression line equation:

$$\bar{\sigma} = 1.8 \times 10^{-3}\left[\frac{Eg}{\gamma}\right]^{1/4} \frac{a^{0.46}}{t^{0.73}h^{0.23}} \cdot \frac{\Phi_{(f)}^{1/2}}{\delta^{0.36}} f(ar)^{0.73} \tag{92b}$$

For aluminum alloy, Equation (92b) becomes

$$\bar{\sigma} = 0.90 \frac{a^{0.46}}{t^{0.73}h^{0.23}} \frac{\Phi_{(f)}^{0.50}}{\delta^{0.36}} f(ar)^{0.73} \tag{92c}$$

Equation (92c) above is used in Section V to develop a design nomograph for honeycomb sandwich facing sheets.

D. Simple Panel Curvature Effects

Correlation of the theory developed in Section II for evaluating panel curvature effects on stress response and the test data contained in Reference 12 will be described in this section.

The specimens tested in Reference 12 were defined by the parameters

TABLE XIV

DATA FOR CORRELATING HONEYCOMB SANDWICH PANEL FACING SHEET RESPONSE PARAMETERS WITH MEASURED STRESS

Designation	Dimensionless group $\left(\frac{a^2}{th}\right)\frac{f_{(ar)}}{\delta^{1/2}} \times 10^{-5}$	Dimensionless group $\frac{\bar{\sigma}}{\left(\frac{qE}{\gamma}\right)^{1/4}\left(\frac{h}{a^2}\right)^{1/2}\Phi_{(f)}^{1/2}} \times 10^{-1}$
11A	2.62	2.18
B	2.62	2.00
12A	2.24	1.44
B	2.24	1.86
13A	2.32	1.72
B	2.32	1.45
14A	1.43	1.62
B	1.43	1.76
15B	6.05	3.16
16A	3.77	2.39
B	3.77	2.35
17A	1.68	1.26
B	1.68	1.64
18A	1.64	1.19
B	1.64	1.19
19A	2.08	1.27
B	2.08	1.38
20A	3.08	2.19
B	3.08	2.06
21A	5.36	3.50
B	5.36	3.24
23A	3.71	2.39
B	3.71	2.29
25A	3.78	2.45
B	3.78	1.94

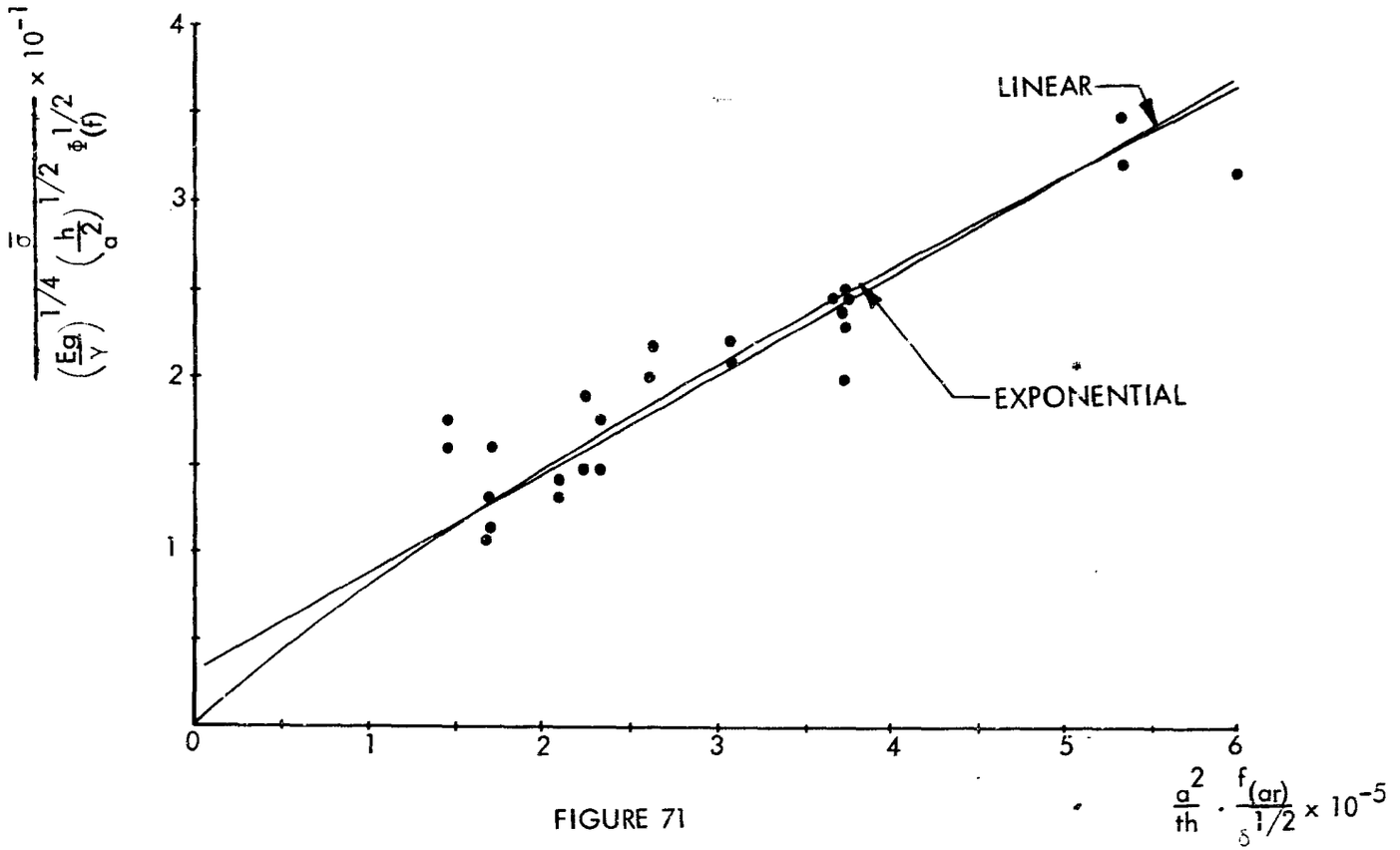

FIGURE 71

PLOT OF $\frac{\bar{\sigma}}{\left(\frac{Eg}{\gamma}\right)^{1/4}\left(\frac{h}{2a}\right)^{1/2}\Phi_{(f)}^{1/2}}$ VS. $\frac{a^2}{th} \cdot \frac{f_{(ar)}}{\delta^{1/2}}$

$A = 0.82$

$L = 344$

$\phi = 0$, 0.094, 0.125, and 0.188 radians

Equation (111), rewritten below, was used to evaluate C_1 and C_2. The specimen parameters listed above and ratios of rms curved panel stress to rms flat panel stress shown in Table XV were used to accomplish the evaluation.

$$\frac{\sigma_c}{\sigma_f} = \left[1 + \frac{C_2(AL\phi)^2}{A^4 + 0.61A^2 + 1}\right]^{-3/4} \left[1 + C_1\left(\frac{A^2 + 0.034}{A^4 + 9.62A^2 + 1}\right)AL\phi\right] \qquad (111a)$$

The stress ratios are:

TABLE XV

EXPERIMENTAL CURVED AND FLAT PANEL RMS STRESS RATIOS

ϕ	σ_c/σ_f
0.00	1.00
0.094	0.80
0.125	0.45
0.188	0.23

The constants C_2 and C_1 were determined to be 0.006 and 0.453.

Even though Equation (111a) is not exact, a method is available for predicting the effects or radius of curvature, aspect ratio, and length to thickness ratio. Equation (111a) will be used in Section V to develop a design nomograph for assessing curvature effects of skin-stringer panels.

E. Honeycomb Sandwich Curvature Effects

Strain data were measured on one curved honeycomb sandwich test specimen. These data were used to check (1) the ratio of the facing sheet stresses at the center of the panel and (2) the ratio of the y component of the stress to the x component of the stress at the same point on the curved panel. In an attempt to validate the effect of curvature on facing sheet stress at the center of the panel and also the effect on edge stress, strain data were measured on a similar flat sandwich panel. The strains were transformed by the theory developed herein to accomplish the comparison.

In the experimental determination of strain ratios, both flat and curved panels were tested at a discrete frequency sound pressure level of 130 decibels. The frequency in each case was set at the (1,1) mode response. Absolute strain was not determined; however, the strain for both panels was normalized to the same base.

The flat and curved panel parameters are listed in Table XVI. The non-dimensional parameters are given in Table XVII, and the relative strain data are tabulated in Table XVIII.

TABLE XVI

TEST SPECIMEN PHYSICAL PARAMETERS

	Curved Panel	Flat Panel
a	23.0"	20.0"
b	29.0"	30.0"
h_1	.125"	.145"
t_2	.008"	.025"
R	84"	∞
G_{yz}	9,000 psi	15,000 psi
G_{xz}	18,000 psi	30,000 psi
E	16.2×10^6 psi	10×10^6 psi
t_e	.045"	.101" - 4 ply -.040

TABLE XVII

TEST SPECIMEN NON-DIMENSIONAL PARAMETERS

Parameter	Curved Panel	Flat Panel
θ	.345 Radians	0
L	2875.	800
b/t_e	511.	198
A	1.26	1.50
g	15.6	5.8
s	.000495	.00133
c	2.0	2.0

TABLE XVIII

RELATIVE MEASURED FACING SHEET STRAIN (NO SCALE)

Outside ($z=h_1$)	Curved Panel	Flat Panel
ϵ_y center	34.2	14.5
ϵ_x center	25.3	31.0
ϵ_y edge	38.0	15.5
ϵ_x edge	26.5	18.0
Inside ($z=-h_1$)		
ϵ_y center	10.0	17.0
ϵ_x center	13.5	27.5

The stress values for the flat panel stress data were derived using Equation (137) for σ_y with $\emptyset$ set zero. In addition, Equations (149), (155), and (156) were used to define the generalized displacement, W_{mn}. To obtain the stress transformation between flat panel designs the equation is

$$\sigma_{y1\ \text{center}} = \frac{\left[\frac{A^2L^2S_3}{g\,S_1}\right]_1}{\left[\frac{A^2L^2S_3}{g\,S_1}\right]_2}\ \sigma_{y2\ \text{center}} \tag{158}$$

for converting from a design 2 to a desired design 1. A similar transformation for edge stress was derived from the relationship

$$\sigma_y = \frac{Et_e}{2(1-\nu^2)}\left(\frac{\partial^2 w}{\partial y^2} + \nu\frac{\partial^2 w}{\partial x^2}\right) \tag{25a}$$

The term $\frac{\partial^2 w}{\partial x^2}$ is zero along the edge, $y = 0$. Again Equations (149), (155), and (156) were used to determine the generalized deflections. The stress transformation ratio for the edge is,

$$\sigma_{y1}\Big|_{edge} = \frac{\left[\frac{L}{t_e}\left(\frac{AL}{g}\right)^2 \frac{S_2}{S_1}\right]_1}{\left[\frac{L}{t_e}\left(\frac{AL}{g}\right)^2 \frac{S_2}{S_1}\right]_2} \sigma_{y2}\Big|_{edge} \qquad (159)$$

A comparison of the calculated and measured data is presented in Table XIX. Although magnitudes do not correlate exactly the trends are apparent.

TABLE XIX

STRESS RATIO COMPARISON

	Calculated	Measured
$\frac{\sigma_{yc}}{\sigma_{xc}}\Big\|_{center}$	1.71	1.16
$\frac{\sigma_{yc,\ z=h_1}}{\sigma_{yc,\ z=h_1}}\Big\|_{center}$	1.86	2.93
$\frac{\sigma_{yc}}{\sigma_{yf}}\Big\|_{center}$	0.873	0.337
$\frac{\sigma_{yc}}{\sigma_{yf}}\Big\|_{edge}$	2.04	1.23

V - DEVELOPMENT OF DESIGN EQUATIONS AND NOMOGRAPHS

A. Introduction

The information required to produce a design nomograph for a specific type of structure is an analytical expression for the stress which is caused by the random acoustical excitation and the allowable fatigue stress and life relationship. The analytical expression, as derived in Section IV, has empirically determined edge fixity and built-in stress concentration factors.

To be useful and practical, the design nomograph also must be as free as possible of complexities, easy to use, and give an accurate representation of the test results from which it was derived.

B. Skin-Stringer

1. Skin Design

Figure 72 is a sketch showing the nomenclature for a simple flat panel that is representative of a single bay of skin stringer construction. The analytical expression used for developing the skin-stringer nomograph, Figure 73, is Equation (36d) and the fatigue curve, Figure 34. An example problem is also presented to illustrate the use of the nomograph.

2. Stringer Flange Stresses

The prying action of the attached flange on the fasteners (rivets) causes stresses in the attached flange which may be critical. Since there were no stringer or rib flange failure experienced during the experimental phase of this program, the design nomograph is identical to the one developed in Reference 1. The stress in the flange of the rib was expressed as:

$$\bar{\sigma}_r \propto \frac{Pa}{t_r^2} \tag{160}$$

One factor entering the rib-moment equation is the stringer flange width. In Reference 1 it was stated that this dimension varies only with stringer thickness for good design practice and is evaluated through the test results. Figure 74 is a sketch of skin-stringer construction details and Figure 75 is the stringer and rib flange design nomograph.

3. Design Nomograph for Supporting Structure

In order to develop the design nomographs for stiffened flat panels, it was convenient to restrict considerations to a panel with constant rib spacing and constant stringer spacing covered by a uniform thin sheet. The ribs and stringers are considered to be uniform members, each characterized by its bending rigidity and its torsion rigidity. The above situation is illustrated in Figure 76.

As mentioned previously, there are three modes of interest for sonic fatigue considerations. These modes are broadly characterized as rib bending - stringer trosion, rib - torsion - stringer bending, and coupled rib - stringer bending - torsion. Hence, the nomograph can be used to predict three frequencies for each design. The purpose of this analysis is to consider the motion of the structure as a whole and is not concerned with component

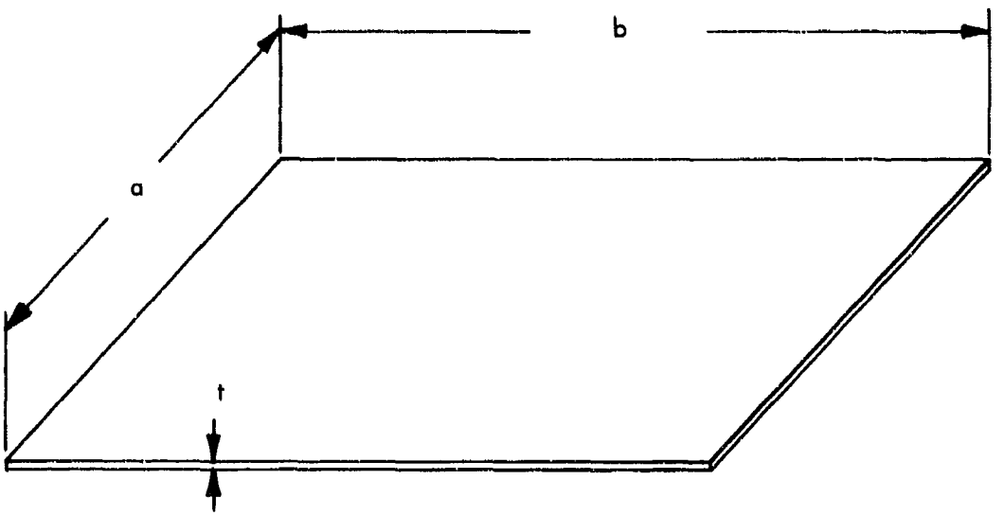

FIGURE 72. NOMENCLATURE FOR SIMPLE FLAT PANEL (REPRESENTATIVE OF A SINGLE BAY)

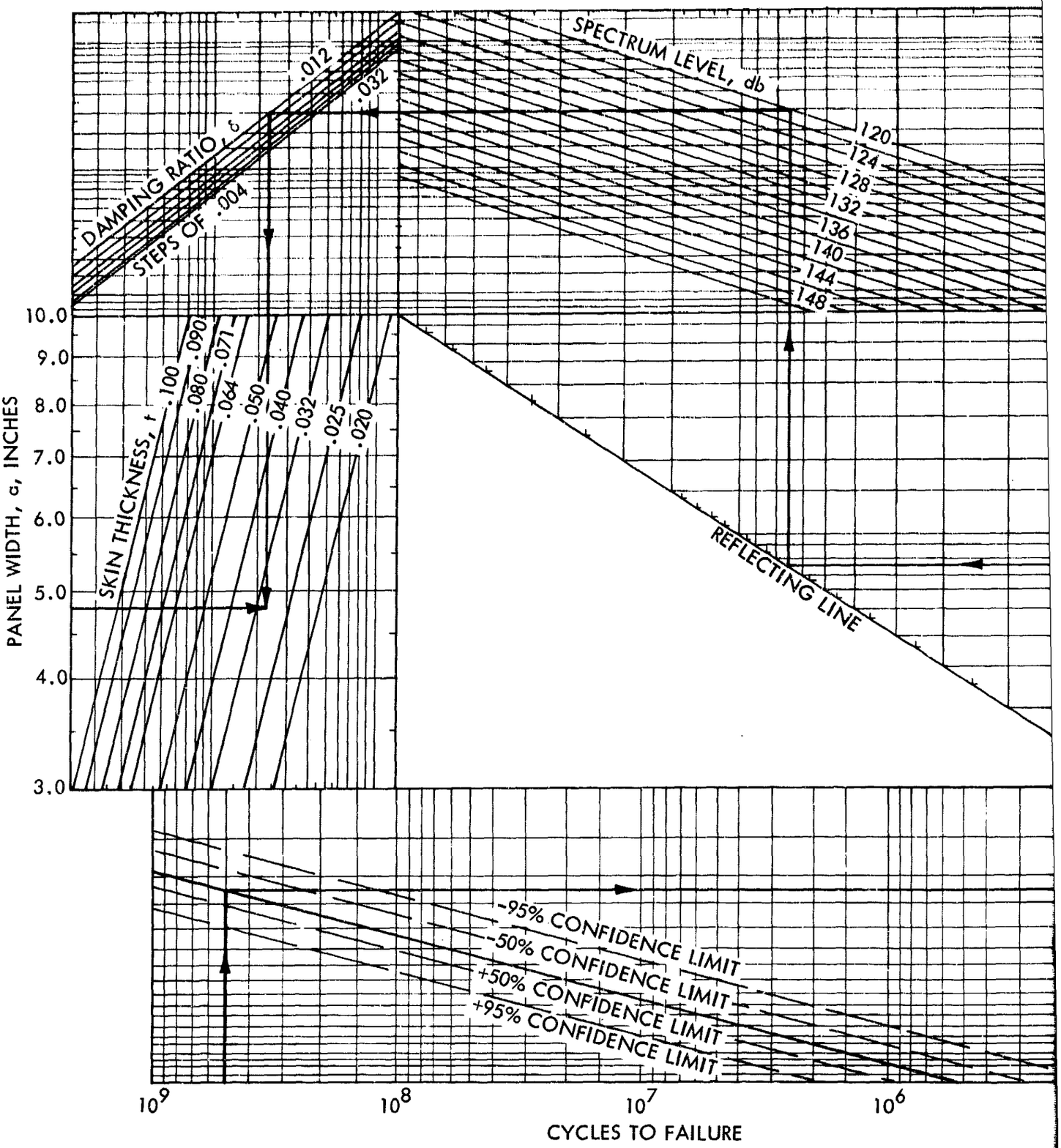
SPECTRUM LEVEL, db
120
124
128
132
136
140
144
148
DAMPING RATIO, ζ
.012
.032
STEPS OF .004
SKIN THICKNESS, t
.100
.090
.080
.071
.064
.050
.040
.032
.025
.020
REFLECTING LINE
PANEL WIDTH, a, INCHES
10.0
9.0
8.0
7.0
6.0
5.0
4.0
3.0
-95% CONFIDENCE LIMIT
-50% CONFIDENCE LIMIT
+50% CONFIDENCE LIMIT
+95% CONFIDENCE LIMIT
10^9
10^8
10^7
10^6
CYCLES TO FAILURE

A.

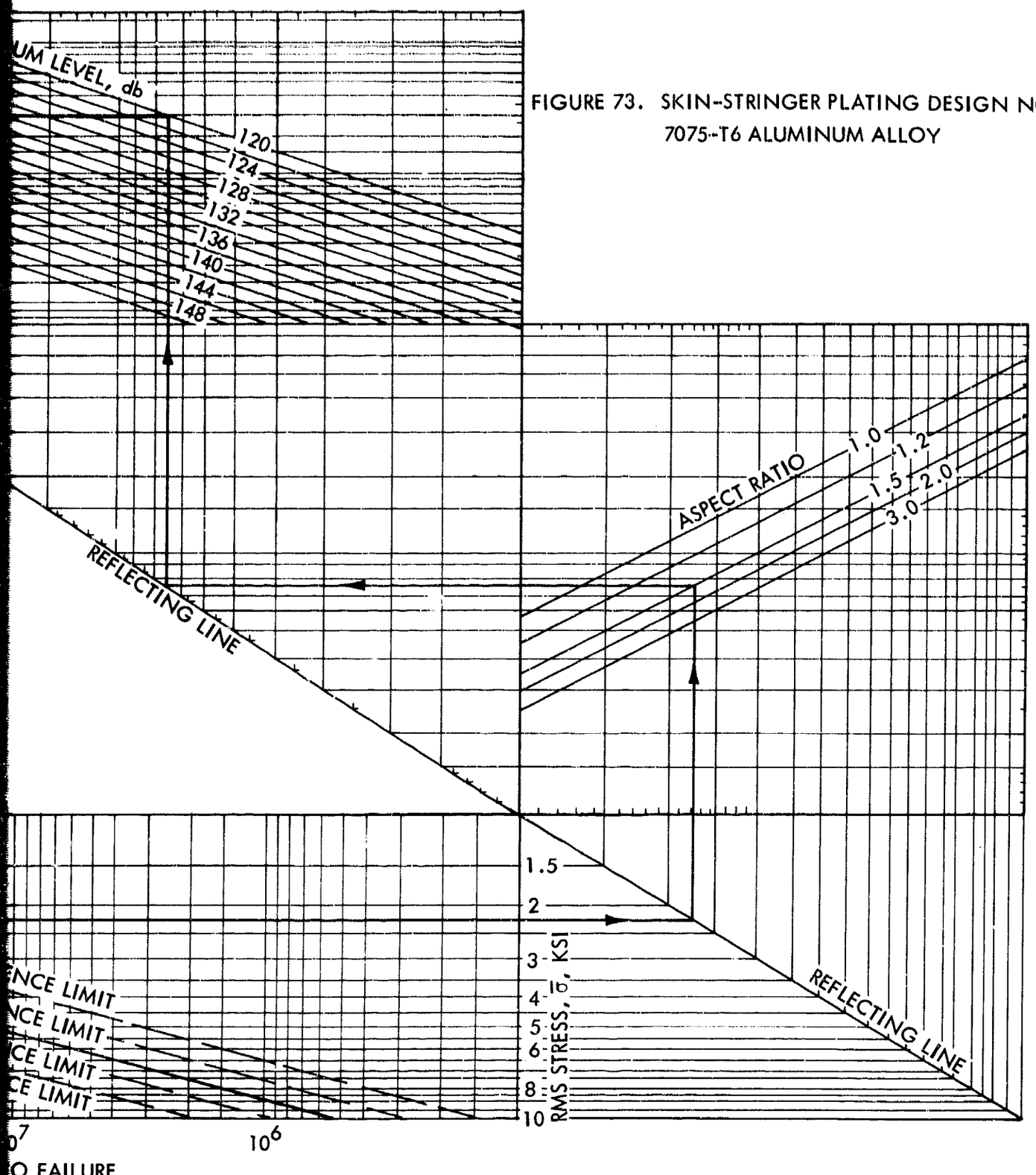

FIGURE 73. SKIN-STRINGER PLATING DESIGN NOMOGRAPH
7075-T6 ALUMINUM ALLOY

B.

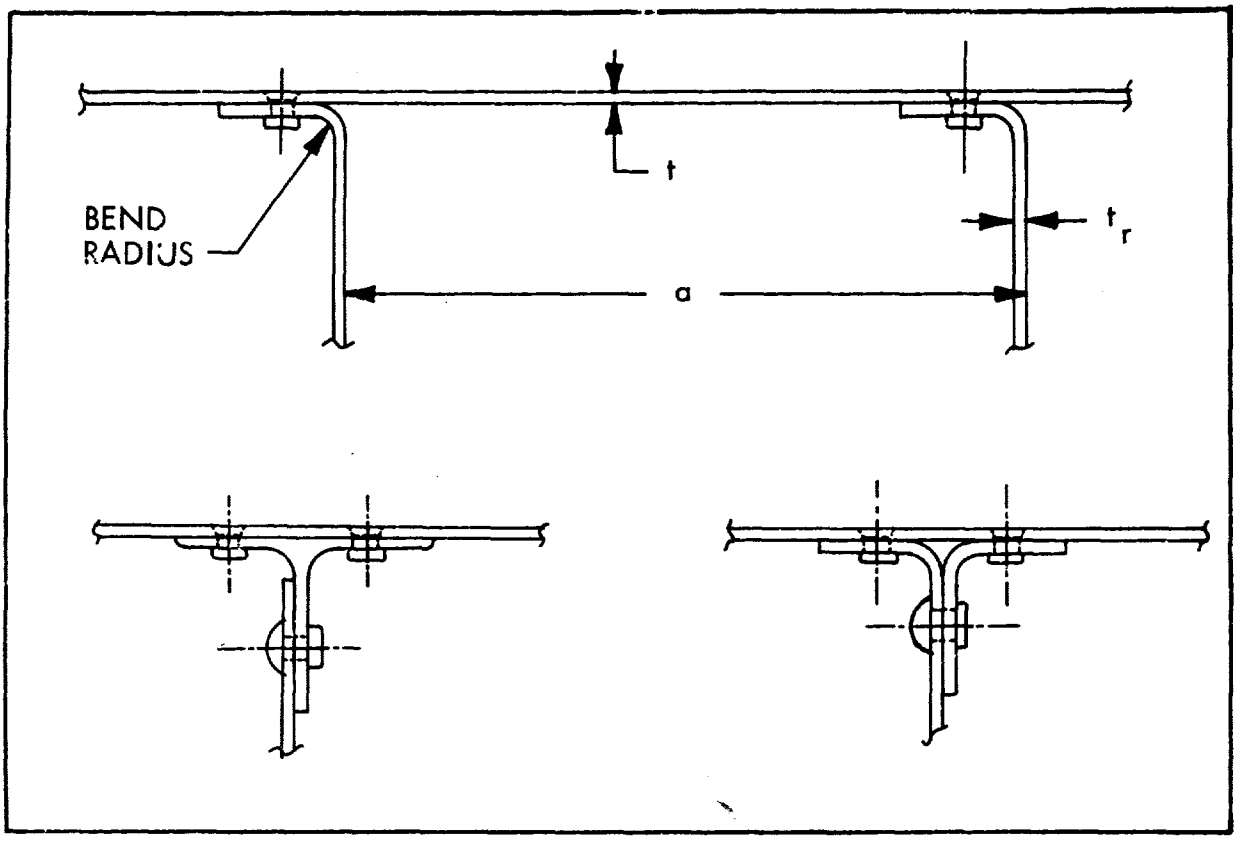

EXAMPLE: A flat aluminum-alloy, skin-stringer structure is required to withstand an estimated service noise spectrum level of 120 db. The design life is 5×10^8 cycles, the damping ratio is assumed to be 0.012, the assumed stringer spacing a = 4.75", and the aspect ratio is assumed to be 1.5. Follow through the nomograph, Figure 73, as indicated by the arrows and the skin thickness t = 0.032". Next, follow through the stringer or rib flange nomograph, Figure 75, as indicated by the arrows to $t_r \approx 0.043$". The fundamental frequency can be estimated using Figure AVI-1, Appendix VI, and in this case is calculated to be 290 Hz. At this frequency, the service environment noise spectrum level is checked with the noise spectrum level used above. If necessary, an iteration is made to obtain agreement.

If other materials such as titanium, etc., are to be considered, Figure 48, Reference 1, should be used to make the necessary fatigue curve conversion.

FIGURE 74. SKETCH OF SKIN-STRINGER CONSTRUCTION DETAILS

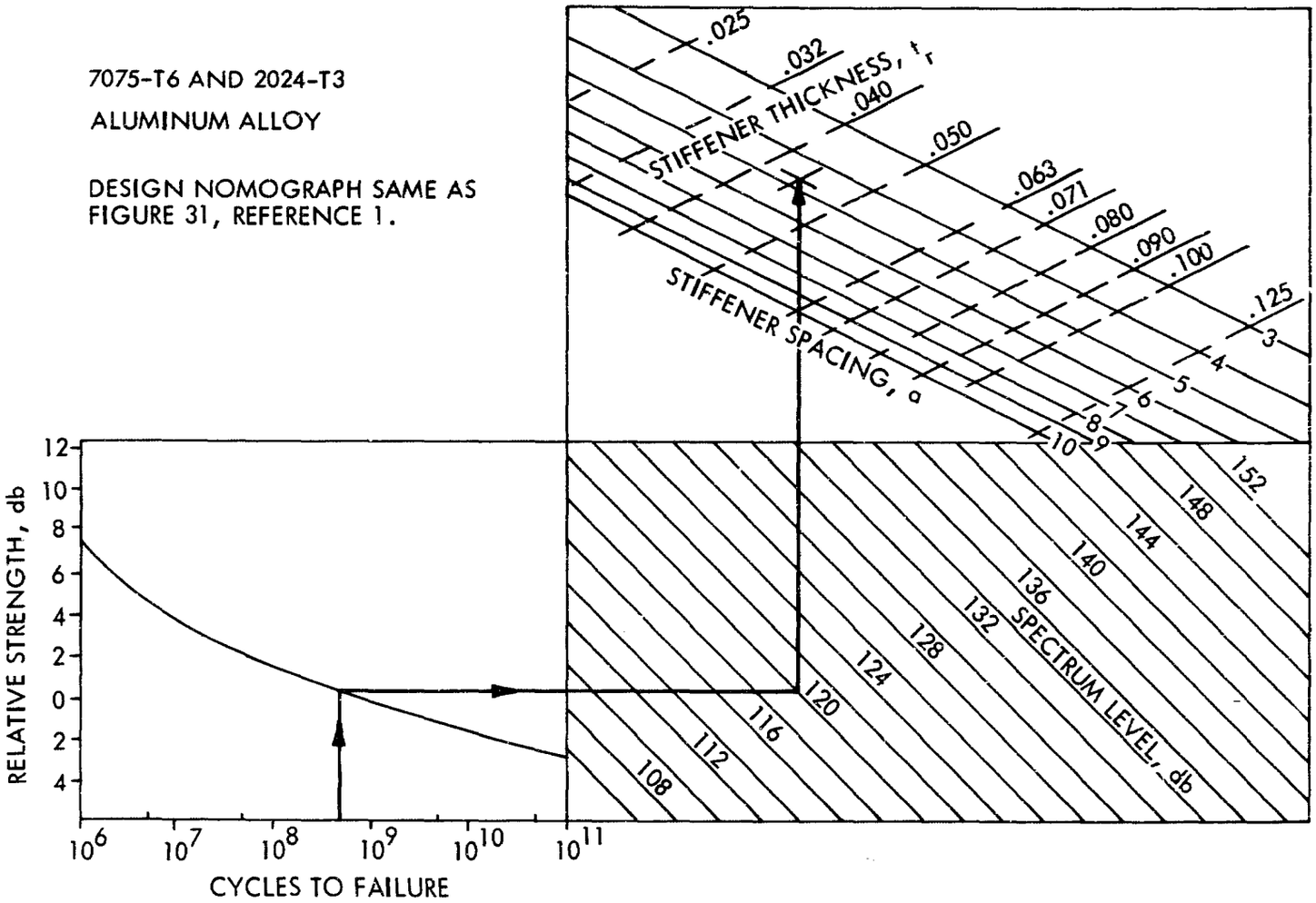

FIGURE 75. STRINGER OR RIB FLANGE DESIGN NOMOGRAPH

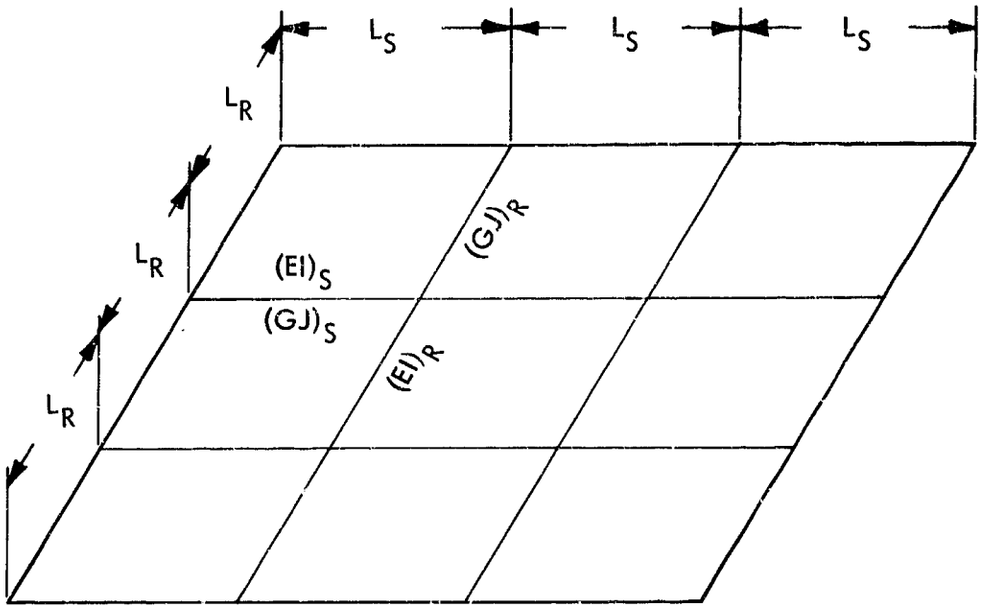

FIGURE 76. SKIN-STRINGER NOMENCLATURE

modes, such as individual panel motion. If the cover sheet is thin, then the sheet affects the frequency mainly by its mass effect. Thus, the stiffness of the cover sheet will be neglected as small compared to the stiffness of the supporting structure.

From Equations (55a) through (55f), it is seen that, if terms on the order of βL and β are neglected as small compared to βL^2, the stiffness matrix reduces to consideration of only $[K_{xx}]$ and $[K_{zz}]$. Similarly, since the rib and stringer spacing is considered to be uniform, the mass matrix uncouples so that the general eigenvalue problem can be reduced by considering only the diagonal submatrices:

$$\left| \left[K_{xx} \right] - \omega^2 \left[I_{xx} \right] \right| = 0 \tag{161}$$

$$\left| \left[K_{zz} \right] - \omega^2 \left[I_{zz} \right] \right| = 0 \tag{162}$$

$$\left| \left[K_{yy} \right] - \omega^2 \left[I_{yy} \right] \right| = 0 \tag{163}$$

Equation (161) governs the rib-bending stringer-torsion mode, Equation (162) governs the rib-torsion stringer-bending mode, and Equation (163) governs the coupled rib-stringer bending-torsion mode.

The lowest eigenvalue of each of the above problems can be approximated as:

$$\omega^2 = \frac{1}{M_{11}} \left[K_{11} - \left[K_{12}^2 + K_{13}^2 \right]^{1/2} \right] \tag{164}$$

where K_{11}, K_{12}, K_{13}, and M_{11} depend upon the mode under consideration. For the rib-bending stringer-torsion mode, the constants are

$$\begin{aligned} K_{11} &= 2.0\,(GJ/L)_S + 8.0\,(EI/L)_R \\ K_{12} &= (GJ/L)_S \\ K_{13} &= 2.0\,(EI/L)_R \\ M_{11} &= (L_R^2 - L_R L_S + L_S^2)\,(2.0\,W_P L_R L_S + W_R L_R)/579 \end{aligned} \tag{165}$$

For the rib-torsion stringer-bending mode the constants are

$$\begin{aligned} K_{11} &= 2.0\,(GJ/L)_R + 8.0\,(EJ/L)_S \\ K_{12} &= 2.0\,(EI/L)_S \\ K_{13} &= (GJ/L)_R \\ M_{11} &= (L_R^2 - L_R L_S + L_S^2)\,(2.0\,W_P L_R L_S + W_S L_S)/579. \end{aligned} \tag{166}$$

Finally, for the coupled rib-stringer bending-torsion mode, the constants are

$$K_{11} = 24. \left| (EI/L^3)_S + (EI/L^3)_R \right|$$
$$K_{12} = 12\,(EI/L^3)_S \qquad (167)$$
$$K_{13} = 12\,(EI/L^3)_R$$
$$M_{11} = (2.0\,W_p L_R L_S + W_R L_R + W_S L_S)/193$$

Equation (164) is evaluated for the appropriate K_{11}, K_{12}, K_{13}, and M_{11} by use of Figures 77 through 78 .

As an example, consider a panel with the following characteristics

$(EI)_R = 9 \times 10^4$ lb.in.^{2} $\qquad$ $(EI)_S = 4.5 \times 10^4$ lb.in.^{2}

$(GJ)_R = 1.5 \times 10^3$ lb.in.^{2} $\qquad$ $(GJ)_S = 2.0 \times 10^2$ lb.in.^{2}

$W_R = 0.1$ lb.in. $\qquad$ $W_S = 0.05$ lb.in.

$L_R = 6$ in. $\qquad$ $L_S = 8$ in.

$T_{skin} = 0.032$ in. $\qquad$ $W_P = 0.0032$ lb/in.^{2}

The frequency for the rib-bending stringer-torsion mode is computed as follows:

1. Enter Figure 77 with $(GJ)_S = 2.0 \times 10^2$, move to the left until $L_S = 8.0$, and project up to read $K_{12} = 25.0$. At $(EI)_R = 9 \times 10^4$ move down to $L_R = 6.0$ and to the right to read $K_{13} = 3.0 \times 10^4$. Projecting the K_{12} line downward and the K_{13} line to the left, $K_{11} = 1.1 \times 10^5$ is read in the lower left hand corner of the chart.

2. Enter Figure 78 at the lower left hand side with $L_1 = L_R = 6$, project to the right until $L_2 = L_S = 8$ is reached, move vertically to $W_P = 0.0032$, and then project to the right. With $L_1 = 6$ enter the lower right hand side of the chart, move left until $W_1 = W_R = 0.1$ is reached, and project upward. At the intersection point read the value of Q. Enter Q in the lower right hand side of the chart, move vertically to the line P = 52, and project to the right to read $M_{11} = 0.09$.

3. Enter Figure 79 in the left hand side with $K_{11} = 1.1 \times 10^5$ and project horizontally. Moving downward from $K_{12}^2 + K_{13}^2 = 9 \times 10^8$, read the value at the intersection point of $K_{11} - \sqrt{K_{12}^2 + K_{13}^2} = 1 \times 10^5$. On the right hand side enter $K_{11} - \sqrt{K_{12}^2 + K_{13}^2}$, move left to the $M_{11} = 0.09$ line, and project vertically to read f = 180 Hz.

The frequency for the rib-torsion stringer-bending mode is computed in a similar fashion with only slight changes. Enter Figure 77 with $(GJ)_R$ and $(EI)_S$ and proceed as before to read K_{12}, K_{13}, and K_{11} (follow the dashed line). Enter Figure 78 with $L_1 = L_S$, $L_2 = L_R$, $W_1 = W_S$ and read M_{11}. Enter Figure 79 with K_{11} and $K_{12}^2 + K_{13}^2$ and compute the frequency as before.

The frequency for coupled rib-stringer bending-torsion mode is computed using Figure 80 through 82. Enter Figure 80 with $(EI)_R$ and L_R^3 as the scales to the right. Connect $(EI)_R$ and L_R^3 to read $12(EI/L^3)_R = K_{13}$. Similarly, with $(EI)_S$ and L_S^3, read $12(EI/L^3)_S = K_{12}$. In the left hand portion of Figure 80, enter K_{12} and K_{13} and at the intersection point read K_{11}. On Figure 81, enter the three scales on the left by connecting W_R with L_R and W_S with L_S to read the numbers $W_R L_R$ and $W_S L_S$. In the center portion connect L_R and L_S to read $L_R L_S$. Connect $L_R L_S$ to W_P to read $2 W_P L_R L_S$. Enter $2 W_P L_R L_S + W_R L_R + W_S L_S$ on the scale to the right and move laterally to read M_{11}. Finally, enter Figure 82 with K_{11} and $K_{12}^2 + K_{13}^2$ as in Figure 79. Enter $K_{11} - \sqrt{K_{12}^2 + K_{13}^2} = 7.8 \times 10^3$ on the right side, move laterally to $M_{11} = 6.7 \times 10^{-3}$, and project vertically to read f = 160 Hz.

C. Honeycomb Sandwich

1. Edge Design

The mathematical expression used for estimating the honeycomb sandwich edge stress is Equation (86c). It was used in combination with the appropriate fatigue curve, Figure 50, to derive the honeycomb sandwich edge design nomograph. Figure 83 is the design nomograph and Figure 84 is a drawing of the construction details with an example problem solved.

2. Facing Sheet Design

Equation (92c) was used to derive the honeycomb sandwich facing sheet design nomograph. Figure 51, the facing sheet fatigue curve, was used to relate facing sheet stresses to number of positive crossings to failure. Figure 85 is the resulting honeycomb sandwich facing sheet design nomograph. Figure 84 is a sketch of the construction details with an example problem solved.

3. Core Shear Design

The maximum shear stress in the core of a flat honeycomb sandwich panel occurs in the neighborhood of the edges regardless whether the panel is simply supported or clamped. The mathematics expressing the core shear for simply supported edges is less complicated and slightly conservative compared to clamped edges and can be used for purposes of checking the core shear fatigue resistance.

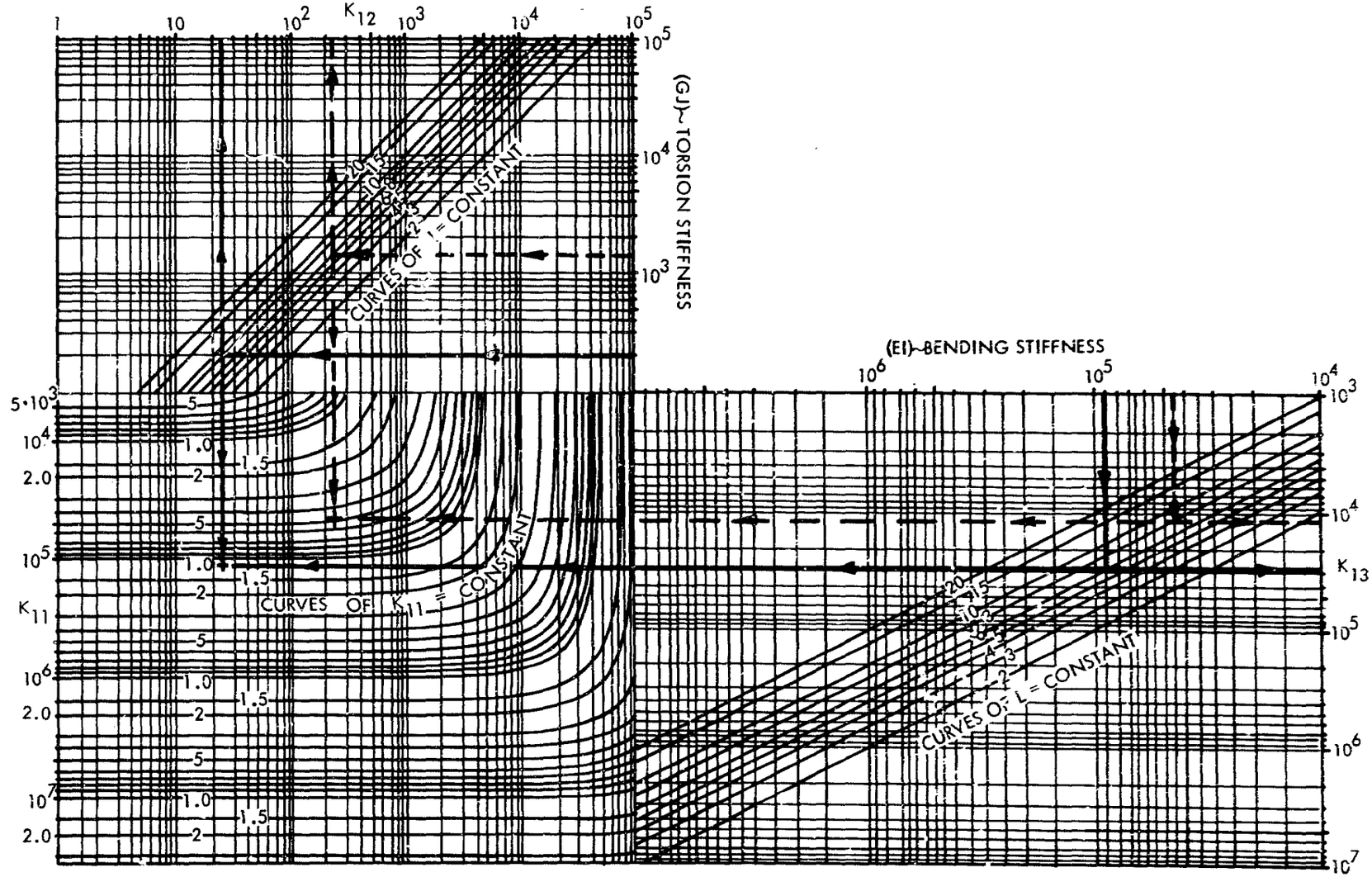

FIGURE 77. NOMOGRAPH FOR COMPUTING K_{11}, K_{12}, AND K_{13} FOR RIB BENDING-STRINGER TORSION AND RIB-TORSION STRINGER BENDING MODES OF SKIN-STRINGER PANELS

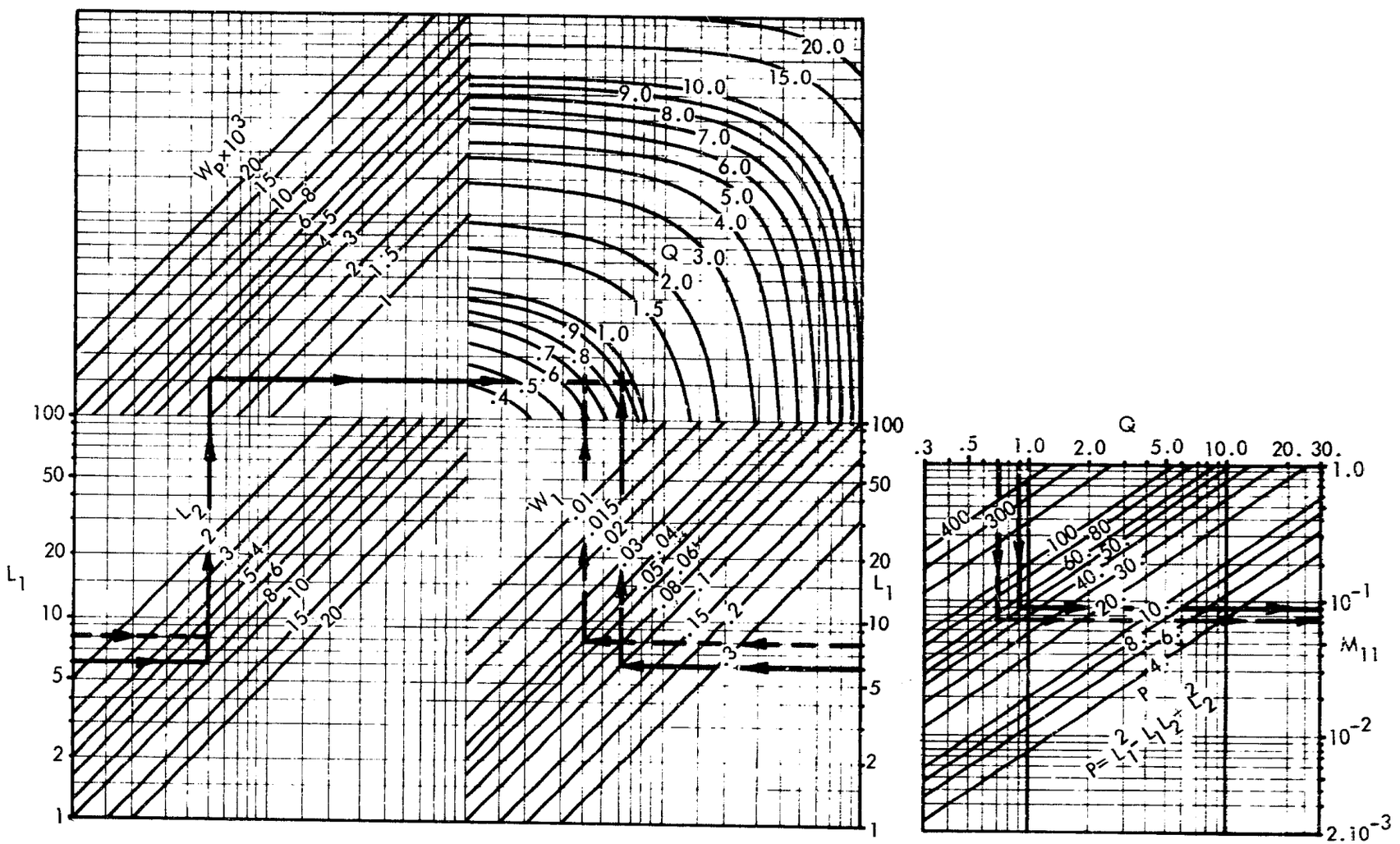

FIGURE 78. NOMOGRAPH FOR COMPUTING M_{11} FOR RIB-BENDING STRINGER-TORSION MODE AND RIB-TORSION STRINGER-BENDING MODE

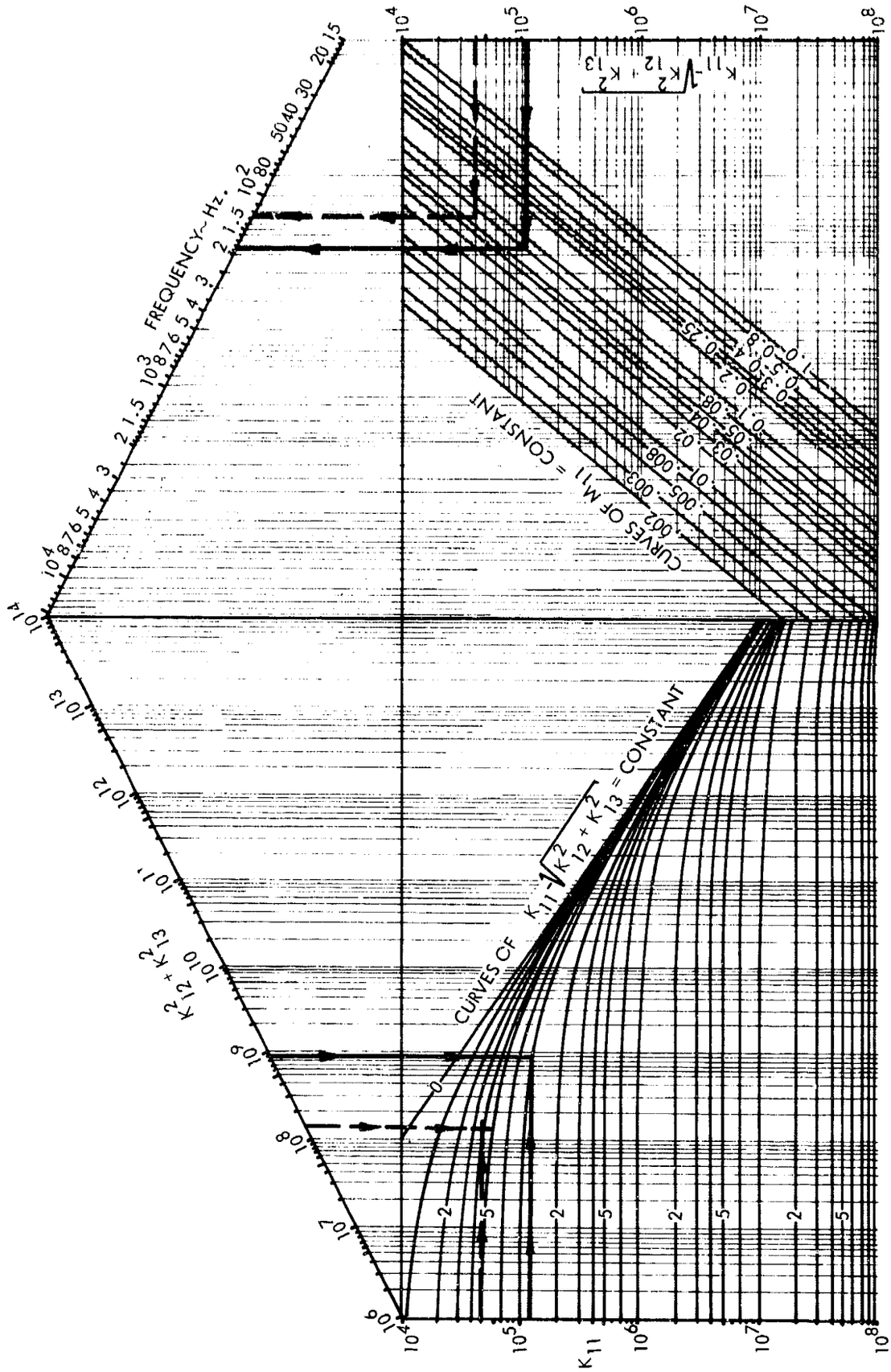

FIGURE 79. NOMOGRAPH FOR COMPUTING FREQUENCIES OF RIB-BENDING STRINGER-TORSION AND RIB-TORSION STRINGER-BENDING MODES

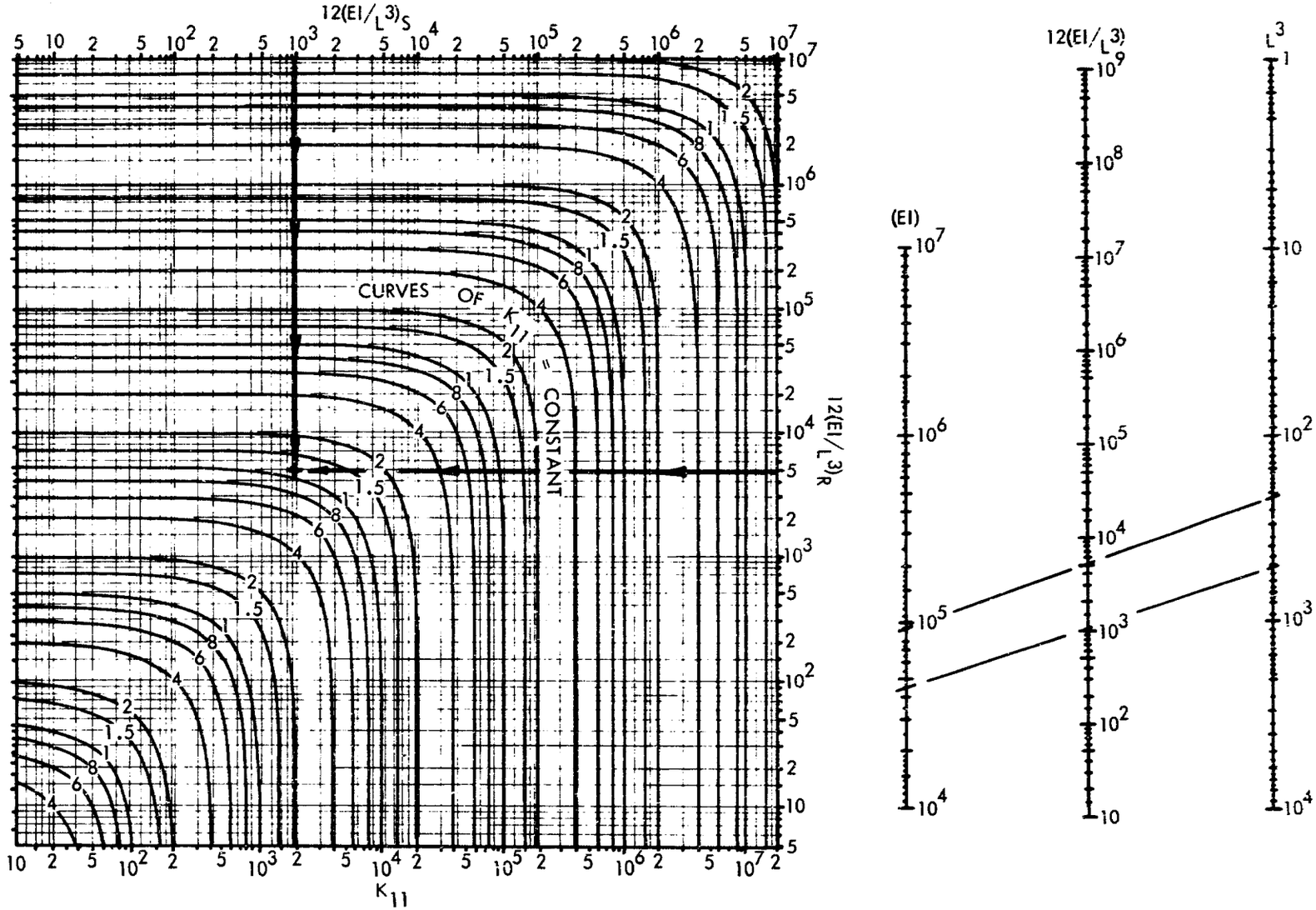

FIGURE 80. NOMOGRAPH FOR COMPUTING K_{11}, K_{12}, AND K_{13} FOR COUPLED RIB-STRINGER BENDING-TORSION MODES

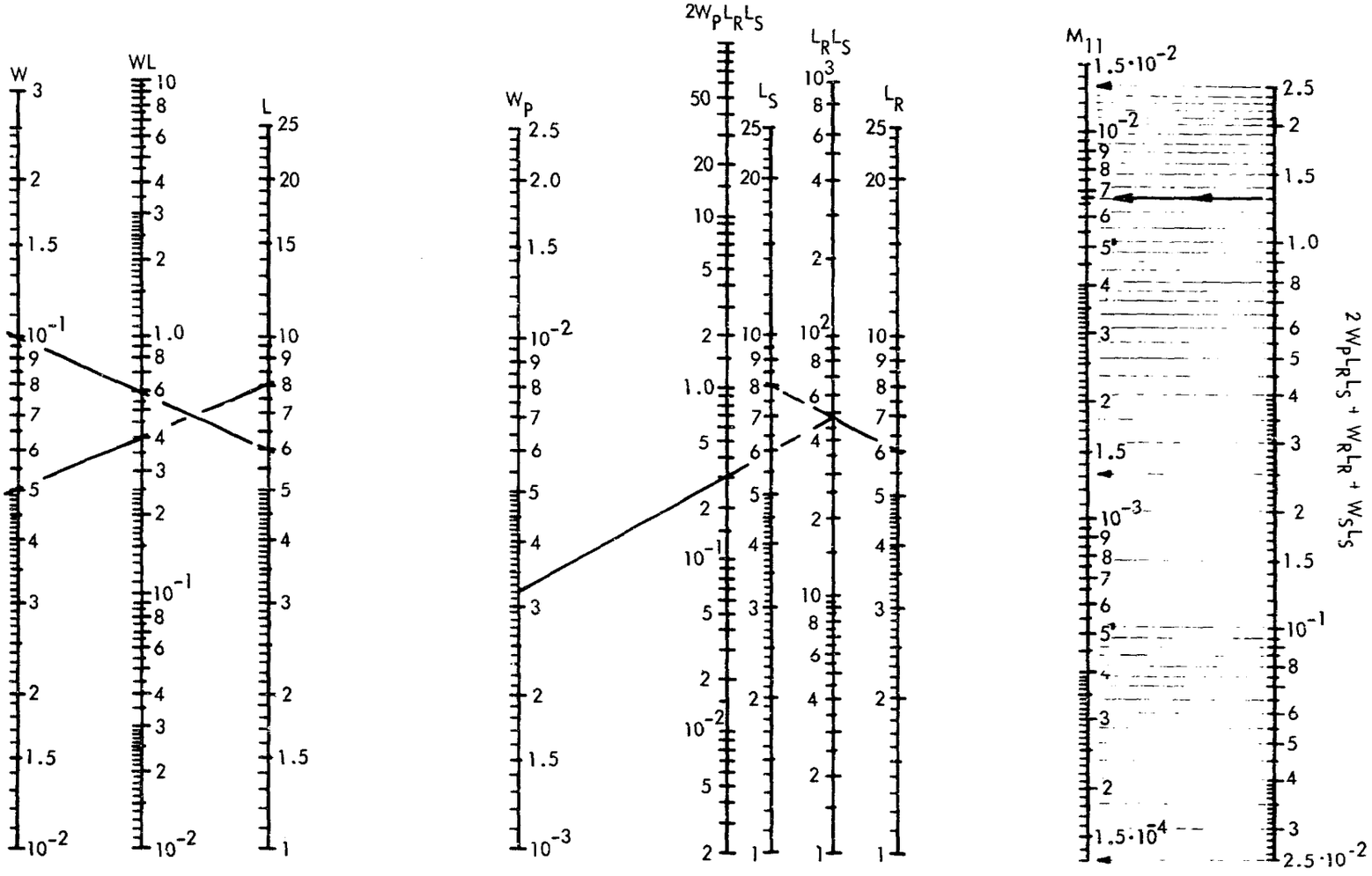

FIGURE 81. NOMOGRAPH FOR COMPUTING M_{11} FOR THE COUPLED RIB-STRINGER BENDING TORSION MODE

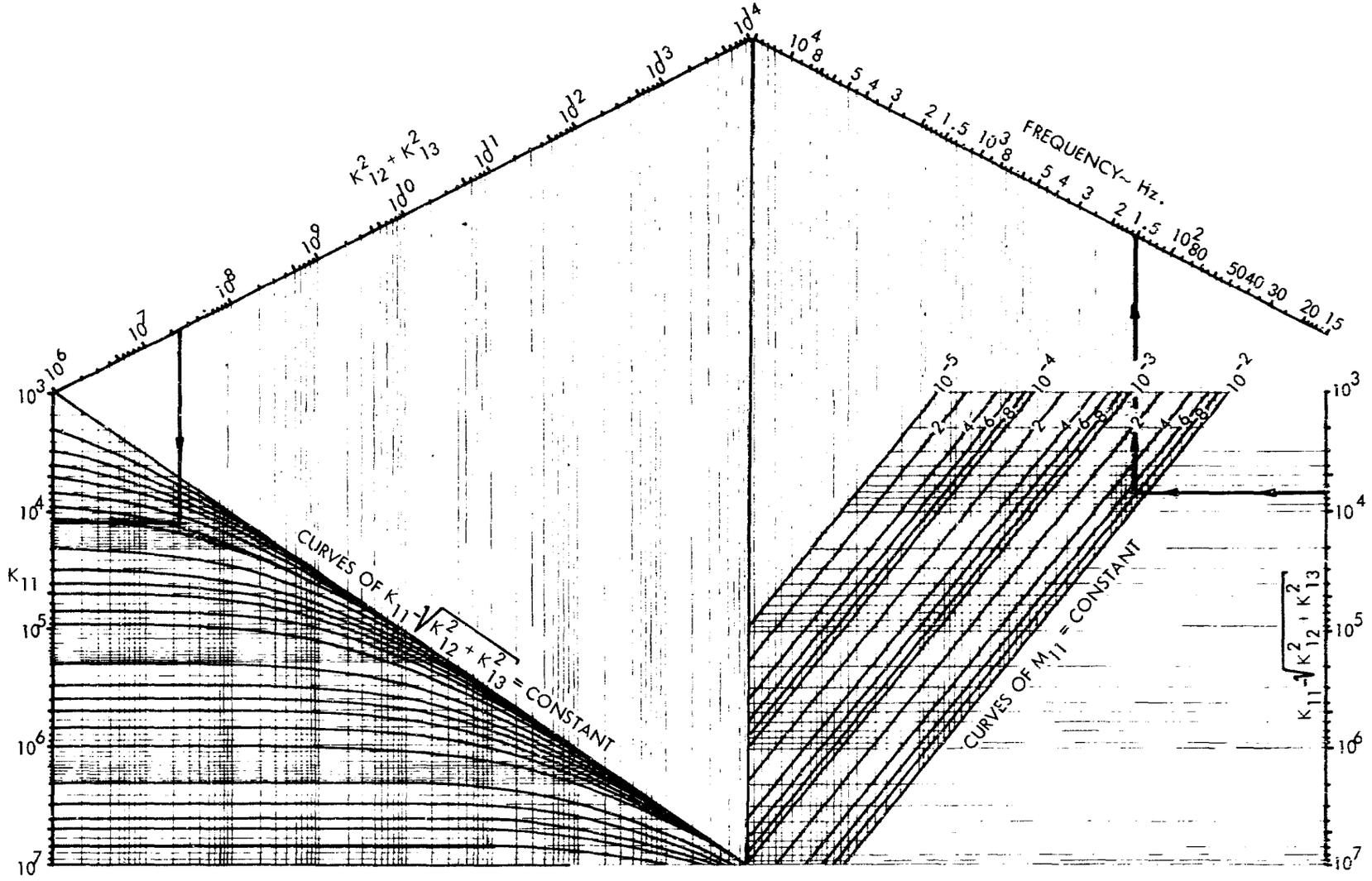

FIGURE 82. NOMOGRAPH FOR COMPUTING FREQUENCY OF COUPLED RIB-STRINGER BENDING TORSION MODE

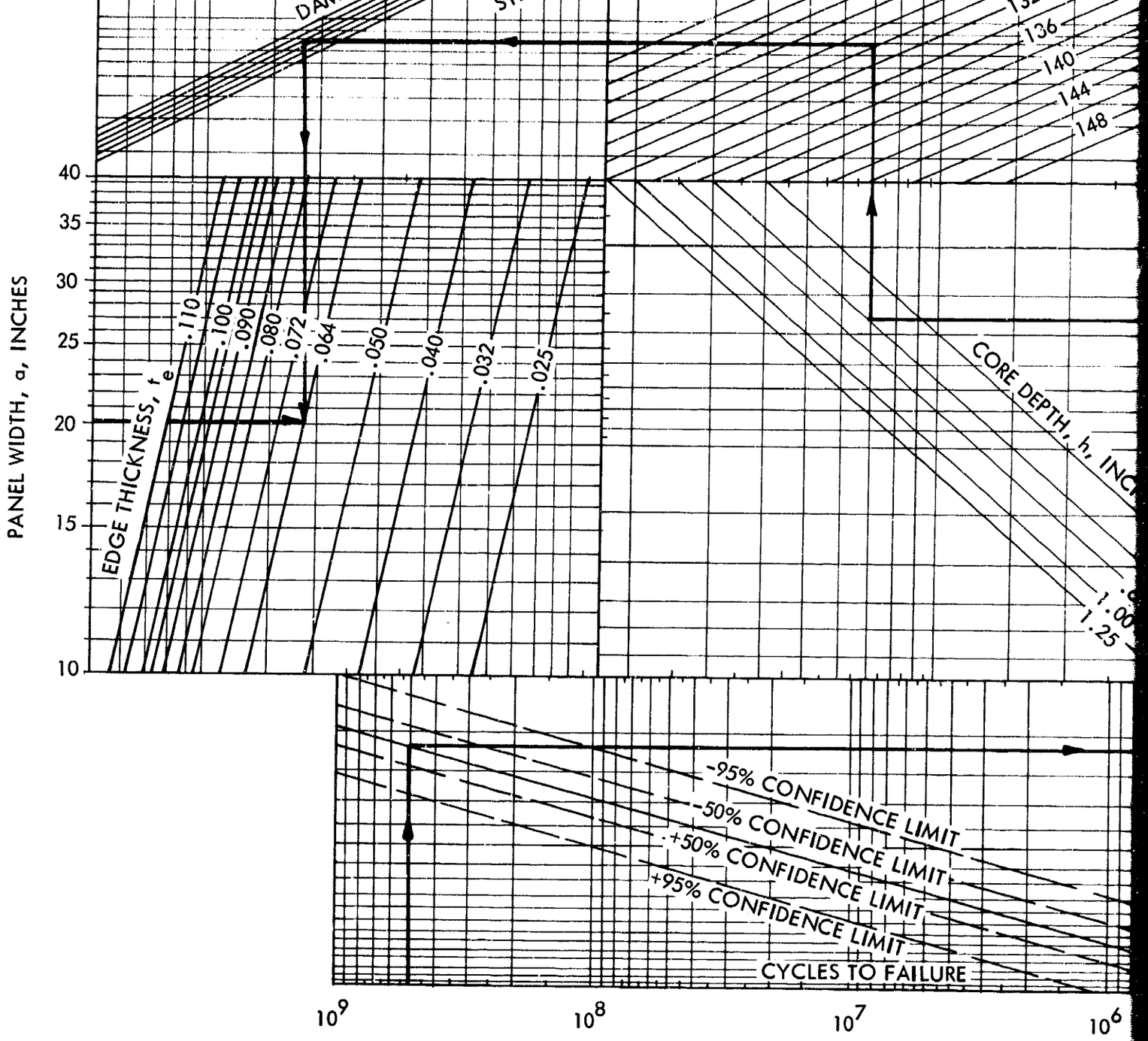
DAMPING RATIO, δ .012
.032
STEPS OF .004
SPECTRUM LEVEL, db
120
124
128
132
136
140
144
148
PANEL WIDTH, a, INCHES
40
35
30
25
20
15
10
EDGE THICKNESS, t_e
.110
.100
.090
.080
.072
.064
.050
.040
.032
.025
CORE DEPTH, h, INCH
1.00
1.25
-95% CONFIDENCE LIMIT
-50% CONFIDENCE LIMIT
+50% CONFIDENCE LIMIT
+95% CONFIDENCE LIMIT
CYCLES TO FAILURE
10^9
10^8
10^7
10^6

A.

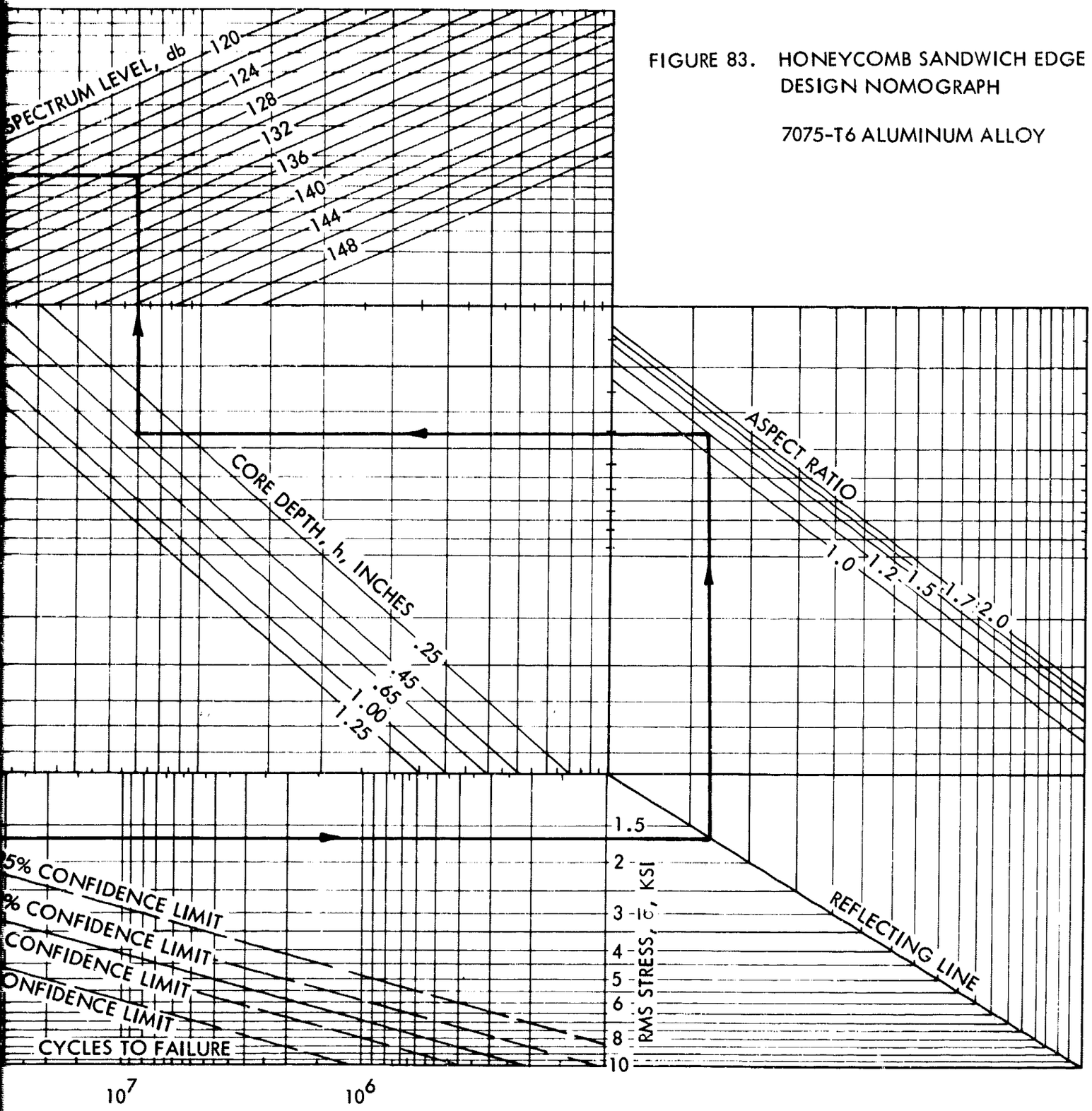

FIGURE 83. HONEYCOMB SANDWICH EDGE DESIGN NOMOGRAPH

7075-T6 ALUMINUM ALLOY

B.

EXAMPLE: A flat aluminum-alloy, honeycomb sandwich structure is required to withstand an estimated service environment noise spectrum level of 130 db. The design life is 5×10^8 cycles, the average damping is considered to be 0.019, the assumed panel width a = 20", an aspect ratio of 1.2, and a honeycomb core depth h = 0.45". Follow through Figure 83 as indicated by the arrows and obtain an edge thickness, t_e = 0.064". Move to Figure 85, using the same design conditions specified above, and follow the arrows to obtain the required facing sheet thickness, t = 0.015". The fundamental frequency can be calculated using Figure AVI-2, Appendix VI, and is found to be 290 Hz. At this frequency the service environment noise spectrum level is checked with the noise spectrum level used above. If necessary, an iteration is made to obtain agreement.

If other materials such as titanium, etc., are to be considered, Figure 48, Reference 1, should be used to make the necessary fatigue curve conversion.

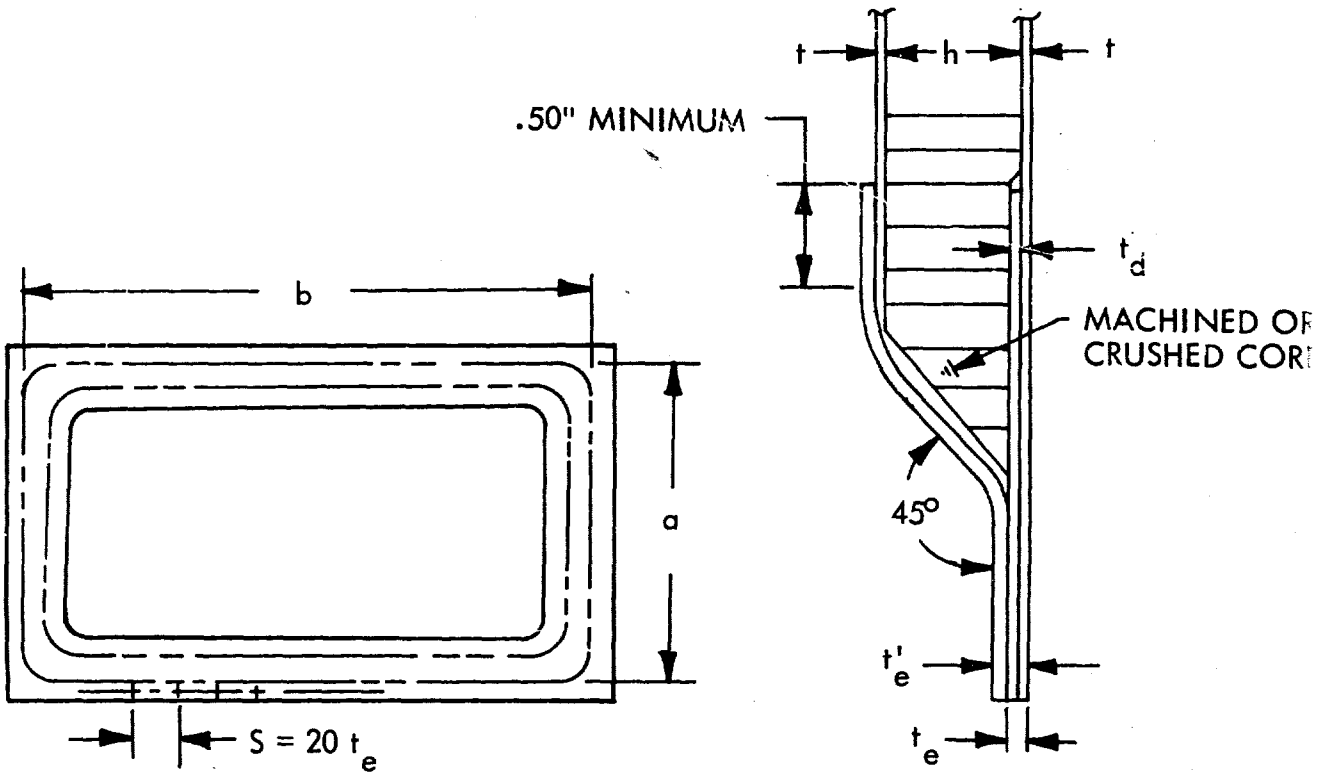

NOTE: t'_e is edge thickness with metal pan only.

FIGURE 84. HONEYCOMB SANDWICH CONSTRUCTION DETAILS

Preceding Page Blank

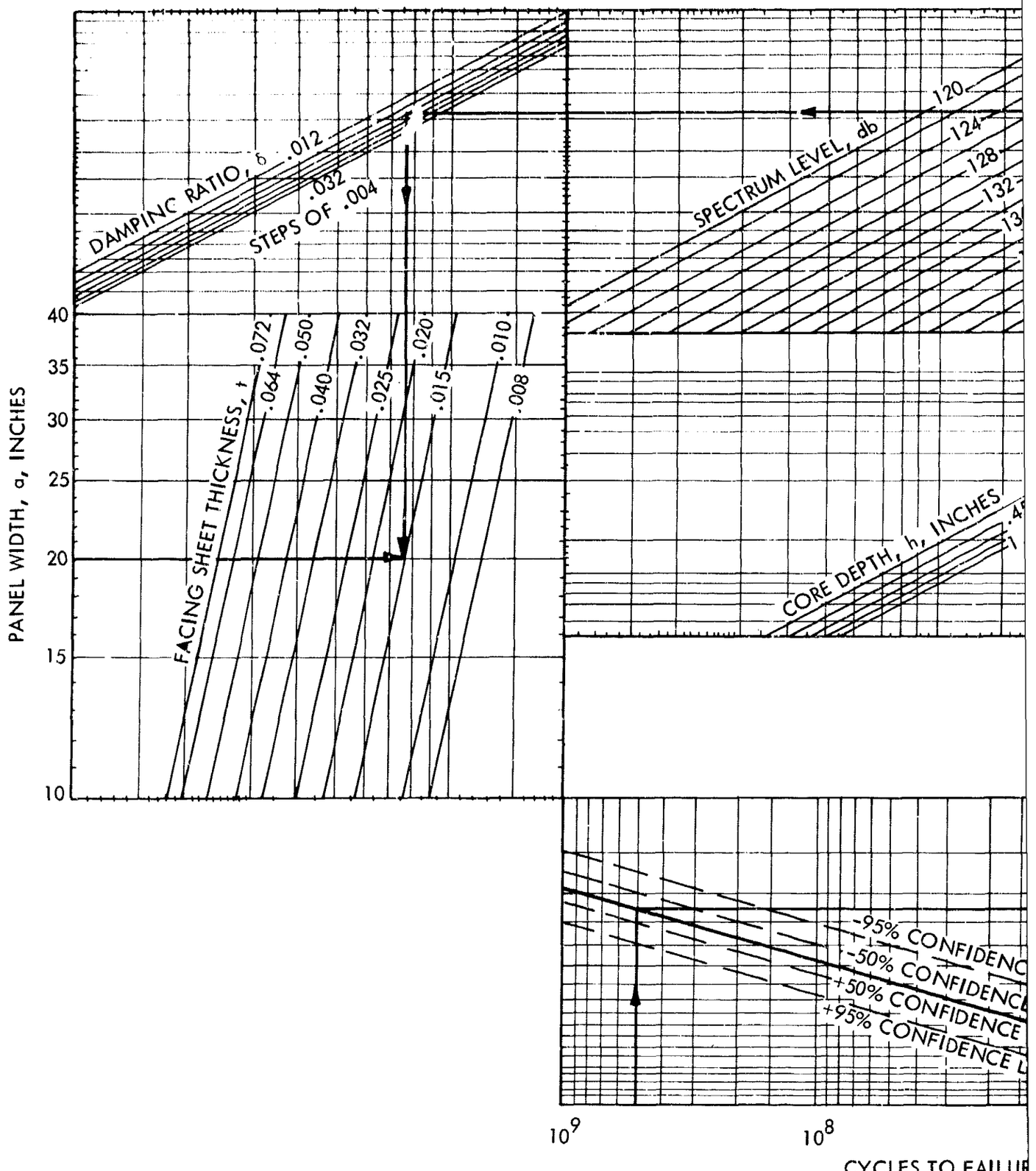
DAMPINC RATIO, δ
.012
.032
STEPS OF .004
SPECTRUM LEVEL, db
120
124
128
132
PANEL WIDTH, a, INCHES
40
35
30
25
20
15
10
FACING SHEET THICKNESS, t
.072
.064
.050
.040
.032
.025
.020
.015
.010
.008
CORE DEPTH, h, INCHES
-95% CONFIDENC
-50% CONFIDENCE
+50% CONFIDENCE
+95% CONFIDENCE L
10^9
10^8
CYCLES TO FAILUR

A.

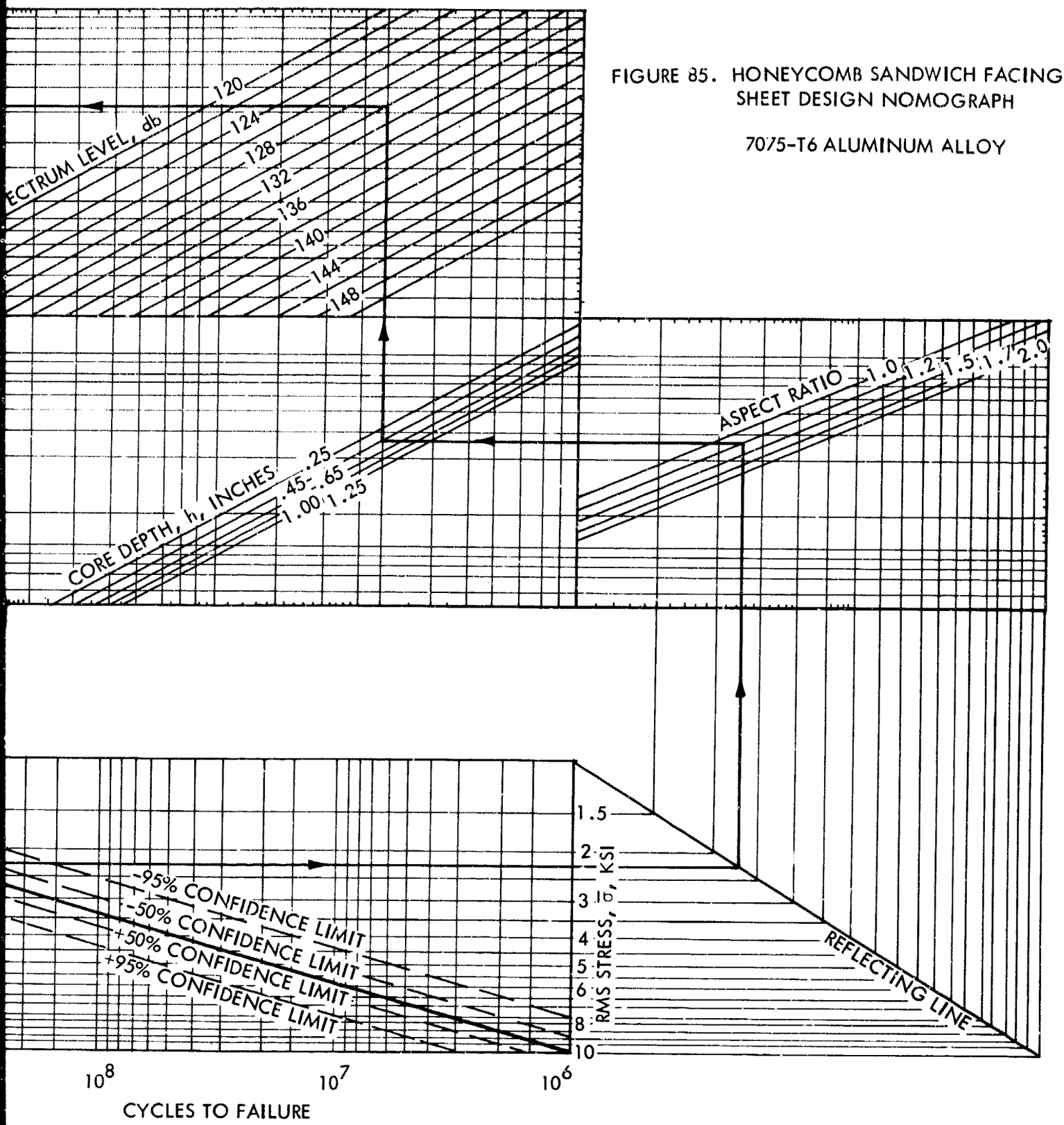

FIGURE 85. HONEYCOMB SANDWICH FACING SHEET DESIGN NOMOGRAPH

7075-T6 ALUMINUM ALLOY

B.

The shearing stress in the core of a flat honeycomb sandwich panel subjected to static load can be approximated by the following equation, derived in Reference 17:

$$\tau = \frac{W_o D \pi^3}{h a} \left[\frac{1}{a^2} + \frac{1}{b^2} \right] \tag{168}$$

where W_o is evaluated by Equation (40).

The maximum static shear stress resulting from a uniform pressure of unit magnitude is

$$\tau = \frac{16}{\pi^3 h a} \frac{1}{\left[\frac{1}{a^2} + \frac{1}{b^2} \right]} \tag{169}$$

The rms core shear stress for a lightly damped, simply supported flat honeycomb sandwich panel exposed to random acoustical excitation can be estimated by combining Equations (5), (83), and (169). The result is

$$\bar{\tau} = \frac{187 b}{a} \left[\frac{\Phi(f)}{h \delta} \right]^{1/2} \frac{1}{\left[a^2 + b^2 \right]^{1/2}} \tag{170}$$

where the damping was assumed to be an average value of 1.85%. (See Table IX.)

The required core density (lbs/ft^3) can be estimated using Equation (170) and the core shear fatigue curve extracted from Reference 23. This fatigue curve was derived from flexural tests of bonded sandwich panels subjected to bending conditions producing high core shear and facing sheet stresses. The constant amplitude core shear stresses were converted into rms core shear stresses using the method recommended by Crede and Lunny (Reference 24). This simple relationship is

$$\bar{\tau} = \frac{\tau}{\left[a/2 \right]^{1/2} \left[\pi a \right]^{1/2} a} = \frac{\tau}{1.80} \tag{171}$$

where $\bar{\tau}$ is the rms shear stress.
τ is the constant amplitude shear stress.
a is the inverse negative slope of the fatigue curve equal to 6.2.

There are only two core shear fatigue points available to check the accuracy of the fatigue curve: HC-15A and one from a recently conducted C-5A sonic fatigue test. (The latter is reported in Reference 25.) The core shear for each panel was estimated using Equation (170) and the parameters listed in the table below:

TABLE XX

CORE SHEAR STRESS PARAMETERS

Designation	a	b	h	SPL db	Core density	Damping ratio, %
HC-15A	20	24	0.27	140	3.4	2.0
C-5A panel	23	35	0.50	139	2.4	2.2

The rms shear stress for HC-15A was computed to be 60.1 psi and it developed a core shear failure in 1.08 million zero crossings. The rms shear stress for the C-5A panel was computed to be 35.1 psi and it developed a shear failure in 2.1 million zero crossings. These points are plotted on Figure 87 to show a comparison of predicted life and test lift.

Equation 170 and its companion fatigue curve, Figure 86, can be used to select the required core density (lb/ft^3) for a given design.

D. Skin-Stringer Curvature Effects

The effect of curvature on stress ratio, expressed by Equation (111a), Section V-D, was used to develop the curvature effects nomograph for skin-stringer construction.

The curvature effects nomograph is designed to be used in connection with the design nomograph for flat skin-stringer plating. Figure 73 is used to estimate the panel dimensions. Using these dimensions, a stress reduction ratio due to curvature is obtained from Figure 87. The procedure is repeated until a satisfactory convergence is obtained. Two to three iterations are generally sufficient for satisfactory convergence.

E. Design Equations for Curved Honeycomb Panels

The equations below were developed as a design aid for curved honeycomb panels. Although the equations are accurate within the assumptions, it was deemed impractical to design nomographs for solution and/or evaluation of the equations presented.

To determine the effect of curvature on face sheet ($z = h_1$) tensile stress at the center of the panel, in the direction of curvature (y), use the following equation:

$$\sigma_{yc} = \left[1 + .0527 \left(1 + .049 A^2\right) \frac{S_2}{S_3} \left(\frac{AL\theta}{g}\right) \right] \frac{W_c}{W_f} \sigma_{yf} \qquad (172)$$

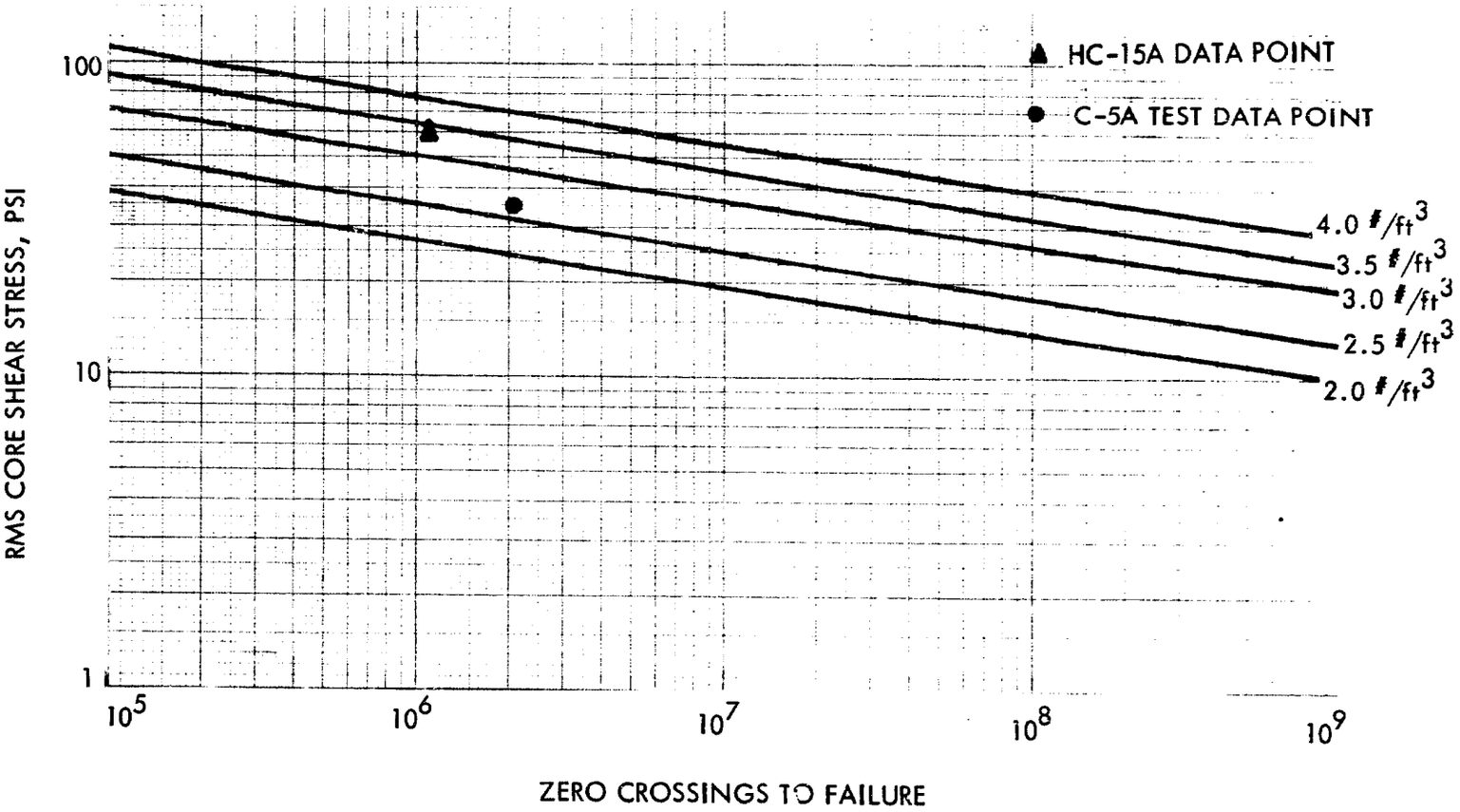

FIGURE 86. 5052-H39 ALUMINUM ALLOY CORE SHEAR FATIGUE CURVE

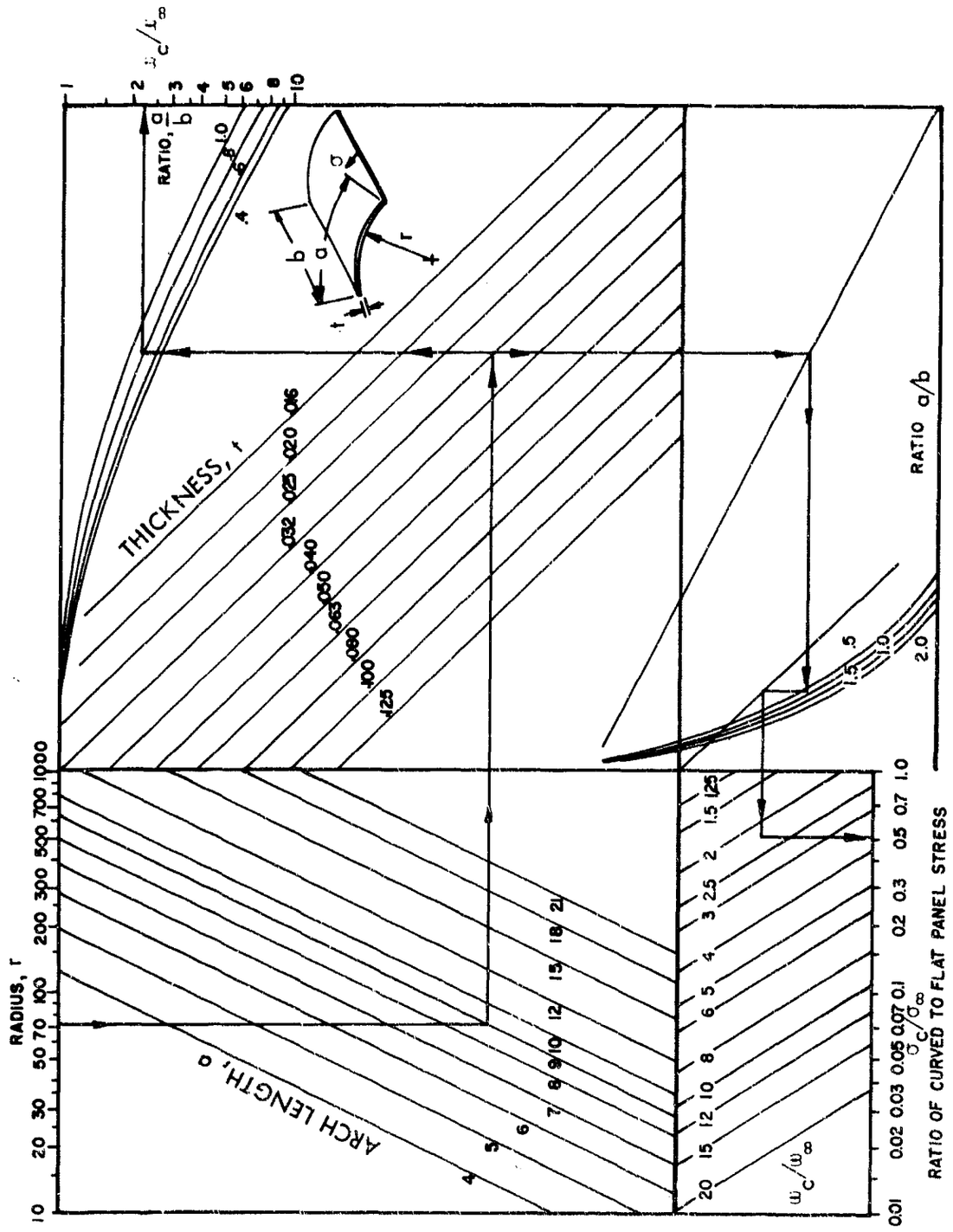

FIGURE 87. EFFECT OF CURVATURE ON STRESS RATIO FOR SKIN-STRINGER PANELS WITH RANDOM LOADING

The effect of curvature on face sheet ($z = h_1$) tensile stress in the longitudinal direction (x), at the center of the panel, is determined by the relationship which follows:

$$\sigma_{xc} = \left[1 + .0396 (1 + .103 A^2) \frac{S_2}{S_4} \left(\frac{AL\theta}{g} \right) \right] \frac{W_c}{W_f} \sigma_{xf} \tag{173}$$

The ratio of σ_x to σ_y at the center of the panel in the outer face sheet ($z = h_1$) is found from the following relationship, which holds for flat as well as curved panels,

$$\frac{\sigma_y}{\sigma_x} = 2.58 \left[\frac{(1 + .049 A^2) \left(\frac{AL\theta}{g} \right) + 19.0 \frac{S_3}{S_2}}{(1 + .0285 A^2) \left(\frac{AL\theta}{g} \right) + 16.3 \frac{S_4}{S_2}} \right] \tag{174}$$

The ratio of tensile stress at the panel center in the outer face sheet ($z = h_1$) to tensile stress in the inner face sheet ($z = -h_1$) is

$$\frac{\sigma_{y, z = h_1}}{\sigma_{y, z = -h_1}} = \frac{.0527 (1 + .049 A^2) \frac{S_2}{S_3} \left(\frac{AL\theta}{g} \right) + 1}{.0527 (1 + .049 A^2) \frac{S_2}{S_3} \left(\frac{AL\theta}{g} \right) - 1} \tag{175}$$

The effect of curvature on edge stress at the center of straight edge ($y = 0$ or a, $x = b/2$) is given by the following equation:

$$\sigma_{yc} = \left[1 + \frac{.445 (A^2 + .108) A L_e \theta}{1 + 9.62 A^2 + A^4} \right] \frac{W_c}{W_f} \sigma_{yf} \tag{176}$$

The effect of curvature on transverse shear stress is simply stated as the ratio of generalized coordinates

$$\tau_{xzc} = \frac{W_c}{W_f} \tau_{xzf}$$
$$\tau_{yzc} = \frac{W_c}{W_f} \tau_{yzf} \tag{177}$$

If the excitation is broad-band random noise, the ratio W_c/W_f is

$$\frac{W_c}{W_f} = \left[1 + .002 \frac{S_2}{S_1} \left(\frac{AL\theta}{g} \right)^2 \right]^{3/4} \tag{178}$$

If the excitation is sinusoidal, the ratio becomes

$$\frac{W_c}{W_f} = 1 + .002 \frac{S_2}{S_1} \left(\frac{AL\theta}{g} \right)^2 \tag{179}$$

It is assumed in Equations (172), (173), (176), and (177) that the damping ratio for the first mode does not change as curvature increases (frequency increases). If this assumption is not acceptable for certain designs, then the ratio of W_c/W_f is expressed as

(a) for random excitation

$$\frac{W_c}{W_f} = \left(\frac{\delta f}{\delta c} \right)^{1/2} \left[1 + .002 \frac{S_2}{S_1} \left(\frac{AL\theta}{g} \right)^2 \right]^{3/4} \tag{180}$$

(b) for sinusoidal excitation

$$\frac{W_c}{W_f} = \frac{\delta f}{\delta c} \left[1 + .002 \frac{S_2}{S_1} \left(\frac{AL\theta}{g} \right)^2 \right] \tag{181}$$

The parameters S_1 to S_4 are determined by the following relationships

$$S_1 = 1 + A^4 + 40.7 \left(\frac{g}{scL^2} \right) (1 + cA^2)$$

$$S_2 = 1 + 40.7 \left(\frac{g}{scL^2} \right) \left(1 + \frac{c}{A^2} \right) + 1655 \left(\frac{g}{scL^2} \right)^2 \frac{c}{A^2} \tag{182}$$

$$S_3 = 1 + .33A^2 + 38.0 \left(\frac{g}{scL^2} \right) (1 + .143\, c)$$

$$S_4 = 1 + 3.0A^2 + 16.3 \left(\frac{g}{scL^2} \right) (1 + 7.0c)$$

Due to simplifying assumptions made in the derivation of these equations, certain restrictions are placed on the variables. These limits are

$$\theta \leq .35$$
$$g \geq 5$$
$$s \leq .01$$
$$L \geq 100$$
$$.3 \leq A \leq 3$$
$$L_e \geq 100$$

The equations derived in this section are too complicated for graphical solution. If extensive calculations are to be made, the computer program described in detail in Appendix IV-B can be used. While the program is coded in Fortran IV, slight modifications may be necessary for compatibility with various computers. This specific program was developed for use on the IBM 360 system.

VI. CONCLUSIONS

A. The results of the analytical and experimental investigations reported here indicate that the overall rms stresses induced in flat skin-stringer plating and honeycomb sandwich construction by broad-band noise can be estimated with sufficient accuracy for design purposes by a development involving plate theory and Miles' response theory.

B. The skin-stringer plating and honeycomb sandwich design nomographs presented in this report give estimates of fatigue life well within the ±95-percent confidence limits of their respective fatigue curves. Obviously the accuracy of the nomographs can be established only in the range of the test conditions. Additional testing is required to define the accuracy of the extrapolated portion of the fatigue curves.

C. Skin-stringer and honeycomb sandwich construction designed using the nomographs and procedures presented here will be lightweight and sonic-fatigue-resistant.

D. Back-up structure, ribs, and stringers, designed using the nomographs and procedures described in this report, will be conservative. None of the 30 skin-stringer designs that were tested experienced rib or stringer flange cracks.

E. The dynamic analysis of back-up structure indicates that the motion is highly coupled and that the phase relations between adjacent bays is extremely important for fatigue considerations. Hence, in order to realize the degree of constraint along a boundary of an individual panel, the coupled effect of rib and stringer motion must be taken into account. This approach is necessary since the back-up structure represents some 60 percent of the weight of skin-stringer construction. The back-up structure must then be considered as an integral part of the fatigue analysis in order to design a system which is optimum from a weight standpoint. In addition, consideration must be given to multi-bay effects for structure which deviates from the model considered here.

F. The experimental data contained in Reference 12, when compared with the various analytical studies reported here, indicate that aircraft-type, skin-stringer construction does not realize the degree of in-plane restraint represented in the classical clamped panel analysis. An analytical solution that more nearly determines the fundamental frequency of an aircraft-type curved panel can be obtained by relaxing the in-plane restraint along the length through appropriate changes in the energy representation and the assumed eigenmodes.

G. The effects of curvature in honeycomb sandwich construction evaluated by state-of-the-art analysis techniques are (1) the vibratory stresses in the outer facing sheet, in the direction of curvature, are of greater magnitude than the stresses in the inner facing sheet, when the facing sheets are of equal thickness; (2) the vibratory facing sheet stress at the center of a panel increases with curvature, because of membrane influences; and (3) honeycomb core shear stress decreases with panel curvature.

H. The design nomographs and computer program for skin-stringer and honeycomb sandwich construction which account for structural curvature effects will increase sonic fatigue design capabilities.

APPENDIX I

TEST DETAILS AND INSTRUMENTATION

A. Modal Frequency Investigation

The test arrangement for the modal frequency investigation is shown in Figure AI-1. This was accomplished by placing the frame-mounted specimens over two 15-inch loudspeakers, one of which was equipped with a phase-reversal switch so that the test specimen could be excited with an in-phase or out-of-phase forcing function. The mode shapes (Chladni patterns) were obtained by sprinkling cork particles on the surface of the vibrating panel, and then varying the input frequency until the cork was aligned along the mode lines. When a well-defined pattern was observed, the input frequency was recorded. After a study of the mode shapes, it was decided that the strain gages should be located in the positions shown in Figures 22 and 23, Section III.

B. Damping Studies

The test setup for performing damping studies is shown in Figure AI-2. The test specimens were mounted over two loudspeakers in the same manner as was done for the modal frequency investigation. An oscilloscope and a Polaroid Oscilloscope Camera was used to photograph the decaying strain oscillations. The photographs were obtained by using a 3-way switch which turned off the loudspeaker and at the same time triggered the oscilloscope. When the trace appeared on the oscilloscope a photograph was made.

The logarithmic decrement was found using the following equation

$$D = \frac{1}{n} \ln X_o/X_n$$

where D = the logarithmic decrement

X_o = the amplitude of the damped wave at point 0

X_n = the amplitude of the damped wave after n cycles

n = the number of cycles.

The damping ratio δ was determined using the log decrement and the equation

$$\delta = \frac{\ln X_o/X_n}{2 \pi n}$$

In order to get an average value for each panel, several decaying strain oscillations were analyzed. The mean damping ratio was calculated using

$$\delta_A = \frac{1}{N} \sum_{1}^{n} \delta_i$$

where δ_A = the average damping ratio

N = the number of decaying strain oscillations taken into account for a specific panel.

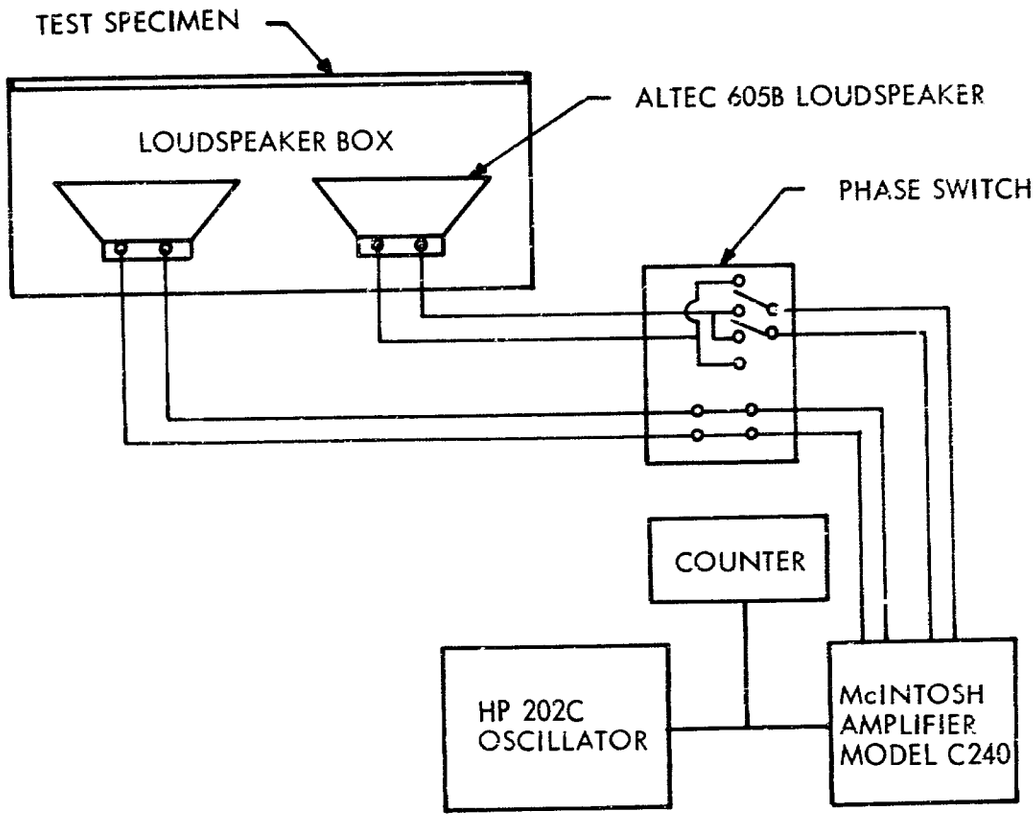

FIGURE AI-1. TEST SET-UP FOR MODAL STUDIES

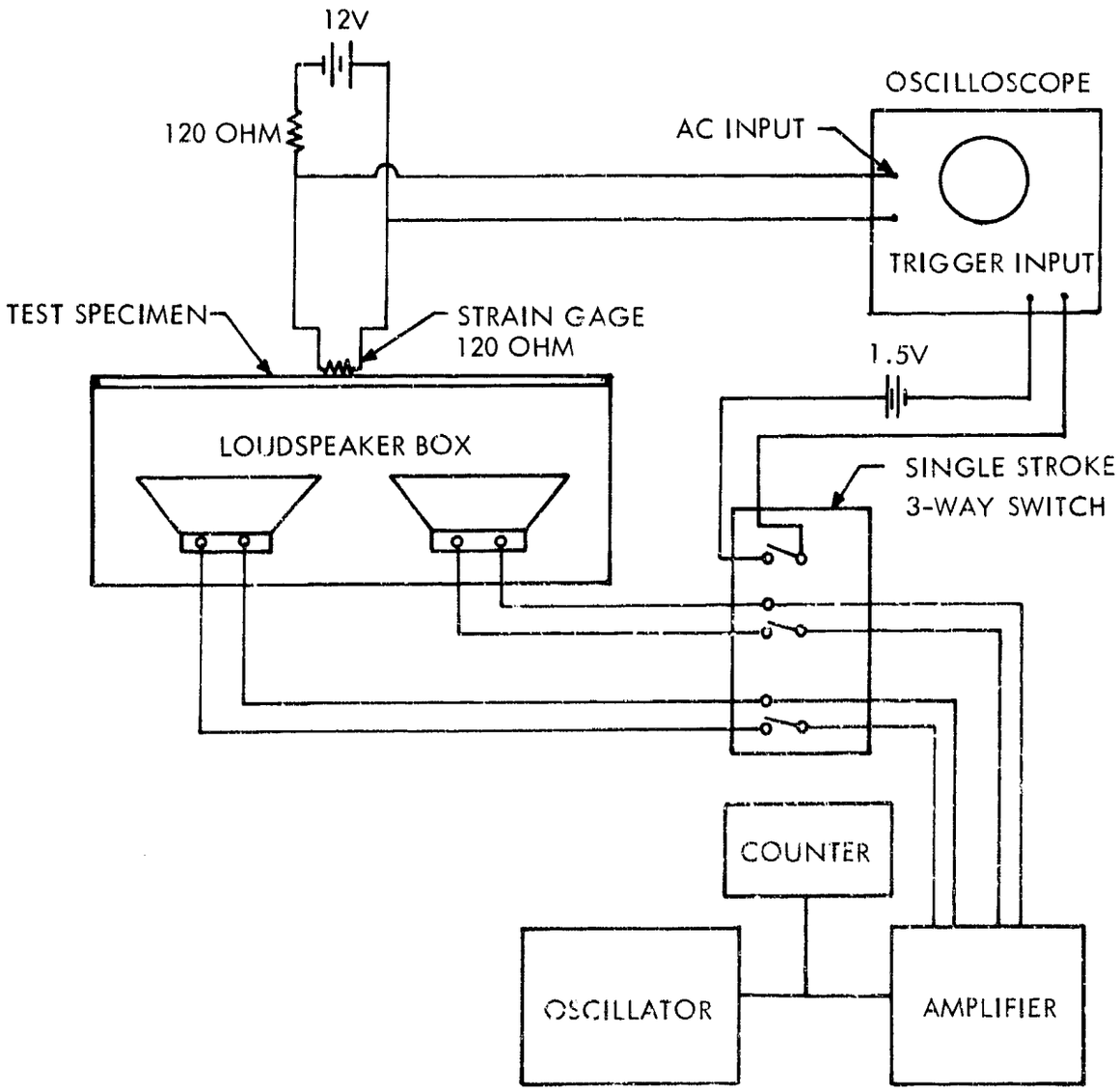

FIGURE AI-2. SCHEMATIC OF TEST SET-UP FOR DAMPING MEASUREMENTS

C. Discrete Frequency Sweeps

The test arrangement for conducting the sinusoidal frequency sweeps is shown in Figure AI-3. The test specimens were instrumented with strain gages and mounted in the test facility.

Each strain gage was connected in a four-arm bridge circuit and subsequently connected to a 6-channel signal conditioning unit. The test panels were then excited by using two transducers for a frequency range of 80 Hz to 2000 Hz. The strain gage signal was amplified and then analyzed using a Spectral Dynamics Analyzer with a narrow band (2 Hz) filter. The output was plotted on an x-y recorder.

During the frequency sweeps, accelerometers mounted on the test fixture were monitored to see if test fixture resonance was interfering with the test specimen response. There was no indication of significant test frame resonances in the frequency range of 80 Hz to 2000 Hz.

D. Panel Response

The strain gaged specimens were mounted in the test facility as shown in Figure 25, Section III, and exposed to broadband noise excitation. The response of the panels were obtained by using the same procedure that was used for the frequency sweeps. A simplified diagram of the set-up is shown in Figure AI-4. From the response plots the most active gage was determined for each set of test specimens. This gage was then recorded on magnetic tape using the set-up shown in Figure AI-5. Before each recording was made, a calibration signal from the strain gage was recorded on tape.

A tape loop, which included the calibration signal, was made from the recorded data. The loop was used to obtain PSD and peak strain probability analyses. The data analysis systems are shown in Figure AI-6, and a block diagram of the set-up is shown in Figure AI-7.

E. Spectrum Set-up

The block diagram for plotting of the spectrum is shown in Figure AI-8. The spectrum for each set of panels was shaped to concentrate the acoustical energy in a desired range of frequencies. The bandwidth of the test spectrum was chosen to be at least three times the bandwidth of the panel response.

F. Calibration of Test Section

A detailed survey of the sound pressure level distribution in the test section of the High Intensity Structural Test Facility was made. Discrete frequency sweeps were used to make the evaluation. Discrete frequency sound pressure levels were recorded at the locations shown on Figure AI-9. This figure is also a plot of the sound pressure level distribution for 145 decibels reference level and frequencies of 125 Hz, 150 Hz, and 275 Hz. This range of frequencies encompasses the (1,1) mode response of most of the specimens tested for this program. It can be seen that the distribution of sound pressure level over the test section at 125 Hz is uniform with a maximum positive deviation of 3 db and a maximum negative deviation of 1 db relative to the reference 145 db at the center of the test section. The distribution is somewhat better at 150 Hz with a maximum positive deviation of 3 db and no negative deviation. The distribution at 275 Hz showed a maximum positive deviation of 2 db and a maximum negative deviation of 3 db.

G. Microphone Calibration

The microphones were calibrated before each test spectrum was shaped. This was accomplished by using a Photocon Model PC-125 calibrator, which is traceable to a secondary

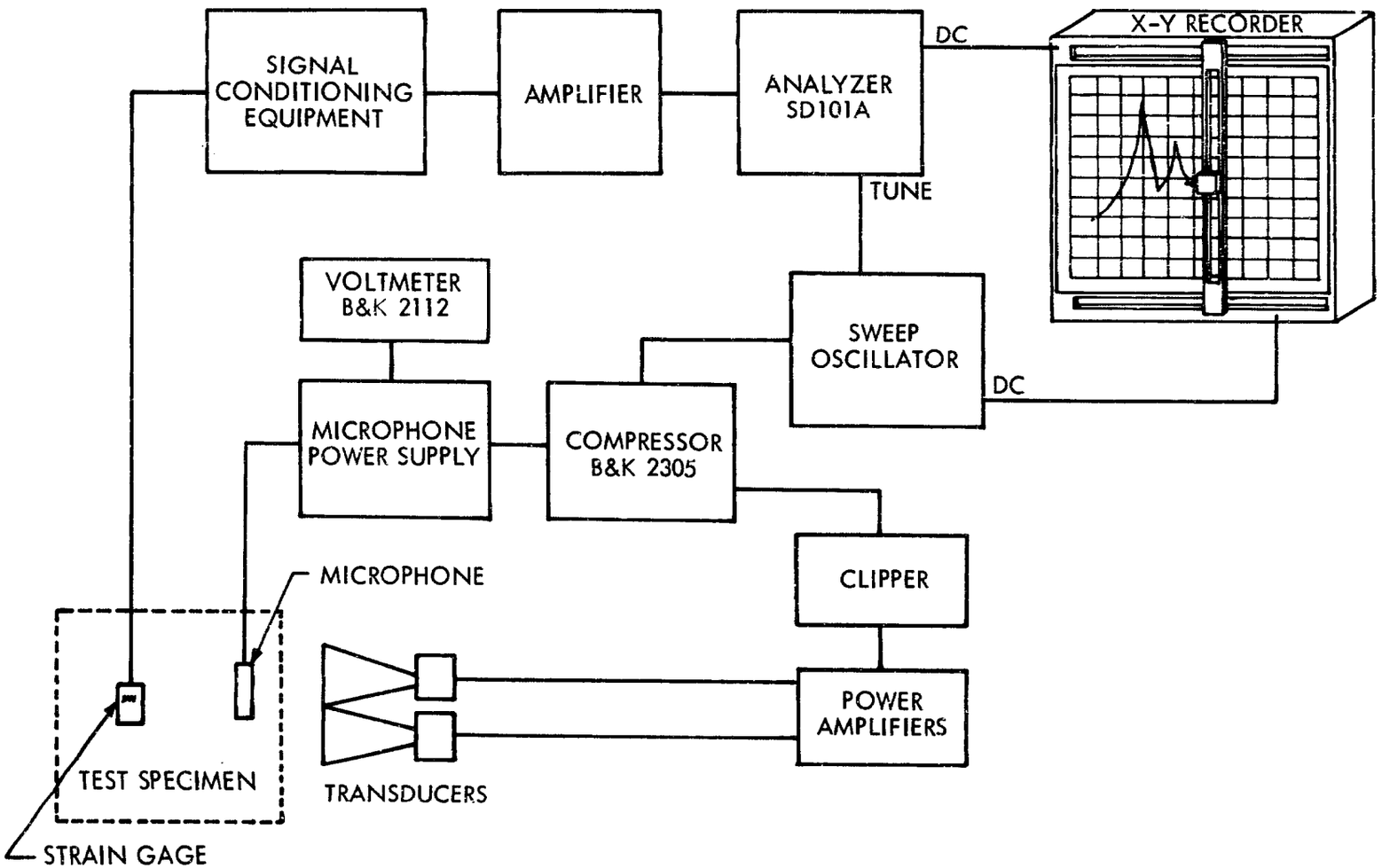

FIGURE AI-3. BLOCK DIAGRAM OF FREQUENCY SWEEP TEST SET-UP

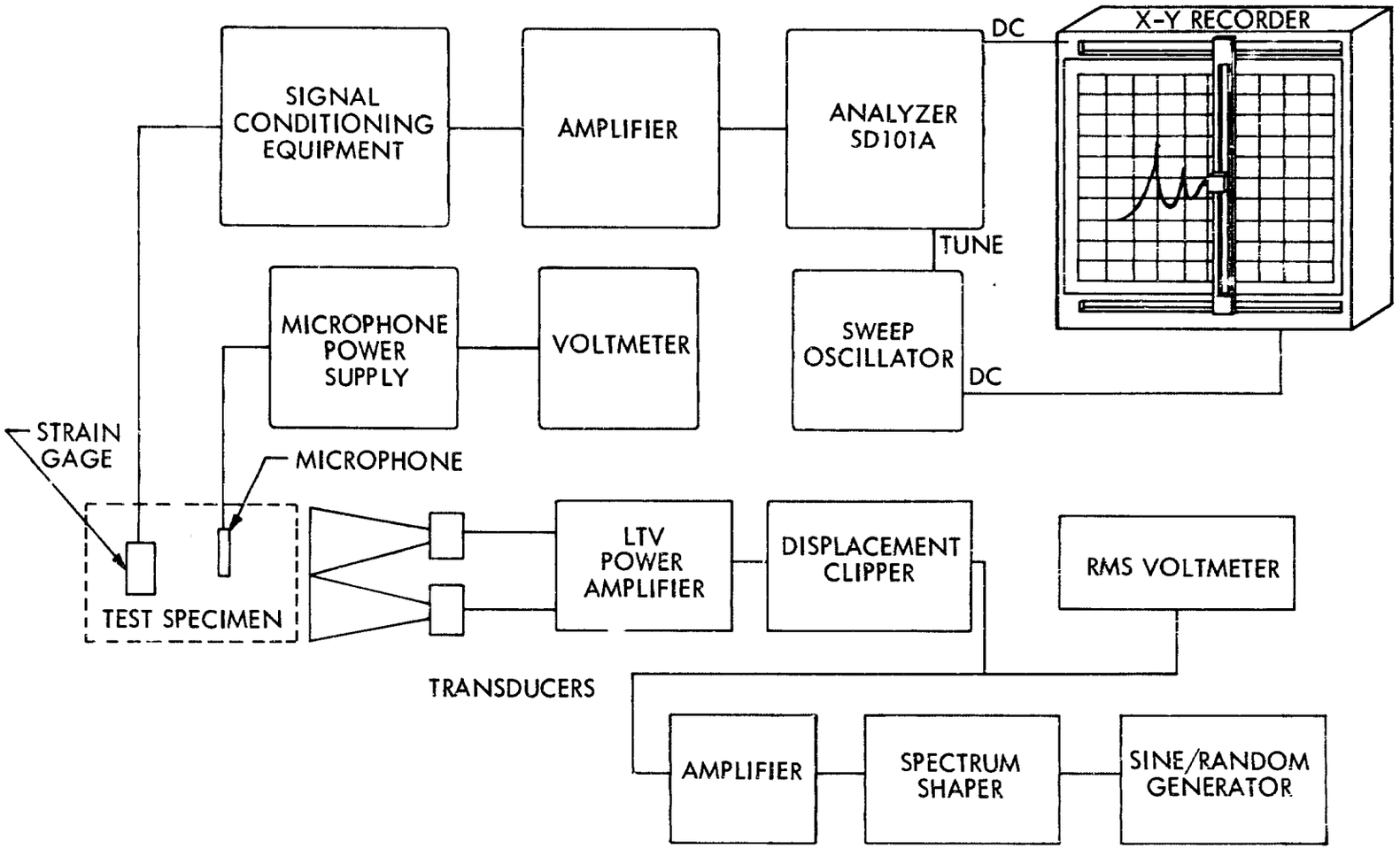

FIGURE AI-4. BLOCK DIAGRAM OF TEST SET-UP FOR PLOTTING PANEL RESPONSE

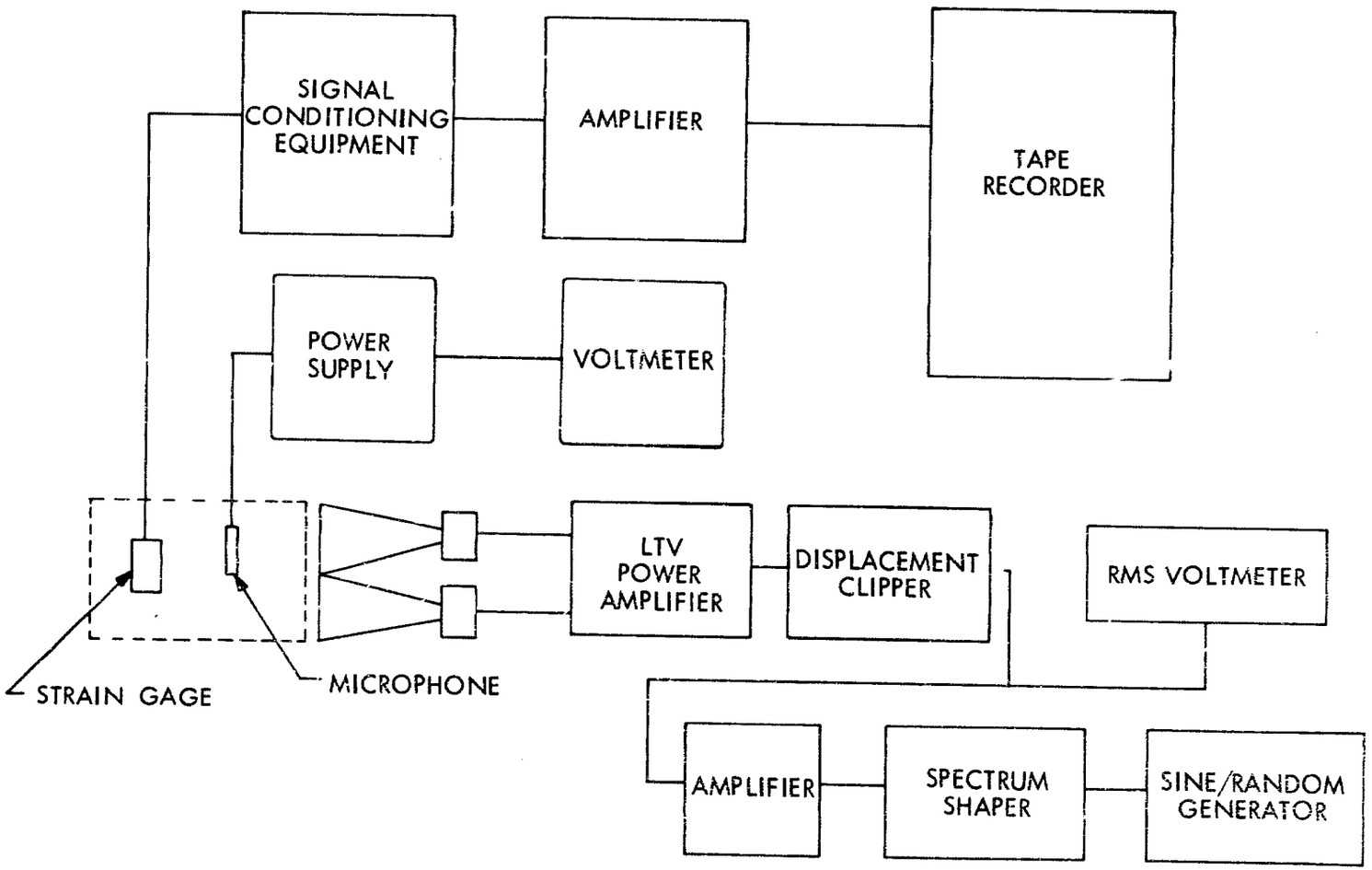

FIGURE AI-5. BLOCK DIAGRAM OF TEST SET-UP FOR DATA RECORDING

FIGURE AI-6. DATA ANALYSIS SYSTEM

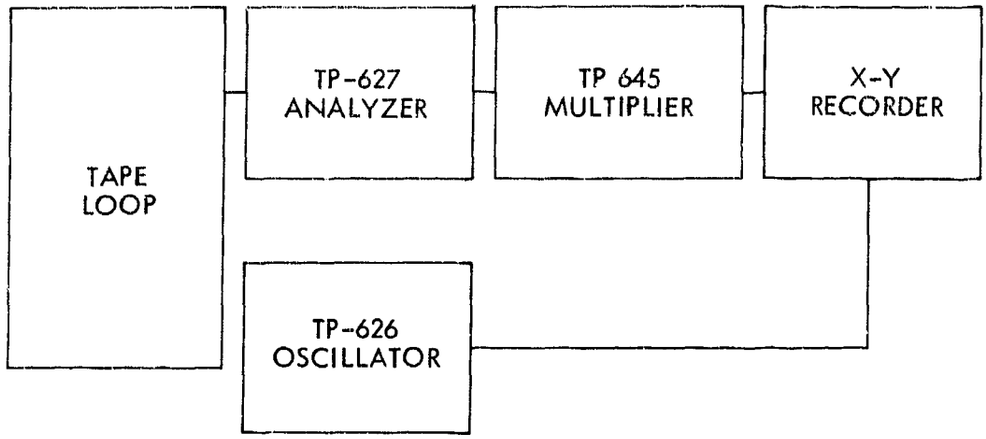

a. Block Diagram of PSD Analysis

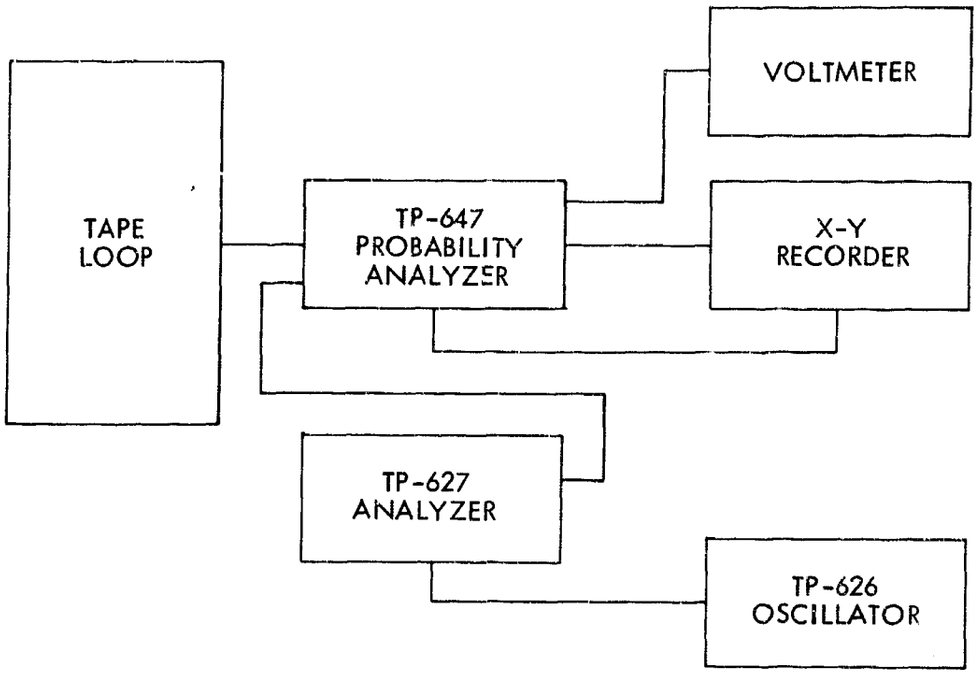

b. Block Diagram of Peak Strain Probability Analysis

FIGURE AI-7. BLOCK DIAGRAMS FOR STATISTICAL ANALYSIS OF TEST DATA

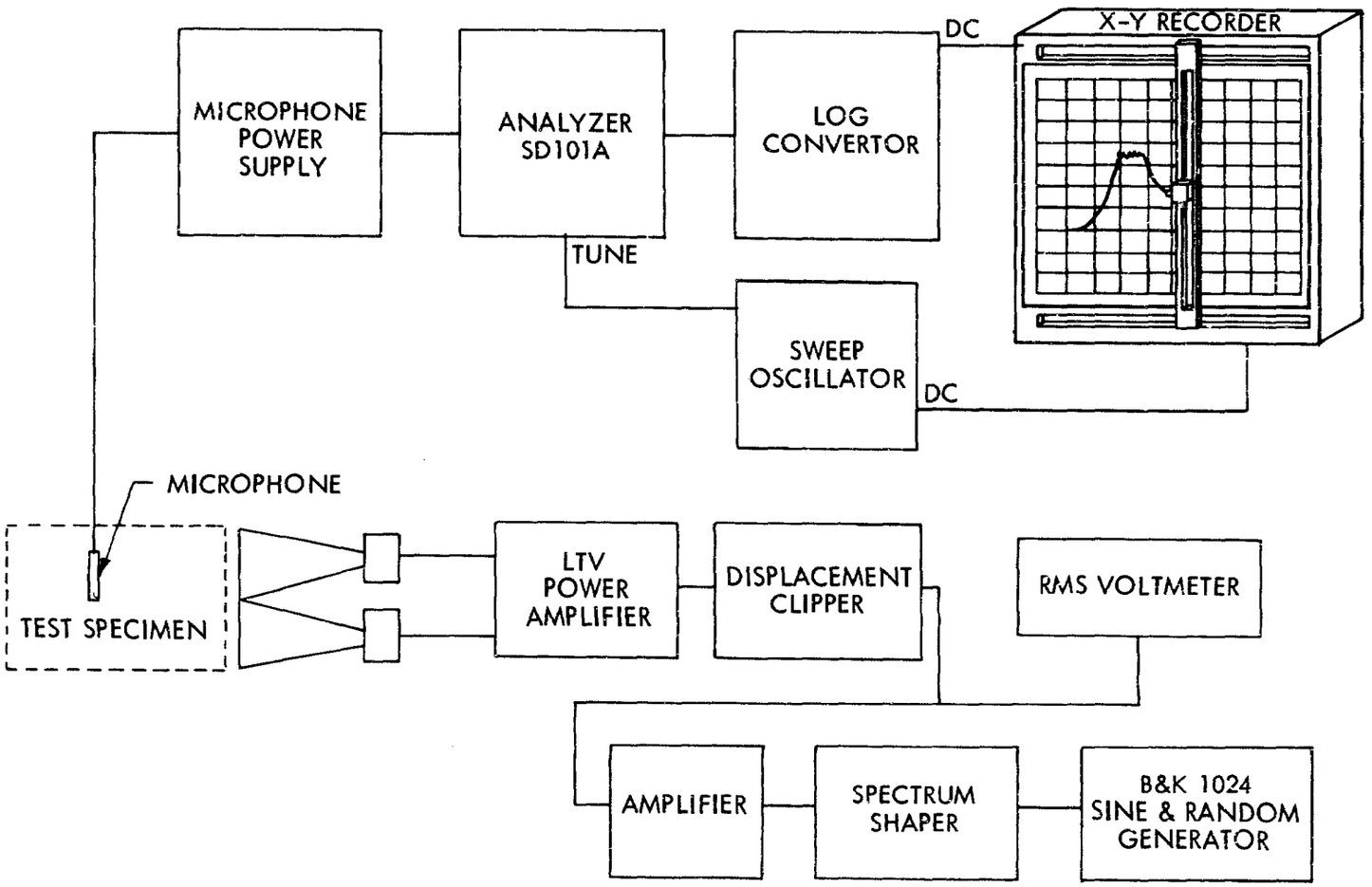

FIGURE AI-8. BLOCK DIAGRAM OF TEST SET-UP FOR PLOTTING SPECTRUM

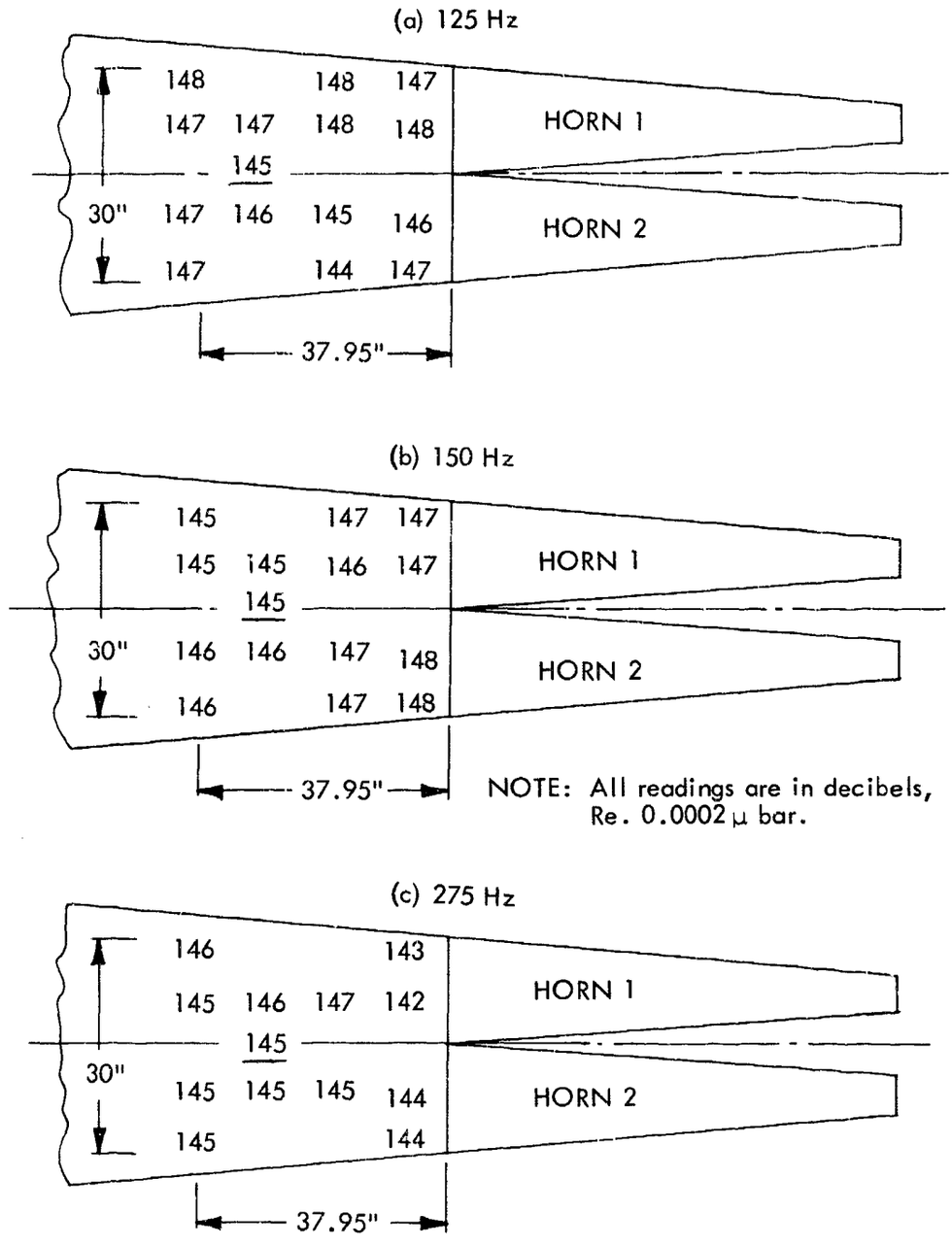

FIGURE AI-9. SOUND PRESSURE LEVEL DISTRIBUTION IN TEST SECTION

standard. The signal from the microphone, proportional to the calibration sound pressure level, was sent though the analyzing equipment to the x-y recorder. The displacement of the recorder pen was equal to the level applied to the microphone.

When the same spectrum was used for several days of testing, the microphones were calibrated at the beginning and the end of each day to see if there was any change in the sensitivity.

H. Strain Gage Curcuit

A four arm bridge circuit shown in Figure AI-10 was used for all strain measurements. The mathematical expression for this bridge circuit is as follows:

$$E_o = \frac{V_B R_G}{R_G + R_2} - \frac{V_B R_C}{R_C + R_1}$$

where V_B = excitation voltage

R_G = strain gage resistance (120 ohm)

R_C = dummy gage 120 ohm (for temperature compensation)

$R_1 = R_2$ = fixed resistance (120 ohm)

F = gage factor ($F = 2$)

E_o = gage output (volts)

Differentiating with respect to R_G

$$\frac{dE_o}{dR_G} = \frac{(R_G + R_2)V_B - V_B R_G}{(R_G + R_2)^2}$$

and

$$dE_o = V_B \frac{R_2}{(R_G + R_2)^2} dR_G .$$

The gage factor is

$$F = \frac{dR/R}{dL/L} ,$$

then $dR_G = F R_G \, dL/L$

and

$$dE_o = V_B \frac{R_2 R_G}{(R_G + R_2)^2} F \, dL/L$$

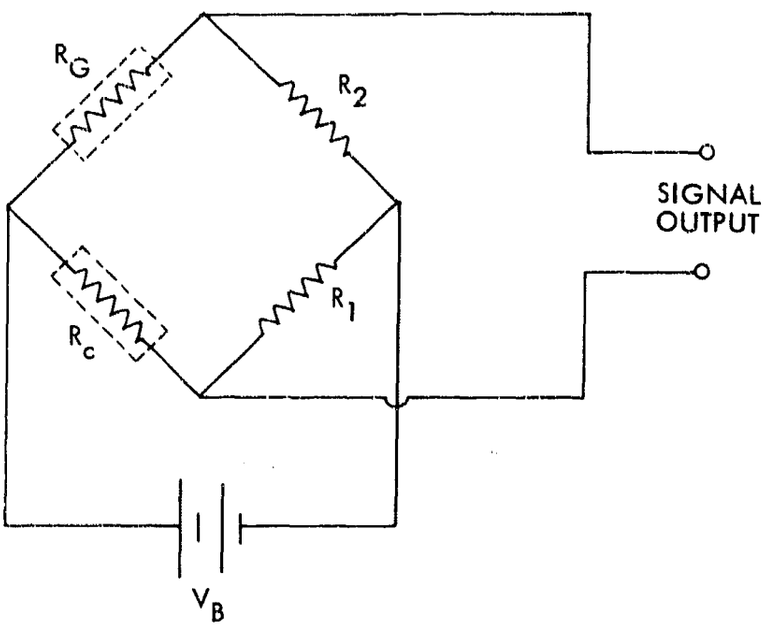

FIGURE AI-10. STRAIN GAGE CIRCUIT

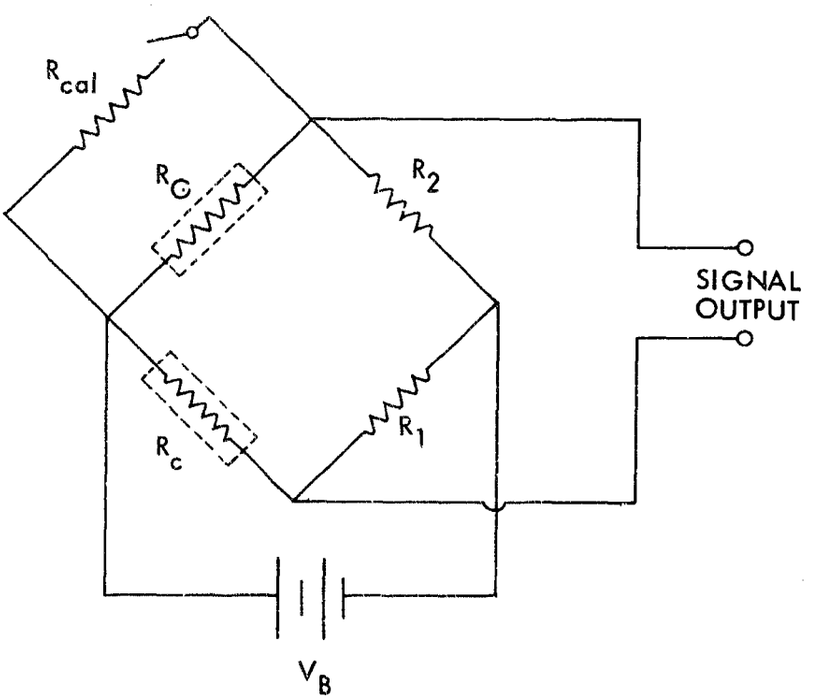

FIGURE AI-11. STRAIN GAGE CIRCUIT FOR CALIBRATION

where $R_2 = R_G$.

Therefore $\frac{R_2 R_G}{(R_G + R_2)^2} = \frac{R_2^2}{(2R_2)^2} = \frac{1}{4}$,

then $dE_o = V_B \frac{1}{4} F \, dL/L$

and $dL/L = \epsilon$ = strain.

Consequently, $dE_o = \frac{V_B}{4} F \epsilon$.

Example:

For 100 μ in/in strain

V_B = 11 volts

$F = 2$

$$dE_o = \frac{11(2)}{4} \times 100 \times 10^{-6}$$

$$dE_o = \frac{22}{4} \times 100 \times 10^{-6}$$

$$dE_o = 550 \times 10^{-6} = .550 \text{ millivolts for 100 } \mu \text{ in/in strain}$$

1. Strain Gage Calibration

The strain gages were calibrated using the shunt calibration method. This was accomplished by pressing a switch on the Signal Conditioning equipment. This switched a resistor in parallel with the strain gage. A simplified diagram of the circuit is shown in Figure AI-11. The parallel combination of the strain gage, R_G and the calibration resistor R_{cal} caused a ΔR change in the resistance of the active arm of the bridge circuit. Four calibration resistors were chosen so that the ΔR change in resistance of the parallel combination would be equivalent to 500, 1000, 1500 & 2000 micro in/in of strain. When the strain gages were being calibrated the output of the signal conditioning equipment was a d-c voltage. To facilitate the data analysis, this d-c signal was changed to an a-c signal. This was accomplished by monitoring the d-c voltage on an oscilloscope and then using an oscillator to provide an a-c signal with a peak to peak value equal to the d-c voltage. To compensate for possible gain or attenuation due to analyzing equipment the a-c calibration signal was sent through the same equipment as the strain gage signal. The calibration signal provided a deflection of the x-y recorder pen which corresponded to units of strain. Each plot of panel response was preceded by a calibration which gave a very accurate measure of the panel response in terms of strain.

An example of the method used for determining the values of the calibration resistor R_{cal}, Figure AI-11, is given below.

Example:

Find R_{cal} for an equivalent strain of 1000 μ in/in

$$F = \frac{\Delta R/R_G}{\Delta L/L} \;\&$$

$$\Delta R/R = F\ \Delta L/L = F\epsilon$$

For $\frac{\Delta R}{R_G} = 2000 \times 10^{-6}$ where $R_G = 120$ ohm

$$\Delta R = \epsilon R_G = (2000 \times 10^{-6}) \times 120 = .2400 \text{ ohm}$$

$$\Delta R = R_G - \frac{R_G R_{cal}}{R_G + R_{cal}}$$

$$\frac{R_G R_{cal}}{R_G + R_{cal}} = R_G - .240 \text{ ohm}$$

$$\frac{120 R_{cal}}{120 + R_{cal}} = 120 - .24$$

$$120 R_{cal} = (120)^2 + 120 R_{cal} - .24 R_{cal}$$

$$R_{cal} = \frac{(120)^2}{.24} \approx 60,000 \text{ or } 60K \text{ ohms}$$

J. Test Equipment List

Microphones:	Bruel & Kjaer type 4136
Microphone power supply:	Bruel & Kjaer type 2801
Microphone calibrator:	Photocon model PC-125
Signal conditioning:	Endevco model 4400.10
Data amplifier:	Hewlett Packard model 8875A
X-Y recorder:	Moseley model 2FRA
Sweep oscillator:	Spectral Dynamics model SD-104-2
Power amplifier:	Ling model RP-3/5
Transducer:	Ling model EPT 200
Random signal generator:	Bruel & Kjaer type 1024C
True R.M.S. voltmeter:	Bruel & Kjaer type 2416
Spectrum Shaper:	Bruel & Kjaer model 1612S/2
Tape recorder:	Ampex FR-1300
Time code generator:	Ampex TCS-100
Log convertor:	Technical Products model TP-662
Power amplifier:	McIntosh model Mc 240
Speaker:	Altec model 605B
Counter:	CMC model 800A
DC power supply:	Kron-Hite model RS-3610 SR
Multi-channel averaging control:	Spectral Dynamics model SD-22
Accelerometers:	Endevco model 2223
Accelerometer amplifier:	Endevco 2711A
Strain Gages:	BLH type DLB-A12-4AS13 & Dentronics type 202C13
Level recorder:	Bruel & Kjaer type 2305CS
Oscillator:	Hewlett Packard model 202C
Narrowband analyzer:	Spectral Dynamics model SD-101A
Octave band analyzer:	Bruel & Kjaer type 2112C
Oscilloscope:	Tektronix type 502A
Oscillator:	Technical Products TP-626T
Analyzer:	Technical Products TP-627T
Multiplier:	Technical Products TP-645

APPENDIX II

STATISTICAL ANALYSIS OF DATA

Frequently it is necessary to determine whether an apparent relation between two variables is significant and having shown it to be significant, to determine the best form of representation.

When pairs of observations on the two variables plotted on rectangular coordinate or functional curve paper give something that looks approximately like a straight line, there are some reasons to suspect that the relationship could have the forms:

$$y = a + bx$$

or if transformed

$$Y = AX^B .$$

In the fitting of the best straight line to data, the definition of the best line is that line which makes a minimum the sum of squares of the deviations from the line of the measurements of y; the independent variable x is assumed to be free of errors. When this process is applied to a pair of variables transformed in the manner indicated above what is being minimized is not the deviations of Y but the deviations of log Y.

To test for the significance of an apparently linear relation a correlation coefficient r defined by

$$r = \frac{\Sigma (x - \bar{x})\ (y - \bar{y})}{\left[\Sigma (x - \bar{x})^2 \quad \Sigma (y - \bar{y})^2 \right]}^{1/2}$$

where

$$\Sigma (x - \bar{x})^2 = \Sigma x^2 - \frac{(\Sigma x)^2}{n}$$

$$\Sigma (y - \bar{y})^2 = \Sigma y^2 - \frac{(\Sigma y)^2}{n}$$

$$\Sigma (x - \bar{x})\ (y - \bar{y}) = \Sigma x y - \frac{\Sigma x \ \Sigma y}{n}$$

n = number of pairs of observations

The correlation coefficient has the characteristics such that if the relationship between the data can be represented exactly by a straight line then $r = \pm 1$, positive if the straight line has positive slope and negative if the line has negative slope. If on the other hand there is no relation at all between the variables than r is zero.

If r proves to be significantly greater than zero the matter can be taken farther. The values of a and b can be evaluated from

$$a = \frac{\Sigma y}{n} - \frac{b \Sigma x}{n}$$

$$b = \frac{\Sigma (x - \bar{x})(y - \bar{y})}{\Sigma (x - \bar{x})^2}$$

The regression line will have an equation of the type

$$y = a + bx$$

or

$$Y = AX^B$$

etc.

It is assumed that the regression line is established with points scattered about on either side of it. The standard deviation of this scatter E, measured in units of y parallel to the y axis, is given by

$$E = \sqrt{1 - r^2} \sqrt{\frac{\Sigma (y - \bar{y})^2}{n - 2}} \quad .$$

Suppose it is desired to draw 95% confidence limits on either side of the regression line, within which 95% of all points should lie. First, the value of t for n - 2 degrees of freedom and the 5% level of significance is found from a Student's t table. The product of tE is determined next. Last, two lines are drawn parallel to the regression line, but one displaced tE units of y downwards and one displaced tE units of y upwards. Thus, if the regression line is used to predict the value of y from a known value of x, these confidence limits give the approximate limits between which there is a 95% chance of obtaining a correct prediction.

APPENDIX III

BRIEF DERIVATION OF THE PLATE ELEMENT STIFFNESS MATRIX

Consider the thin plate element shown below

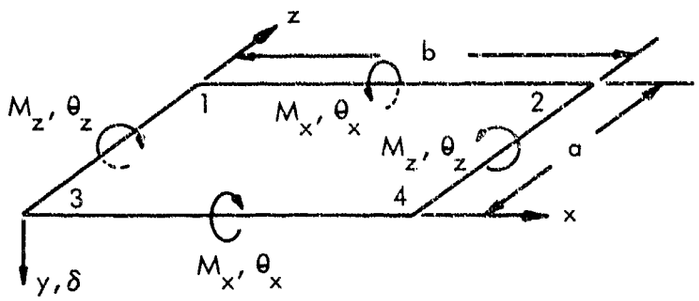

FIGURE AIII- 1 PLATE ELEMENT

Assuming a deformation of the form

$$\left.\begin{aligned} &w_1(x) = X(x) \quad \text{along lines of } z = \text{constant} \\ &w_2(z) = Z(z) \quad \text{along lines of } x = \text{constant} \\ &\text{where } X(x) = A_3x^3 + A_2x^2 + A_1x + A_o \\ &\qquad Z(z) = B_3z^3 + B_2z^2 + B_1z + B_o \end{aligned}\right\} \quad (1)$$

the coefficients A_i and B_i will be determined from the boundary conditions at the corner of the plate element.

Along the edge $z = 0$

$$\left.\begin{aligned} &X(o) = A_o = \delta_3 \\ &X(b) = A_3b^3 + A_2b^2 + A_1b + A_o = \delta_4 \\ &X'(o) = A_1 = \theta_{z3} \\ &X'(b) = 3A_3b^2 + 2A_2b + A_1 = -\theta_{z4} \end{aligned}\right\} \quad (2)$$

where δ_i is the displacement at the i^{th} corner

θ_{zi} is the rotation about the z axis at the i^{th} corner

θ_{xi} is the rotation about the x axis at the i^{th} corner

Solving Equations (2) for the coefficients, A_i,

$$\left.\begin{aligned} A_o &= \delta_3 \\ A_1 &= \theta_{z3} \\ A_2 &= -\frac{2}{b}\theta_{z3} + \frac{1}{b}\theta_{z4} - \frac{3}{b^2}\delta_3 + \frac{3}{b^2}\delta_4 \\ A_3 &= \frac{1}{b^2}\theta_{z3} - \frac{1}{b^2}\theta_{z4} + \frac{2}{b^3}\delta_3 - \frac{2}{b^3}\delta_4 \end{aligned}\right\} \quad (3)$$

Then, along the edge $z = 0$

$$X_o(x) = \left(\frac{x^3}{b^2} - \frac{2x^2}{b} + x\right)\theta_{z3} - \left(\frac{x^3}{b^2} - \frac{x^2}{b}\right)\theta_{z4} + \left(\frac{2x^3}{b^3} - \frac{3x^2}{b^2} + 1\right)\delta_3 - \left(\frac{2x^3}{b^3} - \frac{3x^2}{b^2}\right)\delta_4 \quad , \quad (4)$$

Similarly, along the edge $z = a$

$$X_a(x) = \left(\frac{x^3}{b^2} - \frac{2x^2}{b} + x\right)\theta_{z1} - \left(\frac{x^3}{b^2} - \frac{x^2}{b}\right)\theta_{z2} + \left(\frac{2x^3}{b^3} - \frac{3x^2}{b^2} + 1\right)\delta_1 - \left(\frac{2x^3}{b^3} - \frac{3x^2}{b^2}\right)\delta_2 \quad , \quad (5)$$

along the edge $x = 0$

$$Z_o(z) = \left(\frac{z^3}{a^2} - \frac{2z^2}{a} + z\right)\theta_{x3} - \left(\frac{z^3}{a^2} - \frac{z^2}{a}\right)\theta_{x1} + \left(\frac{2z^3}{a^3} - \frac{3z^2}{a^2} + 1\right)\delta_3 - \left(\frac{2z^3}{a^3} - \frac{3z^2}{a^2}\right)\delta_1 \quad , \quad (6)$$

and along the edge $x = b$

$$Z_b(z) = \left(\frac{z^3}{a^2} - \frac{2z^2}{a} + z\right)\theta_{x4} - \left(\frac{z^3}{a^2} - \frac{z^2}{a}\right)\theta_{x2} + \left(\frac{2z^3}{a^3} - \frac{3z^2}{a^2} + 1\right)\delta_4$$

$$- \left(\frac{2z^3}{a^3} - \frac{3z^2}{a^2}\right)\delta_2 \qquad (7)$$

For thin plates the strain energy expression is

$$U = \frac{1}{2}D \int_0^a \int_0^b \left[(w_{,xx} + w_{,zz})^2 - 2(1-\nu)\ (w_{,xx}w_{,zz} - w_{,xz}^2)\right]dx\,dz \qquad (8)$$

Letting $w(x,z) = w_1(x) + w_2(z)$ (9)

the assumed deformation pattern will be taken as

$$\left.\begin{aligned}
w(x,z) &= X_o(x) + Z_o(z) && 0 \le x \le b/2,\ 0 \le z \le a/2 \\
w(x,z) &= X_o(x) + Z_b(z) && 0 \le x \le b/2,\ a/2 \le z \le a \\
w(x,z) &= X_a(x) + Z_o(z) && b/2 \le x \le b,\ 0 \le z \le a/2 \\
w(x,z) &= X_a(x) + Z_b(z) && b/2 \le x \le b,\ a/2 \le z \le a
\end{aligned}\right\} \qquad (10)$$

Equations (10) are used to evaluate the bending contributions to the strain energy through the terms $w_{,xx}$ and $w_{,zz}$. The contribution to the strain energy for the torsion of the plate is obtained by considering the curvature to be defined as

$$w_{,xz} = (-\delta_1 + \delta_2 + \delta_3 - \delta_4)/ab \qquad (11)$$

Then, substituting Equations (10) and Equation (11) into the strain energy expression (Equation (8)) and performing the integrations, the strain energy is obtained in terms of the corner displacements δ_i, θ_{xi}, and θ_{zi}. The stiffness matrix is obtained by application of Castigliano's Theorem.

From the definitions given in Equation (58) the plate stiffness matrix is (see Equation (43)) for the i^{th} plate element.

$$\left[K_{xx}\right]_i = \begin{bmatrix} 2\alpha_i & 0 & \alpha_i & 0 \\ 0 & 2\alpha_i & 0 & \alpha_i \\ \alpha_i & 0 & 2\alpha_i & 0 \\ 0 & \alpha_i & 0 & 2\alpha_i \end{bmatrix} \tag{12}$$

$$\left[K_{xy}\right]_i = \begin{bmatrix} -\rho_i & 30(\delta/b)_i & \sigma_i & -6(\delta/b)_i \\ 30(\delta/b)_i & -\rho_i & -6(\delta/b)_i & \sigma_i \\ -\sigma_i & 6(\delta/b)_i & \rho_i & -30(\delta/b)_i \\ 6(\delta/b)_i & -\sigma_i & -30(\delta/b)_i & \rho_i \end{bmatrix} \tag{13}$$

$$\left[K_{zz}\right]_i = \begin{bmatrix} 2\beta_i & \beta_i & 0 & 0 \\ \beta_i & 2\beta_i & 0 & 0 \\ 0 & 0 & 2\beta_i & \beta_i \\ 0 & 0 & \beta_i & 2\beta_i \end{bmatrix} \tag{14}$$

$$\left[K_{zy} \right]_i = \begin{bmatrix} \chi_i & -\tau_i & -30(\delta/a)_i & 6(\delta/a)_i \\ \tau_i & -\chi_i & -6(\delta/a)_i & 30(\delta/a)_i \\ -30(\delta/a)_i & 6(\delta/a)_i & \chi_i & -\tau_i \\ -6(\delta/a) & 30(\delta/a)_i & \tau_i & -\chi_i \end{bmatrix} \tag{15}$$

$$\left[K_{yy} \right]_i = \begin{bmatrix} \kappa_i & -\lambda_i & -\mu_i & \gamma_i + 72(\delta/ab)_i \\ -\lambda_i & \kappa_i & \gamma_i + 72(\delta/ab)_i & -\mu_i \\ -\mu_i & \gamma_i + 72(\delta/ab)_i & \kappa_i & -\lambda_i \\ \gamma_i + 72(\delta/ab)_i & -\mu_i & -\lambda_i & \kappa_i \end{bmatrix} \tag{16}$$

where only the upper diagonal sub matrices have been shown.

APPENDIX IV

COMPUTER PROGRAMS

A. Substructure Dynamic Analysis

The computer program given below uses the equations developed in Section II-D and the method of solution given in Section II-D-3.

The only option is whether or not eigenvectors are desired. For print out of eigenvectors set MV = 0. The input data are defined as

E(I)	Young's Modulus for the i^{th} stiffener
J1(I)	St. Venant's torsion constant for the i^{th} stiffener
I1(I)	second area moment of Inertia for the i^{th} stiffener
L1(I)	length of the i^{th} stiffener
EP(I)	Young's Modulus for the i^{th} panel element
HP(I)	thickness of the i^{th} panel element
AP(I)	length of the i^{th} panel element in the z direction
BP(I)	length of the i^{th} panel element in the x direction
WP	weight of panel element per unit area
WR	weight of rib per unit length
WS	weight of stringer per unit length

All dimensions are in inches and weight in pounds.

B. Effect of Curvature on Stress in Honeycomb Panels

The program uses the equations, summarized in Section V-2 in the calculation of stress ratio.

There are two input options. OPT1 selects the type of excitation; 0 for random noise, 1 for sinusoidal excitation. OPT2 allows the inclusion of variations of damping due to change in natural frequency with curvature; 0 leaves out damping, 1 includes variable damping.

There are three lines of input data. The first two lines contain the physical data. The data are

A	arc length
B	panel length
E	modulus of elasticity of skin
GXZ	Transverse shear modulus for core
GYZ	Transverse shear modulus for core
H	core thickness
R	panel radius of curvature
T	skin thickness
TE	edge thickness
RO	skin mass density
DELC	damping ratio for first mode of curved panel
DELF	damping ratio for first mode of flat panel

The data are prepared as follows:

1st and 2nd line

COL

1	11	21	41	51
A	B	E	GXZ	GYZ
H	R	T	TE	RO

1	2	3	10
OPT1	OPT2	DELC	DELF

Two of the four possible output combinations are shown at the end of the program.

```
C       THIS PROGRAM COMPUTES NATURAL FREQUENCIES AND MODE SHAPES
C       OF A NINE BAY ORTHOGONALLY STIFFENED PANEL ARRAY WITH CLAMPED
C       EDGES. SUBROUTINES REQUIRED ARE LOC,EIGEN,AND NROOT.
        REAL E(12),J1(12),I1(12),L1(12),B(12),T(12),K1(12,12)
        REAL EP(9),HP(9),AP(9),BP(9),L(9),AL(9),BE(9),GM(9),DE(9)
        REAL P1(9),P2(9),P3(9),P4(9),P5(9),P6(9),P7(9)
        REAL KP(12,12),K2(12,12),MM(12,12)
        DOUBLE PRECISION EVL(12),EVC(144),AA(144),BB(144)
        INTEGER Q,S
C       IF EIGENVALUES AND EIGENVECTORS ARE DESIRED, SET MV=0 .
C       IF ONLY EIGENVALUES ARE DESIRED, SET MV=1 .
C       SEE COMMENTS IN SUBROUTINE ' EIGEN'.
  111   READ(5,1) MV
        READ(5,2) WP,WR,WS
        N=12
        S= 9
        READ(5,3) (E(I),I1(I),J1(I),L1(I), I=1,N)
        READ(5,3) (EP(I),HP(I),AP(I),BP(I), I=1,S)
    1   FORMAT(3I3)
    2   FORMAT(3E12.5)
    3   FORMAT(4E12.5)
        WRITE(6,4)
    4   FORMAT(1H1,5X,'VIBRATION ANALYSIS OF A STIFFENED PANEL')
C       COMPUTE STIFFNESS OF SUPPORTING STRUCTURE
        DO 5 Q=1,N
        B(Q)= E(Q)*I1(Q)/L1(Q)**3
        T(Q)= 0.384*E(Q)*J1(Q)/L1(Q)
    5   CONTINUE
        K1(1,1)= T(2)+T(3)+4.0*(B(4)*L1(4)**2+B(12)*L1(12)**2)
        K1(1,2)=-T(3)
        K1(1,3)= 2.0*B(12)*L1(12)**2
        K1(1,9)= 6.0*(B(12)*L1(12)-B(4)*L1(4))
        K1(1,11)=-6.0*B(12)*L1(12)
        K1(2,2)= T(3)+T(7)+4.0*(B(5)*L1(5)**2+B(6)*L1(6)**2)
        K1(2,4)= 2.0*B(6)*L1(6)**2
        K1(2,10)= 6.0*(B(6)*L1(6)-B(5)*L1(5))
        K1(2,12)=-6.0*B(6)*L1(6)
        K1(3,3)= T(1)+T(9)+4.0*(B(11)*L1(11)**2+B(12)*L1(12)**2)
        K1(3,4)=-T(9)
        K1(3,9)= 6.0*B(12)*L1(12)
        K1(3,11)= 6.0*(B(11)*L1(11)-B(12)*L1(12))
        K1(4,4)= T(8)+T(9)+4.0*(B(6)*L1(6)**2+B(10)*L1(10)**2)
        K1(4,10)= 6.0*B(6)*L1(6)
        K1(4,12)= 6.0*(B(10)*L1(10)-B(6)*L1(6))
        K1(5,5)= T(4)+T(12)+4.0*(B(2)*L1(2)**2+B(3)*L1(3)**2)
        K1(5,6)= 2.0*B(3)*L1(3)**2
        K1(5,7)=-T(12)
        K1(5,9)= 6.0*(B(3)*L1(3)-B(2)*L1(2))
        K1(5,10)=-6.0*B(3)*L1(3)
```

FIGURE A-IV-1. COMPUTER PROGRAM FOR FREQUENCY ANALYSIS OF SUBSTRUCTURE (CONTINUED)

```
      K1(6,6)= T(5)+T(6)+4.0*(B(3)*L1(3)**2+B(7)*L1(7)**2)
      K1(6,8)=-T(6)
      K1(6,9)= 6.0*B(3)*L1(3)
      K1(6,10)= 6.0*(B(7)*L1(7)-B(3)*L1(3))
      K1(7,7)= T(11)+T(12)+4.0*(B(1)*L1(1)**2+B(9)*L1(9)**2)
      K1(7,8)= 2.0*B(9)*L1(9)**2
      K1(7,11)= 6.0*(B(9)*L1(9)-B(1)*L1(1))
      K1(7,12)=-6.0*B(9)*L1(9)
      K1(8,8)= T(6)+T(10)+4.0*(B(8)*L1(8)**2+B(9)*L1(9)**2)
      K1(8,11)= 6.0*B(9)*L1(9)
      K1(8,12)= 6.0*(B(8)*L1(8)-B(9)*L1(9))
      K1(9,9)= 12.0*(B(2)+B(3)+B(4)+B(12))
      K1(9,10)=-12.0*B(3)
      K1(9,11)=-12.0*B(12)
      K1(10,10)= 12.0*(B(3)+B(5)+B(6)+B(7))
      K1(10,12)=-12.0*B(6)
      K1(11,11)= 12.0*(B(1)+B(9)+B(11)+B(12))
      K1(11,12)=-12.0*B(9)
      K1(12,12)= 12.0*(B(6)+B(8)+B(9)+B(10))
C     COMPUTE STIFFNESS OF COVER PLATES
      DO 6 Q=1,S
      D(Q)=0.0912*EP(Q)*HP(Q)**3
      AL(Q)=D(Q)*BP(Q)/AP(Q)**2
      BE(Q)=D(Q)*AP(Q)/BP(Q)**2
      GM(Q)=1.4*D(Q)/(AP(Q)*BP(Q))
      DE(Q)= 0.01875*D(Q)
      P1(Q)= 3.0*(AL(Q)+10.0*DE(Q)/BP(Q))
      P2(Q)= 3.0*(BE(Q)+10.0*DE(Q)/AP(Q))
      P3(Q)= 3.0*(AL(Q)+2.0*DE(Q)/BP(Q))
      P4(Q)= 3.0*(BE(Q)+2.0*DE(Q)/AP(Q))
      P5(Q)= GM(Q)+72.0*DE(Q)/(AP(Q)*BP(Q))
      P6(Q)= 6.0*AL(Q)/AP(Q)
      P7(Q)= 6.0*BE(Q)/BP(Q)
6     CONTINUE
      KP(1,1)= 2.0*(AP(5)*AL(5)+AP(4)*AL(4)+AP(2)*AL(2)+AP(1)*AL(1))
      KP(1,3)= AP(5)*AL(5)+AP(4)*AL(4)
      KP(1,9)= P1(1)+P1(2)-P1(4)-P1(5)
      KP(1,10)= 30.0*(DE(5)/BP(5)-DE(2)/BP(2))
      KP(1,11)= P3(4)+P3(5)
      KP(1,12)=-6.0*DE(5)/BP(5)
      KP(2,2)= 2.0*(AP(6)*AL(6)+AP(5)*AL(5)+AP(3)*AL(3)+AP(2)*AL(2))
      KP(2,4)= AP(5)*AL(5)+AP(6)*AL(6)
      KP(2,9)= 30.0*(DE(5)/BP(5)-DE(2)/BP(2))
      KP(2,10)= P1(2)+P1(3)-P1(5)-P1(6)
      KP(2,11)=-6.0*DE(5)/BP(5)
      KP(2,12)= P3(5)+P3(6)
      KP(3,3)= 2.0*(AP(8)*AL(8)+AP(7)*AL(7)+AP(5)*AL(5)+AP(4)*AL(4))
      KP(3,9)=-P3(4)-P3(5)
```

FIGURE A-IV-1. (CONTINUED)

```
      KP(3,10)= 6.0*DE(5)/BP(5)
      KP(3,11)= P1(4)+P1(5)-P1(7)-P1(8)
      KP(3,12)= 30.0*(DE(8)/BP(8)-DE(5)/BP(5))
      KP(4,4)=2.0*(AP(9)*AL(9)+AP(8)*AL(8)+AP(6)*AL(6)+AP(5)*AL(5))
      KP(4,9)= 6.0*DE(5)/BP(5)
      KP(4,10)=-P3(5)-P3(6)
      KP(4,11)= 30.0*(DE(8)/BP(8)-DE(5)/BP(5))
      KP(4,12)= P1(5)+P1(6)-P1(8)-P1(9)
      KP(5,5)= 2.0*(BP(1)*BE(1)+BP(2)*BE(2)+BP(4)*BE(4)+BP(5)*BE(5))
      KP(5,6)= BP(5)*BE(5)+BP(2)*BE(2)
      KP(5,9)= P2(2)+P2(5)-P2(1)-P2(4)
      KP(5,10)=-P4(2)-P4(5)
      KP(5,11)= 30.0*(DE(4)/AP(4)-DE(5)/AP(5))
      KP(5,12)= 6.0*DE(5)/AP(5)
      KP(6,6)= 2.0*(BP(2)*BE(2)+BP(3)*BE(3)+BP(5)*BE(5)+BP(6)*BE(6))
      KP(6,9)= P4(2)+P4(5)
      KP(6,10)= P2(3)+P2(6)-P2(2)-P2(5)
      KP(6,11)=-6.0*DE(5)/AP(5)
      KP(6,12)= 30.0*(DE(5)/AP(5)-DE(6)/AP(6))
      KP(7,7)= 2.0*(BP(4)*BE(4)+BP(5)*BE(5)+BP(7)*BE(7)+BP(8)*BE(8))
      KP(7,8)= BP(8)*BE(8)+BP(5)*BE(5)
      KP(7,9)= 30.0*(DE(4)/AP(4)-DE(5)/AP(5))
      KP(7,10)= 6.0*DE(5)/AP(5)
      KP(7,11)= P2(5)+P2(8)-P2(4)-P2(7)
      KP(7,12)=-P4(5)-P4(8)
      KP(8,8)= 2.0*(BP(5)*BE(5)+BP(6)*BE(6)+BP(8)*BE(8)+BP(9)*BE(9))
      KP(8,9)=-6.0*DE(5)/AP(5)
      KP(8,10)= 30.0*(DE(5)/AP(5)-DE(6)/AP(6))
      KP(8,11)= P4(5)+P4(8)
      KP(8,12)= P2(6)+P2(9)-P2(5)-P2(8)
      KP(9,9)= P5(1)+P6(1)+P7(1)+P5(2)+P6(2)+P7(2)
     1         +P5(4)+P6(4)+P7(4)+P5(5)+P6(5)+P7(5)
      KP(9,10)=-P5(2)-P7(2)-P5(5)-P7(5)
      KP(9,11)=-P5(4)-P6(4)-P5(5)-P6(5)
      KP(9,12)= P5(5)
      KP(10,10)= P5(2)+P6(2)+P7(2)+P5(3)+P6(3)+P7(3)
     1           +P5(5)+P6(5)+P7(5)+P5(6)+P6(6)+P7(6)
      KP(10,11)= P5(5)
      KP(10,12)=-P5(5)-P6(5)-P5(6)-P6(6)
      KP(11,11)= P5(4)+P6(4)+P7(4)+P5(5)+P6(5)+P7(5)
     1           +P5(7)+P6(7)+P7(7)+P5(8)+P6(8)+P7(8)
      KP(11,12)=-P5(5)-P7(5)-P5(8)-P7(8)
      KP(12,12)= P5(5)+P6(5)+P7(5)+P5(6)+P6(6)+P7(6)
     1           +P5(8)+P6(8)+P7(8)+P5(9)+P6(9)+P7(9)
C     COMPUTE STIFFNESS OF STIFFENED PANEL ARRAY
      DO 7 I=1,N
      DO 7 J=1,N
```

FIGURE A-IV-1. (CONTINUED)

```
      K1(I,J)= K1(I,J)+KP(I,J)
      K1(J,I)= K1(I,J)
      K2(I,J)= K1(I,J)
 7    CONTINUE
C     COMPUTE MASS MATRIX
      WP=WP/386.0
      WR=WR/386.0
      WS=WS/386.0
      DP1=WP*(L1(12)+L1(4))*(L1(2)+L1(3))
      DR1=WR*(L1(12)+L1(4))
      DS1=WS*(L1(2)+L1(3))
      P11=L1(2)**2-L1(2)*L1(3)+L1(3)**2
      P21= L1(12)**2-L1(12)*L1(4)+L1(4)**2
      P31= L1(3)-L1(2)
      P41= L1(4)-L1(12)
      MM(1,1)= P21*(DP1+DR1)/3.0
      MM(1,5)=-P31*P41*DP1/4.0
      MM(1,9)=-P41*(DP1+DR1)/2.0
      MM(5,5)=P11*(DP1+DS1)/3.0
      MM(5,9)=P31*(DP1+DS1)/2.0
      MM(9,9)= DP1+DR1+DS1
      DP2= WP*(L1(6)+L1(5))*(L1(3)+L1(7))
      DR2= WR*(L1(6)+L1(5))
      DS2= WS*(L1(3)+L1(7))
      P12= L1(3)**2-L1(3)*L1(7)+L1(7)**2
      P22= L1(6)**2-L1(6)*L1(5)+L1(5)**2
      P32= L1(7)-L1(3)
      P42= L1(5)-L1(6)
      MM(2,2)= P22*(DP2+DR2)/3.0
      MM(2,6)=-P32*P42*DP2/4.0
      MM(2,10)=-P42*(DP2+DR2)/2.0
      MM(6,6)= P12*(DP2+DS2)/3.0
      MM(6,10)= P32*(DP2+DS2)/2.0
      MM(10,10)= DP2+DR2+DS2
      DP3= WP*(L1(11)+L1(12))*(L1(1)+L1(9))
      DR3= WR*(L1(11)+L1(12))
      DS3= WS*(L1(1)+L1(9))
      P13= L1(1)**2-L1(1)*L1(9)+L1(9)**2
      P23= L1(11)**2-L1(11)*L1(12)+L1(12)**2
      P33= L1(9)-L1(1)
      P43= L1(12)-L1(11)
      MM(3,3)= P23*(DP3+DR3)/3.0
      MM(3,7)=-P33*P43*DP3/4.0
      MM(3,11)=-P43*(DP3+DR3)/2.0
      MM(7,7)=P13*(DP3+DS3)/3.0
      MM(7,11)= P33*(DP3+DS3)/2.0
      MM(11,11)= DP3+DR3+DS3
```

FIGURE A-IV-1. (CONTINUED)

```
      DP4= WP*(L1(10)+L1(6))*(L1(9)+L1(8))
      DR4= WR*(L1(10)+L1(6))
      DS4= WS*(L1(9)+L1(8))
      P14= L1(9)**2-L1(9)*L1(8)+L1(8)**2
      P24= L1(10)**2-L1(10)*L1(6)+L1(6)**2
      P34= L1(8)-L1(9)
      P44= L1(6)-L1(10)
      MM(4,4)= P24*(DP4+DR4)/3.0
      MM(4,8)=-P34*P44*DP4/4.0
      MM(4,12)=-P44*(DP4+DR4)/2.0
      MM(8,8)= P14*(DP4+DS4)/3.0
      MM(8,12)= P34*(DP4+DS4)/2.0
      MM(12,12)= DP4+DR4+DS4
      DO 8 I=1,N
      DO 8 J=1,N
      MM(J,I)= MM(I,J)
 8    CONTINUE
      DO 9 I=1,N
      DO 9 J=1,N
      CALL LOC(I,J,IJ,N,0)
      AA(IJ)= K1(I,J)
      BB(IJ)= MM(I,J)
 9    CONTINUE
C     COMPUTE EIGENVALUES AND EIGENVECTORS
      CALL NROOT(N,AA,BB,EVL,EVC)
      DO 13 I=1,N
      IF(EVL(I)) 10,11,11
 10   EVL(I)= DABS(EVL(I))
 11   EVL(I)= 0.1591*DSQRT(EVL(I))
      WRITE(6,14) EVL(I)
      IF(MV) 12,12,13
 12   WRITE(6,15)
      IX= 1+N*(I-1)
      IY= N+N*(I-1)
      WRITE(6,16) (EVC(J), J=IX,IY)
 13   CONTINUE
 14   FORMAT(5X,'FREQUENCY=',1X,E12.5,1X,'HZ.')
 15   FORMAT(5X,'MODE SHAPE')
 16   FORMAT(5X,4E12.5)
      DO 17 I=1,12
      DO 17 J=1,12
      K1(I,J)= 0.0
      K2(I,J)= 0.0
      KP(I,J)= 0.0
      CALL LOC(I,J,IJ,12,0)
      AA(IJ)= 0.0
      BB(IJ)= 0.0
 17   CONTINUE
      GO TO 111
```

FIGURE A-IV-1. (CONTINUED)

```
C
C     ******************************************************************
C
C        SUBROUTINE EIGEN
C
C        PURPOSE
C           COMPUTE EIGENVALUES AND EIGENVECTORS OF A REAL SYMMETRIC
C           MATRIX
C
C        USAGE
C           CALL EIGEN(A,R,N,MV)
C
C        DESCRIPTION OF PARAMETERS
C           A - ORIGINAL MATRIX (SYMMETRIC), DESTROYED IN COMPUTATION.
C               RESULTANT EIGENVALUES ARE DEVELOPED IN DIAGONAL OF
C               MATRIX A IN DESCENDING ORDER.
C           R - RESULTANT MATRIX OF EIGENVECTORS (STORED COLUMNWISE,
C               IN SAME SEQUENCE AS EIGENVALUES)
C           N - ORDER OF MATRICES A AND R
C           MV- INPUT CODE
C                     0   COMPUTE EIGENVALUES AND EIGENVECTORS
C                     1   COMPUTE EIGENVALUES ONLY (R NEED NOT BE
C                         DIMENSIONED BUT MUST STILL APPEAR IN CALLING
C                         SEQUENCE)
C
C        REMARKS
C           ORIGINAL MATRIX A MUST BE REAL SYMMETRIC (STORAGE MODE=1)
C           MATRIX A CANNOT BE IN THE SAME LOCATION AS MATRIX R
C
C        SUBROUTINES AND FUNCTION SUBPROGRAMS REQUIRED
C           NONE
C
C        METHOD
C           DIAGONALIZATION METHOD ORIGINATED BY JACOBI AND ADAPTED
C           BY VON NEUMANN FOR LARGE COMPUTERS AS FOUND IN 'MATHEMATICAL
C           METHODS FOR DIGITAL COMPUTERS', EDITED BY A. RALSTON AND
C           H.S. WILF, JOHN WILEY AND SONS, NEW YORK, 1962, CHAPTER 7
C
C     ******************************************************************
C
      SUBROUTINE EIGEN(A,R,N,MV)
      DIMENSION A(1),R(1)
C
C     ******************************************************************
C
C        IF A DOUBLE PRECISION VERSION OF THIS ROUTINE IS DESIRED, THE
C        C IN COLUMN 1 SHOULD BE REMOVED FROM THE DOUBLE PRECISION
C        STATEMENT WHICH FOLLOWS.
```

FIGURE A-IV-1. (CONTINUED)

```
C
      DOUBLE PRECISION A,R,ANORM,ANRMX,THR,X,Y,SINX,SINX2,
     1                 COSX2,SINCS,COSX
C
C         THE C MUST ALSO BE REMOVED FROM DOUBLE PRECISION STATEMENTS
C         APPEARING IN OTHER ROUTINES USED IN CONJUNCTION WITH THIS
C         ROUTINE.
C
C         THE DOUBLE PRECISION VERSION OF THIS SUBROUTINE MUST ALSO
C         CONTAIN DOUBLE PRECISION FORTRAN FUNCTIONS.  SQRT IN STATEMENTS
C         40, 68, 75, AND 78 MUST BE CHANGED TO DSQRT.  ABS IN STATEMENT
C         62 MUST BE CHANGED TO DABS.
C
C         ...,.........................,.....................
C
C         GENERATE IDENTITY MATRIX
C
      IF(MV-1) 10,25,10
   10 IQ=-N
      DO 20 J=1,N
      IQ=IQ+N
      DO 20 I=1,N
      IJ=IQ+I
      R(IJ)=0.0
      IF(I-J) 20,15,20
   15 R(IJ)=1.0
   20 CONTINUE
C
C         COMPUTE INITIAL AND FINAL NORMS (ANORM AND ANORMX)
C
   25 ANORM=0.0
      DO 35 I=1,N
      DO 35 J=I,N
      IF(I-J) 30,35,30
   30 IA=I+(J*J-J)/2
      ANORM=ANORM+A(IA)*A(IA)
   35 CONTINUE
      IF(ANORM) 165,165,40
   40 ANORM=1.414*DSQRT(ANORM)
      ANRMX=ANORM*1.0E-6/FLOAT(N)
C
C         INITIALIZE INDICATORS AND COMPUTE THRESHOLD, THR
C
      IND=0
      THR=ANORM
   45 THR=THR/FLOAT(N)
   50 L=1
   55 M=L+1
C
C         COMPUTE SIN AND COS
C
```

FIGURE A-IV-1. (CONTINUED)

```
   60 MQ=(M*M-M)/2
      LQ=(L*L-L)/2
      LM=L+MQ
   62 IF(DABS(A(LM))-THR) 130,65,65
   65 IND=1
      LL=L+LQ
      MM=M+MQ
      X=0.5*(A(LL)-A(MM))
   68 Y=-A(LM)/DSQRT(A(LM)*A(LM)+X*X)
      IF(X) 70,75,75
   70 Y=-Y
   75 SINX=Y/DSQRT(2.0*(1.0+(DSQRT(1.0-Y*Y))))
      SINX2=SINX*SINX
   78 COSX=DSQRT(1.0-SINX2)
      COSX2=COSX*COSX
      SINCS =SINX*COSX
C
C        ROTATE L AND M COLUMNS
C
      ILQ=N*(L-1)
      IMQ=N*(M-1)
      DO 125 I=1,N
      IQ=(I*I-I)/2
      IF(I-L) 80,115,80
   80 IF(I-M) 85,115,90
   85 IM=I+MQ
      GO TO 95
   90 IM=M+IQ
   95 IF(I-L) 100,105,105
  100 IL=I+LQ
      GO TO 110
  105 IL=L+IQ
  110 X=A(IL)*COSX-A(IM)*SINX
      A(IM)=A(IL)*SINX+A(IM)*COSX
      A(IL)=X
  115 IF(MV-1) 120,125,120
  120 ILR=ILQ+I
      IMR=IMQ+I
      X=R(ILR)*COSX-R(IMR)*SINX
      R(IMR)=R(ILR)*SINX+R(IMR)*COSX
      R(ILR)=X
  125 CONTINUE
      X=2.0*A(LM)*SINCS
      Y=A(LL)*COSX2+A(MM)*SINX2-X
      X=A(LL)*SINX2+A(MM)*COSX2+X
      A(LM)=(A(LL)-A(MM))*SINCS+A(LM)*(COSX2-SINX2)
      A(LL)=Y
      A(MM)=X
```

FIGURE A-IV-1. (CONTINUED)

```
C
C          TESTS FOR COMPLETION
C
C          TEST FOR M = LAST COLUMN
C
  130 IF(M-N) 135,140,135
  135 M=M+1
      GO TO 50
C
C          TEST FOR L = SECOND FROM LAST COLUMN
C
  140 IF(L-(N-1)) 145,150,145
  145 L=L+1
      GO TO 55
  150 IF(IND-1) 160,155,160
  155 IND=0
      GO TO 50
C
C          COMPARE THRESHOLD WITH FINAL NORM
C
  160 IF(THR-ANRMX) 165,165,45
C
C          SORT EIGENVALUES AND EIGENVECTORS
C
  165 IQ=-N
      DO 185 I=1,N
      IQ=IQ+N
      LL=I+(I*I-I)/2
      JQ=N*(I-2)
      DO 185 J=I,N
      JQ=JQ+N
      MM=J+(J*J-J)/2
      IF(A(LL)-A(MM)) 170,185,185
  170 X=A(LL)
      A(LL)=A(MM)
      A(MM)=X
      IF(MV-1) 175,185,175
  175 DO 180 K=1,N
      ILR=IQ+K
      IMR=JQ+K
      X=R(ILR)
      R(ILR)=R(IMR)
  180 R(IMR)=X
  185 CONTINUE
      RETURN
      END
```

FIGURE A-IV-1. (CONTINUED)

```
C
C     ..........................................................
C
C         SUBROUTINE NROOT
C
C         PURPOSE
C            COMPUTE EIGENVALUES AND EIGENVECTORS OF A REAL NONSYMMETRIC
C            MATRIX OF THE FORM B-INVERSE TIMES A.  THIS SUBROUTINE IS
C            NORMALLY CALLED BY SUBROUTINE CANOR IN PERFORMING A
C            CANONICAL CORRELATION ANALYSIS.
C
C         USAGE
C            CALL NROOT (M,A,B,XL,X)
C
C         DESCRIPTION OF PARAMETERS
C            M  - ORDER OF SQUARE MATRICES A, B, AND X.
C            A  - INPUT MATRIX (M X M).
C            B  - INPUT MATRIX (M X M).
C            XL - OUTPUT VECTOR OF LENGTH M CONTAINING EIGENVALUES OF
C                 B-INVERSE TIMES A.
C            X  - OUTPUT MATRIX (M X M) CONTAINING EIGENVECTORS COLUMN-
C                 WISE.
C
C         REMARKS
C            NONE
C
C         SUBROUTINES AND FUNCTION SUBPROGRAMS REQUIRED
C            EIGEN
C
C         METHOD
C            REFER TO W. W. COOLEY AND P. R. LOHNES, 'MULTIVARIATE PRO-
C            CEDURES FOR THE BEHAVIORAL SCIENCES', JOHN WILEY AND SONS,
C            1962, CHAPTER 3.
C
C     ..........................................................
C
      SUBROUTINE NROOT (M,A,B,XL,X)
      DIMENSION A(1),B(1),XL(1),X(1)
C
C     ...............................................................
C
C         IF A DOUBLE PRECISION VERSION OF THIS ROUTINE IS DESIRED, THE
C         C IN COLUMN 1 SHOULD BE REMOVED FROM THE DOUBLE PRECISION
C         STATEMENT WHICH FOLLOWS.
C
      DOUBLE PRECISION A,B,XL,X,SUMV
C
C         THE C MUST ALSO BE REMOVED FROM DOUBLE PRECISION STATEMENTS
C         APPEARING IN OTHER ROUTINES USED IN CONJUNCTION WITH THIS
C         ROUTINE.
```

FIGURE A-IV-1. (CONTINUED)

```
C
C          THE DOUBLE PRECISION VERSION OF THIS SUBROUTINE MUST ALSO
C          CONTAIN DOUBLE PRECISION FORTRAN FUNCTIONS.  SQRT IN STATEMENTS
C          110 AND 175 MUST BE CHANGED TO DSQRT.  ABS IN STATEMENT 110
C          MUST BE CHANGED TO DABS.
C
C          ...........................................................
C
C      COMPUTE EIGENVALUES AND EIGENVECTORS OF B
C
       K=1
       DO 100 J=2,M
       L=M*(J-1)
       DO 100 I=1,J
       L=L+1
       K=K+1
  100  B(K)=B(L)
C
C          THE MATRIX B IS A REAL SYMMETRIC MATRIX.
C
       MV=0
       CALL EIGEN (B,X,M,MV)
C
C      FORM RECIPROCALS OF SQUARE ROOT OF EIGENVALUES.  THE RESULTS
C      ARE PREMULTIPLIED BY THE ASSOCIATED EIGENVECTORS.
C
       L=0
       DO 110 J=1,M
       L=L+J
  110  XL(J)=1.0/DSQRT(DABS(B(L)))
       K=0
       DO 115 J=1,M
       DO 115 I=1,M
       K=K+1
  115  B(K)=X(K)*XL(J)
C
C      FORM (B**(-1/2))PRIME * A * (B**(-1/2))
C
       DO 120 I=1,M
       N2=0
       DO 120 J=1,M
       N1=M*(I-1)
       L=M*(J-1)+I
       X(L)=0.0
       DO 120 K=1,M
       N1=N1+1
       N2=N2+1
  120  X(L)=X(L)+B(N1)*A(N2)
```

FIGURE A-IV-1. (CONTINUED)

```
      L=0
      DO 130 J=1,M
      DO 130 I=1,J
      N1=I-M
      N2=M*(J-1)
      L=L+1
      A(L)=0.0
      DO 130 K=1,M
      N1=N1+M
      N2=N2+1
  130 A(L)=A(L)+X(N1)*B(N2)
C
C     COMPUTE EIGENVALUES AND EIGENVECTORS OF A
C
      CALL EIGEN (A,X,M,MV)
      L=0
      DO 140 I=1,M
      L=L+I
  140 XL(I)=A(L)
C
C     COMPUTE THE NORMALIZED EIGENVECTORS
C
      DO 150 I=1,M
      N2=0
      DO 150 J=1,M
      N1=I-M
      L=M*(J-1)+I
      A(L)=0.0
      DO 150 K=1,M
      N1=N1+M
      N2=N2+1
  150 A(L)=A(L)+B(N1)*X(N2)
      L=0
      K=0
      DO 180 J=1,M
      SUMV=0.0
      DO 170 I=1,M
      L=L+1
  170 SUMV=SUMV+A(L)*A(L)
  175 SUMV=DSQRT(SUMV)
      DO 180 I=1,M
      K=K+1
  180 X(K)=A(K)/SUMV
      RETURN
```

FIGURE A-IV-1. (CONTINUED)

```
      SUBROUTINE LOC(I,J,IJ,N,MS)
      IX=I
      JX=J
      IF(MS-1)10,20,30
   10 IJX=N*(JX-1)+IX
      GO TO 36
   20 IF(IX-JX)22,24,24
   22 IJX=IX+(JX*JX-JX)/2
      GO TO 36
   24 IJX=JX+(IX*IX-IX)/2
      GO TO 36
   30 IJX=0
      IF(IX-JX)36,32,36
   32 IJX=IX
   36 IJ=IJX
      RETURN
      END
```

FIGURE A-IV-1. COMPUTER PROGRAM FOR FREQUENCY ANALYSIS OF SUBSTRUCTURE (CONCLUDED)

```
/JOB GO
      REAL L,LE
1     READ(5,100)A,B,E,GXZ,GYZ
      READ(5,100)H,R,T,TE,RO
      READ(5,109)OPT1,OPT2,DELC,DELF
      IND=0
      THETA=A/R
      L=B/T
      AR=A/B
      G=H/(2.*T)
      S=.889*GYZ/E
      LE=B/TE
      C=GXZ/GYZ
      IF(THETA-.35)3,3,2
2     WRITE(6,101)THETA
      IND=1
3     IF(L-100.)4,5,5
4     WRITE(6,102)L
      IND=1
5     IF(AR-3.)7,7,6
6     WRITE(6,103)AR
      IND=1
7     IF(AR-.3)8,9,9
8     WRITE(6,103)AR
      IND=1
9     IF(G-5.)10,11,11
10    WRITE(6,104)G
      IND=1
11    IF(S-.01)13,13,12
12    WRITE(6,105)S
      IND=1
13    IF(C-3.)15,15,14
14    WRITE(6,106)C
      IND=1
15    IF(C-.3)16,17,17
16    WRITE(6,106)C
      IND=1
17    IF(LE-100.)18,19,19
18    WRITE(6,107)LE
      IND=1
19    IF(IND)26,26,50
50    WRITE(6,108)
      GO TO 1
26    C1=AR*L*THETA/G
      C2=G/(S*C*L**2)
      S1=1.+AR**4+40.7*C2*(1.+C*AR**2)
      S2=1.+40.7*C2*(1.+C/AR**2)+1655.*C2**2*C/AR**2
      S3=1.+.33*AR**2+38.*C2*(1.+.143*C)
      S4=1.+3.*AR**2+16.3*C2*(1.+7.*C)
      FR2=1.+.002*S2*C1**2/S1
```

FIGURE A-IV-2. COMPUTER PROGRAM FOR CURVATURE EFFECTS ON STRESS IN HONEYCOMB PANELS

```
      FR=SQRT(FR2)
      IF(OPT2)20,20,23
20    IF(OPT1)21,21,22
21    WCF=1./FR2**.75
      GO TO 30
22    WCF=1./FR2
      GO TO 30
23    IF(OPT1)24,24,25
24    WCF=(DELF/DELC)**.5/FR2**.75
      GO TO 30
25    WCF=DELF/(DELC*FR2)
30    SIGYCF=(1.+.0527*(1.+.049*AR**2)*S2*C1/S3)*WCF
      SIGXCF=(1.+.036*(1.+.103*AR**2)*S2*C1/S4)*WCF
      SIGXYC=2.58*((1.+.049*AR**2)*C1+19.*S3/S2)/
     1((1.+.0258*AR**2)*C1+16.3*S4/S2)
      C3=.0527*(1.+.049*AR**2)*S2*C1/S3
      SIGH1=(C3+1.)/(C3-1.)
      SIGCFE=(1.+.445*(AR**2+.108)*AR*LE*THETA/
     1(1.+9.62*AR**2+AR**4))*WCF
      TAUXZC=WCF
      TAUYZC=WCF
      WRITE(6,120)
      IF(OPT1)33,33,34
33    WRITE(6,121)
      GO TO 35
34    WRITE(6,122)
35    IF(OPT2)32,32,36
36    WRITE(6,123)
32    WRITE(6,124)
      WRITE(6,125)A,B,H,T,TE,R
      WRITE(6,126)RO,E,GXZ,GYZ
      IF(OPT2)38,38,37
37    WRITE(6,127)DELC,DELF
38    WRITE(6,128)
      WRITE(6,129)
      WRITE(6,130)THETA,L,AR,G,S
      WRITE(6,140)
      WRITE(6,130)C,LE
      WRITE(6,131)
      WRITE(6,132)SIGYCF
      WRITE(6,133)SIGXCF
      WRITE(6,134)SIGXYC
      WRITE(6,135)SIGH1
      WRITE(6,136)SIGCFE
      WRITE(6,137)TAUXZC
      WRITE(6,138)TAUYZC
      WRITE(6,139)FR
      GO TO 1
100   FORMAT(8E10.3)
101   FORMAT('C = ',E12.5)
```

FIGURE A-IV-2. (CONTINUED)

```
102   FORMAT('L = ',E12.5)
103   FORMAT('AR = ',E12.5)
104   FORMAT('G = ',E12.5)
105   FORMAT('S = ',E12.5)
106   FORMAT('C = ',E12.5)
107   FORMAT('LE = ',E12.5)
108   FORMAT('CALCULATION TERMINATED FOR THIS CASE.'
     1/'VARIABLE(S) PRINTED ABOVE OUT-OF-RANGE')
109   FORMAT(2I1,2F7.4)
120   FORMAT('1'//////,3X,'EFFECT OF CURVATURE ON HONEYCOMB',
     1' SANDWICH PANEL STRESS')
121   FORMAT(/18X,'WITH RANDOM EXCITATION')
122   FORMAT(/16X,'WITH SINUSOIDAL EXCITATION')
123   FORMAT(/10X,'AND DAMPING WHICH VARIES WITH CURVATURE')
124   FORMAT(//21X,'****INPUT DATA****')
125   FORMAT(/'ARC LENGTH IS ',F14.3,2X,'LENGTH IS ',F19.3,
     1/'CORE THICKNESS IS ',F10.3,2X,'SKIN THICKNESS IS ',F11.3,
     2/'EDGE THICKNESS IS ',F10.3,2X,'RADIUS IS ',F19.1)
126   FORMAT(/'SKIN DENSITY IS ',F12.7,2X,'SKIN MODULUS IS ',F13.0,
     1/'CORE MODULUS, GXZ IS',F8.0,2X,'GYZ IS ',F22.0)
127   FORMAT(/'CURVED PANEL DAMPING RATIO IS',3X,F5.3
     1,/'FLAT PANEL DAMPING RATIO IS',5X,F5.3)
128   FORMAT(//14X,'***NON-DIMENSIONAL PARAMETERS***')
129   FORMAT(/,5X,'THETA',9X,'L',11X,'AR',10X,'G',11X,
     1'S')
130   FORMAT(7(2X,E10.3))
131   FORMAT(//20X,'****STRESS RATIOS****')
132   FORMAT(//,'STRESSES AT PANEL CENTER',//,
     1'RATIO OF SIGMA Y CURVED TO SIGMA Y FLAT IS',5X,E12.5)
133   FORMAT('RATIO OF SIGMA X CURVED TO
     1,'SIGMA X FLAT IS ',4X,E12.5)
134   FORMAT('RATIO OF SIGMA Y CURVED TO ',
     1'SIGMA X CURVED IS ',2X,E12.5)
135   FORMAT('RATIO OF SIGMA Y OUTER FACE TO ',
     1/26X,'SIGMA Y INNER FACE IS ',E12.5)
136   FORMAT(//'RATIO OF SIGMA Y CURVED TO',/5X,'SIGMA Y ',
     1'FLAT AT CENTER OF STRAIGHT EDGE IS ',E12.5)
137   FORMAT('RATIO OF TAU XZ CURVED TO TAU XZ FLAT IS ',6X,E12.5)
138   FORMAT('RATIO OF TAU YZ CURVED TO TAU YZ FLAT IS ',6X,E12.5)
139   FORMAT(//'THE FREQUENCY RATIO IS ',E12.5)
140   FORMAT(/6X,'C',11X,'LE')
      END
```

FIGURE A-IV-2. (CONTINUED)

```
/DATA
29.          23.          17000000.  18000.     9000.
.25          84.          .008       .045       .000453
00   0.      0.
29.          23.          17000000.  18000.     9000.
.25          84.          .008       .045       .000453
01   .001    .002
29.          23.          17000000.  18000.     9000.
.25          84.          .008       .045       .000453
10   0.      0.
29.          23.          17000000.  18000.     9000.
.25          84.          .008       .045       .000453
11   .001    .002
/END
```

FIGURE A-IV-2. (CONTINUED)

EFFECT OF CURVATURE ON HONEYCOMB SANDWICH PANEL STRESS

WITH RANDOM EXCITATION

****INPUT DATA****

ARC LENGTH IS	29.000	LENGTH IS	23.000
CORE THICKNESS IS	0.250	SKIN THICKNESS IS	0.008
EDGE THICKNESS IS	0.045	RADIUS IS	84.0
SKIN DENSITY IS	0.0004530	SKIN MODULUS IS	17000000.
CORE MODULUS, GXZ IS	18000.	GYZ IS	9000.

NON-DIMENSIONAL PARAMETERS

THETA	L	AR	G	S
0.345E 00	0.288E 04	0.126E 01	0.156E 02	0.471E-03

C	LE
0.200E 01	0.511E 03

****STRESS RATIOS****

STRESSES AT PANEL CENTER

RATIO OF SIGMA Y CURVED TO SIGMA Y FLAT IS	0.13080E 01
RATIO OF SIGMA X CURVED TO SIGMA X FLAT IS	0.49356E 00
RATIO OF SIGMA Y CURVED TO SIGMA X CURVED IS	0.17134E 01
RATIO OF SIGMA Y OUTER FACE TO SIGMA Y INNER FACE IS	0.18530E 01

RATIO OF SIGMA Y CURVED TO SIGMA Y FLAT AT CENTER OF STRAIGHT EDGE IS	0.29898E 01
RATIO OF TAU XZ CURVED TO TAU XZ FLAT IS	0.30106E 00
RATIO OF TAU YZ CURVED TO TAU YZ FLAT IS	0.30106E 00

THE FREQUENCY RATIO IS 0.22262E 01

FIGURE A-IV-2. (CONTINUED)

EFFECT OF CURVATURE ON HONEYCOMB SANDWICH PANEL STRESS

WITH SINUSOIDAL EXCITATION

****INPUT DATA****

ARC LENGTH IS	29.000	LENGTH IS	23.000
CORE THICKNESS IS	0.250	SKIN THICKNESS IS	0.008
EDGE THICKNESS IS	0.045	RADIUS IS	84.0
SKIN DENSITY IS	0.0004530	SKIN MODULUS IS	17000000.
CORE MODULUS, GXZ IS	18000.	GYZ IS	9000.

NON-DIMENSIONAL PARAMETERS

THETA	L	AR	G	S
0.345E 00	0.288E 04	0.126E 01	0.156E 02	0.471E-03

C	LE
0.200E 01	0.511E 03

****STRESS RATIOS****

STRESSES AT PANEL CENTER

RATIO OF SIGMA Y CURVED TO SIGMA Y FLAT IS	0.87665E 00
RATIO OF SIGMA X CURVED TO SIGMA X FLAT IS	0.33079E 00
RATIO OF SIGMA Y CURVED TO SIGMA X CURVED IS	0.17134E 01
RATIO OF SIGMA Y OUTER FACE TO SIGMA Y INNER FACE IS	0.18530E 01

RATIO OF SIGMA Y CURVED TO SIGMA Y FLAT AT CENTER OF STRAIGHT EDGE IS	0.20038E 01
RATIO OF TAU XZ CURVED TO TAU XZ FLAT IS	0.20177E 00
RATIO OF TAU YZ CURVED TO TAU YZ FLAT IS	0.20177E 00

THE FREQUENCY RATIO IS 0.22262E 01

FIGURE A-IV-2. COMPUTER PROGRAM FOR CURVATURE EFFECTS ON STRESS IN HONEYCOMB PANELS (CONCLUDED)

APPENDIX V

EMPIRICALLY DETERMINED NATURAL FREQUENCIES

A. Skin-Stringer Plating

To obtain an estimate of the fundamental frequency of the skin-stringer plating, data from the sine-sweep tests were used to establish an empirically derived frequency equation. The procedure used in developing the frequency equation was as follows:

1. The fundamental frequency of each configuration was adjusted by dividing by the aspect ratio function, $1 + (b/a)^2$.
2. The parameter t/a^2, determined from Equation (24b), was then computed for each configuration.
3. The adjusted fundamental frequency was plotted versus the parameter t/a^2.
4. A "least-squares" fit of the data was determined to obtain a regression line equation.

Figure A-V-1 is a plot of the equation resulting from the correlation of test data and theory. Clamped and simply supported edge conditions are shown in dotted lines to afford a comparison of the edge fixities.

B. Honeycomb Sandwich

The fundamental frequency data from the tests involving the honeycomb sandwich test panels were also correlated as described in the section above. The parameter $(h+t)/a^2$ was plotted versus the adjusted frequencies.

Figure A-V-2 is a plot of the "least-squares" fit of data.

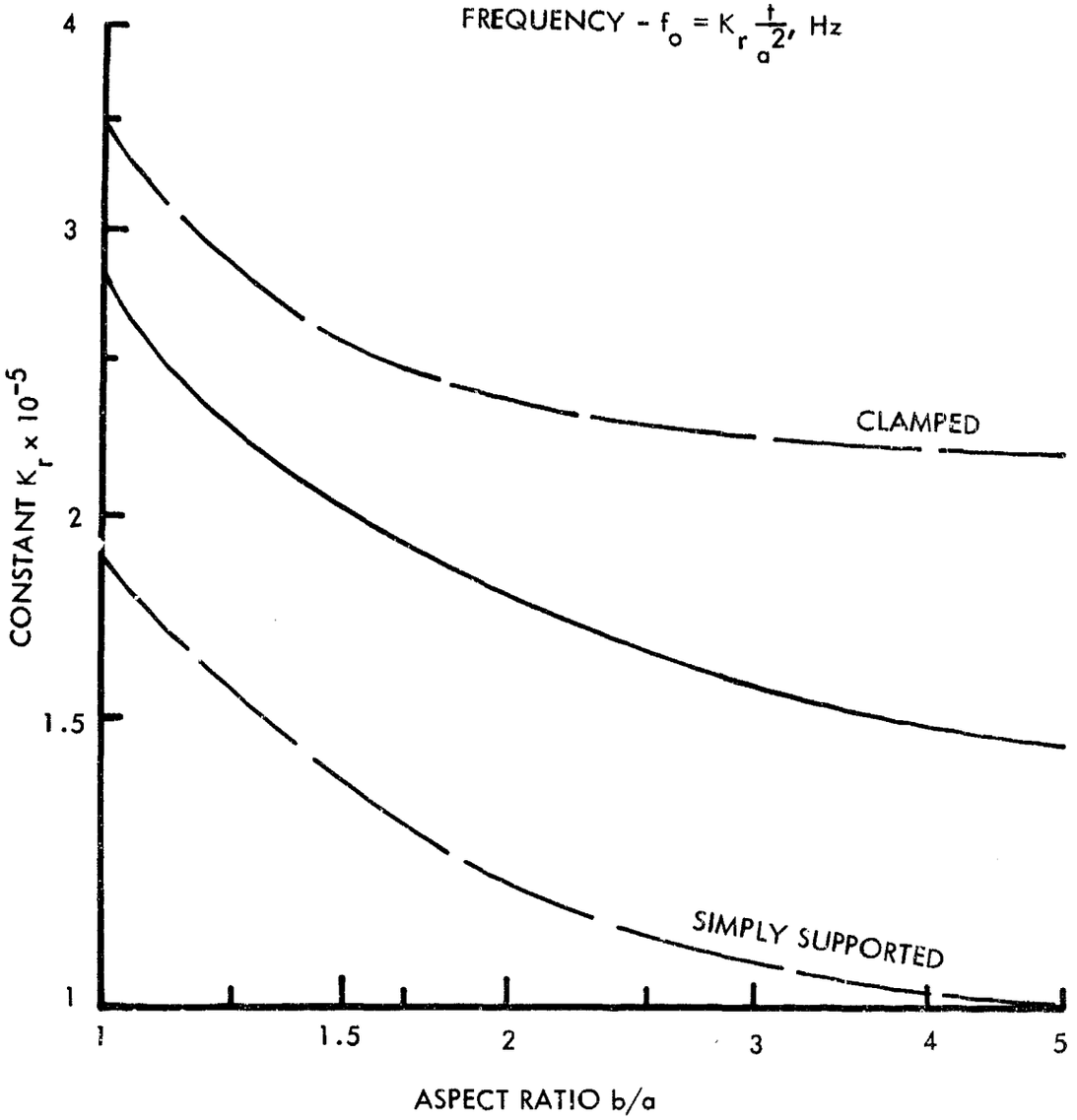

FIGURE AV-1. FUNDAMENTAL FREQUENCY OF SKIN-STRINGER PANEL

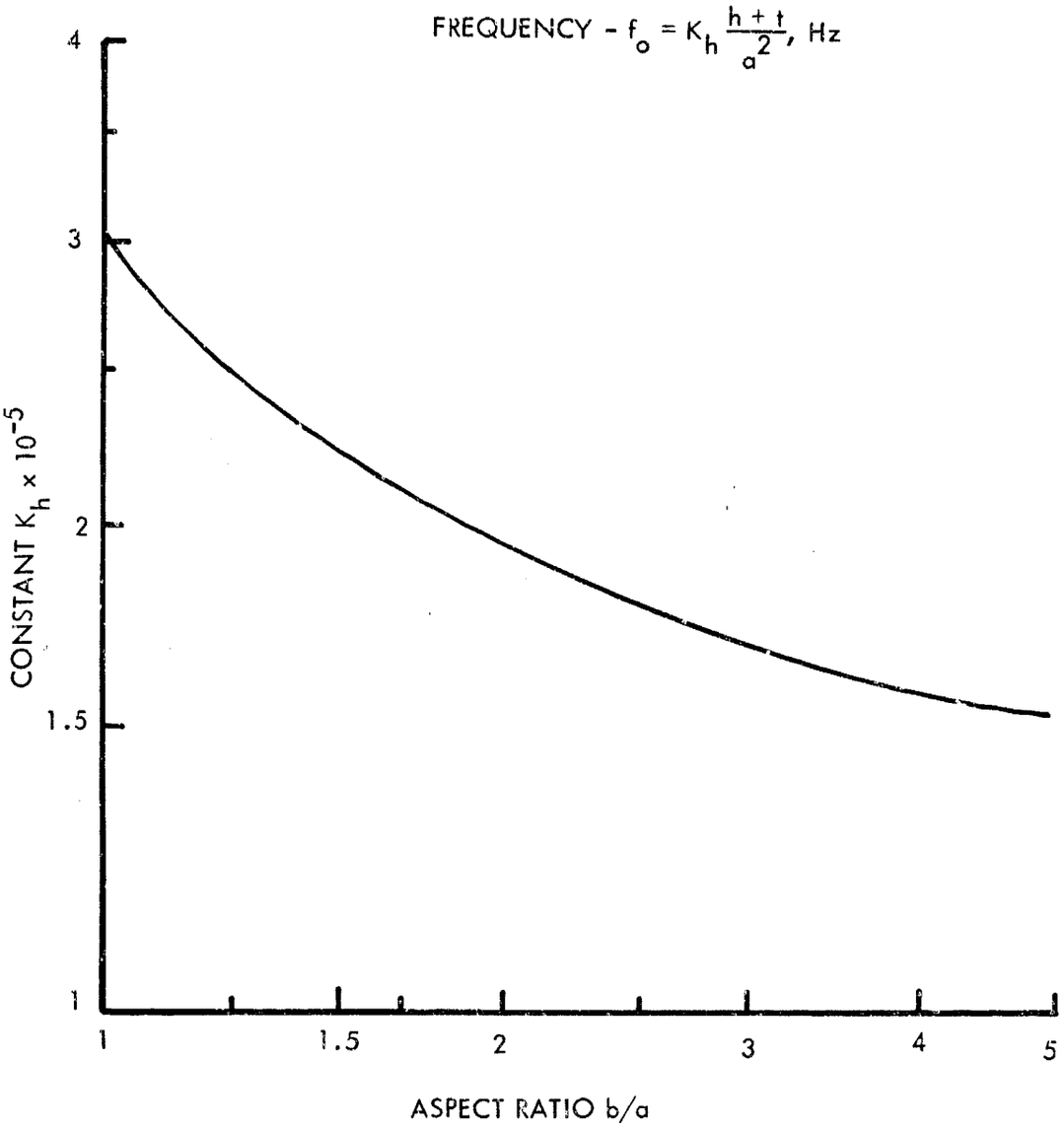

FIGURE AV-2. FUNDAMENTAL FREQUENCY OF HONEYCOMB SANDWICH PANEL

APPENDIX VI

SKIN-STRINGER TEST SPECIMEN DETAILS

Details of the skin-stringer test specimens are shown in Figure A-VI-1 and Table AVI-1.

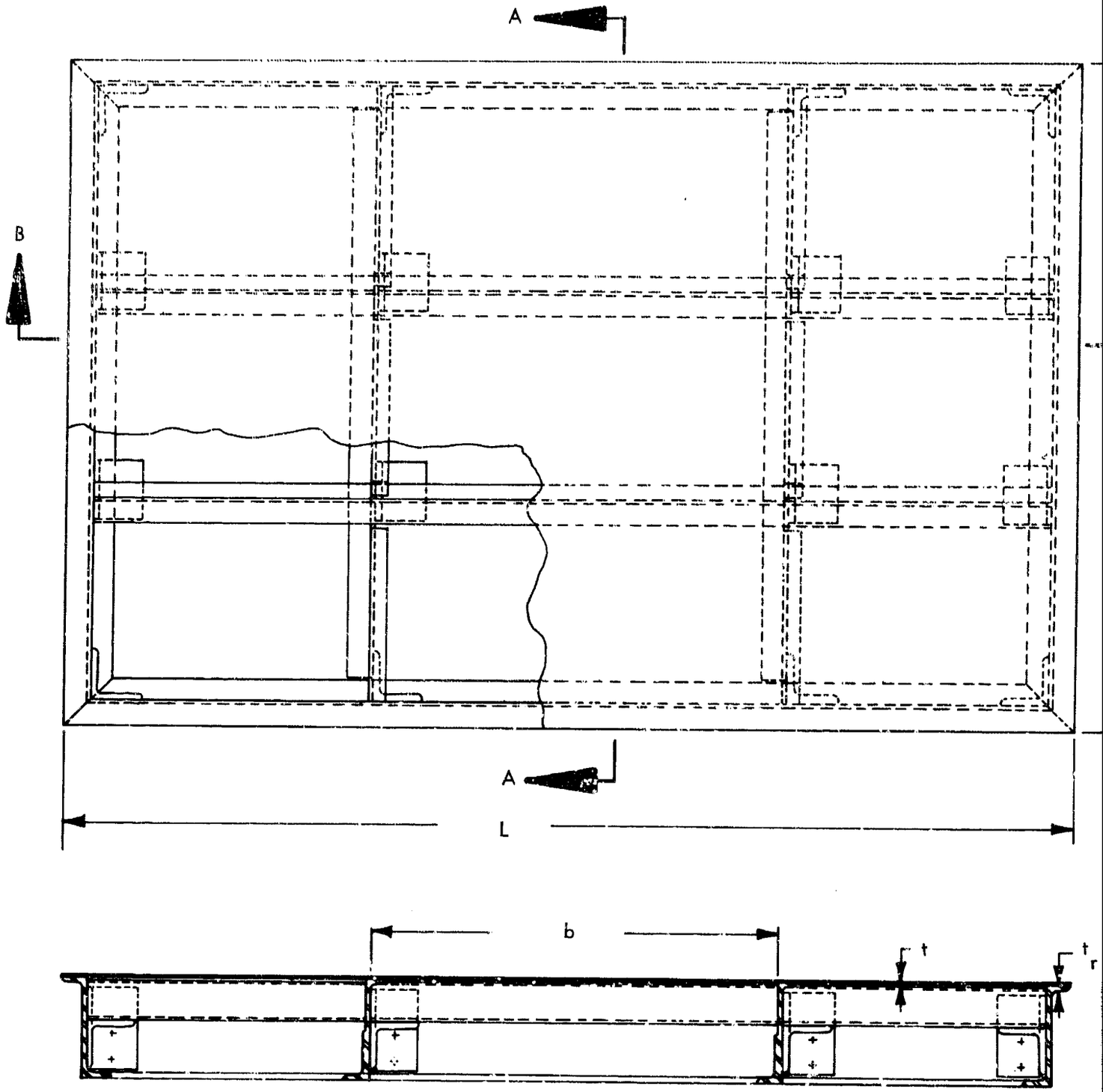

SECTION B-B

A.

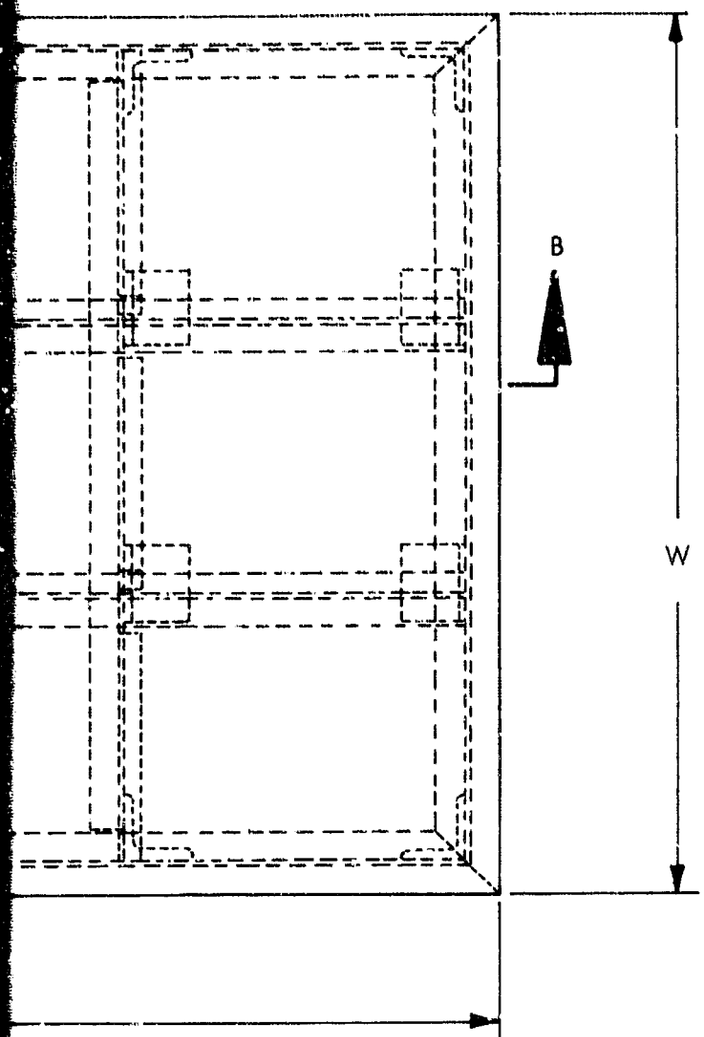

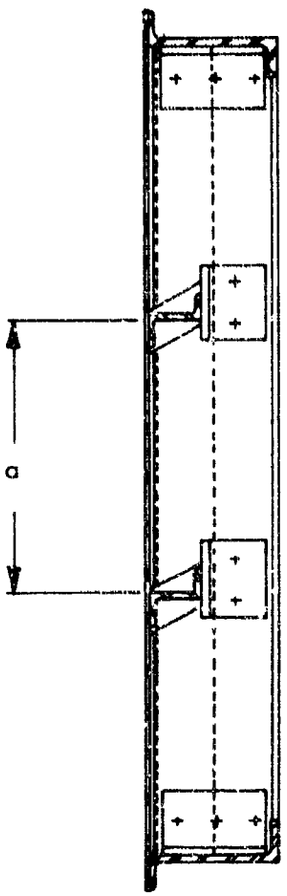

SECTION A-A

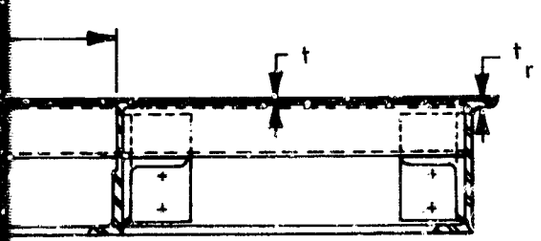

FIGURE AVI-1. SKIN-STRINGER TEST SPECIMEN DETAILS

B.

TABLE A-VI-I

BILL OF MATERIALS FOR SKIN STRINGER TEST SPECIMENS

Designation	Quantity	No. Bays	Dimensions*							Remarks
			L	W	a	b	t	t_r	b/a	
STR-1	2	9	30	20	6.00	12.00	.032	.040	2.0	lipped stringer
STR-2	2	9	30	20	6.00	12.00	.032	.040	2.0	
STR-3	2	9	30	20	6.00	12.00	.032	.040	2.0	
STR-4	2	12	30	20	4.00	8.00	.032	.050	2.0	
STR-5	2	9	30	20	5.00	10.00	.050	.071	2.0	
STR-6	2	9	30	20	9.00	18.00	.071	.071	2.0	
STR-7	2	9	30	20	5.00	10.00	.020	.027	2.0	
STR-8	2	9	30	20	6.00	12.00	.100	.125	2.0	
STR-9	2	9	30	20	9.00	18.00	.040	.040	2.0	
STR-10	2	9	30	20	6.00	9.00	.032	.040	1.5	
STR-11	2	9	30	20	8.00	16.00	.032	.032	2.0	
STR-12	2	9	30	20	5.00	10.00	.025	.032	2.0	
STR-13	2	12	30	20	4.00	8.00	.020	.032	2.0	
STR-14	2	9	30	20	9.00	18.00	.050	.050	2.0	
STR-15	2	12	30	20	3.00	6.00	.025	.040	2.0	
STR-16	2	9	30	20	5.00	10.00	.040	.050	2.0	
STR-17	2	9	30	20	7.00	14.00	.050	.063	2.0	
STR-18	2	12	30	20	4.00	8.00	.040	.063	2.0	
STR-19	2	9	30	20	6.00	12.00	.063	.080	2.0	
STR-20	2	9	30	20	10.00	20.00	.090	.090	2.0	
STR-21	2	9	30	20	6.00	12.00	.032	.040	2.0	same as STR-3
STR-22	2	9	30	20	5.00	10.00	.051	.070	2.0	same as STR-5
STR-23	2	12	30	20	6.00	9.00	.032	.040	1.5	redesign of STR-10
STR-24	2	9	30	20	9.00	18.00	.040	.040	2.0	
STR-25	2	12	30	20	4.00	6.00	.040	.063	1.5	
STR-26	2	9	30	20	6.00	9.00	.063	.080	1.5	
STR-27	2	12	30	20	4.00	12.00	.040	.063	3.0	
STR-28	2	9	30	20	6.00	18.00	.063	.080	3.0	
STR-29	2	9	30	20	5.00	10.00	.032	.050	2.0	
STR-30	2	9	30	20	8.00	16.00	.050	.064	2.0	

*Letters representing test specimen dimensions refer to Figure AVI-1, Skin-Stringer Test Specimen Drawing

REFERENCES

1. McGowan, P. R., et al., "Structural Design for Acoustic Fatigue," ASD-TDR-62-820, October 1963

2. Miles, J. W., "On Structural Fatigue Under Random Loading," Journal of Aeronautical Sciences, Vol. 21, November 1954

3. Miner, M. A., "Cumulative Damage in Fatigue," Journal of Applied Mechanics, Vol. 12, 1954.

4. Palmgren, A., "Die Lebensdaur von Kugellagern," Zietschrift Verein Deutscher Ingenieure, Vol. 68, pp 339-341, 1924

5. Powell, A., "On the Fatigue Failure of Structure Due to Vibration Excited by Random Pressure Fields," Journal Acoustical Society of America, Vol. 30, December 1958

6. Clarkson, B. L., "Stresses in Skin Panels Subjected to Random Acoustic Loading," Institute of Sound and Vibration Report, May 1967.

7. Timoshenko, S. P., and Winowsky-Kreiger, S., Theory of Plates and Shells, Second Edition, McGraw-Hill, Inc., New York, 1959

8. Livesley, R. K., Matrix Methods of Structural Analysis, Pergamon Press, Ltd., London, 1964

9. Melosh, R. J., "A Stiffness Matrix for the Analysis of Thin Plates in Bending," Journal of the Aeronautical Sciences, Vol. 28, No. 1, January 1961, pp 34-42, 64.

10. Kuo, Shan S., Numerical Methods and Computers, Addison-Wesley, Reading, Mass., 1965

11. IBM Application Program, H20-0205-1, System/360 Scientific Subroutine Package (360A-CM-03X) Verson II Programmer's Manual

12. Ballentine, J. R., et al., "Sonic Fatigue in Combined Environment," AFFDL-TR-66-7, May 1966

13. Sweers, J. E., "Prediction of Response and Fatigue Life of Honeycomb Sandwich Panels Subjected to Acoustical Excitation," Acoustical Fatigue in Aerospace Structures

14. Mead, D. J. and Sivakumaron, S., "The Stodola Method Applied to Sandwich Beam Vibration," Proceedings of Symposium on Numerical Methods for Vibration Problems, University of Southampton, 1966

15. Plumblee, H. E., "Free Vibration of a Cylindrically Curved Honeycomb Sandwich Panel with Clamped Edges," Master's Thesis, M.S. in Engr. Mech., Georgia Institute of Technology, May 1967.

16. Young, Dana and Felgar, R. P., "Tables of Characteristic Functions Representing Normal Modes of Vibration of a Beam", Engineering Research Series No. 44, Bureau of Engineering Research, University of Texas.

17. Wallace, C. E., "Stress Response and Life of Sandwich Panels," Acoustical Fatigue in Aerospace Structures, Syracuse University Press, Syracuse, New York, 1965

18. Donnell, L. H., "The Effect of Transverse Shear Deformation on the Bending of Elastic Plates," Journal of Applied Mechanics, Vol. 13, 1946

19. Royal Aeronautical Society, "Data Sheets on Fatigue," No. 66022, 1966.

20. Johnston, G. S., "Skin Cracking Due to Engine Noise," McDonnell Aircraft Corporation Report 4885, August 1957

21. Spice, B. J., "Sonic Fatigue Tests on Lockheed C-141A Structural Panels," North American Aviation Report NA62H-359, June 1962

22. Hoel, P. G., Introduction to Mathematical Statistics, Third Edition, John Wiley & Sons, Inc., New York, 1962

23. Thompson, J. R., "Model C-5A, Flexural Fatigue Tests of Bonded Sandwich Panels," Lockheed-Georgia Company Report ER 8355, December 1966

24. Lunney, E. J., and Crede, C. E., "The Establishment of Vibration and Shock Tests for Airborne Electronics," WADC Technical Report 57-75, January 1958

25. Rasor, J. O., "Sonic Fatigue Tests of Low Density Core Honeycomb Sandwich Panels," Lockheed-Georgia Company Report ER 8601, July 1966.

Unclassified

Security Classification

DOCUMENT CONTROL DATA - R&D

(Security classification of title, body of abstract and indexing annotation must be entered when the overall report is classified)

1. ORIGINATING ACTIVITY (Corporate author)
Lockheed-Georgia Company
South Cobb Drive
Marietta, Georgia 30061

2a. REPORT SECURITY CLASSIFICATION
Unclassified

2b. GROUP

3. REPORT TITLE

REFINEMENT OF SONIC FATIGUE STRUCTURAL DESIGN CRITERIA

4. DESCRIPTIVE NOTES (Type of report and inclusive dates)
Final - August 1966 to November 1967

5. AUTHOR(S) (Last name, first name, initial)

Ballentine, John R., Rudder, F. F. Jr., Mathis, J. T., Plumblee, H. E. Jr.

6. REPORT DATE	7a. TOTAL NO. OF PAGES	7b. NO. OF REFS
January 1968	234	25

8a. CONTRACT OR GRANT NO.	9a. ORIGINATOR'S REPORT NUMBER(S)
AF 33(615)-3816	ER-9546
b. PROJECT NO 1471	
c. 147101	9b. OTHER REPORT NO(S) (Any other numbers that may be assigned this report)
d.	AFFDL-TR-67-156

10. AVAILABILITY/LIMITATION NOTICES
This document is subject to special export controls and each transmittal to foreign governments or foreign nationals may be made only with prior approval of the Flight Dynamics Laboratory (FDDA) Wright-Patterson Air Force Base, Ohio 45433.

11. SUPPLEMENTARY NOTES	12. SPONSORING MILITARY ACTIVITY
	Air Force Flight Dynamics Laboratory Wright-Patterson AFB, Ohio 45433

13. ABSTRACT

Accurate nomographs for designing conventional skin-stringer and honeycomb sandwich construction to meet sonic fatigue requirements are presented. The nomographs were derived from the results of sonic fatigue tests of 30 skin-stringer and 30 honeycomb sandwich designs, totaling 60 test specimens for each design. Emphasis is also placed on assessing the effect of structural curvature on sonic fatigue and structural response. Nomographs for determining the curvature effects are included.

DD FORM 1 JAN 64 1473

Unclassified

Security Classification

Unclassified

Security Classification

14 KEY WORDS	LINK A		LINK B		LINK C	
	ROLE	WT	ROLE	WT	ROLE	WT
Sonic Fatigue						
Dynamic Response						
Structural Design						
Curvature Effects						

INSTRUCTIONS

1. ORIGINATING ACTIVITY: Enter the name and address of the contractor, subcontractor, grantee, Department of Defense activity or other organization *(corporate author)* issuing the report.

2a. REPORT SECURITY CLASSIFICATION: Enter the overall security classification of the report. Indicate whether "Restricted Data" is included. Marking is to be in accordance with appropriate security regulations.

2b. GROUP: Automatic downgrading is specified in DoD Directive 5200.10 and Armed Forces Industrial Manual. Enter the group number. Also, when applicable, show that optional markings have been used for Group 3 and Group 4 as authorized.

3. REPORT TITLE: Enter the complete report title in all capital letters. Titles in all cases should be unclassified. If a meaningful title cannot be selected without classification, show title classification in all capitals in parenthesis immediately following the title.

4. DESCRIPTIVE NOTES: If appropriate, enter the type of report, e.g., interim, progress, summary, annual, or final. Give the inclusive dates when a specific reporting period is covered.

5. AUTHOR(S): Enter the name(s) of author(s) as shown on or in the report. Enter last name, first name, middle initial. If military, show rank and branch of service. The name of the principal author is an absolute minimum requirement.

6. REPORT DATE: Enter the date of the report as day, month, year; or month, year. If more than one date appears on the report, use date of publication.

7a. TOTAL NUMBER OF PAGES: The total page count should follow normal pagination procedures, i.e., enter the number of pages containing information.

7b. NUMBER OF REFERENCES: Enter the total number of references cited in the report.

8a. CONTRACT OR GRANT NUMBER: If appropriate, enter the applicable number of the contract or grant under which the report was written.

8b, 8c, & 8d. PROJECT NUMBER: Enter the appropriate military department identification, such as project number, subproject number, system numbers, task number, etc.

9a. ORIGINATOR'S REPORT NUMBER(S): Enter the official report number by which the document will be identified and controlled by the originating activity. This number must be unique to this report.

9b. OTHER REPORT NUMBER(S): If the report has been assigned any other report numbers *(either by the originator or by the sponsor)*, also enter this number(s).

10. AVAILABILITY/LIMITATION NOTICES: Enter any limitations on further dissemination of the report, other than those imposed by security classification, using standard statements such as:

(1) "Qualified requesters may obtain copies of this report from DDC."

(2) "Foreign announcement and dissemination of this report by DDC is not authorized."

(3) "U. S. Government agencies may obtain copies of this report directly from DDC. Other qualified DDC users shall request through

_____."

(4) "U. S. military agencies may obtain copies of this report directly from DDC. Other qualified users shall request through

_____."

(5) "All distribution of this report is controlled. Qualified DDC users shall request through

_____."

If the report has been furnished to the Office of Technical Services, Department of Commerce, for sale to the public, indicate this fact and enter the price, if known.

11. SUPPLEMENTARY NOTES: Use for additional explanatory notes.

12. SPONSORING MILITARY ACTIVITY: Enter the name of the departmental project office or laboratory sponsoring *(paying for)* the research and development. Include address.

13. ABSTRACT: Enter an abstract giving a brief and factual summary of the document indicative of the report, even though it may also appear elsewhere in the body of the technical report. If additional space is required, a continuation sheet shall be attached.

It is highly desirable that the abstract of classified reports be unclassified. Each paragraph of the abstract shall end with an indication of the military security classification of the information in the paragraph, represented as *(TS), (S), (C), or (U)*.

There is no limitation on the length of the abstract. However, the suggested length is from 150 to 225 words.

14. KEY WORDS: Key words are technically meaningful terms or short phrases that characterize a report and may be used as index entries for cataloging the report. Key words must be selected so that no security classification is required. Identifiers, such as equipment model designation, trade name, military project code name, geographic location, may be used as key words but will be followed by an indication of technical context. The assignment of links, rules, and weights is optional.

GPO 886-551

Unclassified

Security Classification

AD831 118*

Errata: AFFDL-TR-67-156
"Refinement of Sonic Fatigue Structural Design Criteria"

Page	Correction
xiii	g $h_1/t = h/(2t)$
xiv	L b/t
	L_e b/t_e
xvii	ρ mass per unit area of a plate
	mass per unit volume - Section F
19	The (2, 1) element in the matrix of Equation (56b) should read $(30[(\delta/b)_5 - (\delta/b)_2])$
54	The line following Equation (128) should read, "where it has been assumed that $t_2 = t_3 = t$."
54	Changes in the definitions in Equation (129) should be L = b/t, $g = h_1/t$.
57	Following Table III the data should read L = b/t = 1031.25 $g = h_1/t = 11.625$
60	In Equation (146) the "L" in the numerator should be "L_e".
62	In Equations (156) and (157) the subscript "2" should be deleted from t.
146	In Table XVI change "a" to "b" change "b" to "a" delete the subscript "2" on t
148	In Table XIX the definition on the second line should be $\left.\frac{\sigma_{yc,z=h_1}}{\sigma_{yc,z=-h_1}}\right\|_{center}$
171	Equation (120) should read $\bar{\tau} = 18.7\left(\frac{b}{h}\right)\left(\frac{D}{\rho}\right)^{1/4}\left[\frac{\Phi(f)}{(a^2+b^2)}\right]^{1/2}$

Page	Correction
171	The first sentence in the next paragraph should read: "The required core density (lbs/in^3) can ...".
176	In Equation (178) the exponent on the right hand side should be -3/4. In Equation (179) the entire right hand side should be raised to the power -1. In Equation (180) the exponent on the bracketed term should be -3/4. In Equation (181) the bracketed term should be raised to the power -1.